NOVEL HYBRID POLYMERIC MATERIALS FOR BARRIER COATINGS

A Dissertation
Submitted to the Graduate Faculty
of the
North Dakota State University
of Agriculture and Applied Science

By

Erin Christine Pavlacky

In Partial Fulfillment
for the Degree of
DOCTOR OF PHILOSOPHY

Major Department:
Coatings and Polymeric Materials

January 2012

Fargo, North Dakota

North Dakota State University

Graduate School

Title

Novel Hybrid Polymeric Materials for Barrier Coatings

By

Erin Pavlacky

The Supervisory Committee certifies that this ***disquisition*** complies with North Dakota State University's regulations and meets the accepted standards for the degree of

DOCTOR OF PHILOSOPHY

SUPERVISORY COMMITTEE:

Dean C. Webster

Chair

Andriy Voronov

Pinjing Zhao

Amy O'Connor

Approved by Department Chair:

01/18/2012 — Date

Dean C. Webster — Signature

ABSTRACT

Polymer-clay nanocomposites, described as the inclusion of nanometer-sized layered silicates into polymeric materials, have been widely researched due to significant enhancements in material properties with the incorporation of small levels of filler (1 – 5 wt.%) compared to conventional micro- and macro-composites (20 – 30 wt.%). One of the most promising applications for polymer-clay nanocomposites is in the field of barrier coatings.

The development of UV-curable polymer-clay nanocomposite barrier coatings was explored by employing a novel in situ preparation technique. Unsaturated polyesters were synthesized in the presence of organomodified clays by in situ intercalative polymerization to create highly dispersed clays in a precursor resin. The resulting clay-containing polyesters were crosslinked via UV-irradiation using donor-acceptor chemistry to create polymer-clay nanocomposites which exhibited significantly enhanced barrier properties compared to alternative clay dispersion techniques. The impact of the quaternary alkylammonium organic modifiers, used to increase compatibility between the inorganic clay and organic polymer, was studied to explore influence of the organic modifier structure on the nanocomposite material properties. An alternative in situ preparation method was explored to further increase the dispersion of organomodified clay within the precursor polyester resins. In stark contrast to traditional in situ polymerization methods, a novel “reverse” in situ preparation method was developed, where unmodified montmorillonite clay was added *during* polyesterification to a reaction mixture

containing the alkylammonium organic modifier. The resulting nanocomposite films exhibited reduced water vapor permeability and increased mechanical properties.

The novel preparation of hybrid films coupling the advantageous properties of organic-inorganic hybrids formed through sol-gel chemistry with polymer-clay nanocomposite technology was also explored. Alkoxysilane-functional copolymer-clay nanocomposites were first synthesized, followed by crosslinking via simultaneous hydrolysis and condensation reactions to create the novel hybrid barrier films. By dispersing organomodified clay throughout the hybrid network, dramatic improvements in several film properties were observed, particularly regarding the viscoelastic properties. Additional studies with the same organic-inorganic preparation technique were performed to incorporate amine-functionality into the hybrid film for potential applications as protective membranes in CO_2 capture and separation technologies. Finally, controlled free-radical polymerization techniques were combined with the preparation of the organic-inorganic hybrids.

ACKNOWLEDGEMENTS

I am incredibly grateful for my family, friends, and colleagues who have been a constant source of encouragement throughout my collegiate education. I have been very blessed to have the unconditional support of so many wonderful people as I pursued my goal of obtaining a Ph.D. in Coatings and Polymeric Materials. Dr. Webster, thank you so much for your advice and guidance over the past three years. I am very lucky to have been a member of your research group, and I appreciate the time and efforts put into making my graduate school experience very rewarding. Dr. Voronov, Dr. Zhao, and Dr. O'Connor, thank you very much for serving as a member of my advisory committee. You each have been so helpful and supportive throughout my graduate career at NDSU, and I am very appreciative of the time taken to provide assistance and advice regarding my research.

I would not have achieved any of the success in my professional and personal life without the amazing love, support, kindness, and humor of my family and friends. I cannot imagine going through all the ups and downs of graduate school without my wonderful husband Drew. We will always remember our last year of graduate school as the first year of our marriage, and I know we will look back on these years and be so happy we were able to share them together. You make me laugh every single day, and I could not ask for more. Mom and Dad, others may say they have the best parents in the world, but I know for a fact that I truly do. All of my professional and personal achievements are because of you and the love and encouragement you have

unconditionally given to me. My drive and motivation is a result of your parenting, and I am so appreciative to all you have given me. Tara, you have always been a much needed source of humor and encouragement when life gets stressful. I am looking forward to hopefully not living four hours apart and spending much more time with you, including watching Survivor in person! I have been very blessed with making such wonderful friends in the Fargo area. Linda and Teddi, I hope our friendship continues to grow as we all begin our careers and we continue to have so many fun memories.

I would like to thank the members of the Webster research group for helping to make graduate school more enjoyable and making the days pass by very quickly. Jaci, Kathy, and Carol, thank you for your assistance and help over the past years in the CPM office. Heidi, thank you for the countless hours you have helped me and every other student in the instrument room. I hope you know how appreciated you are, and I am very grateful for all your advice. Finally, I would like to thank the National Science Foundation (ND EPSCoR) and the Department of Energy for funding my graduate research.

DEDICATION

To my amazing, wonderful, hilarious, kind, smart, and loving husband Drew, I dedicate my Ph.D. dissertation to you. I cannot wait to begin the next stage of our life after graduate school, and I know we can accomplish anything together.

TABLE OF CONTENTS

LIST OF TABLES

LIST OF FIGURES

LIST OF SCHEMES

CHAPTER 1. INTRODUCTION: POLYMER-CLAY NANOCOMPOSITES

1.1. Introduction

Traditionally, the incorporation of inorganic or synthetic fillers into polymers to create composite systems has been a relatively simple approach to reduce cost or enhance material properties, but the dispersed particulate phase may also increase the composite weight, brittleness, and opacity.[1] Recently, a new class of composite materials, referred to as nanocomposites, have garnered significant attention as a low cost, facile approach to develop high performance materials which exhibit significantly improved properties compared to conventional micro- or macro-composites.[2] Nanocomposites are described as filled polymeric materials where at least one dimension of the dispersed particulate phase is in the nanometer (nm) range, such as layered silicates, carbon nanotubes, and whiskers.[3] Of the nanocomposite classes, polymer-clay nanocomposites have received the most attention due to the profound material property improvements with the incorporation of relatively low levels of loading (1 – 5 wt. %) compared to conventional composite systems (20 – 30 wt.%) along with their wide-spread availability and low processing costs.[4]

Polymer-clay nanocomposites are described as the incorporation of layered silicates (clay) into a polymer matrix by various dispersion techniques including sonication and intercalative methods. Although polymer-clay nanocomposite research dates back over 50 years,[5-8] the studies conducted by the Toyota Central Research Laboratories were the catalyst for significant nanocomposite advances. The initial studies by Toyota prepared nylon 6-montmorillonite clay

nanocomposites to be used in timing belt covers for the Toyota Camry automobile.[9-10] With the incorporation of montmorillonite clay into the nylon 6 polymer, the Toyota research group reported enhanced modulus, barrier protection, and heat distortion temperatures compared to an unfilled nylon 6 sample. Additionally, high optical clarity was maintained for the nylon 6-montmorillonite clay nanocomposites when compared to the neat nylon 6.

From the success of the Toyota polymer-clay nanocomposite research, several other applications have utilized the incorporation of layered silicates to enhance product properties and performance including food and beverage packages, marine fuel tanks, and flame retardant compounds.[11-13] With a continuously growing volume of publications in both industrial and academic institutions, the implementation of polymer-clay nanocomposites to produce new and innovative products is certain.

1.2. Layered silicate structure

Layered silicates are the by-product of volcanic eruptions which occurred throughout the world millions of years ago.[14] The ash from volcanic activity was deposited under water sources such as oceans and alkaline lakes. Oceans, which previously covered what is now the western United States of America, gradually formed clay-containing deposits during the Cretaceous Age (85 – 125 million years ago).[15] The instability of the volcanic ash with water readied the particulates for chemical reactions. Interactions with excess magnesium located in the marine sediment environment and contact with water helped to form the uncharged and

charged clay species mined in deposits around the world today. Currently, it is estimated Wyoming alone contains over one billion tons of available clay.[16]

The most common layered silicates used in polymer-clay nanocomposite research belong to the 2:1 phyllosilicate family, possessing crystal structures composed of two tetrahedral silicon sheets fused to one octahedral aluminum or magnesium oxide sheet (Figure 1.1).[17] Examples of 2:1 phyllosilicates include montmorillonite, saponite, and hectorite clays, and the general formulas are reported in Table 1.1 (M = monovalent cation and χ = degree of isomorphic substitution).[18-19]

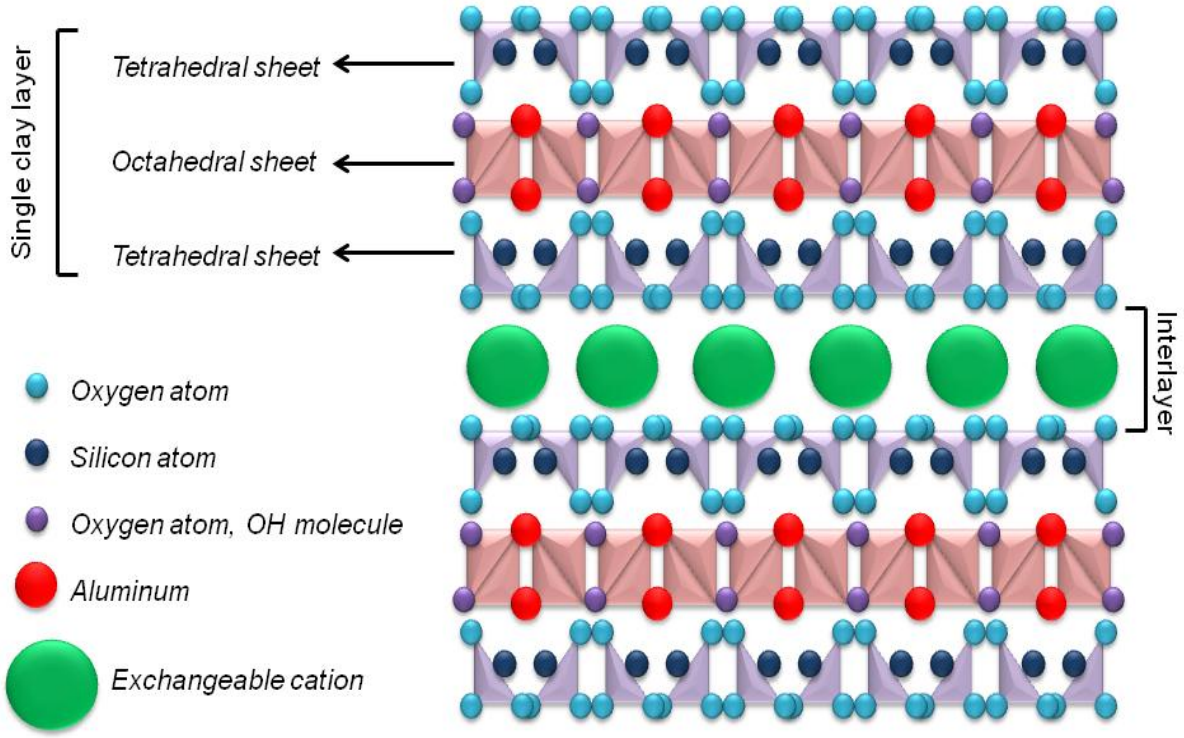

Figure 1.1: Illustration of 2:1 phyllosilicate structure.

TABLE 1.1
2:1 phyllosilicate general formulas

2:1 phyllosilicate	General formula
Montmorillonite	$M_x(Al_{4-x}Mg_x)Si_8O_{20}(OH)_4$
Saponite	$M_xMg_6(Si_{8-x}Al_x)Si_8O_{20}(OH)_4$
Hectorite	$M_x(Mg_{6-x}Li_x)Si_8O_{20}(OH)_4$

The fusion of the three sheets forms a single clay layer with a thickness of approximately one nm and lateral dimensions ranging from 30 nm to several microns depending on the clay type and processing conditions. Therefore, the layered silicate aspect ratio, or the ratio of clay layer width to thickness, may range from 100 to over 1,000.[2, 20-21]

Recently, a study to determine the lateral dimensions of commercially-available montmorillonite clay was performed by atomic force microscopy (AFM). The montmorillonite clay was first deposited onto mica substrates from a very dilute solution, followed by AFM analysis assuming a circular shape to create equation (1.1) where A is the clay platelet area, D is the clay diameter, and t is the clay thickness. With an approximate thickness of one nm, the lateral dimensions of the montmorillonite platelets were determined to be 100 – 200 nm.[22]

$$\sqrt{A/t} = \sqrt{\pi/4}\left(\frac{D}{t}\right) = 0.89(\frac{D}{t}) \qquad (1.1)$$

Isomorphic substitutions within the octahedral sheet produce clay sheets bearing negative charges. More specifically, the Al^{3+} may be replaced with Mg^{2+} or Fe^{2+} and Mg^{2+} may be replaced with Li^{1+} to create a negative charge distribution throughout the octahedral sheet resulting from the differences in valence. In order to balance the negative charge created from the isomorphic substitutions, positive alkaline and alkali counterions are located in the clay interlayer. Most commonly,

Na^+ and K^+ cations are found in naturally-produced 2:1 phyllosilicates. Layered silicates typically exist in stacked formations due to favorable electrostatic interactions between the negatively charged clay platelets and positively charged counterions. The interlayer or gallery refers to the van der Waals gap between each clay platelet, and is the location of the counterions. The interlayer cations are critical to the final dispersion of layered silicates within a polymer matrix as the cations will dictate the affinity of the clay to the polymer as well as provide a source for organic modification to the clay sheet.

1.3. Layered silicate organomodification

Organic modification of layered silicates is commonly performed to render the inorganic clay platelets more organophilic to facilitate their incorporation into a polymer matrix. The alkali counterions, or “exchangeable” cations located within the clay interlayers, may be exchanged with other cationic molecules to increase wettability between the clay and polymers, functionalize the silicate surface, and lower the surface energy of the inorganic clay platelets. The quantity of negative charge from the clay surface may be quantified to obtain a cation exchange capacity (CEC) value. The CEC is dependent on the location the clay source is mined and the extent of isomorphic substitutions within the tetrahedral and octahedral sheets. The CEC surface charge, generally expressed in milliequivalents/gram, is a characteristic average as the negative charge will vary between individual clay layers.

Immiscibility between inorganic and organic components may reduce material properties such as mechanical strength and thermal stability. Hence, the

organomodification of layered silicates is often necessary to improve compatibility and aid in the formation of nanocomposites. The alkali or alkaline earth cations situated within the clay interlayer will increase compatibility with hydrophilic polymers, such as polyvinyl alcohol (PVA).[23] To increase layered silicate organophilicity, ion exchange reactions are conducted to replace the interlayer earth cations with various organic surfactants, which increases clay-polymer affinity. Interlayer cations are referred to as exchangeable cations due to the ease of replacement as the cations are not covalently incorporated into the clay sheet structure.[24]

Quaternized alkylammonium cations are commonly exchanged with cations to modify clay platelets. The impact of alkylammonium ion modifiers on the properties of epoxy-clay nanocomposites was studied by Xidas et al.[25] The structure, functionality, polarity, and hydrophobicity of the modifiers resulted in varying degrees of clay dispersion as well as changes in mechanical, thermo-mechanical, and thermal properties of the nanocomposite films. Fornes et al. examined how the length of the alkyl chain attached to the nitrogen atom of various organic modifiers affected the final clay dispersion in nylon 6 nanocomposites.[26] Modifiers with one alkyl chain provided the highest degree of exfoliation compared to modifiers with zero or two alkyl chains. Two alkyl chains showed poorer dispersion than one alkyl chain due to the increased repulsive interactions between the modifier hydrocarbon chains and the polyamide matrix.

The superiority of quaternary ammonium modifiers over primary, secondary, and tertiary ammonium clays was reported by Kim and White in a study on the

impact of organic modifiers on montmorillonite clays in the formation of polymer-clay nanocomposites.[27] The quaternary ammonium modifiers demonstrated the best compatibility with polar polymers. This observation was attributed to the greatest surface area interaction between the long alkyl chains of the modifier and the polar polymeric material as the quaternary ammonium modifier will cover more of the clay platelet than shorter alkyl chains. Additionally, the longer alkyl chains permitted a higher degree of intercalation of the polymer into the montmorillonite clay interlayer.

In addition to increased affinity between the primarily hydrophilic clay and polymer matrices, the organic modifier may also serve as an initiation source in a wide variety of polymerization reactions. Fan et al. described a technique for ionically binding organic modifiers to clay platelets that may be activated to initiate polymerization reactions.[28-29] The surface-initiated polymerizations were performed by cationic free radical initiators to synthesize polystyrene-clay nanocomposites. Free-radical grafting was also performed by Mansoori et al. in the preparation of polyacrylamide-clay nanocomposites.[30] A silylation reaction was employed to modify montmorillonite clay with vinyltrichlorosilane, followed by chemical grafting of polyacrylamide to the clay surface to produce intercalated nanocomposites. Photoinduced polymerizations have also been successfully performed with the utilization of layered silicate organomodification as a photoinitiation source.[31-34] Recently, living radical polymerization (LRP) methods have been employed to produce nanocomposites exhibiting well-defined polymer functionality and architecture. The modification of layered silicates has been used to facilitate atom

transfer radical polymerization (ATRP),[35-38] nitroxide mediated polymerization (NMP),[39-41] and reverse addition-fragmentation chain transfer (RAFT)[42-45] in multiple studies.

1.4. Nanocomposite morphology and characterization

1.4.1. Morphology classifications

The dispersion of layered silicates within a polymer matrix is classified into three distinct morphological groups: phase-separated (agglomerated), intercalated, and exfoliated (Figure 1.2).

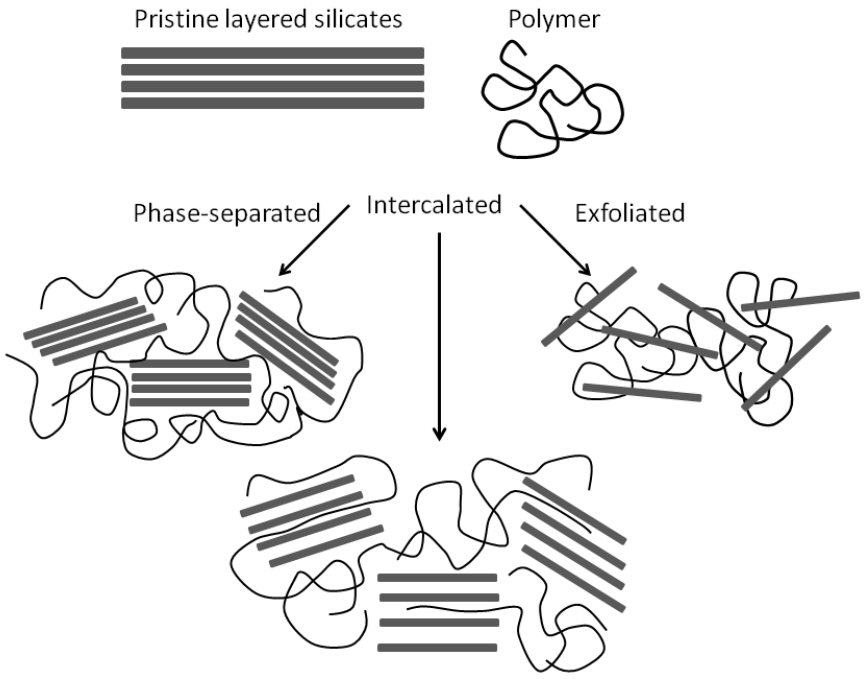

Figure 1.2: Polymer-clay nanocomposite morphological classifications: phase-separated, intercalated, and exfoliated.

Each morphological classification describes the extent of polymer and clay interfacial interaction based on polymer intercalation.[46] Due to the inherent incompatibility between the inorganic clay fillers and organic polymeric materials, phase-separated polymer-clay nanocomposites are the most likely morphological

classification. Phase-separation occurs in nanocomposites when the polymeric material does not penetrate between clay platelets, and flocculation of layered silicates manifest throughout the polymer matrix. With poor dispersion, clay agglomerates diminish the final material properties, and the composite behaves similarly to conventional, micro- and macro-composite systems.[47] Stacked clay formation tends to persist with phase-separated systems.

Intercalated morphologies are described as the intercalation of polymer chains into the clay interlayer to increase the basal spacing between layered silicates and enhance the interfacial interaction between the clay and polymer components; however, overall order is maintained within the nanocomposite as the clays still exhibit face-to-face stacking. A characteristic repeat distance forms in between the clay platelets, typically increasing the interlayer distance to 2 – 3 nm.

The final classification of polymer-clay nanocomposite morphology is an exfoliated state, where individual clay platelets are well-dispersed throughout the polymer matrix. Often, the clay delamination produces randomly oriented silicates, a stark contrast to the well-ordered stacking of phase-separated and intercalated morphologies. Exfoliated morphologies also produce the highest interfacial interactions between the clay filler and polymer matrix, thereby maximizing the contribution of the inorganic particulates and most significantly enhancing the material properties.[48] In particular, the mechanical properties of exfoliated polymer-clay nanocomposites have exceeded those of intercalated nanocomposites. By dispersing individual clay platelets, the reinforcing impact of the layered silicates improves, as does the nanocomposite's ability to withstand cracks and carry

applied loads. The final spacing between the clay platelets may reach upwards of 8 – 10 nm. Expectedly, complete exfoliation within polymer-clay nanocomposite is difficult due to clay anisotropy, volume fraction, and favorable electrostatic interactions.

1.4.2. Structural characterization

X-ray diffraction (XRD) and transmission electron microscopy (TEM) are the two most common techniques to confirm nanocomposite formation and classify morphology. Characterization of the nanocomposite structure may be performed by quantifying the basal spacing of the layered silicates. Bragg's Law is utilized to determine the structural spacing as shown in equation (1.2) where n is an integer, λ is the X-ray radiation wavelength, d is the diffractional spacing, and θ is the angle of diffraction.

$$\sin\theta = n\lambda/2d \tag{1.2}$$

Generally, diffraction peaks occurring in the 2 – 9 2θ range have been employed for structural characterization as higher diffraction angles tend to produce diffraction peaks from polymer crystallinity. The location of diffraction peaks indicates the degree of clay dispersion in the nanocomposite system. Intercalated nanocomposite morphologies have a characteristic shift in the diffraction peak to lower angles as compared to the pristine clay (Figure 1.3), representing an increase in the structural spacing from polymer intercalation according to Bragg's Law. Because the well-ordered arrangement of the layered silicates is preserved with intercalated morphologies, the basal spacing may be determined. Conversely, exfoliated nanocomposite morphologies do not have characteristic diffraction

peaks at low angles due to the disruption of order and possible random orientation of the clay platelets throughout the polymer matrix. The absence of peaks in the XRD diffractograms may indicate the spacing between layered silicates has achieved too great of a distance between the delaminated clay layers to produce a characteristic peak.

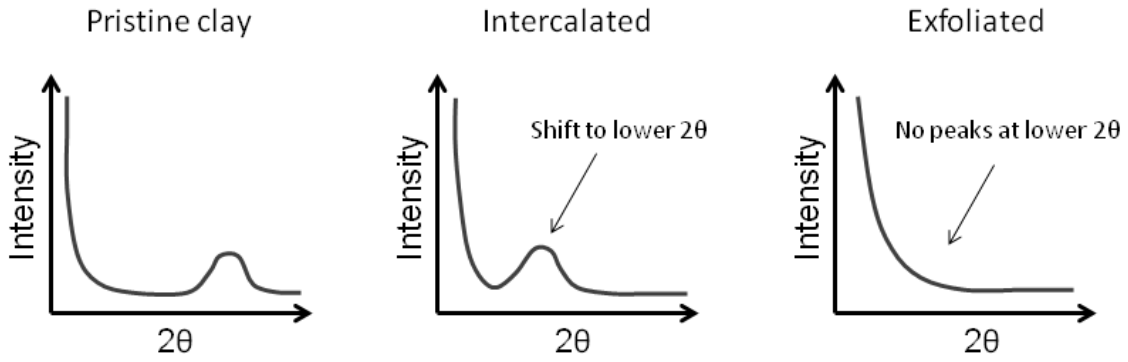

Figure 1.3: Schematic representation of XRD diffractograms indicating the degree of clay dispersion.

Although XRD has widely been employed to study the structural characteristics of polymer-clay nanocomposites, the utilization of this technique can only indicate the final morphology. A featureless diffractogram may not necessarily confirm the formation of an exfoliated state. Low instrument sensitivity may limit the ability to detect order within a nanocomposite system, particularly when low amounts of clay are incorporated in polymer matrices (1 – 5 wt.%). Morgan and Gilman studied the inaccuracies associated with XRD analysis to confirm the final nanocomposite structure.[49] At times, immiscible and intercalated morphologies were incorrectly identified as exfoliated morphologies from XRD analysis. Factors such as orientation, poor calibration at low angles, and clay concentration may produce misleading XRD diffractograms.[50] Due to the potential

inaccuracies associated with structural determination via XRD, TEM provides a complimentary and qualitative assessment of nanocomposite structural characteristics. Cross-sections of the layered silicates appear as dark, bold lines due to their composition of primarily heavier elements than polymeric materials, thus providing an easily identifiable marking in the bright-field images produced from TEM. TEM is also particularly useful when mixed morphologies, such as intercalated and partially intercalated-exfoliated, are present in the nanocomposite sample.

1.5. Preparation of nanocomposites

The arbitrary mixing of layered silicates and polymeric species will not necessarily form intercalated or exfoliated polymer-clay nanocomposites due to the inherent incompatibility between the inorganic clay filler and organic polymeric material. Four principle processes have been employed to overcome the polymer and clay incompatibility to form polymer-clay nanocomposites with high degrees of clay dispersion: template synthesis, polymer or prepolymer intercalation, melt intercalation, and in situ intercalative polymerization.

1.5.1. Template synthesis

The template synthesis method to produce polymer-clay nanocomposites utilizes sol-gel chemistry to create silicate minerals in situ. With this technique, an aqueous polymer gel serves as a template for clay layer formation from the hydrothermal crystallization of magnesium hydroxide or lithium fluoride precursors with a silica sol.[51] As the silicate building blocks are formed, the aqueous polymer will aid in nucleation and growth, eventually becoming entrapped between the clay

minerals. Template synthesis has been typically employed for the production of double-layer hydroxide-based nanocomposites.

Anionic polymers poly(styrenesulfonate) and poly(vinylsulfonate) were utilized in the production of layered double hydroxide nanocomposites via template synthesis to study their intercalation with organomodified silicate sheets.[52] The anionic polymers successfully intercalated between the in situ formed silicate particulates, but also strongly adsorbed onto the clay aggregate outer surface, and thus controlled the electrokinetic behavior. Despite the apparent advantage of synthesizing the clay minerals in situ with the polymeric material in a one-step process, the high temperature processing conditions have limited the use of template synthesis due to polymer decomposition. One notable exception is the hectorite clay, which may be processed at much milder reaction conditions.[53] However, the likelihood of silicate aggregation has severely hindered the implementation of template synthesis for nanocomposite production, so the remaining three methods of polymer-clay nanocomposite preparation are primarily used.

1.5.2. Polymer or prepolymer intercalation

With the polymer or prepolymer intercalation nanocomposite preparation technique, clay is first swollen in a suitable solvent, followed by polymer or prepolymer addition to intercalate between the silicate layers (Figure 1.4). The electrostatic attraction between silicate layers may easily be overcome with dissolution into a suitable solvent, thereby creating a solution of exfoliated clay layers. The target polymer, which is readily soluble in the selected solvent, is

added to the swollen clays and intercalated between the silicate layers. The final step of the polymer intercalation is removal of the solvent by precipitation or vaporization. Upon solvent removal, the layered silicate reassembly will produce nanocomposites with polymer intercalated between the silicate layers. To successfully produce polymer-clay nanocomposites with this intercalation method, the entropy reduction from polymer intercalation between silicates must be compensated with an entropy increase from intercalated solvent molecule desorption. Therefore, the driving force for successful polymer or prepolymer intercalation is the entropy gained from solvent molecule desorption.

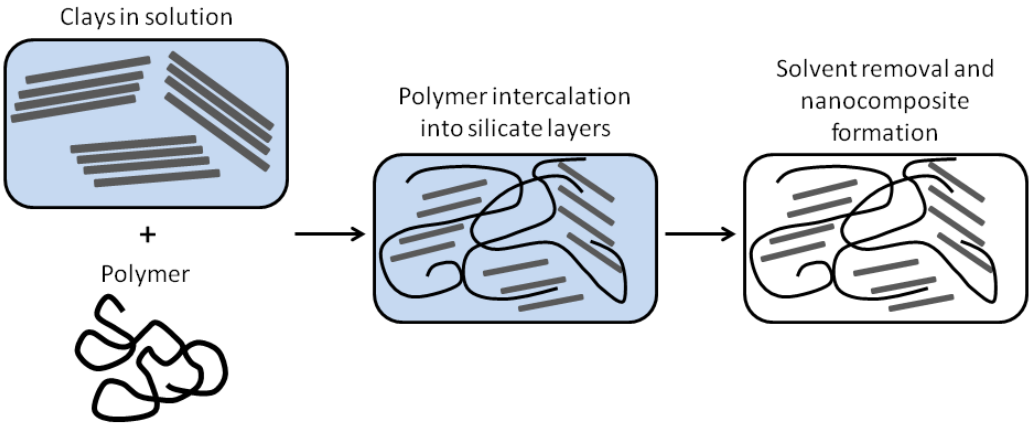

Figure 1.4: Polymer-clay nanocomposite formation via polymer intercalation in solution.

Water soluble polymers are most often employed in the polymer intercalation preparation of nanocomposites. Ogata and coworkers studied the intercalation of PVA and poly(ethylene oxide) (PEO) into montmorillonite clay using water as a cosolvent.[54] The resulting PVA-clay nanocomposites were successfully intercalated with well-dispersed montmorillonites, whereas the PEO-clay nanocomposites formed agglomerates due to PEO crystallites forming

perpendicular to the clays. PVA-nanocomposites produced PVA crystallite formation parallel to the montmorillonite layers, thereby contributing to the formation of a nicely intercalated system. Additional water-soluble polymers used in polymer intercalation methods include poly(vinyl pyrrolidone),[55-56] poly(acrylic acid),[57-58] and poly(vinyl ethylene).[59]

Interestingly, polymers insoluble or infusible in organic solvents may also be used in the preparation of nanocomposites by a similar intercalation technique. Instead of intercalating the polymer in solution, a prepolymer precursor is intercalated then converted to the desired polymeric species thermally or through chemical reactions. Poly(imide)-clay nanocomposites have been prepared using a prepolymer intercalation method by the Toyota research group.[60] Organically-modified montmorillonite clays were dispersed in dodecylammonium hydrochloride followed by addition of poly(amic acid), a poly(imide) precursor. After solvent removal, the poly(amic acid)-clay film was thermally treated at 300 °C to initiate imidization and create a poly(imide)-clay nanocomposite. Additional clays used in the preparation of the poly(imide)-based nanocomposites through a prepolymer intercalation in solvent technique include hectorite, saponite, and synthetic mica.[61]

Although the facile nature of the polymer or prepolymer intercalation approach is a significant advantage in the preparation of nanocomposites, the large quantities of solvent required has limited its use to small-batch syntheses and hindered its implementation in industrial settings. Consequently, the most commonly used polymer-clay nanocomposite preparation methods are melt intercalation and in situ intercalative polymerization.

1.5.3. Melt intercalation

The melt intercalation technique to prepare polymer-clay nanocomposites may be the most suitable for industrial applications as the nanocomposite formation occurs in a one-step, potentially solvent-free process. Melt intercalation is described as the blending of layered silicates with molten polymer, typically under shear, to induce intercalation or exfoliation within the polymer matrix. Nanocomposite preparation via melt intercalation has significant advantages over the other principle techniques including low or no solvent use, increased efficiency, and lower costs. Both entropic and enthalpic effects contribute to the overall thermodynamically-driven melt intercalation process. Although entropy is reduced from the confinement of polymer chains, an overall entropy increase is observed due to the increased freedom of the silicate organic modifiers such as alkylammonium cationic surfactants. The enthalpic contribution to induce polymer intercalation is much greater than the entropic contribution; therefore, the success of the melt intercalation process depends on the total enthalpic change. To favorably reduce the enthalpy of mixing, the polymer and silicate surface interactions should be maximized as high clay and polymer compatibility is crucial to successfully form nanocomposites through melt intercalation. As previously discussed, layered silicate organomodification significantly improves polymer-clay affinity; thus, proper selection of the organic modifier is critical to successfully employ melt intercalation.

Nylon 6-clay nanocomposites prepared via melt intercalation were studied by Fornes et al. to examine the impact of the organic modifier chain length,

composition, and concentration on nanocomposite morphology and physical properties.[26] By systematically varying the composition of the organic modifier, structure-property relationships were analyzed to understand the ability of organomodification to alter nanocomposite properties. Three distinct trends in the alkylammonium surfactants were associated with improvements in clay dispersion and mechanical properties: one long chain instead of two alkyl chains, replacement of hydroxy-ethyl with methyl functionalities on the amine group, and equivalent, not excessive, surfactant concentration on the clay surface. Di et al. studied the impact of hydroxy-functional organic modifiers to induce exfoliation of poly(caprolactone)-clay nanocomposites by melt intercalation.[62] Montmorillonite clays modified with a quaternary ammonium ion containing methyl tallow bis-2-hydroxyethyl aided in the exfoliation throughout the poly(caprolactone) matrix compared to modifications with a methyl dihydrogenated tallow ammonium surfactant. Several additional studies have explored the impact of the layered silicate modifiers on producing nanocomposites by melt intercalation with poly(methyl methacrylate),[63] poly(styrene),[64] poly(L-lactide),[65] poly(ethylene terephthalate),[66] rubber,[67] and polyurethanes.[68]

Apart from organomodification of layered silicates, the processing conditions of the melt intercalation technique may also dictate the extent of clay dispersion. Variables such as shear intensity, extruder design, and residence time will impact clay delamination.[69-73] Dennis et al. reported three cases where melt intercalation may lead to exfoliation of layered silicates.[69] First, high compatibility between the organic modifier and polymer may produce exfoliated

nanocomposites in almost all processing conditions. Second, when the organic modifier and polymer are somewhat compatible, optimization of the processing conditions may also produce delamination within the polymer matrix. Third, limited organic modifier and polymer compatibility cannot be overcome by melt intercalation to produce exfoliated nanocomposites. Instead, optimization of the processing conditions may only partially intercalate the polymer between the silicate layers. Compatibility between the layered silicate organic modifiers and polymeric species as well as optimized processing conditions cannot overcome the possibility of polymer or modifier thermal degradation during melt intercalation, thereby somewhat limiting the usefulness of this nanocomposite preparation method.[74-75]

1.5.4. In situ intercalative polymerization

The preparation of polymer-clay nanocomposites by in situ intercalative polymerization utilizes the increased volume associated with growing polymer chains to intercalate or exfoliate layered silicates within a polymer matrix (Figure 1.5).

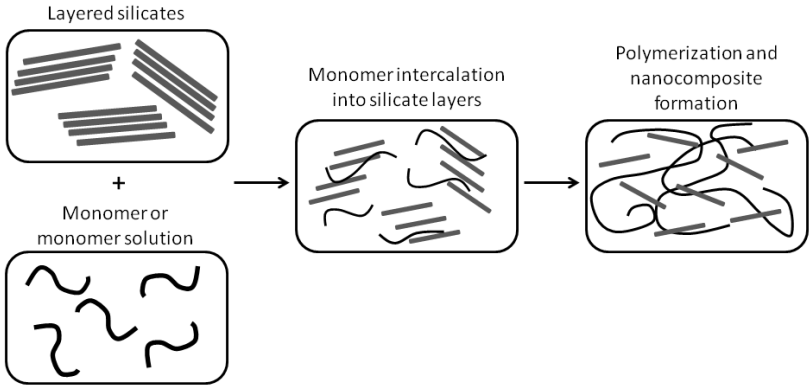

Figure 1.5: Polymer-clay nanocomposite preparation by in situ intercalative polymerization with precursor monomer and clay dispersion.

With in situ intercalative polymerizations, layered silicates are swollen in a monomer or monomer solution to intercalate the monomeric species in the silicate interlayer. Upon initiation, the polymerization reaction occurs within and surrounding the clay platelets to produce intercalated or exfoliated nanocomposite systems. In situ intercalative polymerizations are also referred to as monomer intercalation.

The first polymer-clay nanocomposite prepared by in situ intercalative polymerization was conducted by the Toyota Research group to create nylon 6 (polycaprolactam)-clay nanocomposites.[9-10, 76-77] Montmorillonite clay was first modified via an ion exchange reaction with several ω-amino acids of varying alkyl chain length, and then swollen with molten ε-caprolactam. Ring opening polymerization of the ε-caprolactam monomer was catalyzed by ω-amino acid, and the length of the alkyl chain significantly impacted monomer intercalation and the final nanocomposite morphology. Based on XRD analysis, alkyl chain lengths with fewer than eight carbons did not increase the montmorillonite basal spacing, whereas ω-amino acids containing over 11 carbons in the alkyl chain exhibited large improvements in the silicate spacing. The ω-amino acid 12-aminodedecanoic acid was ion-exchanged onto a natural Na^+-montmorillonite clay, followed by swelling with the ε-caprolactam and subsequent ring opening polymerization to produce the first nylon 6-clay nanocomposites. Several material properties significantly improved with small loadings of the modified clay (2 – 5 wt.%) in the nylon 6 matrix. Tensile strength, tensile modulus, and thermal stability all increased compared to the conventional, unfilled nylon 6 hybrid films. An additional notable

improvement with the incorporation of the modified montmorillonite was the reduction in oxygen gas permeability. With the addition of just 2 wt.% clay, the oxygen gas permeability decreased approximately 50% compared to the neat nylon 6 hybrids.

Several additional thermoplastic polymer-clay nanocomposites have been produced by in situ intercalative polymerization. Polyethylene-clay nanocomposites were prepared by Alexandre and coworkers to study the impact of the organomodification of montmorillonite and hectorite clays on morphology and mechanical properties.[78] After the modification of the clay species with trimethylaluminum-depleted methylaluminoxane and a Ti-based catalyst, the in situ intercalative polymerization of ethylene was performed in both the presence and absence of a hydrogen chain transfer agent. Nanocomposites prepared in the presence of the hydrogen transfer agent demonstrated improved tensile and shear properties as well as exfoliated morphologies. Well-exfoliated polystyrene-clay nanocomposites were produced by the in situ intercalative polymerization of styrene in the presence of montmorillonite clay functionalized with the cationic initiator 2,2'-azobis(2-methyl-*N*-(2-acetoxy-(2-*N*,*N*,*N*-tributylammonium bromide)-ethyl) propionamide (ABTBA).[79] Polystyrene-clay nanocomposites containing 1 and 3 wt.% ABTBA-modified clay had highly exfoliated morphologies, which was attributed to the successful polymerization of styrene within the clay interlayers. Once the loading increased to 5 wt.% ABTBA-modified clay, the extent of exfoliation decreased as a result of more extra-gallery polymerization. Enhancements in degradation temperature were observed up to 3 wt.% ABTBA-

modified clay. Additional thermoplastic-based nanocomposites prepared through in situ intercalative polymerization include poly(methyl methacrylate),[80-82] poly(vinyl chloride),[83-84] and poly(propylene).[85-86]

Currently, in situ intercalative polymerizations are the only viable nanocomposite preparation route to support the use of thermosetting polymers in commercial applications as melt intercalation methods cannot support the balance between intra- and extra-gallery crosslinking reactions.[87-88] Proper exfoliation of nanocomposites derived from thermosetting polymers depends on the equivalent curing reactions within and surrounding the silicate layers. When the intra- and extra-gallery curing reactions are approximately equal, the heat of curing can overcome the electrostatic interactions between silicate layers and promote exfoliation. If the extra-gallery curing reactions exceed intra-gallery curing, the thermosetting polymer or resin will gel before the curing heat can induce exfoliation within the silicate layers. The catalytic effect of organomodification, silicate structural spacing, and the compatibility between the thermosetting polymer and clay will greatly affect the degree of dispersion to create thermoset polymer-clay nanocomposites. Based on these factors, in situ intercalative polymerization is currently the only viable nanocomposite preparation method for thermosetting polymers.

Epoxy-amine polymer-clay nanocomposites prepared through in situ intercalative polymerizations have been widely studied. Several alkylammonium-exchanged clays were researched to determine the feasibility of successful epoxy monomer intercalation to produce exfoliated nanocomposites.[89] The epoxy resin, a

diglycidyl ether of bisphenol A (Epon 828), was mixed with organomodified clays, followed by the addition of one equivalent *m*-phenyldiamine as a crosslinking agent. Exfoliation was achieved when the acidic onium ions modified to the silicate layers facilitated comparable intra- and extra-gallery amine curing reactions. While the epoxy component of the nanocomposite materials provides several important material properties, the rate of curing has been found to be primarily controlled by the amine crosslinker. Several amine-functional curing agents were studied for their ability to exfoliate epoxy-based nanocomposites by Messersmith and Giannelis.[2, 90] Primary and secondary amines were shown to only produce intercalated morphologies as a consequence of the bifunctional amine crosslinking agents forming “bridge” linkages between silicate layers to only partially expand the silicate spacing. Also, the strong polarity of the N-H groups from the primary and secondary amines may have contributed to a favorable intercalated structure. Delamination observed with nadic methyl anhydride and benzyldimethylamine curing agents was attributed to the amine crosslinkers catalyzing the reactions between the hydroxy-functional organic modifiers of the silicates and the epoxy precursor. In addition to epoxy thermosetting polymers, unsaturated polyester[4, 91-92] and polyurethane[93-95] thermoset nanocomposites have been produced through in situ intercalative polymerization.

1.6. Nanocomposite properties

Dramatic improvements in material properties with the incorporation of small levels of clay loading into polymer matrices have propelled polymer-clay nanocomposite research. Pristine layered silicates possess several extraordinarily

unique characteristics and properties including moduli approaching 180 GPa, surface areas of 750 m^2/gram, and a non-toxic FDA classification.[96] While multiple enhancements in material properties are associated with nanocomposite formation, three prominent properties commonly improved with layered silicate inclusion will be discussed: mechanical performance, thermal stability, and barrier protection.

1.6.1. Mechanical performance

Tensile strength, yield strength, and modulus enhancements represent a small sampling of the mechanical property improvements observed with polymer-clay nanocomposites compared to neat polymeric systems. Currently, two prevailing theories exist regarding polymer reinforcement from silicate incorporation. The first reinforcement theory is equivalent to the reinforcement mechanism provided by conventional composite systems. Layered silicates are characteristically rigid and resistant to straining due to their high moduli. By incorporating the inorganic, higher moduli dispersed phase throughout a softer polymeric matrix, the polymer chains are reinforced mechanically due to high restraint between silicate layers.[19, 97] With adequate adhesion between the clay and polymeric species, the silicate fillers bear the majority of applied loads. Because the enhanced mechanical properties directly depend on the interfacial interactions between the clay and polymer, the high silicate surface area could produce a larger reinforcing effect. With higher surface area interactions, the addition of the nanosized silicates may more drastically improve the mechanical performance with small loading compared to conventional composite fillers.

Polymer-clay nanocomposites demonstrate a much sharper improvement in the mechanical properties than traditional composite systems with lower filler loading.

The second reinforcement theory describes the improved mechanical properties as a result higher moduli physisorbed polymer surrounding the silicate layers.[98-99] According to this theory, the layer of polymer in contact with the clay fillers will be stiffer than the bulk polymeric material, leading to improvements in mechanical performance. High affinity and adhesion between the clay and polymer are necessary for the surrounding polymer to increase in moduli. With high surface area exposure between the silicate layers and polymeric materials, the reinforcing effect of clay incorporation may be observed. Numerous studies have reported increased mechanical properties based on nanocomposite formation including increased tensile strength,[93, 100-101] modulus,[102-104] yield strength,[105-106] and toughness.[107]

To further understand the fundamental reasons for enhanced physical properties with the intercalation of organically modified clays into polymer matrices, Katti et al. have employed molecular dynamics to study the qualitative and quantitative constituents in polymer-clay nanocomposites.[108] Through molecular dynamic simulations, the total energy of the nanocomposite system, a combination of bonded and non-bonded energies, was studied. Attractive non-bonded energy interactions, or the summation of van der Waals, electrostatic, and hydrogen bonding energies, were found to increase in strength as the magnitude of the interaction decreased. The total energy of the model polymer-clay nanocomposite system was less than the summation of energies from the organically modified clay

and polymer, thus indicating the polymer-clay nanocomposite formation was more stable than an immiscible mixture of clay and polymer. Additionally, the strongest interactions occurred between the organic modifier and clay, particularly the end functional groups.

1.6.2. Thermal stability

Similar to enhancements in mechanical properties, increased thermal stability with the formation of nanocomposites has been attributed to contributions from both the inorganic clay fillers and the surrounding polymer chains. Thermal stability improvements based on nanocomposite formation was first reported by Blumstein with poly(methyl methacrylate)(PMMA)-clay nanocomposites as a result of restricted thermal motion from polymer chain confinement.[6] Interestingly, even the PMMA extracted from the clay exhibited degradation temperatures 40 – 50 °C greater than the neat PMMA films, a phenomenon Blumstein suggested was a result of fewer macromolecular species terminated with double bonds as the PMMA polymers were restricted within the silicate layers.

Traditionally, thermogravimetric analysis (TGA) has been employed to examine the thermal degradation and stability of polymer-clay nanocomposite systems in both inert and oxygen-rich atmospheres. Two popular explanations for the enhanced thermal stability associated with nanocomposite formation have been suggested.[109] First, the final nanocomposite system may act as a barrier to the degradation products, such as slowing the mass transport of volatile by-products caused from high temperature exposure, essentially acting as an insulator. Second, the dispersed inorganic phase may contribute to the formation

of char with the onset of degradation. With an increase in char formation, higher polymer-clay nanocomposite degradation temperatures may be attributed to an increase in the interaction between the organic polymer matrix and inorganic clay platelets.

1.6.3. Barrier protection

Barrier properties of polymer-clay nanocomposites are directly affected by the degree of clay dispersion and orientation of clay layers. Exceptional protection from gas and vapor molecules may be achieved as the impermeable nanoclay layers force a tortuous path of diffusion. Several models currently exist to simulate the diffusion process through nanocomposites by incorporating the impact of aspect ratio, volume fraction, and orientation among others variables.

The regular, parallel arrangement of clays within a polymer matrix is the basis of many permeability models for polymer-clay nanocomposites. Beginning work regarding permeability modeling was reported by Barrer and Petropoulos.[110] This study examined the diffusion in a heterogeneous media with a lattice of regular parallelepipeds of a different diffusion coefficient. The aspects of particle shape and orientation were included in this model. An average diffusion coefficient may be produced using equation (1.3), where D_B is the regular permeability of the parallelepiped, and a and b are the length and width of the cross section. Equation (1.3) dictates that the average diffusion coefficient is dependent upon the fractional cross section of the parallelepiped and the tortuosity of the diffusant path.

$$\overline{D} = D_B b(2a + b)\gamma'{\beta'}_B/(a + b)^2 \qquad (1.3)$$

Nielsen famously proposed a simple permeability model for the regular arrangement of plate-like shaped particles with a finite width and thickness but infinite length.[111] The schematic representation of the Nielsen permeability model is illustrated in Figure 1.6, where width is L and thickness is W. The orientation of the regular plate-like particles is directly perpendicular to the diffusion direction but does not account for the morphology of the distinct nanocomposite phases.

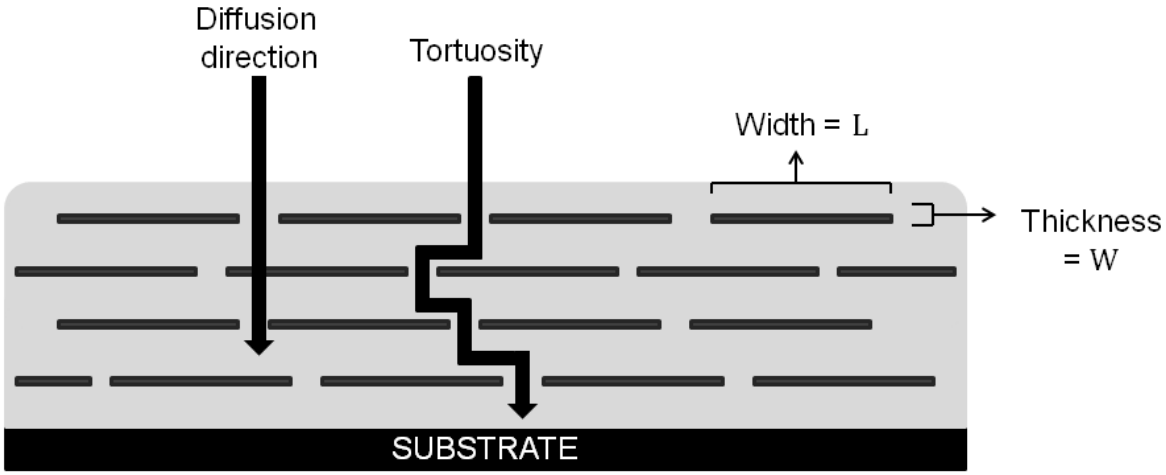

Figure 1.6: Schematic representation of Nielsen polymer-clay nanocomposite permeability model.[111]

The tortuosity factor (τ), calculated from equation (1.4), depends on the nanoplatelet aspect ratio, shape, and orientation where l represents the thickness of sample and l' is the prolonged diffusion path due to impermeable clay fillers

$$\tau = l'/l \tag{1.4}$$

Nielsen's model for nanocomposite permeability depends on the volume fraction of nanoplatelets ϕ and their aspect ratio fillers α (filler length/width). Assuming that each nanoplatelet contributes to prolonging the diffusion length by $L/2$ and the mean number of nanoplatelets encountered by the diffusant is <N> = $L\phi/W$, the permeability through a nanocomposite is determined by equation (1.5).

$$\frac{K_{COMPOSITE}}{K_{MATRIX}} = \frac{1-\phi}{1+\frac{\alpha}{2}\phi} \tag{1.5}$$

From equation (1.5), a decrease in permeability will be observed with an increase in α and ϕ. This result may not be applicable to systems where the $\phi \geq 10\%$ as the nanoplatelets will tend to agglomerate instead of dispersing uniformly throughout the polymer matrix.

Bharadwaj expanded upon Nielsen's model to account for random orientation of nanoclay layers within the polymer matrix.[112] An orientation factor S is used in the model, and is defined in equation (1.6) where θ describes the angle between the preferred direction orientation and the nanoplatelet sheet.

$$S = \frac{1}{2}\left\langle 3\cos^2\theta - 1 \right\rangle \tag{1.6}$$

The orientation factor S can vary from 1 to -0.5. When the S factor is exactly 1, perfect parallel orientation of the nanoplatelet to the surface exists. The S factor can also be 0, indicating random orientation of nanoplatelets within the polymer matrix. The third possible S factor is -0.5 and represents the nanoclay platelets are perfectly perpendicular to the surface. The model for permeability described by Bharadwaj is displayed in equation (1.7).

$$\frac{K_{COMPOSITE}}{K_{MATRIX}} = \frac{1-\phi}{1+\alpha\phi\frac{2}{3}(S+\frac{1}{2})} \quad . \tag{1.7}$$

Bharadwaj's model includes clay volume fraction and aspect ratio as well as the orientation factor. If the orientation factor S is 1, the model reduces to the Nielsen model, equation (1.5). The permeability models described relate the diffusion of gas and vapor molecules through a polymer matrix containing nanoclay

particles. The main factors affecting the permeability through nanocomposites are dependent on the nanoclay volume fraction, dispersion, and orientation. Additional permeability models include parameters for non-platelet like particles such as disks. Manias conducted a review of current tortuosity based permeability models to predict the consequences of morphology on diffusion.[113] This study determined that an exfoliated montmorillonite, with aspect ratio of approximately 500, at volume fraction loading of 2% had comparable permeability with a partially-exfoliated montmorillonite at volume fraction loading of 3% and mostly-intercalated montmorillonite at volume fraction loading of 5%. The implication from this portion of the study is that exfoliated nanocomposites utilize lower volume fractions of nanoclay to produce comparable permeability results to intercalated states. Polycaprolactone/montmorillonite nanocomposites were studied by Gorrasi et al. to examine the effect of nanoclay dispersion on vapor diffusion.[114] Intercalated nanocomposites were prepared via melt blending, whereas exfoliated nanocomposites were prepared by an in situ intercalative polymerization. Microcomposites were also prepared as a point of reference. This study found diffusion parameters for the microcomposites and intercalated nanocomposites very comparable to the neat polycaprolactone. Exfoliated nanocomposites produced much lower diffusion values.

The aggregation of inorganic silicates decreases permeation properties of the nanocomposite due to an increased presence of pores in the matrix.[115] When the nanoclay layers agglomerate, gas and vapor molecules encounter less resistance through the matrix, and therefore have a lower resistance to reach a

substrate. Nazarenko et al. modified Nielsen's model of permeability to account for the number of nanoclay layers.[116] Incorporating the nanoclay layers parameter and the orientation into a permeability model, equation (1.8) may be applied, where N represents the number of nanoclay layers.

$$\frac{K_{COMPOSITE}}{K_{MATRIX}} = \frac{1-\phi}{1+\frac{\alpha}{3N}(S'+\frac{1}{2})\phi} \tag{1.8}$$

Permeation of gases through polymer-clay nanocomposites may be directly measured using a permeability cell. The typical set-up for a permeability cell includes a nanocomposite membrane separating the cell into two compartments. One compartment of the permeability cell has a constant pressure applied to the membrane. The flux density is measured in the second compartment. Once the concentration of gas in the nanocomposite reaches a steady distribution, a steady state flux of the system is reached. This steady state flux density will depend on the nanocomposite membrane thickness and pressure applied in the initial chamber. The equation relating the steady state flux is given in equation (1.9) where the steady state flux is J_∞, the permeability coefficient is *K*, the nanocomposite membrane thickness is *d*, and the constant pressure is P_0.

$$J_\infty = K\frac{P_0}{d} \tag{1.9}$$

Another use of the permeability cell for direct gaseous diffusion measurement is to apply two constant pressures in each chamber. The first chamber will be set at a constant pressure greater than the constant pressure of the second pressure. The pressure will be measured over time to observe any

diffusion through the nanocomposite membrane. When the gas present permeates through the membrane, the first chamber's pressure will fall whereas the second chamber will experience an increase in pressure. Nanocomposites permitting extremely low gaseous diffusion will not see any recordable changes in the constant pressures.

The permeability cells may also be supplemented with the addition of a mass spectrometer to track gaseous diffusion. The first chamber will consist of a test gas or gases, such as carbon dioxide, and the second chamber will be fed with a pure, reference gas, such as nitrogen. The chambers will both be subjected to the same constant pressure. As the experiment continues, the second chamber will also contain any test gas that has permeated through the nanocomposite membrane. The test gas and reference gas of the second chamber are then fed to a mass spectrometer to analyze the amount of test gas present. This permeability cell test is referred to as the Wicke-Kallenbach device.[117]

The diffusion of gas and vapor molecules through a nanocomposite consists of distinct stages: the sorption of gas or vapor onto the surface, the dissolution through the surface, the diffusion through the nanocomposite, and desorption of the opposite side of the surface. The sorption and desorption measurements are considered an indirect measure of permeability. The basis for these indirect experiments is the measurement of gas or vapor molecule mass uptake. Typically, sorption experiments involve a nanocomposite membrane subjected to vacuum pressure while a constant gas or vapor pressure is applied. Gaseous vapors will be dissolved, and the dissolved gases or vapor molecules will then diffuse through the

nanocomposite membrane over time. The mass uptake is measured by periodic weighing of the nanocomposite. For these measurements, fractional mass uptake is measured as a function of time. This fractional permeability assessment may be approximated by equation (1.10) where M_t and M_∞ represent the mass uptake at times *t* and ∞ , and d is the thickness of the nanocomposite membrane.

$$\frac{M_t}{M_\infty} = \frac{8}{\pi^{1/2}}\left(\frac{Dt}{d^2}\right)^{1/2} \tag{1.10}$$

The diffusion coefficient *D* is calculated by plotting the fractional permeability mass uptake as a function of time and thickness. The slope of this diagram will produce the diffusion coefficient. Conversely, at long convergence times, the fractional permeability mass uptake is determined by equation (1.11). The diffusion coefficient of the nanocomposite may be determined by plotting the right side of the equation as a function of time.

$$\ln(1-\frac{M_t}{M_\infty}) = \ln(\frac{8}{\pi^2}) - \frac{\pi^2 Dt}{d^2} \tag{1.11}$$

An additional method of vapor diffusion can be determined following ASTM E 96. This ASTM is a test method describing the vapor diffusion through membranes. The nanocomposite sample is securely fastened to a container of distilled water. The container is placed in a controlled atmosphere and routinely measured to determine the amount of water that has diffused through the nanocomposite and evaporated.

Multiple applications for high-barrier nanocomposites exist in the coatings industry. When gas and vapor molecules diffuse through a coating to the substrate,

degradation and corrosion may occur. This corrosive behavior greatly shortens the life of many substrates, and therefore increases the cost of production. The following applications require extremely low permeability of nanocomposites to maintain the substrate for which the nanocomposite coating protects.

Electronic devices processed on flexible substrates have seen increased popularity due to decreased device weight and easier production at lower cost while maintaining their electrical conductivity.[118] The performance of the flexible devices greatly depends on the performance of the optical and electrical properties of the system. Polymer-clay nanocomposites have been utilized as a protective coating for these electronic applications to prevent the diffusion of gas and vapor molecules. The inorganic nanoclays are embedded into the encapsulating material of the coating to produce a tortuous diffusion path. Nanoclay use is advantageous as the fillers do not interfere with the electronic properties of the device.[119]

Currently, most materials used in the food industry for packaging are undegradable. New bio-based materials have entered the market, but these systems have demonstrated poor protection from gas and vapor diffusion that leads to food spoilage. The addition of nanoclays to bio-based materials for food packaging has received attention to not only decrease permeability, but decrease brittleness and cost.[120] Polymer/clay nanocomposite packaging systems also protect unwanted aromas and unusual flavors from interacting with the food.[121] However, it is also important to study the safety of using nanoclays for packaged food applications in terms of the environment and personal health. An additional application of low permeability polymer/clay nanocomposites is the protection of

storage tanks. The incorporation of nanoclays to the polymer coating system has drastically reduced the permeability of gases while greatly decreasing the tank weight.[122] Additionally, nanocomposite formation decreased microcracking of tanks due to stress but maintained high strength and barrier protection compared to the corresponding neat polymer resin.

1.7. UV-curable nanocomposites

In stark contrast to thermally-induced curing of polymer-clay nanocomposites, ultraviolent (UV)-induced cure of nanocomposite coatings relies on cross-linking initiated by radiation as opposed to heat. The implementation of UV-curing mechanisms to polymer-clay nanocomposite technology offers several significant advantages including ambient temperature cure, rapid cross-linking, direct contact to heat-sensitive substrates, and low or zero volatile organic compounds (VOC) used during nanocomposite formation.[123] The utilization of UV-curing technologies to produce UV-curable polymer-clay nanocomposites couples the advantageous properties of the UV-curing mechanism with nanocomposite formation to create high performance materials.

1.7.1. UV-curing mechanism

Two mechanisms for UV-curing are widely employed to induce polymerization: free radical and cationic. Free radical photopolymerization describes the polymerization of vinyl double bonds from a photogenerated free radical, whereas cationic-initiated photopolymerization produces ring-opening polymerization reactions by the propagation of a cationic species upon UV-

irradiation. Scheme 1.1 depicts an illustration of free radical and cationic UV-curing.

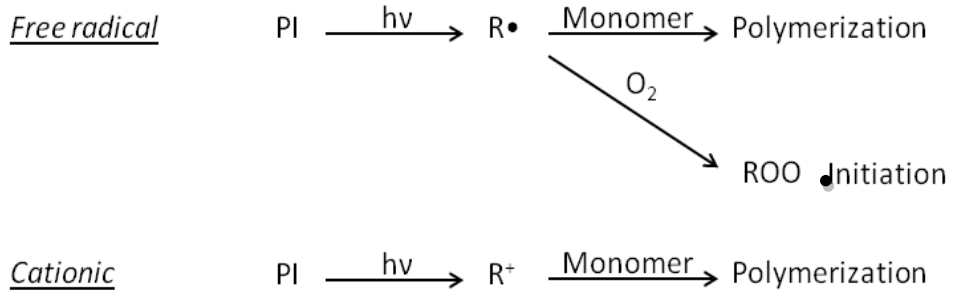

Scheme 1.1: Free radical and cationic UV-curing mechanisms.

The first step in free radical photopolymerization is the generation of a free radical from a UV-source. Commonly, the UV source may stem from an electrode lamp, an electrodeless lamp (powered by microwaves), or an excimer lamp. Once the photoinitator is excited, the free radical-bearing species will initiate polymerization by reacting with a vinyl bond-containing monomer, and subsequent monomer addition will lead to propagation. Cationic photopolymerization undergoes a similar polymerization mechanism, but the UV source photogenerates a cationic species for initiation and subsequent polymer propagation.

Each UV-curing mechanism has characteristic advantages and disadvantages. Free radical photopolymerization may be applied to a wider variety of monomer precursors. Several functionalities may be incorporated into the polymer backbone by employing vinyl-functional monomers. However, oxygen inhibition may hinder polymer formation and limits the usefulness of free radical UV-curing. Oxygen may react with the propagating chain bearing a free radical to create a peroxy radical and eventually terminates polymerization. Additionally, oxygen quenches the excited state of some photoinitiators, significantly reducing

polymer chain growth. Unlike the free radical UV-curing mechanism, cationic photopolymerization does not succumb to oxygen inhibition. The monomeric precursors used in cationic UV-curing tend to be less irritating than the free radical precursors, particularly acrylate-functional compounds. Cationic photopolymerization is limited by exposure to high humidity environments as water readily reacts with the cationic intermediate.

1.7.2. Nanocomposites from UV-curable polymers

UV-curable polymer-clay nanocomposites couple the advantageous properties associated with UV-curing with nanocomposite formation. UV-curable nanocomposites were first reported by Zahouily, Decker, and coworkers in the early 2000s.[124-125] Polyurethane-acrylate nanocomposites containing bentonite clay cured by UV-irradiation demonstrated over 95% conversion as determined by real-time infrared (RTIR) spectroscopy.[126] The morphological state of the UV-curable nanocomposites was classified as exfoliated by XRD analysis as no diffraction peaks were observed in the 2 – 9 2θ range. Multifunctional acrylic resins were also utilized to create polymer-clay nanocomposites at various levels of clay loading.[127] Modification of the clays with alkylammonium cations increased affinity with the acrylic precursor resin and contributed to high clay dispersion throughout the polymer matrix. The resulting nanocomposites demonstrated superior mechanical performance and barrier protection compared to both an unfilled acrylic resin and an acrylic microcomposite system. Subsequently, Decker et al. studied the formation of nanocomposites by both free radical and cationic UV-curing using both acrylate- and epoxy-functional oligomeric precursors.[128] The epoxy-based

nanocomposites experienced more drastic improvements in the viscoelastic properties than the acrylate-based systems, but both nanocomposites demonstrated high solvent and moisture resistance compared to an unfilled system. Uhl and coworkers researched the impact of organically modified montmorillonite clays on acrylate polymers bearing both urethane and epoxy functionalities to create UV-curable nanocomposites.[129-131] Overall, significant enhancements in thermal and mechanical properties were observed with the formation of nanocomposite systems derived from UV-curable polymers.

1.8. Summary

Polymer-clay nanocomposites are widely reported to drastically improve material properties due to the interfacial interactions between the polymeric matrix and dispersed clay fillers. The low cost and high accessibility of clays, particularly 2:1 phyllosilicates, contribute to the growing popularity of nanocomposite research. To overcome the inherent incompatibility between the inorganic clay species and organic polymer resins, organomodification of clay surface is performed to improve polymer-clay affinity and functionalize the clay platelets. Three morphological states arise based on the degree of clay dispersion throughout the polymer matrix with an exfoliated morphology representing the highest degree of polymer and clay surface area interaction. Four main processing routes have been established to produce polymer-clay nanocomposites. Of these processes, melt intercalation and in situ intercalative polymerization may currently be applied to industrial applications, and only in situ intercalative polymerizations may incorporate thermosetting polymers. After nanocomposite preparation, several material

properties have been reported to increase including mechanical strength, thermal stability, and barrier protection. Recently, high performance UV-curable nanocomposites have been researched as viable alternatives to thermally-initiated nanocomposite systems. By coupling the advantageous properties of nanocomposite formation with the low heat, high conversion of UV-curable polymers, a new class of nanocomposites is created with superior properties for a multitude of applications including protection of flexible electronics and food and beverage packaging.

1.9. Research scope and purpose

The purpose of this research was to develop high performance barrier coatings from novel hybrid polymeric materials. Preparation of nanocomposites was performed using in situ intercalative polymerization techniques with a focus of creating exfoliated morphologies. Two novel in situ preparation techniques were explored to develop UV-curable unsaturated polyester precursor resins containing highly dispersed organically-modified montmorillonite clays. The impact of clay loading, organic modification, and clay dispersion technique on the morphological and physical properties of the resulting UV-curable nanocomposites was the primary focus of this research. The unsaturated polyesters containing the dispersed montmorillonite clays were characterized using gel permeation chromatography (GPC), differential scanning calorimetry (DSC), ^{1}H nuclear magnetic resonance (NMR) spectroscopy, and cone and plate viscometry. Nanocomposite morphology was characterized through the complimentary techniques of XRD and TEM. Barrier protection from silicate incorporation was

determined by measuring both water vapor and oxygen gas permeation through the nanocomposite films. Mechanical, thermal, and optical properties were also explored to determine the impact of clay dispersion, loading, and processing route on the nanocomposite physical properties.

1.10. References

1. Mallick, P. K., *Fiber-reinforced composites: materials, manufacturing, and design*. CRC Press: 1993; Vol. 83.

2. Messersmith, P. B.; Giannelis, E. P., *Chemistry of Materials* **1994,** *6* (10), 1719-1725.

3. Thostenson, E. T.; Li, C.; Chou, T. W., *Composites Science and Technology* **2005,** *65* (3-4), 491-516.

4. Bharadwaj, R. K.; Mehrabi, A. R.; Hamilton, C.; Trujillo, C.; Murga, M.; Fan, R.; Chavira, A.; Thompson, A. K., *Polymer* **2002,** *43* (13), 3699-3705.

5. Bower, C. A., *Studies on the forms and availability of soil organic phosphorus*. Agricultural Experiment Station, Iowa State College of Agriculture and Mechanic Arts: 1949; Vol. 362.

6. Blumstein, A., *Journal of Polymer Science Part A: General Papers* **1965,** *3* (7), 2653-2664.

7. Blumstein, A., *Journal of Polymer Science Part A: General Papers* **1964,** *3* (7), 2653-2664.

8. Theng, B. K. G., *Formation and properties of clay-polymer complexes*. Elsevier: 1979; Vol. 9.

9. Usuki, A.; Kawasumi, M.; Kojima, Y.; Okada, A.; Kurauchi, T.; Kamigaito, O., *Journal of Materials Research* **1993,** *8* (5), 1174–1178.

10. Usuki, A.; Kojima, Y.; Kawasumi, M.; Okada, A.; Fukushima, Y.; Kurauchi, T.; Kamigaito, O., *Journal of Materials Research* **1993,** *8* (05), 1179-1184.

11. Sorrentino, A.; Gorrasi, G.; Vittoria, V., *Trends in Food Science & Technology* **2007,** *18* (2), 84-95.

12. Hussain, F.; Hojjati, M.; Okamoto, M.; Gorga, R. E., *Journal of Composite Materials* **2006,** *40* (17), 1511.

13. Laoutid, F.; Bonnaud, L.; Alexandre, M.; Lopez-Cuesta, J. M.; Dubois, P., *Materials Science and Engineering: R: Reports* **2009,** *63* (3), 100-125.

14. Drits, V., *Clay Minerals* **2003,** *38* (4), 403.

15. Moll Jr, W. F., *Clays and Clay Minerals* **2001,** *49* (5), 374.

16. Kamena, K., *Functional fillers for plastics* **2005**, 163-174.

17. Odom, I., *Philosophical Transactions of the Royal Society of London. Series A, Mathematical and Physical Sciences* **1984,** *311* (1517), 391.

18. Alexandre, M.; Dubois, P., *Materials Science and Engineering: R: Reports* **2000,** *28* (1-2), 1-63.

19. Pavlidou, S.; Papaspyrides, C., *Progress in Polymer Science* **2008,** *33* (12), 1119-1198.

20. Krishnamoorti, R.; Giannelis, E. P., *Macromolecules* **1997,** *30* (14), 4097-4102.

21. Dong, Y.; Bhattacharyya, D., *Composites Part A: Applied Science and Manufacturing* **2008,** *39* (7), 1177-1191.

22. Ploehn, H. J.; Liu, C., *Industrial & Engineering Chemistry Research* **2006,** *45* (21), 7025-7034.

23. Chang, J. H.; Jang, T. G.; Ihn, K. J.; Lee, W. K.; Sur, G. S., *Journal of Applied Polymer Science* **2003,** *90* (12), 3208-3214.

24. Zhou, C. H., *Applied Clay Science* **2011,** *53* (2), 87-96.

25. Xidas, P. I.; Triantafyllidis, K. S., *European Polymer Journal* **2010,** *46* (3), 404-417.

26. Fornes, T. D.; Hunter, D. L.; Paul, D. R., *Macromolecules* **2004,** *37* (5), 1793-1798.

27. Kim, Y.; White, J. L., *Journal of Applied Polymer Science* **2005,** *96* (5), 1888-1896.

28. Fan, X.; Xia, C.; Fulghum, T.; Park, M.-K.; Locklin, J.; Advincula, R. C., *Langmuir* **2002,** *19* (3), 916-923.

29. Fan, X.; Xia, C.; Advincula, R. C., *Langmuir* **2003,** *19* (10), 4381-4389.

30. Mansoori, Y.; Atghia, S.; Zamanloo, M.; Gh, I.; Sirousazar, M., *European Polymer Journal* **2010,** *46* (9), 1844-1853.

31. Nese, A.; Sen, S.; Tasdelen, M. A.; Nugay, N.; Yagci, Y., *Macromolecular Chemistry and Physics* **2006,** *207* (9), 820-826.

32. Qin, X.; Wu, Y.; Wang, K.; Tan, H.; Nie, J., *Applied Clay Science* **2009,** *45* (3), 133-138.

33. Tan, H.; Nie, J., *Journal of Applied Polymer Science* **2007,** *106* (4), 2656-2660.

34. Tan, H.; Yang, D.; Han, J.; Xiao, M.; Nie, J., *Applied Clay Science* **2008,** *42* (1-2), 25-31.

35. Zhao, H.; Farrell, B. P.; Shipp, D. A., *Polymer* **2004,** *45* (13), 4473-4481.

36. Yang, Y.; Wu, D.; Li, C.; Liu, L.; Cheng, X.; Zhao, H., *Polymer* **2006,** *47* (21), 7374-7381.

37. Bharathwaj, R.; Natarajan, U.; Dhamodharan, R., *Applied Clay Science* **2010,** *48* (3), 300-306.

38. Djouani, F.; Herbst, F.; Chehimi, M. M.; Benzarti, K., *Construction and Building Materials* **2011,** *25* (2), 424-431.

39. Weimer, M. W.; Chen, H.; Giannelis, E. P.; Sogah, D. Y., *Journal of the American Chemical Society* **1999,** *121* (7), 1615-1616.

40. Ghannam, L.; Parvole, J.; Laruelle, G.; Francois, J.; Billon, L., *Polymer International* **2006,** *55* (10), 1199-1207.

41. Konn, C.; Morel, F.; Beyou, E.; Chaumont, P.; Bourgeat-Lami, E., *Macromolecules* **2007,** *40* (21), 7464-7472.

42. Salem, N.; Shipp, D. A., *Polymer* **2005,** *46* (19), 8573-8581.

43. Samakande, A.; Sanderson, R. D.; Hartmann, P. C., *European Polymer Journal* **2009,** *45* (3), 649-657.

44. Samakande, A.; Juodaityte, J. J.; Sanderson, R. D.; Hartmann, P. C., *Macromolecular Materials and Engineering* **2008,** *293* (5), 428-437.

45. Samakande, A.; Sanderson, R. D.; Hartmann, P. C., *Polymer* **2009,** *50* (1), 42-49.

46. Balazs, A. C.; Singh, C.; Zhulina, E.; Lyatskaya, Y., *Accounts of Chemical Research* **1999,** *32* (8), 651-657.

47. Zunjarrao, S.; Sriraman, R.; Singh, R., *Journal of Materials Science* **2006,** *41* (8), 2219-2228.

48. Dasari, A.; Yu, Z. Z.; Mai, Y. W.; Hu, G. H.; Varlet, J., *Composites Science and Technology* **2005,** *65* (15-16), 2314-2328.

49. Morgan, A. B.; Gilman, J. W., *Journal of Applied Polymer Science* **2003,** *87* (8), 1329-1338.

50. Vaia, R. A.; Weathers, M. S.; Bassett, W. A., *Powder Diffraction* **1994,** *9*, 44.

51. Lagaly, G., *Applied Clay Science* **1999,** *15* (1-2), 1-9.

52. Wilson Jr, O.; Olorunyolemi, T.; Jaworski, A.; Borum, L.; Young, D.; Siriwat, A.; Dickens, E.; Oriakhi, C.; Lerner, M., *Applied Clay Science* **1999,** *15* (1-2), 265-279.

53. Boulet, P.; Bowden, A. A.; Coveney, P. V.; Whiting, A., *Journal of Materials Chemistry* **2003,** *13* (10), 2540-2550.

54. Ogata, N.; Kawakage, S.; Ogihara, T., *Journal of Applied Polymer Science* **1997,** *66* (3), 573-581.

55. Levy, R.; Francis, C., *Journal of Colloid and Interface Science* **1975,** *50* (3), 442-450.

56. Komori, Y.; Sugahara, Y.; Kuroda, K., *Chemistry of Materials* **1998,** *11* (1), 3-6.

57. Billingham, J.; Breen, C.; Yarwood, J., *Vibrational Spectroscopy* **1997,** *14* (1), 19-34.

58. Filippi, S.; Mameli, E.; Marazzato, C.; Magagnini, P., *European Polymer Journal* **2007,** *43* (5), 1645-1659.

59. Zhao, X.; Urano, K.; Ogasawara, S., *Colloid and Polymer Science* **1989,** *267*, 899-906.

60. Yano, K.; Usuki, A.; Okada, A.; Kurauchi, T.; Kamigaito, O., *Journal of Polymer Science Part A: Polymer Chemistry* **1993,** *31* (10), 2493-2498.

61. Yano, K.; Usuki, A.; Okada, A., *Journal of Polymer Science Part A: Polymer Chemistry* **1997,** *35* (11), 2289-2294.

62. Di, Y.; Iannace, S.; Di Maio, E.; Nicolais, L., *Journal of Polymer Science Part B: Polymer Physics* **2003,** *41* (7), 670-678.

63. Ratinac, K. R.; Gilbert, R. G.; Ye, L.; Jones, A. S.; Ringer, S. P., *Polymer* **2006,** *47* (18), 6337-6361.

64. Yoon, J.; Jo, W.; Lee, M.; Ko, M., *Polymer* **2001,** *42* (1), 329-336.

65. Paul, M.-A.; Alexandre, M.; Degée, P.; Henrist, C.; Rulmont, A.; Dubois, P., *Polymer* **2003,** *44* (2), 443-450.

66. Calcagno, C. I. W.; Mariani, C. M.; Teixeira, S. R.; Mauler, R. S., *Polymer* **2007,** *48* (4), 966-974.

67. Samadi, A.; Razzaghi Kashani, M., *Journal of Applied Polymer Science* **2010,** *116* (4), 2101-2109.

68. Barick, A. K.; Tripathy, D. K., *Journal of Applied Polymer Science* **2010,** *117* (2), 639-654.

69. Dennis, H. R.; Hunter, D. L.; Chang, D.; Kim, S.; White, J. L.; Cho, J. W.; Paul, D. R., *Polymer* **2001,** *42* (23), 9513-9522.

70. Lertwimolnun, W.; Vergnes, B., *Polymer Engineering & Science* **2006,** *46* (3), 314-323.

71. Modesti, M.; Lorenzetti, A.; Bon, D.; Besco, S., *Polymer* **2005,** *46* (23), 10237-10245.

72. Lertwimolnun, W.; Vergnes, B., *Polymer* **2005,** *46* (10), 3462-3471.

73. Tanoue, S.; Utracki, L. A.; Garcia Rejon, A.; Tatibouet, J.; Cole, K. C.; Kamal, M. R., *Polymer Engineering & Science* **2004,** *44* (6), 1046-1060.

74. Xie, W.; Gao, Z.; Liu, K.; Pan, W. P.; Vaia, R.; Hunter, D.; Singh, A., *Thermochimica Acta* **2001,** *367*, 339-350.

75. Davis, R. D.; Gilman, J. W.; VanderHart, D. L., *Polymer Degradation and Stability* **2003,** *79* (1), 111-121.

76. Kojima, Y.; Usuki, A.; Kawasumi, M.; Okada, A.; Kurauchi, T.; Kamigaito, O., *Journal of Polymer Science Part A: Polymer Chemistry* **1993,** *31* (7), 1755-1758.

77. Usuki, A.; Kojima, Y.; Kawasumi, M.; Okada, A.; Fukushima, Y.; Kurauchi, T.; Kamigaito, O., *Journal of Materials Research* **1993,** *8* (5), 1185-1189.

78. Alexandre, M.; Dubois, P.; Sun, T.; Garces, J. M.; Jér me, R., *Polymer* **2002,** *43* (8), 2123-2132.

79. Uthirakumar, P.; Nahm, K. S.; Hahn, Y. B.; Lee, Y.-S., *European Polymer Journal* **2004,** *40* (11), 2437-2444.

80. Zhu, J.; Start, P.; Mauritz, K. A.; Wilkie, C. A., *Polymer Degradation and Stability* **2002,** *77* (2), 253-258.

81. Okamoto, M.; Morita, S.; Taguchi, H.; Kim, Y. H.; Kotaka, T.; Tateyama, H., *Polymer* **2000,** *41* (10), 3887-3890.

82. Wei'an, Z.; Yu, L.; Luo, W.; Yue'e, F., *Materials Letters* **2003,** *57* (22-23), 3366-3370.

83. Gong, F.; Feng, M.; Zhao, C.; Zhang, S.; Yang, M., *Polymer Degradation and Stability* **2004,** *84* (2), 289-294.

84. Haiyan, H.; Mingwang, P.; Xiucuo, L.; Xudong, S.; Liucheng, Z., *Polymer International* **2004,** *53* (2), 225-231.

85. He, A.; Hu, H.; Huang, Y.; Dong, J. Y.; Han, C. C., *Macromolecular Rapid Communications* **2004,** *25* (24), 2008-2013.

86. He, A.; Wang, L.; Li, J.; Dong, J.; Han, C. C., *Polymer* **2006,** *47* (6), 1767-1771.

87. Lan, T.; Pinnavaia, T. J., *Chemistry of Materials* **1994,** *6* (12), 2216-2219.

88. Becker, O.; Varley, R.; Simon, G., *Polymer* **2002,** *43* (16), 4365-4373.

89. Lan, T.; Kaviratna, P. D.; Pinnavaia, T. J., *Chemistry of Materials* **1995,** *7* (11), 2144-2150.

90. Giannelis, E. P.; Messersmith, P. B., Method of preparing layered silicate-epoxy nanocomposites. Google Patents: 1996.

91. Kornmann, X.; Berglund, L. A.; Sterte, J.; Giannelis, E., *Polymer Engineering & Science* **1998,** *38* (8), 1351-1358.

92. Suh, D.; Lim, Y.; Park, O., *Polymer* **2000,** *41* (24), 8557-8563.

93. Yao, K.; Song, M.; Hourston, D.; Luo, D., *Polymer* **2002,** *43* (3), 1017-1020.

94. Zilg, C.; Thomann, R.; Mülhaupt, R.; Finter, J., *Advanced Materials* **1999,** *11* (1), 49-52.

95. Cao, X.; James Lee, L.; Widya, T.; Macosko, C., *Polymer* **2005,** *46* (3), 775-783.

96. Beall, G. W.; Powell, C. E., *Fundamentals of polymer-clay nanocomposites*. Cambridge University Press: New York, 2010.

97. Fornes, T.; Paul, D., *Polymer* **2003,** *44* (17), 4993-5013.

98. Takeuchi, H.; Cohen, C., *Macromolecules* **1999,** *32* (20), 6792-6799.

99. Huang, J. C.; Zhu, Z.; Yin, J.; Qian, X.; Sun, Y. Y., *Polymer* **2001,** *42* (3), 873-877.

100. Chen, T. K.; Tien, Y. I.; Wei, K. H., *Polymer* **2000,** *41* (4), 1345-1353.

101. Cho, J.; Paul, D., *Polymer* **2001,** *42* (3), 1083-1094.

102. Liu, X.; Wu, Q., *Polymer* **2001,** *42* (25), 10013-10019.

103. Fu, X.; Qutubuddin, S., *Polymer* **2001,** *42* (2), 807-813.

104. Luo, J.-J.; Daniel, I. M., *Composites Science and Technology* **2003,** *63* (11), 1607-1616.

105. Fornes, T. D.; Yoon, P. J.; Keskkula, H.; Paul, D. R., *Polymer* **2001,** *42* (25), 09929-09940.

106. Shi, H.; Lan, T.; Pinnavaia, T. J., *Chemistry of Materials.* **1996,** *8* (8), 1584-1587.

107. Zhang, M.; Sundararaj, U., *Macromolecular Materials and Engineering* **2006,** *291* (6), 697-706.

108. Sikdar, D.; Katti, D. R.; Katti, K. S.; Bhowmik, R., *Polymer* **2006,** *47* (14), 5196-5205.

109. Gilman, J. W., *Applied Clay Science* **1999,** *15* (1-2), 31-49.

110. Barrer, R.; Petropoulos, J., *British Journal of Applied Physics* **1961,** *12*, 691.

111. Nielsen, L. E., *Journal of Macromolecular Science, Part A* **1967,** *1* (5), 929-942.

112. Bharadwaj, R. K., *Macromolecules* **2001,** *34* (26), 9189-9192.

113. Manias, E.; Polizos, G.; Nakajima, H.; Heidecker, M. J., Fundamentals of Polymer Nanocomposite Technology. In *Flame Retardant Polymer Nanocomposites*, John Wiley & Sons, Inc.: 2006; pp 31-66.

114. Gorrasi, G.; Tortora, M.; Vittoria, V.; Pollet, E.; Lepoittevin, B.; Alexandre, M.; Dubois, P., *Polymer* **2003,** *44* (8), 2271-2279.

115. Choudalakis, G.; Gotsis, A. D., *European Polymer Journal* **2009,** *45* (4), 967-984.

116. Nazarenko, S.; Meneghetti, P.; Julmon, P.; Olson, B. G.; Qutubuddin, S., *Journal of Polymer Science Part B: Polymer Physics* **2007,** *45* (13), 1733-1753.

117. Hiltner, A.; Liu, R.; Hu, Y.; Baer, E., *Journal of Polymer Science Part B: Polymer Physics* **2005,** *43* (9), 1047-1063.

118. Hamers, R. J., *Nature* **2001,** *412* (6846), 489-490.

119. Logothetidis, S., *Materials Science and Engineering: B* **2008,** *152* (1-3), 96-104.

120. Azeredo, H., *Food Research International* **2009,** *42* (9), 1240-1253.

121. Pereira de Abreu, D.; Paseiro Losada, P.; Angulo, I.; Cruz, J., *European Polymer Journal* **2007,** *43* (6), 2229-2243.

122. Miller, S.; Meador, M. In *Polymer-Layered Silicate Nanocomposites for Cryotank Applications*, 48th AIAA/ASME/ASCE/AHS/ASC Structures, Structural Dynamics, and Materials Conference, Honolulu, Hawaii, Honolulu, Hawaii.

123. Wicks, Z. W., *Organic coatings: science and technology*. Wiley-Interscience: 2007; Vol. 33.

124. Zahouily, K. B., S.; Bendaikha, T.; Baron, J.; and Decker, C. RadTech Eur, 2001; p 583.

125. Zahouily, K. D., C.; Benfarhi, S.; and Baron, J. Radtech: The Premier UV/EB Conference and Exhibition, Indiannapolis, IN, April 28 - May 1; Indiannapolis, IN, 2002; pp 309-320.

126. Decker, C.; Zahouily, K.; Keller, L.; Benfarhi, S.; Bendaikha, T.; Baron, J., *Journal of Materials Science* **2002,** *37* (22), 4831-4838.

127. Keller, L.; Decker, C.; Zahouily, K.; Benfarhi, S.; Le Meins, J. M.; Miehe-Brendle, J., *Polymer* **2004,** *45* (22), 7437-7447.

128. Decker, C.; Keller, L.; Zahouily, K.; Benfarhi, S., *Polymer* **2005,** *46* (17), 6640-6648.

129. Uhl, F. M.; Davuluri, S. P.; Wong, S.-C.; Webster, D. C., *Polymer* **2004,** *45* (18), 6175-6187.

130. Uhl, F. M.; Davuluri, S. P.; Wong, S.-C.; Webster, D. C., *Chem. Mat.* **2004,** *16* (6), 1135-1142.

131. Uhl, F. M.; Webster, D. C.; Davuluri, S. P.; Wong, S.-C., *European Polymer Journal* **2006,** *42* (10), 2596-2605.

CHAPTER 2. NOVEL IN SITU SYNTHESIS IN THE PREPARATION OF UV-CURABLE NANOCOMPOSITE BARRIER COATINGS

2.1. Introduction

The degree of clay filler dispersion within polymer matrices is critical to achieving increased barrier protection in polymer-clay nanocomposites; therefore, the process selected for clay dispersion is critical to aid in the intercalation and exfoliation of the clay platelets. In situ intercalative polymerization techniques in the formation of polymer-clay nanocomposites utilize polymerization reactions to produce delaminated clay platelets.[1-2] With these in situ techniques, the clay is swollen with a suitable liquid monomer or monomer solution prior to polymerization. The onset of the polymerization reaction, initiated by radiation or heat, can produce polymer chains within the clay gallery, increase the basal spacing between clay layers, and potentially force delamination. The implementation of an in situ polymerization process was first reported with polyamide nanocomposites.[3] In situ polymerization techniques have been reported to yield exfoliated polyethylene terephthalate (PET) nanocomposites to serve as gas barrier coatings.[4] The production of these PET nanocomposites proceeds through an in situ polymerization mechanism where clay platelet delamination is initiated by PET oligomers, ultimately producing exfoliated polymer-clay nanocomposites. By utilizing this in situ polymerization technique, exfoliated PET nanocomposites were produced with significant reductions in oxygen gas permeability. Katoch et al. have also reported the production of unsaturated polyester-styrene based nanocomposites through an in situ type polymerization.[5]

By introducing the organoclay simultaneously with the monomers, nanocomposites with mixed intercalated-exfoliated morphologies were produced.

UV-curing technology offers many significant advantages over traditional thermal curing including decreased cure time, low-temperature cure, and low to zero volatile emissions. UV-curable nanocomposites were first reported by Zahouily et al.[6-7] Real-time infrared spectroscopy (RTIR) and X-ray diffraction (XRD) were utilized to detect the formation of nanocomposites by quantifying increased spacing between the clay layers.[8] The influence of the organic modifier on cure characteristics, thermal stability, and mechanical properties of radiation-curable nanocomposites has also been reported.[9-11] With regards to UV-curing coatings technologies, donor-acceptor chemistry has been reported as a feasible alternative to acrylate-based systems. With donor-acceptor chemistry, free-radical induced alternating photocopolymerization is achieved by mixing an electron-deficient vinyl group with an electron-rich vinyl group.[12] The benefits of utilizing donor-acceptor chemistry include high flexibility in polymer backbone design, low toxicity of monomers, and comparable cure times to acrylate systems. UV-curable coatings and polymer-clay nanocomposite systems based on maleate-vinyl ether donor-acceptor chemistry have previously been reported.[13-14] Maleic anhydride was used as a monomer in the synthesis of unsaturated polyester resins. These resins were subsequently photocopolymerized with vinyl ether-based reactive diluents to create UV-curable donor-acceptor coatings systems. The composition of the polymer backbone as well as the type and weight loading of clay were found to greatly influence the properties of the final radiation-curable coatings system.

The organomodified clay had been incorporated into the formulation prior to curing using sonication; the morphology of the nanocomposites prepared with donor-acceptor chemistry was classified as intercalated. Additionally, Kim et al. reported the preparation of UV-curable unsaturated polyester- and styrene-clay nanocomposites through a technique of mixing a polyester resin with montmorillonite clay at high shear.[15] Improvements in the dielectric and mechanical properties were observed due to clay inclusion, but X-ray diffraction indicated exfoliation was not achieved as a result of clay aggregation.

The focus of this research was the development of a novel and facile in situ preparation technique to aid in the production of high-performance, UV-curable nanocomposite coatings and to investigate their thermal, mechanical, and barrier properties. Although in situ processes have been reported previously to produce nanocomposite films, much of the focus has been on implementing these in situ techniques in thermoplastic polymer systems. With a desire to prepare UV-cured nanocomposite films having a high degree of nanoclay dispersion, the use of a novel in situ synthesis method to enable the dispersion and subsequent delamination of clay platelets in a polyester resin precursor was explored. The resulting unsaturated polyesters were crosslinked by donor-acceptor chemistry. With this in situ preparation technique, the degree of clay exfoliation is already achieved prior to UV-curing. The objective of this study was to implement a novel in situ preparation process and examine the impact of clay loading and functionalization on the ability to produce exfoliated UV-curable nanocomposite barrier films and explore the nanocomposite physical and mechanical properties.

2.2. Experimental

2.2.1. Materials

Monomers purchased from Sigma Aldrich (Milwaukee, WI) for unsaturated polyester synthesis were maleic anhydride, 1,6-hexanediol, and diethylene glycol. Monomer 1,4-cyclohexanedicarboxylic acid (1,4-CHDA) was obtained from Eastman Chemical Company (Kingsport, TN). Reactive diluent triethyleneglycol divinyl ether (TEGDVE) was obtained from BASF (Ludwigshagen, Germany). Photoinitator, 2-hydroxy-2-methyl-1-phenyl-propan-1-one (Darocur® 1173) was supplied by CIBA (Basel, Germany). Cloisite® Na^+, a natural unmodified montmorillonite clay (cation exchange capacity, CEC = 92 meq/100 g), and Cloisite® 30B, a natural montmorillonite clay modified with methyl tallow bis-2-hydroxyethyl ammonium cations (CEC = 90 meq/100 g), were obtained from Southern Clay Products (Gonzales, TX). The organic modifier cetyltrimethylammonium bromide (CTAB) was also purchased from Sigma Aldrich. All chemicals were used as received without further purification.

2.2.2. Preparation of organomodified clays

CTAB-modified nanoclays were prepared through an ion exchange reaction between unmodified montmorillonite clay Cloisite® Na^+ and alkylammonium surfactant CTAB. 5.00 g of CTAB were added to 200 mL of deionized water in a reaction flask equipped with stirrer and temperature controller. The CTAB-H_2O solution was heated to 50°C for two hours under constant stirring. 1.50 g of Cloisite® Na^+ was added to the solution and stirred for 24 hours at 50°C. The CTAB-modified clay was centrifuged for 15 minutes at 5000 RPM, filtered with

deionizied water and ethanol to remove excess bromine, dried in an oven, and ground using a mortar and pestle. The resulting clay is hereafter referred to as CTAB-modified clay. Cloisite® 30B was used without further modification.

2.2.3. Unsaturated polyester synthesis via in situ technique

Unsaturated polyesters were prepared by standard melt polyesterification. The unsaturated polyester composition is indicated in Table 2.1.

TABLE 2.1
Composition of unsaturated polyesters

Monomer	Maleic anhydride	Diethylene glycol	1,6-hexanediol	1,4-CHDA
Moles	1.000	0.824	0.625	0.172
Weight (g)	40.96	35.99	30.41	12.41

The clay was first added to the liquid monomer diethylene glycol based on the desired loading of the final nanocomposite (1, 2, 5, and 10 wt.%). The diethylene glycol and clay mixture was dispersed at high shear, and then mixed via magnetic stir bar overnight. The diethylene glycol-clay dispersion and remaining monomers were weighed into a 250 mL, three-necked, round bottom flask equipped with nitrogen inlet, condenser, mechanical stirrer, temperature controller, and heating mantle. The polyester synthesis was conducted in a nitrogen atmosphere to prevent oxidation of the double bonds and other side reactions. The reaction was ramped in a controlled manner to 60°C, 120°C, and 180°C. Water was collected from the polyester synthesis as the polymerization proceeded. The polyester reaction was stopped when an acid number of approximately 20 mg of KOH/gram of sample was achieved (determined by titration). A control unsaturated polyester

was synthesized with the same polyester composition but without the incorporation of the organomodified clays.

2.2.4. Unsaturated polyester-clay dispersion via sonication technique

Unsaturated polyester containing no clay, hereafter referred to as the control polyester, was mixed with Cloisite® 30B clay and sonicated for eight hours using an ultrasonic bath to compare the sonication technique of clay dispersion to the in situ process.

2.2.5. Nanocomposite preparation

Nanocomposites were prepared by mixing the unsaturated polyester sample and reactive diluent TEGDVE at a 1:1 stoichiometric ratio based on reactive functional groups: maleate to vinyl ether. Photoinitator Darocur® 1173 was added at 6 wt.% based on total polyester, reactive diluent, and clay. The nanocomposite formulations were mixed for uniformity, and then left undisturbed for two hours to remove air bubbles. Next, samples were cast on glass and aluminum substrates with a Gardco bar-coater at five mil clearance (75 – 85 μm dry film thickness). The cast formulations were cured under UV-light by a Dymax 200 EC silver lamp (UV-A, 365 nm, intensity ≈ 40 mW/cm^2) until the films were tack-free (60 seconds). Testing was performed after 24 hours to allow the nanocomposite coatings to equilibrate.

2.2.6. Nomenclature

Because the polyester composition was kept consistent throughout each polyesterification reaction, the nomenclature for the unsaturated polyesters was designated based on clay loading, clay type, and dispersion method. The name of

each polyester is as follows: wt.% clay_type_dispersion method, such as 1_30B_insitu for an unsaturated polyester containing 1% Cloisite® 30B clay synthesized using the in situ clay dispersion method. The clay type CTAB indicates the Cloisite® Na^+ nanoclay modified with the CTAB organic modifier. The term "sonic" refers to clays dispersed in virgin polyester by sonication. The coatings are named based on the polyester used in its formulation, but the prefix "NC" distinguishes the nanocomposite coating from the polyester.

2.2.7. Characterization

The unsaturated polyesters were characterized for molecular weight, viscosity, glass transition temperature (T_g), and maleate-fumarate isomerization. Molecular weight was determined using a Waters 2410 Gel Permeation Chromatograph equipped with a refractive index detector Polyester was dissolved in solvent tetrahydrofuran (THF) to create a 1% sample solution and filtered by a 0.2 μm PET filter to remove any clay agglomerates. The flow rate was 1 mL/min, and calibration was performed with polystyrene standards. Viscosity measurements were made with an ICI cone and plate viscometer at 100°C. The T_g was determined from differential scanning calorimetry (DSC) using a TA Instruments Q1000 Series DSC. The test method was a heat-cool-heat cycle. Polyester samples were equilibrated at -90°C, heated to 100°C at a rate of 10°C/min, cooled to -90°C at a rate of 10°C/min, then heated once again to 100°C at a rate of 10°C/min. T_g values were determined from the inflection point in the second heating scan. The isomerization from maleate to fumarate in the unsaturated polyester backbone was determined from ^1H nuclear magnetic

resonance (NMR) spectroscopy using a JEOL ECA Series 400 MHz NMR spectrometer with procedure followed from Curtis et al.[16]

The cure characteristics were determined using a Thermo Nicolet Magna-IR 850 spectrometer with detector type DTGS KBr to perform RTIR measurements. A LESCO Super Spot MK II UV-curing lamp equipped with a fiber-optic light guide was UV-irradiation source for curing the samples. The formulations were spin-coated at 3000 RPM onto a KBr window, placed into the spectrometer chamber, and subjected to UV and infrared (IR) irradiation simultaneously. The samples were approximately 20 mm from the end of the fiber-optic cable with a light intensity of 10 mW/cm^2. The degree of conversion was determined from the disappearance of the vinyl ether double bonds (1639 cm^{-1}). The conversion was calculated from equation (2.1) where $(A_{1639})_0$ is the absorbance at time=0 and $(A_{1639})_t$ is the absorbance at time=t.

$$\% \, conversion = \{[(A_{1639})_0 - (A_{1639})_t]/(A_{1639})_0\} \times 100 \qquad (2.1)$$

Nanocomposite morphology was characterized by XRD and TEM. X-ray powder diffraction was collected using a Bruker AXS' D8 Discover diffractometer in Bragg-Brentano geometry, using Cu Kα radiation with a wavelength of 1.5406 Å. The samples were scanned from 1.5 °to 50° 2θ, using a step size of 0.02° 2θ and a run time of 1 second/step. Samples for TEM were thin cut using a diamond knife and RMC MTXL ultramicrotome. The thin sections were placed on 400 mesh copper grids and photographed using a JEOL 100 cx-II transmission electron microscope operating at 80kV. Water vapor transmission testing was performed in accordance with ASTM E96, “Standard Test Methods for Water Vapor

Transmission of Materials," by the Water Method. A controlled humidity chamber was employed to maintain relative humidity at 70% ±2% and 20°C ± 2°C. Under steady state conditions, the mass loss over time correlated with water vapor transmission and permeance. Duplicate samples were performed to verify results. Oxygen gas permeability measurements were conducted with a MOCON Oxtran 2/21 Oxygen Permeability Instrument (Modern Control, Inc., Minneapolis, MN) in accordance with ASTM D3985 (0% RH, 25°C). Duplicate samples of each nanocomposite film were submitted to verify results.

The dynamic mechanical properties were tested using a TA Instruments Q800 Dynamic Mechanical Analyzer in tensile mode. Free films of the cured coatings of approximately 15 mm length, 5 mm width, and 0.070-0.078 mm thickness were characterized using 1 Hz frequency, constant strain of 0.05%, heating rate of 5°C/min over a temperature range of -50°C to 150°C. Film hardness was determined using a BYK-Gardner pendulum hardness tester on aluminum panels. Thermal stability was determined using thermogravimetric analysis (TGA) with a TA Instruments Q500 Thermogravimetric Analyzer. Cured samples were heated in nitrogen from 25°C to 800°C at a rate of 20°C/min. The optical clarity was measured with a Varian Cary 5000 UV-Vis Spectrometer by determining transmittance at 400 nm.

2.3. Results and discussion

2.3.1. In situ synthesis technique

In previous studies, the development of UV-curable coatings and polymer/clay nanocomposites based on the non-acrylate technology of donor-

acceptor chemistry was reported.[13-14] Sonication was employed to disperse the clay and monomers prior to photocopolymerization, and the resulting nanocomposite morphology was classified as intercalated. To further increase clay dispersion, a novel in situ preparation technique was explored to produce highly dispersed clays in a polymer resin prior to crosslinking. With this novel technique, the dispersion of nanoclays in the unsaturated polyester resins prior to crosslinking depends on the diffusion of liquid monomer into the nanoclay interlayers. Scheme 2.1 illustrates the in situ process for nanoclay dispersion. Initially, the nanoclay layers stack face-to-face due to favorable electrostatic interactions between the negatively charged clay platelets and exchangeable cations in the clay interlayer. The interlayer space is equivalent to the organic modifier volume. By introducing a liquid monomer at high shear, the monomer may diffuse into the clay interlayer. The onset of the unsaturated polyester polymerization will lead to oligomeric chain growth. The increase in volume from the growing oligomeric chains may then increase the volume between the nanoclay layers; therefore, the distance between the clay layers will increase. Through this in situ process, it is possible to expand the interlayer spacing to produce highly dispersed clays within the polyester prior to crosslinking. Additionally, the functionality of the clay organic modifier may aid in the exfoliation process. Hydroxy-functional organic modifiers, such as the modifier for Cloisite® 30B, may react with the acid-functional monomers during polyesterification, thereby becoming incorporated into the polyester backbone and further inducing exfoliation of nanoclay platelets. The CTAB-modified clay provided

an organic modification without hydroxy-functionality to explore the impact of the modifier on the final polyester and nanocomposite film properties.

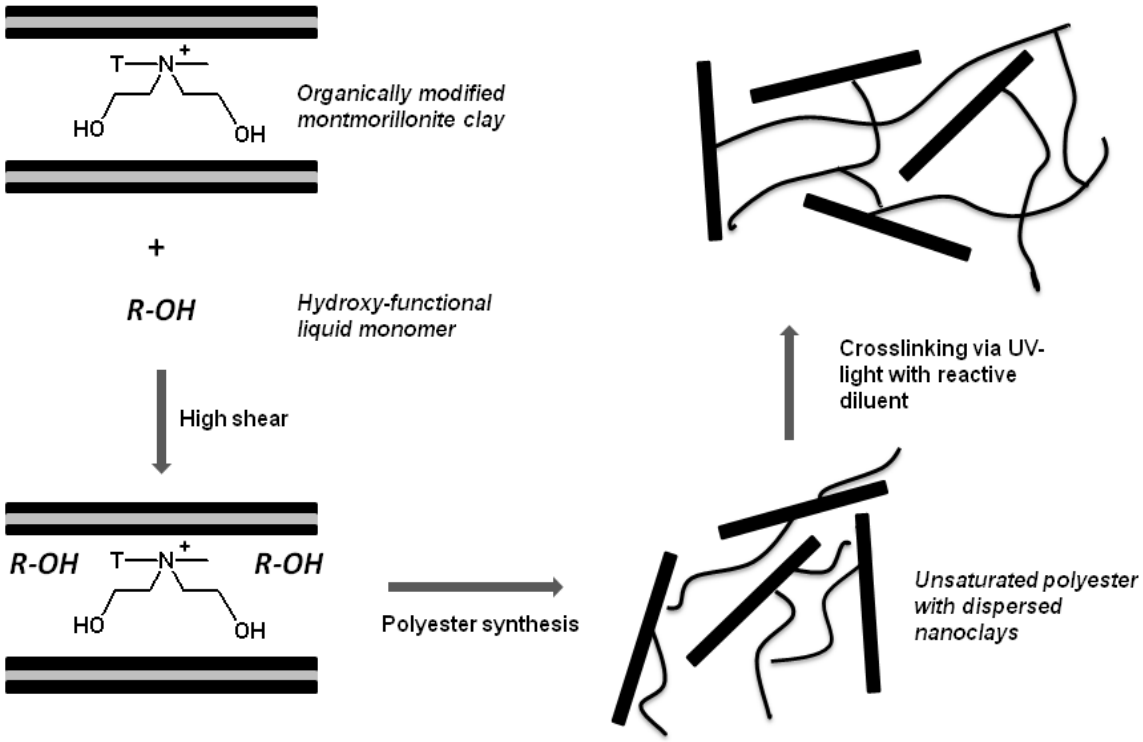

Scheme 2.1: Representation of the in situ technique producing exfoliated clay platelets within the precursor unsaturated polyester resin (T = tallow).

2.3.2. Unsaturated polyester characterization

The properties of the unsaturated polyesters containing organomodified clay were characterized to examine the effect of the clay dispersion technique and loading. Polyester properties provide insight to the properties of the nanocomposite films. Table 2.2 is a comprehensive summary of the polyesters synthesized and their properties. The target acid number was approximately 20 mg of KOH/g of the polyester resins. All polyester reactions were stopped once an acid number near this value was achieved. Comparable acid numbers were

important in the characterization of the unsaturated polyesters as similar acid number values produce similar degrees of polymerization.[17]

TABLE 2.2
Properties of unsaturated polyesters prepared through in situ technique or sonication dispersion route

Polyester	Acid value	M_n (g/mol)	M_w (g/mol)	PDI	Viscosity (Poise)	T_g (°C)	% Fumarate
Control	21	1000	2200	2.2	2.4	-42	33
1_30B_insitu	21	1800	3500	1.9	3.3	-36	46
2_30B_insitu	22	1500	3800	2.5	5.4	-39	39
5_30B_insitu	21	1800	3900	2.2	5.8	-41	41
10_30B_insitu	21	4000	7300	1.8	8.8	-43	64
1_30B_sonic	21	1900	3600	1.9	3.5	-37	19
2_30B_sonic	21	2000	3600	1.8	3.7	-37	17
5_30B_sonic	21	1400	3500	2.4	4.8	-41	24
10_30B_sonic	21	1900	3800	2.0	5.4	-42	18
1_CTAB_insitu	20	2800	6900	2.4	6.0	-32	53
2_CTAB_insitu	21	2400	4700	2.0	6.5	-33	62
5_CTAB_insitu	22	1800	4800	2.7	7.3	-36	52

The molecular weight and polydispersity of the unsaturated polyesters was determined from GPC to examine the impact of the clay. The introduction of clay into the polyester network increased the apparent molecular weight in all unsaturated polyesters. Because the clay was not removed before GPC analysis, the increases in molecular weight may be a reflection of higher hydrodynamic volumes from the polyester oligomers containing the clay fillers. The polydispersity index (PDI) ranged from 1.8 to 2.7, showing higher breadth of molecular weight distribution typical of step-growth polymerizations. The relationship between clay loading and viscosity demonstrated the dramatic influence of the incorporation of even small amounts of clay into a polymer system. The control polyester had a viscosity of 2.4 Poise, and the introduction of just 1 wt. % clay increased the

viscosity regardless of the dispersion route or clay type. Increasing the concentration of clay led to higher unsaturated polyester viscosities. A direct trend between clay loading and viscosity was apparent with higher clay loadings resulting in higher viscosities. The unsaturated polyesters synthesized with the CTAB-modified clay had slightly higher viscosities compared with the Cloisite® 30B at the same clay loading, most likely a consequence of poorer compatibility between the CTAB-modified clay and polyester oligomers. The Cloisite® 30B-containing polyesters prepared through the in situ preparation technique were higher in viscosity than those dispersed through sonication for the same clay loading. The glass transition temperatures (T_g) of these unsaturated polyesters showed an interesting trend with increasing the clay content. The addition of small levels of organomodified clay (1 or 2 wt.%) increased the T_g slightly, up to 10°C higher than the control polyester, but higher clay amounts (5 and 10 wt.%) barely affected the T_g. The small T_g changes observed with clay inclusion into the polyester resin may be a result of the low molecular weight polyester oligomers. Additionally, the control unsaturated polyester resin has a relatively low T_g (-42 °C), so the impact of clay on the polyester T_g may not be as dramatic as polymers with higher T_g values.

The variables influencing maleate-fumarate isomerization have been studied in unsaturated polyesters, where the reaction environment, monomers, and catalyst all affect the final degree of isomerization.[18] Polyesters synthesized from maleic anhydride often exhibit reactivity similar to polyesters synthesized from fumaric acid, a trend attributed to the conversion of maleic to fumaric unsaturation

during polyesterification.[16] Polyesters exhibiting cis-trans conversion along its backbone have also exhibited higher hardness and chemical resistance. The isomerization of the unsaturated polyester backbone from maleate to fumarate was found to be greatest with the polyesters synthesized by the in situ technique.

Curtis et al. have reported the preference of hydroxy-functional monomers to react with the trans isomer in polyesterification reactions when the hydroxyl groups are sterically hindered.[16] Additionally, when the monomers exhibit less steric hindrance, the preference of reacting with the cis or trans isomer decreases. The dispersion of the organomodified clays may greatly influence the final degree of isomerization. If the in situ technique increased clay dispersion, the trans-fumarate isomerization may be promoted as the fumarate isomerization is less influenced by steric effects.[19] The preference to react with the trans isomer is reflected by higher values of fumarate isomerization compared to the control unsaturated polyester.

2.3.3. Cure characteristics – Real-time infrared spectroscopy

Higher conversion with UV-irradiation was observed in every nanocomposite formulation compared to the control sample containing no clay filler. The extent of the reaction was monitored by the disappearance of the vinyl ether double bond (1639 cm^{-1}), indicating the degree of conversion based on donor-acceptor chemistry of the maleate-vinyl ether coatings system. The control sample had a conversion of 72%, whereas each nanocomposite formulation resulted in conversions ranging from 80-87% (Figure 2.1). The increased

conversion achieved with the addition of clay fillers is attributed to the viscosity of the nanocomposite formulations.

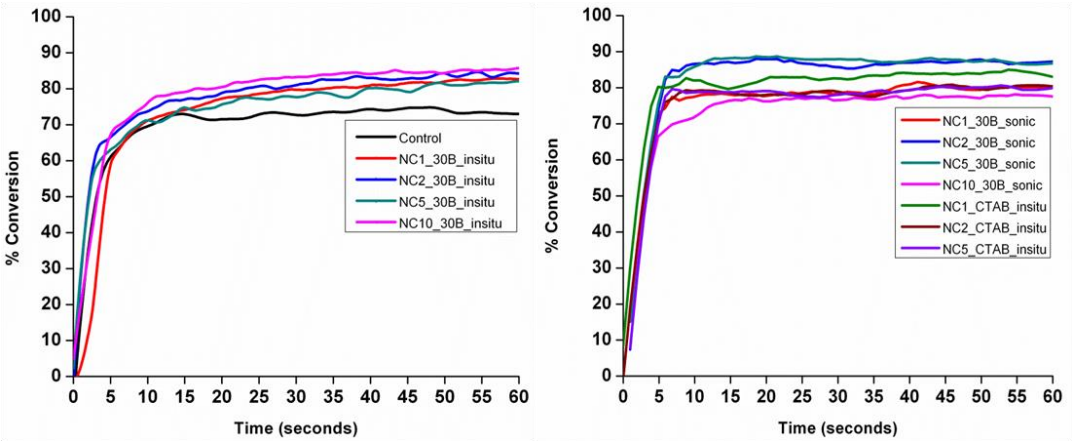

(a) **(b)**

Figure 2.1: Real-time infrared spectroscopy conversions of the vinyl ether double bond (1639 cm^{-1}) with (a) in situ nanocomposite formulations and (b) sonicated and CTAB-modified clay nanocomposite formulations with 60 seconds of UV exposure.

As seen in Table 2.2, the viscosities of the unsaturated polyesters containing clay had significantly greater viscosities than that of the control polyester. Higher viscosities may result in an autoacceleration effect. With the increased viscosity, it becomes more difficult for chain ends bearing radicals to diffuse through the system, thus decreasing the rate of termination. The lower molecular weight reactive diluent and oligomers may more easily diffuse through the system leading to increased conversion. Similar trends regarding increased conversion with the introduction of clay has been reported in other UV-curable nanocomposite systems.[9, 14, 20]

2.3.4. Nanocomposite morphology – X-ray diffraction and transmission electron microscopy

With the in situ technique to incorporate nanoclays, increased organomodified clay delamination may occur as a result of the growing oligomeric polyester chains occupying more volume within the clay interlayer. Increasing the distance between the clay layers leads to a high degree of dispersion within the polymer system. After the unsaturated polyesters are crosslinked by reactive diluent TEGDVE, an exfoliated nanocomposite may be formed. Because the final degree of clay dispersion cannot be changed once curing has occurred, delamination of the clay prior to crosslinking is critical to aiding in the exfoliation process.

The morphology of the UV-curable nanocomposite films has a profound impact on the final coating properties. The degree of dispersion will dictate the extent of polymer-nanoclay surface area interaction with high levels of dispersion leading to the greatest surface area interaction. Therefore, nanocomposite morphology determination is crucial to the explanation of film properties. XRD was conducted to determine the *d*-spacing, or distance of the nanoclay interlayer, of the resulting nanocomposite films. An increase in the *d*-spacing indicates the intercalation of polymer between nanoclay platelets; thus, the formation of nanocomposites. Figure 2.2 displays the XRD patterns of the pristine clays as well as the nanocomposite coatings. With XRD analysis, the presence or absence of diffraction peaks associated with polymer-clay nanocomposites indicates the final morphology.

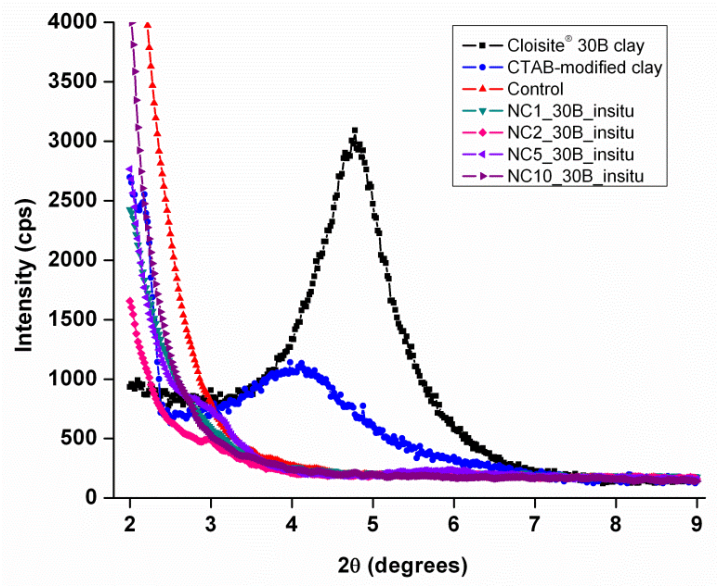

(a)

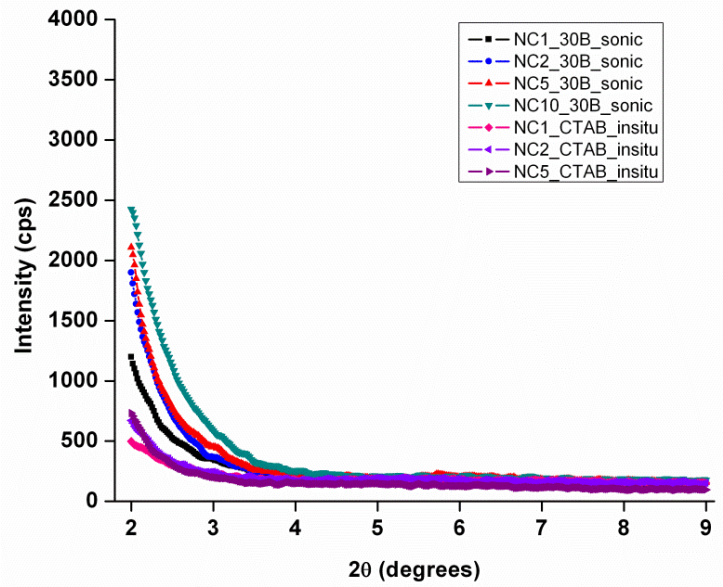

(b)

Figure 2.2: XRD patterns of (a) pristine Cloisite® 30B, CTAB-modified clay, and in situ prepared nanocomposite films, and (b) sonicated and CTAB-modified clay containing nanocomposite films.

Two prominent diffraction peaks were observed at 4.78 and 4.12 2θ for Cloisite® 30B and the CTAB-modified clay, respectively. Using Bragg's Law, the interlayer spacing for Cloisite® 30B was 1.85 nm and 2.14 nm for the CTAB-

modified clay. In stark contrast to the distinct clay diffraction peaks, each nanocomposite film had an absence of any prominent peaks at low 2θ angles. This absence of peaks may indicate the formation of exfoliated nanocomposite morphologies as the clay platelets have been delaminated to a high enough degree to become disoriented and unable to produce diffraction with wide-angle XRD techniques.[21] Although XRD is widely reported to classify polymer-clay nanocomposite morphology, the absence of peaks may also be an indication of poor calibration or clay orientation. Furthermore, low levels of clay loading may fail to produce a Bragg diffraction peak.[22]

While the absence of diffraction peaks from the nanocomposite XRD patterns was a promising indicator for high clay dispersion, TEM was an important and necessary technique to more accurately characterize nanocomposite morphology. TEM micrographs (Figure 2.3) of the nanocomposite samples indicate that the in situ preparation technique produced exfoliated nanocomposites at 1 and 2 wt. % and mostly intercalated at 5 and 10 wt.%. At the lower levels of clay loading, the clay platelets are well-dispersed and randomly oriented, whereas nanocomposites NC5_30B_insitu and NC10_30B_insitu display ordered clay layers, although increased separation between clay platelets was observed. Intercalation was predominantly observed with the sonication dispersion technique; these nanocomposites did not exhibit an exfoliated morphology. The CTAB-modified clay containing nanocomposites also produced predominantly intercalated nanocomposites even with low levels of clay loading, suggesting the

importance of the hydroxyl functionality of the organic modifier to achieve exfoliation through the in situ technique.

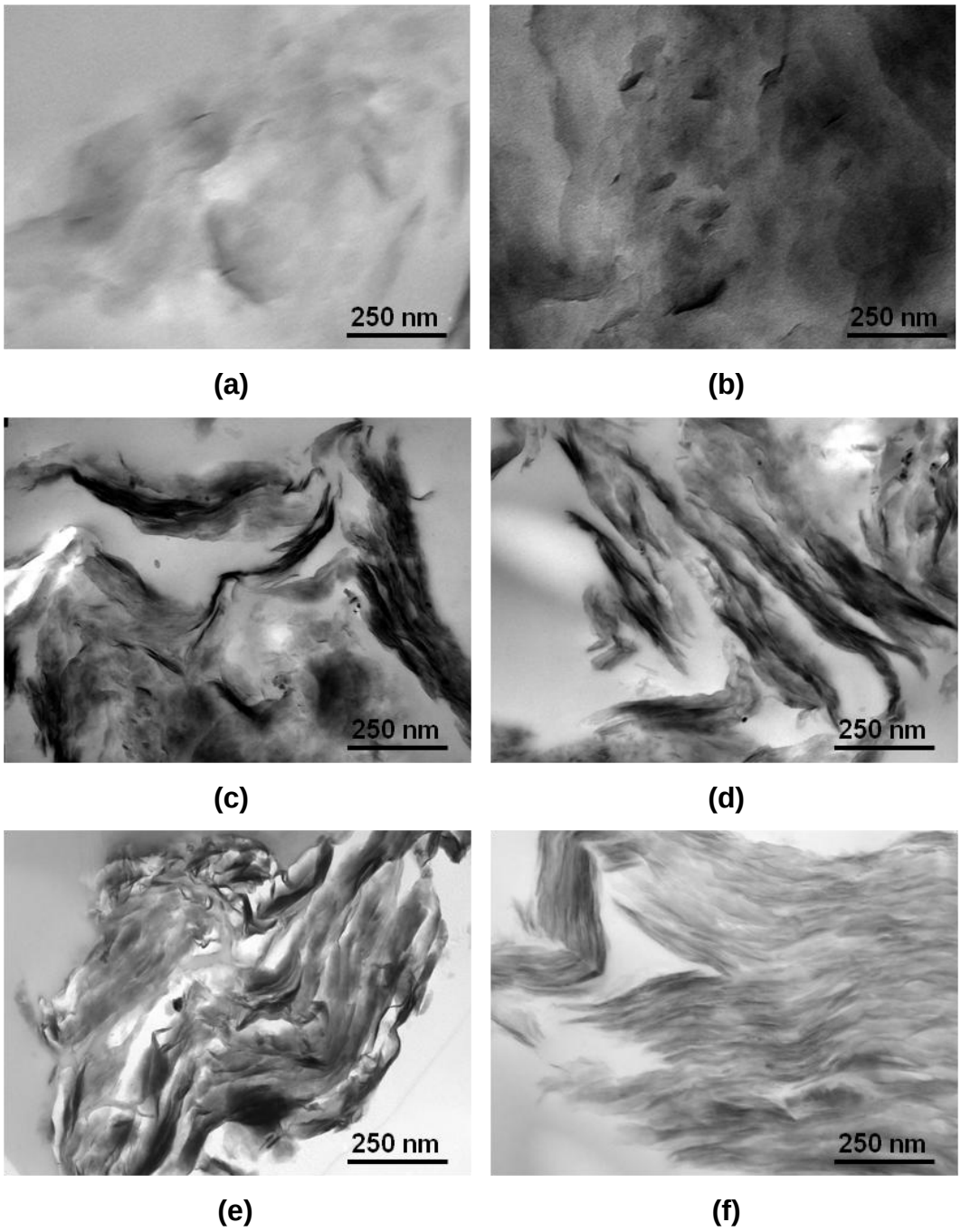

Figure 2.3: Transmission electron micrographs of (a) NC1_30B_insitu, (b) NC2_30B_insitu, (c) NC5_30B_insitu, (d) NC10_30B_insitu, (e) NC5_30B_sonic, and (f) NC1_CTAB_insitu.

2.3.5. Barrier properties – Water vapor transmission and permeability

The results shown in Figure 2.4 and the data summarized in Table 2.3 indicate the in situ preparation technique yielded nanocomposites with lower water vapor transmission (WVT) and permeability (WVP), in accordance with ASTM E96 Water Method. Figure 2.4 demonstrates the superiority of the in situ process in nanocomposite preparation to serve as barriers compared to the sonication preparation technique and CTAB-modified clay containing nanocomposites; the in situ process has the lowest mass loss for every level of clay loading. Figure 2.4a demonstrates that the introduction of just 1 wt. % clay reduced the mass loss of water over time. With the introduction of higher levels of clay loading, the mass loss was more significantly reduced. NC5_30B_insitu and NC10_30B_insitu had the lowest mass loss over time, which correlated into the lowest WVT and WVP of any nanocomposite sample. The performance of the in situ prepared nanocomposites in reducing WVT and WVP is attributed to the higher level of nanoscale dispersion of the clay filler. By utilizing the polyester polymerization to increase the spacing between clay platelets, the clay filler reached a higher degree of dispersion. This dispersion was maintained with the formation of the nanocomposite coatings, resulting in nanocomposites providing a more tortuous diffusion path for water molecules. Although the in situ process did not create perfectly exfoliated nanocomposites with 5 and 10 wt. % clay, the mass loss of water is lower than the sonicated nanocomposite films indicating that a higher degree of dispersion was achieved with the in situ preparation. One noteworthy example of the improvement in barrier protection provided by the in situ process

was the level of clay needed in the in situ process compared to the sonication technique to provide the same level of barrier protection: NC2_30B_insitu recorded approximately the same WVT and WVP as NC10_30B_sonic. Not only did the in situ process produce better barrier protection, but the in situ nanocomposites needed significantly less clay to achieve those barrier properties.

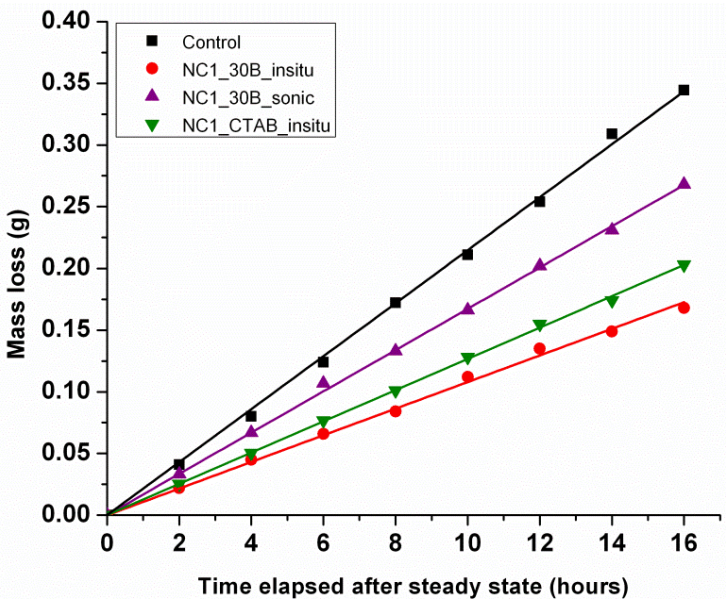

(a)

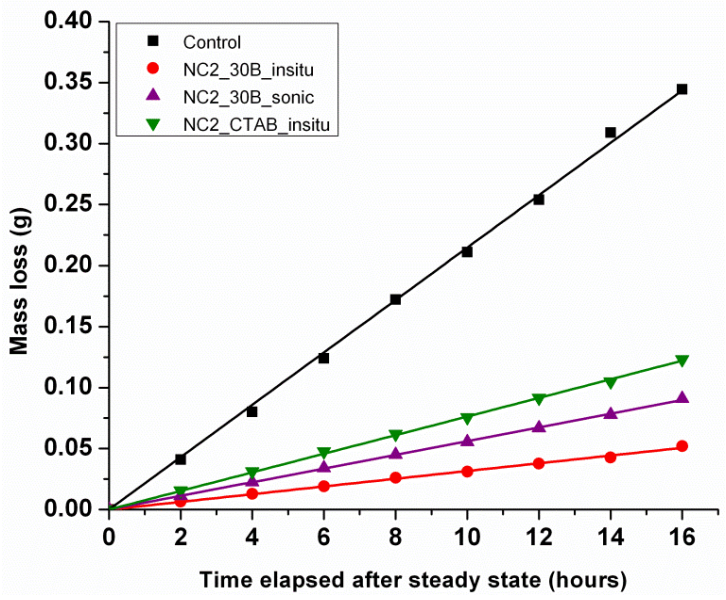

(b)

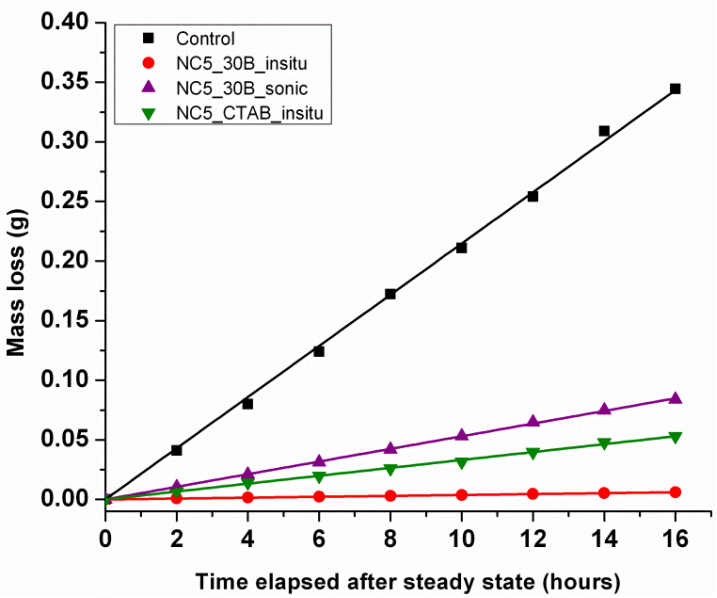

(c)

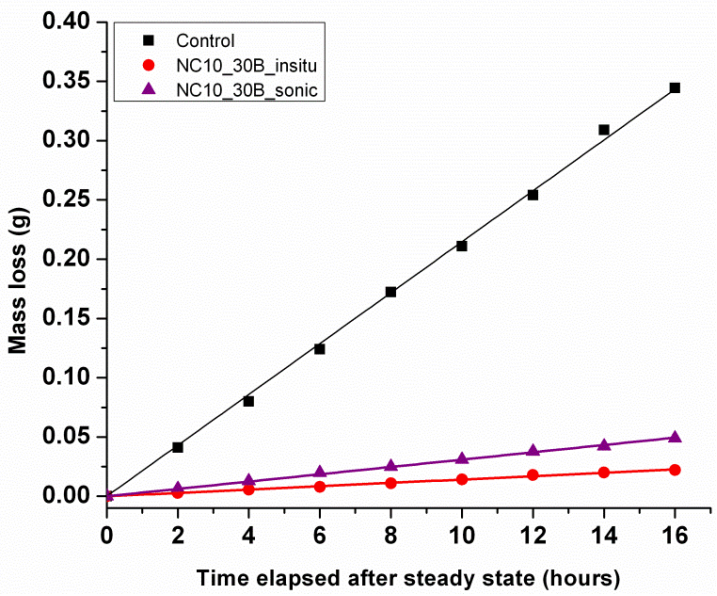

(d)

Figure 2.4: Mass loss versus time once steady state conditions were achieved for nanocomposite films. Comparison of 1 wt.% (a), 2 wt.% (b), 5 wt.% (c), and 10 wt.% (d) displayed.

TABLE 2.3
UV-curable nanocomposite water vapor transmission and permeability results as determined by ASTM E96

Nanocomposite	Mass loss/time (g/hr)	WVT ($g/m^2/s$)	Avg. film thickness (μm)	WVP ($g \cdot m/m^2 \cdot s \cdot Pa$)
Control	2.15 E-02	5.97E-03	86	8.79E-10
NC1_30B_insitu	1.02 E-02	2.83E-03	80	3.88E-10
NC2_30B_insitu	3.17 E-03	8.81E-04	83	1.25E-10
NC5_30B_insitu	3.78 E-04	1.05E-04	78	1.40E-11
NC10_30B_insitu	1.41 E-03	3.92E-04	81	5.43E-11
NC1_30B_sonic	1.67 E-02	4.64E-03	79	6.27E-10
NC2_30B_sonic	5.61 E-03	1.56E-03	84	2.24E-10
NC5_30B_sonic	5.31 E-03	1.48E-03	78	1.97E-10
NC10_30B_sonic	3.09 E-03	8.58E-04	80	1.17E-10
NC1_CTAB_insitu	1.27 E-02	3.53E-03	80	4.83E-10
NC2_CTAB_insitu	7.63 E-03	2.12E-03	78	2.83E-10
NC5_CTAB_insitu	3.31 E-03	9.19E-04	82	1.29E-10

2.3.6. Barrier properties – Oxygen gas transmission

In contrast to the water vapor transmission results reported in the previous section, the in situ technique in the preparation of UV-curable nanocomposites did not demonstrate any concrete trends regarding oxygen gas permeability. Table 2.4 lists the oxygen barrier results obtained from MOCON (Minneapolis, MN) for the series of in situ prepared nanocomposite films containing the hydroxy-functional clay, Cloisite® 30B. Although no direct correlation existed between the clay loading and the oxygen barrier properties of the nanocomposite films, these films still were in the acceptable oxygen transmission rate (OTR) range of a medium barrier layer, such as for certain food and beverage packaging materials.[23] For example, polyethylene terephthalate (PET) is a commonly used material in the packaging of juice, water, beer, meats, and cheeses. The O_2 permeability of PET

films is reported to be approximately 6-10 cc/100in^2/day.[24] The in situ prepared nanocomposites had lower OTR values than PET, ranging from 1.45-2.07 cc/100in^2/day. Unlike the trends observed with WVT, the addition of clay did not drastically lower the oxygen barrier properties of the nanocomposite samples.

TABLE 2.4
UV-curable nanocomposite oxygen gas transmission results as determined by ASTM D3985

Nanocomposite	OTR (cc/100in^2/day)
Control	1.88
NC1_30B_insitu	1.45
NC2_30B_insitu	2.07
NC5_30B_insitu	1.73
NC10_30B_insitu	1.95

Several factors will influence the permeation through the films including clay size, orientation, and compatibility between the permeating species and polymer film. Larger reductions in WVT than OTR were also reported by Osman et al. for polyurethane-clay nanocomposites.[25] One explanation given for the difference in water vapor and oxygen gas permeability was the size of the permeating groups. Because water vapor molecules may form into clusters during their diffusion through polymers, the clusters may increase the diffusion time.[26] Since oxygen gas molecules do not similarly form clusters during diffusion, their diffusion may proceed more readily through polymer films. Additionally, the OTR of the control coating (1.88 cc/100in^2/day) was also considered to be in the range of a medium oxygen barrier.

2.3.7. Mechanical properties – Dynamic mechanical analysis and König hardness

Overall, the nanocomposite films containing lower levels (1 and 2 wt. %) of clay loading exhibited higher storage moduli and hardness values than the nanocomposites with higher clay loading (5 and 10 wt. %), as determined by dynamic mechanical analysis (DMA). A summary of these results are compiled in Table 2.5 and displayed in Figures 2.5 and 2.6. The storage modulus at room temperature of each nanocomposite sample was found to clearly be related to the dispersion technique and clay content. With the in situ preparation technique, the storage modulus was increased over 500 MPa with NC1_30B_insitu compared to the control coating. Further increases in the clay loading led to additional increases in the storage modulus, with NC10_30B_insitu recording a storage modulus of 1500 MPa at room temperature.

TABLE 2.5
UV-curable nanocomposite mechanical and thermal characterization data

Nanocomposite	*E'* (MPa, 25°C)	König hardness (sec)	T_{10}% (°C)
Control	370	83	240
NC1_30B_insitu	890	84	255
NC2_30B_insitu	1020	93	245
NC5_30B_insitu	1250	82	250
NC10_30B_insitu	1500	76	230
NC1_30B_sonic	810	96	270
NC2_30B_sonic	910	89	290
NC5_30B_sonic	625	84	300
NC10_30B_sonic	390	71	280
NC1_CTAB_insitu	610	93	270
NC2_CTAB_insitu	495	87	280
NC5_CTAB_insitu	340	63	260

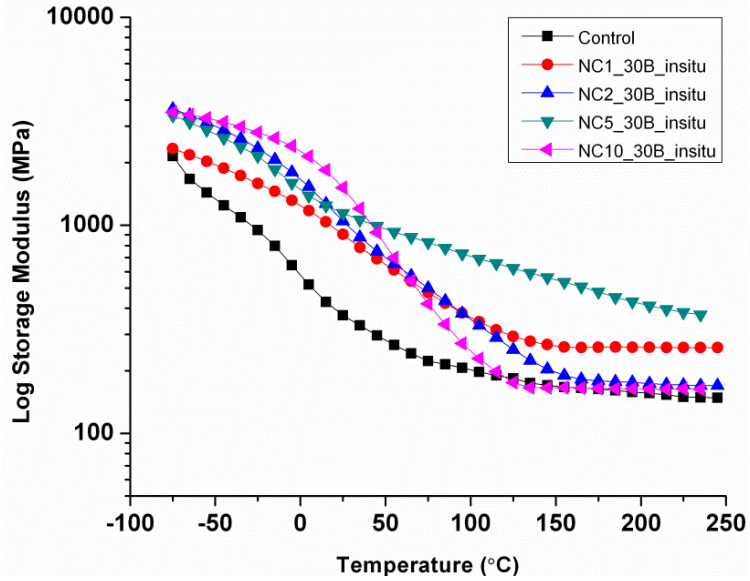

(a)

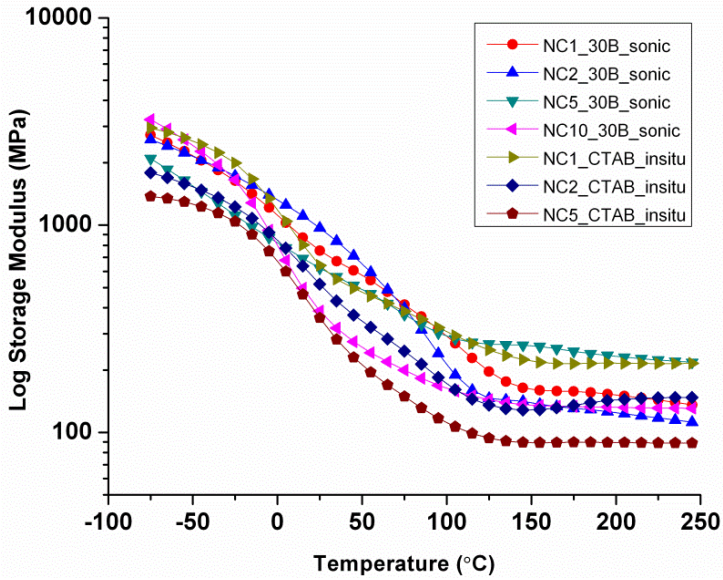

(b)

Figure 2.5: Storage modulus plots from DMTA for (a) in situ nanocomposite films and (b) sonicated and CTAB-modified clay nanocomposite films.

In contrast, the trend of higher storage modulus values with higher levels of clay loading was not reflected with the nanocomposites containing the CTAB-modified clay or the nanocomposites based on the sonication dispersion

technique. With clay loading up to 2 wt. %, these nanocomposites demonstrated increased storage modulus values, but nanocomposites containing 5 and 10 wt. % clay resulted in a decrease in the storage modulus. This trend is most likely a consequence of poorer clay dispersion throughout the nanocomposite film. As seen with TEM analysis, the nanocomposites prepared with the CTAB-modified clay or through the sonication preparation technique were intercalated with portions of phase separation at higher clay loading. With phase-separated clay domains throughout the nanocomposite, the mechanical properties may diminish as the reinforcing effect of the clay fillers decreases from agglomeration. Nanocomposite NC10_30B_sonic had approximately the same storage modulus as the control coating, and nanocomposite NC5_CTAB_insitu actually had a lower storage modulus value than the control. A similar trend is observed with König pendulum hardness of the nanocomposites where coatings containing 1 and 2 wt. % clay loading exhibited higher König hardness values than the coatings with 5 – 10 wt.% clay, regardless of dispersion route (Figure 2.6).

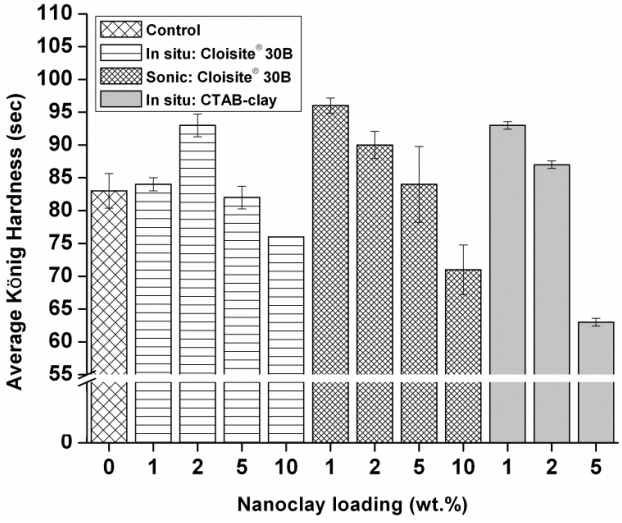

Figure 2.6: König pendulum hardness of the nanocomposite coatings.

2.3.8. Thermal stability – Thermogravimetric analysis

The thermal stability of the nanocomposite samples showed a similar trend as a function of clay loading: nanocomposites containing lower levels of clay loading generally had greater thermal stability. The TGA degradation curves are displayed in Figure 2.7, and Table 2.5 reports the temperature at 10% weight loss (T_{10}%).

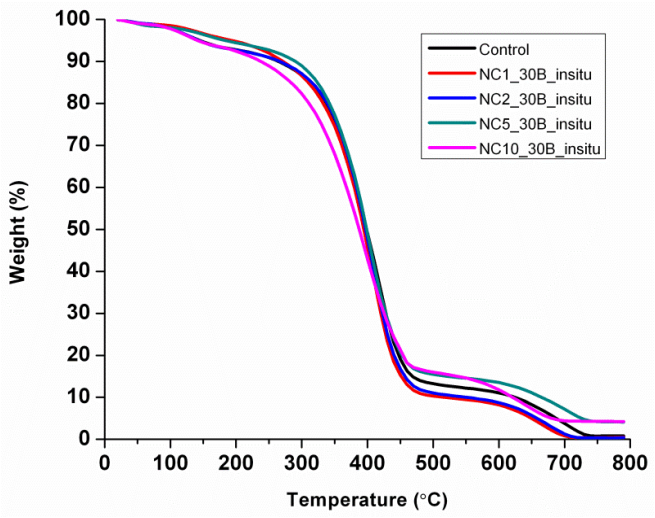

(a)

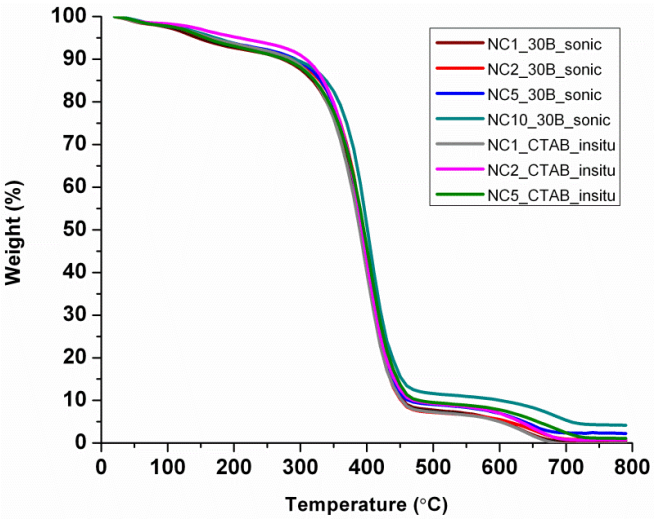

(b)

Figure 2.7: TGA degradation curves of the (a) in situ preparation nanocomposites and (b) sonication and CTAB-modified clay nanocomposites.

The control coating had a T_{10}% of 240°C; NC1_30B_insitu, NC2_30B_insitu, and NC_5_30B_insitu each had slightly higher T_{10}%, up to a 15 °C increase. Conversely, NC10_30B_insitu had the lowest T_{10}% at 230 °C. Increased thermal stability was also observed with each nanocomposite prepared through the sonicated technique as well as the CTAB-modified clay, particularly at 1 -2 wt.% clay. Again, the higher levels of clay loading seemed to diminish the improvement in thermal stability observed with low levels of clay filler.

After examining both the mechanical and thermal properties of the UV-curable nanocomposite films, a significant trend occurred: nanocomposites with lower levels of clay (1 – 2 wt.%) demonstrated increased modulus, hardness, and thermal stability but higher levels of clay (5 – 10wt.%) did not continually increase the material properties. Instead, nanocomposites with higher clay loading demonstrated diminished mechanical and thermal properties when compared to nanocomposites containing lower clay loading. Based on these results, it becomes apparent that there is a significant influence from the clay loading on the final nanocomposite mechanical properties. Miyagawa et al. reported a decrease in the T_g of anhydride-cured epoxy nanocomposites with increased clay volume fraction.[27] The explanation for this phenomenon was hypothesized to be an effect of the organic modifier plasticizing the coatings system. With increased clay amounts in the nanocomposite system, there is also an increase in the amount of the organic modifier within the cured coating. The organic modifier containing a long-chain fatty acid may act as a plasticizer, thus lowering the T_g with increased clay content. Based on trends observed with T_g, the mechanical and thermal

properties of the nanocomposites may also be affected by the increased organic modifier concentration with higher levels of clay loading. Additional experimentation will be conducted to further explore this trend.

2.3.9. Optical clarity – UV-visible spectroscopy

While low concentrations of nanoclays maintained high optical clarity, dramatic decreases in transmittance of the nanocomposite films were observed with higher levels of nanoclay loading. Nanoscale distribution of the silicate platelets contributes to the high optical clarity observed in many polymer-clay nanocomposites.[28] Figure 2.8 shows the transmittance at 400 nm for each nanocomposite. The control coating had high optical clarity with 98% transmittance. The contribution of 1 and 2 wt. % clay, regardless of clay type of dispersion technique, decreased the transmittance slightly (92-97%). The clarity of these nanocomposites is a direct reflection of the low volume fraction of clay present in the sample coupled with the degree of dispersion.

With increases in clay loading to 5 and 10 wt. %, more dramatic decreases in the optical clarity are observed. In particular, the nanocomposites prepared through the sonication technique became much more opaque with the introduction of 5 and 10 wt. % clay, measuring percent transmittance values of 82% and 62%, respectively. Although the in situ preparation of nanocomposites also reflected a decrease in optical clarity with higher clay loadings, the transmittance was much higher than the sonication preparation. NC5_30B_insitu had 85% transmittance, and NC10_30B_insitu had a transmittance value of 84%. The higher optical clarity of the in situ based nanocomposite coatings compared to the sonication technique

may reflect a much greater dispersion of nanoclay fillers, as seen with TEM micrographs. Additionally, the CTAB-modified clay nanocomposites maintained high optical clarity regardless of clay loading.

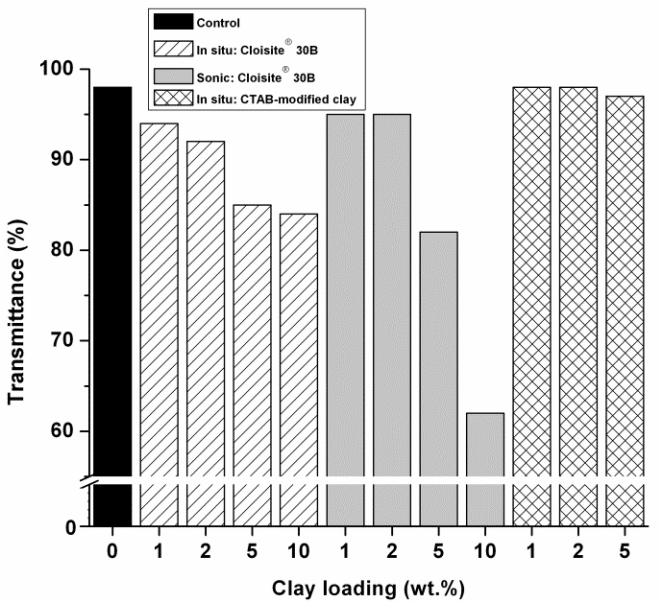

Figure 2.8: Transmittance of nanocomposites at 400 nm as determined by UV-visible spectroscopy.

2.4. Conclusions

UV-curable nanocomposite coatings were successfully prepared by a novel in situ synthesis technique. The unique dispersion technique led to nanocomposite films exhibiting exfoliated morphologies. High clay dispersion was indicated with the absence of XRD diffraction peaks, but exfoliation at low levels of clay loading (1 – 2 wt.% Cloisite® 30B) was confirmed with transmission electron micrographs. The sonicated nanocomposites and CTAB-modified clay containing nanocomposites had predominately intercalated morphologies, demonstrating poorer clay dispersion without applying the in situ process or utilizing the hydroxy-functional organomodified clays. The nanocomposites prepared through this in situ

technique demonstrated lower WVT and WVP values compared to the sonication process. The incorporation of clay fillers increased the overall conversion of the nanocomposite systems up to 15%. The impact of clay loading on final nanocomposite film properties became evident with the trends observed with mechanical and thermal characterization. Introducing low levels of clay filler resulted in increased storage modulus, hardness, and thermal stability, but increasing the clay to higher concentrations diminished these properties. Additionally, optical clarity was shown to have a significant dependence on the volume of clay in each nanocomposite system as well as its dispersion.

2.5. References

1. LeBaron, P. C.; Wang, Z.; Pinnavaia, T. J., *Applied Clay Science* **1999,** *15* (1-2), 11-29.

2. Paul, M.-A.; Delcourt, C.; Alexandre, M.; Degée, P.; Monteverde, F.; Rulmont, A.; Dubois, P., *Macromolecular Chemistry and Physics* **2005,** *206* (4), 484-498.

3. Usuki, A.; Kojima, Y.; Kawasumi, M.; Okada, A.; Fukushima, Y.; Kurauchi, T.; Kamigaito, O., *Journal of Materials Research* **1993,** *8* (05), 1179-1184.

4. Turner, S.; Matabayas, J., *Polymer–clay nanocomposites, John Wiley and Sons, Ltd, Chichester* **2000**, 207–225.

5. Katoch, S.; Kundu, P., *Journal of Applied Polymer Science 122*, 2731-2740.

6. Zahouily, K. B., S.; Bendaikha, T.; Baron, J.; and Decker, C. RadTech Eur, 2001; p 583.

7. Zahouily, K. D., C.; Benfarhi, S.; and Baron, J. Radtech: The Premier UV/EB Conference and Exhibition, Indiannapolis, IN, April 28 - May 1; Indiannapolis, IN, 2002; pp 309-320.

8. Decker, C.; Zahouily, K.; Keller, L.; Benfarhi, S.; Bendaikha, T.; Baron, J., *Journal of Materials Science* **2002,** *37* (22), 4831-4838.

9. Uhl, F. M.; Davuluri, S. P.; Wong, S.-C.; Webster, D. C., *Polymer* **2004,** *45* (18), 6175-6187.

10. Li, F.; Zhou, S.; Wu, L., *Journal of Applied Polymer Science* **2005,** *98* (5), 2274-2281.

11. Uhl, F. M.; Webster, D. C.; Davuluri, S. P.; Wong, S.-C., *European Polymer Journal* **2006,** *42* (10), 2596-2605.

12. Lee, C.; Hall, H. K., *Macromolecules* **1989,** *22* (1), 21-25.

13. Ravindran, N.; Vora, A.; Webster, D. C., *Journal of Coatings Technology and Research* **2006,** *3* (3), 213-219.

14. Ravindran, N.; Vora, A.; Webster, D. C., *Journal of Applied Polymer Science* **2007,** *105* (6), 3378-3390.

15. Kim, H. G.; Han, D. H.; Lim, J. C.; Oh, D. H.; Min, K. E., *Journal of Applied Polymer Science* **2006,** *101* (6), 3609-3615.

16. Curtis, L.; Edwards, D.; Simons, R.; Trent, P.; Von Bramer, P., *Industrial & Engineering Chemistry Product Research and Development* **1964,** *3* (3), 218-221.

17. Carothers, W. H.; Arvin, J. A., *Journal of the American Chemical Society* **1929,** *51* (8), 2560-2570.

18. Yang, Y. S.; Pascault, J. P., *Journal of Applied Polymer Science* **1997,** *64* (1), 133-145.

19. Tolga, A. Nanocomposites based on recycled poly(ethylene tetephthalate). Middle East Technical University, 2005.

20. Uhl, F. M.; Davuluri, S. P.; Wong, S.-C.; Webster, D. C., *Chemistry of Materials* **2004,** *16* (6), 1135-1142.

21. Morgan, A. B.; Gilman, J. W., *Journal of Applied Polymer Science* **2003,** *87* (8), 1329-1338.

22. Ishida, H.; Campbell, S.; Blackwell, J., *Chemistry of Materials* **2000,** *12* (5), 1260-1267.

23. Leterrier, Y., *Progress in Materials Science* **2003,** *48* (1), 1-55.

24. Yeun, J.-H.; Bang, G.-S.; Park, B. J.; Ham, S. K.; Chang, J.-H., *Journal of Applied Polymer Science* **2006,** *101* (1), 591-596.

25. Osman, M. A.; Mittal, V.; Morbidelli, M.; Suter, U. W., *Macromolecules* **2003,** *36* (26), 9851-9858.

26. George, S. C.; Thomas, S., *Progress in Polymer Science* **2001,** *26* (6), 985-1017.

27. Miyagawa, H.; Rich, M. J.; Drzal, L. T., *Polymer Composites* **2005,** *26* (1), 42-51.

28. Strawhecker, K.; Manias, E., *Chemistry of Materials* **2000,** *12*, 2943-2949.

CHAPTER 3. POLYMER-CLAY NANOCOMPOSITE PLASTICIZATION: ELUCIDATING THE INFLUENCE OF QUATERNARY ALKYLAMMONIUM ORGANIC MODIFIERS

3.1. Introduction

Organic modifiers provide crucial alterations to an unmodified layered silicate structure by increasing clay interlayer distance, providing functionality for polymerization reactions, lowering the surface energy of the silicate sheets, and improving the affinity between the clay and polymer. The volume fraction of the modified silicates will have a profound impact on the final properties of both polymeric materials and their coatings. Interestingly, increasing the clay volume fraction within a polymeric matrix has not always been shown to increase the mechanical or thermal properties of a coatings system. Miyagawa and coworkers reported an unexpected decrease in the glass transition temperature (T_g), determined from the maximum point of the tan δ curve from dynamic mechanical testing, of epoxy/clay nanocomposites with increased clay loading.[1] With increases in the clay volume fraction, the T_g decreased from 131 to 117°C instead of increasing, a trend commonly observed with increased clay content due to chain restriction. One explanation given for this phenomenon was the organic modifier, containing a long chain fatty alkyl amine, was thermally dissociated during polymerization. This dissociation would then allow the low molecular weight alkyl amine to act as a plasticizer. As the clay volume fraction was increased, the concentration of the organic modifier, and thus the alkyl amine, would also

increase. Therefore, the alkyl amine could potentially have plasticized the nanocomposite coating to a high enough extent that the T_g would decrease.

Shah and Paul explored the impact of organoclay degradation on melt processed polyethylene-clay nanocomposites with varying melt process temperatures.[2] Decreases in *d*-spacing from X-ray diffraction (XRD) analysis for the nanocomposites prepared at higher temperatures (180 – 200 °C) were observed, a phenomenon attributed to higher concentrations of alkylammonium surfactants leaving the clay interlayer. Continually, Cervantes et al. studied the thermal degradation of commercially-available organomodified clays using thermogravimetric analysis (TGA) coupled with Fourier transform infrared (FTIR) spectroscopy to study the evolved gases during clay thermal decomposition.[3] The thermal decomposition of the organomodified clays was attributed to different mechanisms, depending on the quaternary ammonium surfactant structure, including Hofmann eliminations, nucleophilic substitutions, tallow residue thermal degradation, and unexchanged quaternary ammonium surfactant thermal degradation.

Another instance of decreased T_g values with increased organoclay filler has been reported for polylactide-based nanocomposites.[4] Again, the unexpected trend was hypothesized to be a result of plasticization from the organic modification of the montmorillonite clay. Conversely, Fu et al.[5] and Kim et al.[6] have attributed this trend to the increased viscosity of the polymer system and the decreased polymer density around the silicate fillers, respectively. While the impact of organic modification of layered silicates has been widely shown to

influence several resin and material properties, the influence of the organic modifier, independent of the organomodified clay, has not yet been reported.

Previously, a novel in situ preparation technique to produce UV-curable nanocomposite barrier coatings has shown unexpected decreases in mechanical and thermal properties with increased clay loading (Chapter 2). To explore these unanticipated results, the goal of this study was to isolate the impact of alkylammonium ions used in layered silicate modification on the properties of the same polyester and coatings systems previously developed. By incorporating just the organic modifiers, without layered silicates, into the polyester resins, the impact of these modifiers on the final resin and film properties may be studied. The organic modifier concentrations used in this study were equivalent to the methyl tallow bis-2-hydroxyethyl quaternary ammonium (MTEtOH) concentration in Cloisite® 30B clay and cetyltrimethylammonium bromide (CTAB) concentration in the CTAB-modified Cloisite® Na^+ clay used in the previous study regarding the novel in situ preparation technique. The organic modifiers were once again dispersed by the in situ preparation technique and by a process of mixing and sonication. The impact of the organic composition and concentration on the resulting polyesters and their coatings were studied and compared to the clay-containing polyesters and nanocomposite coatings.

3.2. Experimental

3.2.1. Materials

The monomers maleic anhydride, 1,6-hexanediol, and diethylene glycol were purchased from Sigma Aldrich (Milwaukee, WI), and monomer 1,4-

cyclohexanedicarboxylic acid (1,4-CHDA) was obtained from Eastman Chemical Company (Kingsport, TN). Tri(ethylene glycol) divinyl ether (TEGDVE), the reactive diluent used for creating UV-curable films, was also purchased from Sigma Aldrich, as was the cetyltrimethylammonium bromide (CTAB) organic modifier and iodomethane. Photoinitiator Darocur® 1173, 2-hydroxy-2-methyl-1-phenyl-propan-1-one, was supplied from CIBA (Basel, Germany). Ethomeen T/12, a bis(2-hydroxyethyl) tallow alkyl amine, was generously supplied from AkzoNobel (Houston, TX).

3.2.2. Alkylammonium organic modifier preparation

The organic modifier of Cloisite® 30B, MTEtOH, was reproduced by a quaternization reaction of a tallow amine ethoxylate, similar to a procedure reported by Chen et al.[7] 10.00 g of Ethomeen T/12 was added to 79 mL of dimethylsulfoxide (DMSO) and 11.95 g of iodomethane. The solution was stirred at room temperature (23° C) for 16 hours, precipitated with ice-cold diethyl ether, filtered, and dried in a vacuum oven at 25°C. The CTAB organic modifier was used without further modification. Structures of the both alkylammonium organic modifiers are displayed in Figure 3.1.

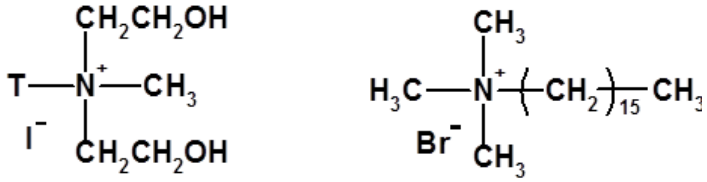

Figure 3.1: Structures of the Cloisite® 30B organic modifier (MTEtOH) and cetyltrimethylammonium bromide (CTAB), two common quaternary alkylammonium cations.

3.2.3. Organic modifier dispersion – In situ and sonication techniques

The concentrations of MTEtOH and CTAB were selected to be equivalent to the modifier concentrations of Cloisite® 30B and CTAB-modified clays used in the preceding study regarding the development of a novel in situ preparation technique. Thermogravimetric analysis (TGA) determined the organic modifier content of Cloisite® 30B and CTAB-modified Cloisite® Na^+ to be approximately 30 wt.% and 48 wt.%, respectively. These values were used to disperse the equivalent amount of organic modifier as would be found in the dispersion of 1, 2, 5, and 10 wt.% Cloisite® 30B and CTAB-modified Cloisite® Na^+ clays. For example, 1 wt.% Cloisite® 30B clay in the in situ preparation technique of clay dispersion is 1.20 g (≈ 120 g total monomer weight), so 30% of 1.20 g, or 0.36 g, was the organic modifier weight incorporated into the polyester resin to maintain equivalent organic modifier concentration to our previous study. The in situ technique was utilized to disperse the organic modifiers in the liquid monomer diethylene glycol prior to unsaturated polyester synthesis. Organic modifiers MTEtOH or CTAB were dispersed at high shear with diethylene glycol to achieve homogeneity, and then mixed overnight at room temperature with a magnetic stir bar. To examine the utility of this in situ technique, MTEtOH was also dispersed into the polyester resin through mixing and sonication to compare properties achieved.

3.2.4. Unsaturated polyester synthesis

The unsaturated polyesters were synthesized by standard melt polyesterification according to the composition previously reported in Chapter 2. Briefly, monomers maleic anhydride (1.000 mol), 1,6-hexanediol (0.625 mol), and

1,4-CHDA (0.172 mol) were combined with the diethylene glycol (0.824 mol)/organic modifier dispersion in a 250 mL 3-neck RBF equipped with mechanical stirrer, nitrogen inlet, temperature probe/controller, condenser, water collection flask, and heating mantle. The reaction mixture was ramped to 60, 120, and 180 °C, then stopped once an acid value of approximately 20 mg KOH/g of sample was achieved. With the sonication dispersion technique, the organic modifiers were dispersed in virgin polyester resin by mixing with a metal spatula, then placing each sample in an ultrasonic bath for eight hours. Polyester compositions are detailed in Table 3.1, where the MTEtOH and CTAB weights are based on the total monomer weight for the in situ preparation technique or based on 10 g of polyester for the mixing and sonication dispersion technique. The control polyester contained no organic modifier.

3.2.5. UV-curable coating preparation

UV-curable coatings were prepared by combining the unsaturated polyesters with the reactive diluent TEGDVE and Darocur® 1173. The polyester and TEGDVE were mixed in a 1:1 ratio based on reactive functional groups: maleate to vinyl ether. The photoinitiator was added based on 6 wt.% of the polyester, modifier, and reactive diluent. The coating formulations were hand mixed to achieve uniformity, then left undisturbed until air bubbles had dissipated. Next, these formulations were cast with a Gardco bar-coater onto glass and aluminum substrates with a five mil clearance. The cast formulations were subjected to UV-irradiation (Dymax 200 EC silver lamp (UV-A, 365 nm, intensity ≈

40 mW/cm^2) for 60 seconds to achieve tack-free films. Coatings were left undisturbed for 24 hours to allow for film equilibration.

3.2.6. Nomenclature

The names of the unsaturated polyesters (displayed in Table 3.1) were designated based on the organic modifier, the wt.% of the organic modifier, and the dispersion method (in situ or sonication technique). The polyester name is as follows: wt.% modifier (derived from the wt.% modifier on the modified clay samples)_type(MTEtOH or CTAB)_dispersion method(insitu or sonic). The prefix "Q" is used to distinguish the polyesters and coatings containing only the quaternary ammonium modifier, instead of the modified clay. "In situ" and "sonic" represent the in situ and sonication clay dispersion techniques.

TABLE 3.1
Unsaturated polyester composition containing alkylammonium organic modifiers

Polyester	Organic modifier	Organic modifier wt. (g)	Dispersion technique
Control	None	---	---
Q1_MTEtOH_insitu	MTEtOH	0.36	In situ
Q2_MTEtOH_insitu	MTEtOH	0.72	In situ
Q5_MTEtOH_insitu	MTEtOH	1.80	In situ
Q10_ MTEtOH _insitu	MTEtOH	3.60	In situ
Q1_ MTEtOH _sonic	MTEtOH	0.03	Mixing/sonication
Q2_ MTEtOH _sonic	MTEtOH	0.06	Mixing/sonication
Q5_MTEtOH _sonic	MTEtOH	0.15	Mixing/sonication
Q10_ MTEtOH _sonic	MTEtOH	0.30	Mixing/sonication
Q1_CTAB_insitu	CTAB	0.58	In situ
Q2_CTAB_insitu	CTAB	1.15	In situ
Q5_CTAB_insitu	CTAB	2.88	In situ

For example, Q1_MTEtOH_insitu describes a polyester containing 1 wt.% MTEtOH, the Cloisite® 30B organic modifier, dispersed through the in situ process.

Polyesters and coatings without the “Q” suffix refer to the unsaturated polyesters and coatings containing clay from our previous study and are shown for comparison of properties.

3.2.7. Characterization

Each unsaturated polyester was characterized to determine molecular weight, viscosity, T_g, and isomerization of the polyester backbone. The polyester molecular weight was determined using a Waters 2410 Gel Permeation Chromatograph equipped with a refractive index detector. Polyester samples were dissolved in tetrahydrofuan (THF) to produce a 1% sample solution. Calibration was performed with polystyrene standards, and the flow rate was 1 mL/minute. The viscosity measurements were performed with an ICI cone and plate viscometer at 100°C. The T_g of each polyester was determined from differential scanning calorimetry (DSC) using TA Instruments Q1000 Series DSC with a heat-cool-heat testing cycle. The polyester samples were equilibrated at -90 °C, heated to 100 °C at a rate of 10 °C/minute, cooled to -90 °C at a rate of 10 °C/minute, then heated once again to 100 °C at a rate of 10 °C/minute. The T_g was determined from the inflection point in the second heating scan. The percent isomerization observed from maleate to fumarate in the unsaturated polyester backbone was determined from ^{1}H nuclear magnetic resonance (NMR) spectroscopy using a JEOL ECA Series 400 MHz NMR spectrometer with procedure followed from Curtis et al.[8] Coatings derived from the unsaturated polyesters were cured by UV-irradiation with a Dymax 200 EC silver lamp (UV-A, 365 nm, intensity ≈ 40 mW/cm^2). The cure characteristics were determined by a Thermo Nicolet Magna-

IR 850 spectrometer with a detector type DTGS KBr to perform real-time IR measurements. The UV-radiation source was a LESCO Super Spot MK II UV-curing lamp equipped with a fiber-optic light guide for curing the samples. Each formulation was spin-coated at 3000 RPM onto a KBr window before being placed in the spectrometer chamber, approximately 20 mm from the end of the fiber-optic cable with a 10 mW/cm^2 light intensity. The samples were subjected to UV and IR irradiation simultaneously. The degree of conversion was calculated based on the disappearance of the vinyl ether double bonds. The conversion was calculated from equation 3.1 where $(A_{1639})_0$ is the absorbance at time=0 and $(A_{1639})_t$ is the absorbance at time=t.

$$\% \, conversion = \{[(A_{1639})_0 - (A_{1639})_t]/(A_{1639})_0\} \times 100 \qquad (3.1)$$

Dynamic mechanical thermal analysis (DMTA) was performed using a TA Instruments Q800 Dynamic Mechanical Analyzer to examine the dynamic mechanical properties of each coating. Free films of the cured coatings were removed from a glass substrate, and cut to dimensions of approximately 15 mm x 5 mm x 0.070 – 0.080 mm thickness. These films were characterized using 1 Hz frequency, a constant strain of 0.05%, a heating rate of 5 °C/minute over a temperature range of -50 °C to 150 °C. The organic modifier wt.% and the coating thermal stability was tested using thermogravimetric analysis (TGA) with a TA Instruments Q500 Thermogravimetric Analyzer. Samples were heated in a nitrogen atmosphere from 25 °C to 800 °C at a rate of 20 °C/minute. The optical clarity of the coatings was examined with a Varian Cary 5000 UV-Vis Spectrometer by determining transmittance at 400 nm.

3.3. Results and discussion

3.3.1. Unsaturated polyester characterization

The development of a novel in situ preparation technique to create highly dispersed clays in a precursor oligomer prior to the formation of UV-curable nanocomposite coatings was reported in Chapter 2. During the characterization of these nanocomposites, several coatings properties reached a maximum, but then decreased or diminished with higher clay concentrations (5-10 wt.%). For example, the storage modulus, degradation temperature, and film hardness increased with the addition of 1-2 wt.% clay, but higher levels of clay led to decreases in these properties. One possible explanation for this phenomenon is the organic modifier of the layered silicate may plasticize the precursor oligomer and coating. When the clay content increases, the organic modifier concentration will also increase, leading to a greater degree of plasticization. Additional theories have also been considered, including decreased polymer density surrounding the clay fillers and increased polymer viscosity. With this study, impact of layered silicate organic modifiers on both polyester and coating properties was explored by synthesizing unsaturated polyester resins in the presence of MTEtOH and CTAB to isolate the impact of each organic modifier. Throughout the discussion of results, the properties obtained from both the clay-containing unsaturated polyesters and UV-curable nanocomposites from our previous study will be shown for comparison.

The characterization of the organic modifier-containing unsaturated polyesters was critical to understanding the impact of the organic modification on

the final coating properties. Table 3.2 contains a summary of the unsaturated polyester properties.

TABLE 3.2
Properties of unsaturated polyesters dispersed with alkylammonium organic modifiers

Polyester	Acid value	M_n (g/mol)	M_w (g/mol)	PDI	Viscosity (Poise)	T_g (°C)	% Fumarate
Control	21	1100	2400	1.9	2.4	-42	33
Q1_ MTEtOH _insitu	21	1100	2400	1.9	1.2	-41	37
Q2_ MTEtOH _insitu	22	1300	2900	1.9	1.8	-40	40
Q5_ MTEtOH _insitu	21	1500	2800	1.9	3.4	-38	37
Q10_ MTEtOH _insitu	22	1700	3400	2.0	6.4	-37	42
Q1_ MTEtOH _sonic	21	1300	2400	1.8	1.4	-43	35
Q2_ MTEtOH _sonic	21	1300	2400	1.8	1.8	-45	34
Q5_ MTEtOH _sonic	21	1300	2400	1.8	1.8	-45	34
Q10_ MTEtOH _sonic	21	1300	2400	1.8	1.8	-49	38
Q1_CTAB_insitu	20	1500	3000	2.0	3.2	-39	50
Q2_CTAB_insitu	21	1300	2700	2.1	3.2	-39	59
Q5_CTAB_insitu	22	2800	4200	1.5	7.0	-34	57
1_30B_insitu[1]	21	1800	3500	1.9	3.3	-36	46
2_30B_insitu	22	1500	3800	2.5	5.4	-39	39
5_30B_insitu	21	1800	3900	2.2	5.8	-41	41
10_30B_insitu	21	4000	7300	1.8	8.8	-43	64
1_30B_sonic	21	1900	3600	1.9	3.5	-37	19
2_30B_sonic	21	2000	3600	1.8	3.7	-37	17
5_30B_sonic	21	1400	3500	2.4	4.8	-41	24
10_30B_sonic	21	1900	3800	2.0	5.4	-42	18
1_CTAB_insitu	20	2800	6900	2.4	6.0	-32	53
2_CTAB_insitu	21	2400	4700	2.0	6.5	-33	62
5_CTAB_insitu	22	1800	4800	2.7	7.3	-36	52

[1]This data and following are reported in Chapter 2.

In accordance with Chapter 2, the two organic modifiers were incorporated into the polyester during polyesterification through the in situ technique as well as after polyester synthesis via sonicating the organic modifier with a control polyester resin. With each polyester resin, the target acid number was 20 mg of KOH/g of polyester. Careful monitoring of the acid number was important to ensure similar

acid number values; therefore, comparable degrees of polymerization were maintained.[9]

GPC was used to examine the molecular weight and polydispersity index (PDI) for the organic modifier-containing polyester resins. The M_n and M_w values obtained for each polyester were less than the molecular weights recorded for the clay-containing polyester counterpart. Whereas increased clay weight led to large increases in polyester molecular weight, increasing the organic modifier concentration produced only slightly larger molecular weight values. The introduction of the MTEtOH organic modifier to a polyester resin via sonication did not change the molecular weight; each polyester sample had a M_n value of 1,300 g/mol and a M_w value of 2,400 g/mol. With the in situ preparation technique, slight increases in the molecular weight values were observed; however, the organic modifier did not affect the molecular weight or polydispersity to the degree observed with the clay-containing polyesters. Without the addition of the clay fillers into the polyester resin, the hydrodynamic volume of the polyester oligomers was rather consistent. Lower PDI values were observed with the organic modifier-containing polyesters (1.8 – 2.1) compared to the clay-containing polyesters (1.8 – 2.7).

The viscosities of the organic modifier-containing polyesters were lower than the control polyester at lower loadings (1 – 2 wt.%) of the organic modifiers. Q1_MTEtOH_insitu, Q2_MTEtOH_insitu, and the polyesters prepared through sonication had viscosities ranging from 1.2 – 1.8 Poise whereas the control polyester viscosity was 2.4 Poise. This trend demonstrates the effect of the organic

modifier of the polyester oligomers where even small additions of the organic modifier can affect the polyester properties. Since the molecular weights of these polyesters were comparable to the control polyester, the introduction of the organic modifier may be reducing the viscosity due to plasticization of the polyester oligomers.

Once the organic modifier concentration was increased to the 5 – 10 wt.% range, the viscosities of Q5_MTEtOH_insitu and Q10_ MTEtOH_insitu were increased to 3.4 and 6.4 Poise, respectively, but still remained lower than their clay-containing counterparts. The polyesters containing the CTAB modifier also showed slight increases in viscosity, ranging from 3.2 to 7.0 Poise. The viscosity increases may be attributed to the higher molecular weights for these polyester oligomers. With increases in the polyester oligomer molecular weight, increased chain entanglement may occur; therefore, the viscosity of the polyester resins may increase with higher clay loading.

The organic modifier did not affect the glass transition temperature (T_g) of each polyester to the extent of the molecular weights and viscosities, but small variations were observed. The sonication dispersion technique produced organic modifier-containing polyesters with T_g values slightly lower (1 – 7 °C) than the control polyester, possibly a sign of oligomer plasticization. The in situ preparation technique, conversely, resulted in the T_g values slightly higher (1 – 8 °C). Higher concentrations of the organic modifier resulted in more significant changes to the T_g. Both Q10_MTEtOH _sonic (T_g = -49 °C) and Q5_CTAB_insitu (T_g = -34 °C) had T_g values ranging further from the control polyester (T_g = -42 °C).

Unlike the clay-containing unsaturated polyesters, the MTEtOH organic modifier did not greatly impact the final maleate-fumarate isomerization of the polyester backbone. Only the polyesters with higher concentrations of the MTEtOH organic modifier demonstrated more significant increases in the isomerization from maleate to fumarate isomers. For example, the fumarate content for Q10_MTEtOH_insitu was 42%, about 10% higher than the control polyester. Without the steric hindrance from the clay fillers, the hydroxy-functional monomers may have exhibited less preference to react with the trans isomer.[8, 10] Polyesters dispersed with the CTAB organic modifier had higher degrees of maleate-fumarate isomerization, ranging from 50 – 59% fumarate isomers. Once again, higher percentages of fumarate isomers with the CTAB-modified polyester systems may be a consequence of higher resin viscosity.

3.3.2. Cure characteristics – Real-time infrared spectroscopy

The final conversion of the UV-curable coatings derived from the organic modifier- containing polyesters had a direct correlation to the polyester viscosity. The extent of the reaction was characterized by monitoring the disappearance of the vinyl ether double bond (1639 cm^{-1}) from the reactive diluent TEGDVE (values reported in Table 3.3). Disappearance of this vinyl ether double bond indicated the degree of conversion of the maleate-vinyl ether coatings system. The coating formulations containing polyesters with viscosities similar to the control formulation had comparable conversions. Figure 3.2 displays RTIR curves representing the difference in conversion of the higher viscosity clay-containing polyesters and the lower viscosity MTEtOH-containing polyesters.

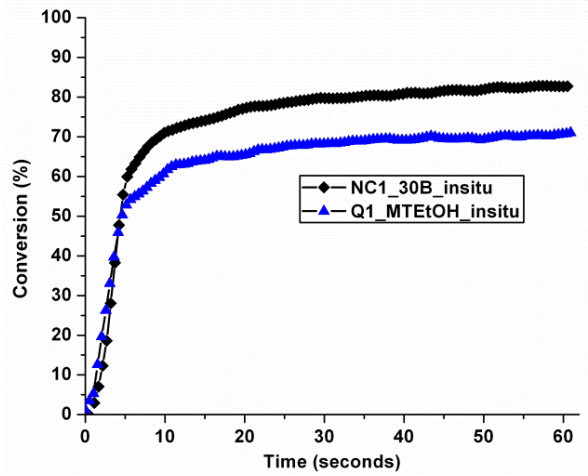

(a)

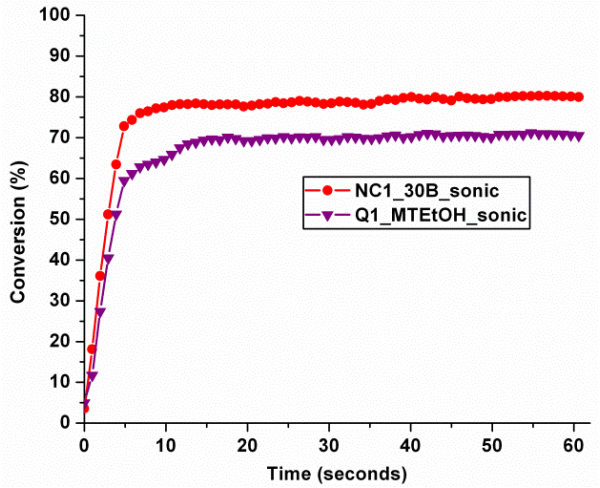

(b)

Figure 3.2: Real-time infrared spectroscopy conversion of 1 wt.% clay and MTEtOH-containing formulations prepared through (a) the in situ synthesis technique and (b) the mixing and sonication dispersion route after 60 seconds of UV-exposure.

As discussed previously, the polyesters Q1_MTEtOH_insitu, Q2_MTEtOH_insitu, and polyesters prepared with sonication had viscosities similar to the control polyester resin. Each coatings system derived from these low viscosity polyesters had comparable conversions (69 – 73 %) to the control coatings system (72%). The more viscous Q5_MTEtOH_insitu,

Q10_MTEtOH_insitu, and the CTAB-organic modifier polyesters also possessed higher conversions (78 – 80 %). This same trend was observed with clay-containing polyesters: higher viscosity resins produced a higher degree of double bond conversion.

TABLE 3.3
UV-curable coating cure, mechanical, thermal, and optical properties characterization data

Coating Name	Conver-sion	*E'* (MPa,25°C)	XLD (mol/cm^3)	T_{10}% (°C)	Transmit-tance (%)
Control	72%	370	0.022	240	98
Q1_MTEtOH_insitu	69%	440	0.019	300	96
Q2_ MTEtOH _insitu	73%	530	0.031	305	98
Q5_ MTEtOH _insitu	80%	285	0.026	305	99
Q10_ MTEtOH _insitu	78%	280	0.011	300	97
Q1_ MTEtOH _sonic	70%	240	0.011	300	99
Q2_ MTEtOH _sonic	73%	340	0.022	300	97
Q5_ MTEtOH _sonic	73%	320	0.016	265	99
Q10_MTEtOH _sonic	72%	280	0.010	250	93
Q1_ CTAB_insitu	77%	730	0.030	305	95
Q2_CTAB_insitu	79%	790	0.031	290	94
Q5_CTAB_insitu	77%	780	0.029	295	94
NC1_30B_insitu[1]	80%	890	0.041	255	94
NC2_30B_insitu	81%	1020	0.042	245	92
NC5_30B_insitu	80%	1250	0.086	250	85
NC10_30B_insitu	83%	1500	0.033	230	84
NC1_30B_sonic	79%	810	0.017	270	95
NC2_30B_sonic	87%	910	0.014	290	95
NC5_30B_sonic	87%	625	0.024	300	82
NC10_30B_sonic	77%	390	0.015	280	62
NC1_CTAB_insitu	83%	610	0.023	270	98
NC2_CTAB_insitu	80%	495	0.016	280	98
NC5_CTAB_insitu	80%	340	0.014	260	97

[1]This data and following are reported in Chapter 2.

Higher viscosity coatings formulations may exhibit decreased rates of termination, a consequence of reactive chain ends difficulty to diffuse through the system, leading to an autoacceleration effect. The clay-containing polyesters prepared by both the in situ preparation and the mixing-sonication techniques

measured higher conversions than the polyesters prepared with just the organic modifiers. The higher conversion of the clay-containing polyesters directly correlates to the higher viscosity polyester resins from clay inclusion within the oligomeric network; therefore, the conversion of these coatings systems appears to be dependent on the viscosity of the precursor polyester resin. The higher viscosity polyesters containing the CTAB organic modifier demonstrated conversions similar to that of the CTAB-modified clay containing polyesters.

3.3.3. Mechanical properties – Dynamic mechanical analysis

The viscoelastic properties of the UV-curable coatings were influenced by the concentration of the MTEtOH and CTAB organic modifiers, as seen in the results obtained from dynamic mechanical analysis (DMA). A summary of these mechanical properties are compiled in Table 3.3 and shown in Figure 3.3. The coatings containing Q1_MTEtOH_insitu and Q2_MTEtOH_insitu had higher storage moduli than the control coating with values of 440 and 530 MPa, respectively. In contrast, the alternative MTEtOH-containing coatings had lower storage moduli than the control coating (240 – 240 MPa).The decreased storage moduli of the MTEtOH-containing coatings demonstrate the impact of the organic modifier on coating mechanical properties. In our previous study, we reported decreases in the storage modulus of nanocomposite coatings with 5 – 10 wt.% organically modified clays (these results are also reported in Table 3.3), a trend that is repeated with the organic modifier-containing coatings. From these trends, the organic modifier appears to be prominently affecting the final mechanical performance of these coatings.

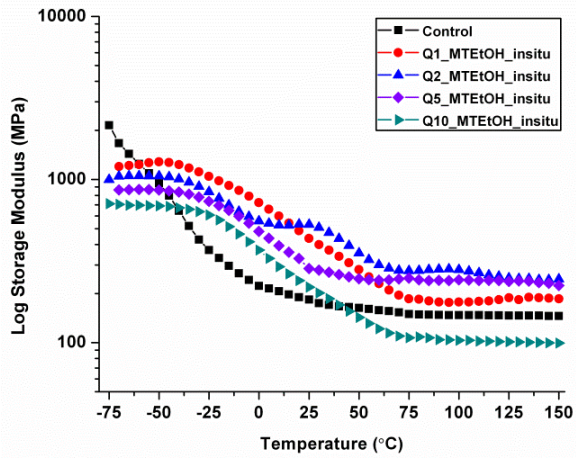

(a)

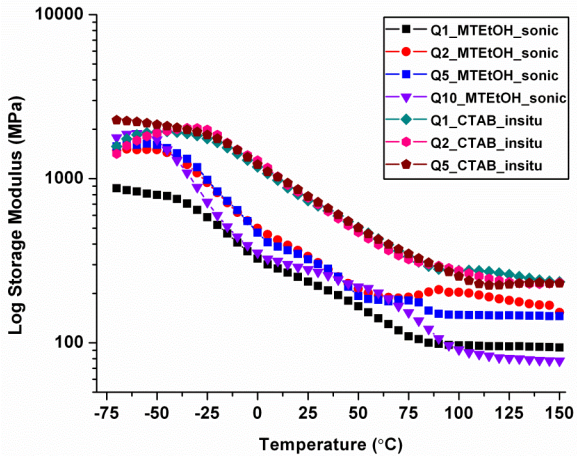

(b)

Figure 3.3: DMA storage modulus plots for (a) in situ preparation MTEtOH-containing coatings and (b) sonication MTEtOH-containing coatings and in situ preparation CTAB-containing coatings.

One possible explanation of the reduction in storage modulus values is the composition of the organic modifier itself. The decreases in mechanical performance of coatings containing Cloisite® 30B clay and the MTEtOH organic modifier at higher concentrations (5 – 10 wt.%) may be a result of plasticization and decreased crosslink density. While the incorporation of 1 – 2 wt.% Cloisite® 30B organic modifier did not significantly affect the storage moduli and crosslink densities, the coatings containing 5 – 10 wt.% Cloisite® 30B organic modifier had

lower storage moduli and crosslink densities compared to the control coating. Coatings Q5_MTEtOH_insitu and Q10_MTEtOH_insitu had storage moduli of 285 and 280 MPa, respectively, which was approximately 100 MPa lower than the control coating (370 MPa). The crosslink density of Q5_MTEtOH_insitu (0.026 mol/cm^3) was similar to the control coating, but the crosslink density of Q10_MTEtOH_insitu was reduced by 50% (0.011 mol/cm^3). Decreases in storage moduli and crosslink density were also observed in the coatings containing polyesters prepared through sonication of the MTEtOH; the storage moduli of each coating was 30 – 130 MPa lower than the control coating. From these results, it is apparent that increasing the MTEtOH organic modifier content decreased the mechanical performance of these coatings. These trends may reflect the decreased storage moduli and crosslink density observed in the nanocomposite samples containing higher concentrations of Cloisite® 30B clay.

Conversely, the coatings containing the CTAB-organic modifier had storage moduli ranging from 730 – 790 MPA, approximately 400 MPa greater than the control coating, as well as higher crosslink densities (0.029 – 0.031 mol/cm^3). These trends may further reinforce the theory of Cloisite® 30B plasticization from MTEtOH as the CTAB organic modifier did not diminish the coating mechanical properties, unlike MTEtOH. However, the nanocomposite coatings containing the CTAB-modified clay had decreased storage moduli and crosslink density with the increased clay loading. As the organic modifier does not appear to be influencing the mechanical performance of the coatings, another explanation may be the inability of the coatings system to adequately surround the clay with higher silicate

volume fractions. High clay volume fractions may hinder adequate polymer/clay dispersion, diminishing the reinforcing nature of the clay fillers on the nanoscale.

Figure 3.4 displays a representative example of the differences observed in the loss factor (tan δ) of the coatings containing MTEtOH compared to the nanocomposite films. The tan δ of each film was broad and bimodal, indicating multiple dampening mechanisms are present within the films containing the Cloisite® 30B clay as well as the MTEtOH organic modifier. The tan δ plot for the nanocomposite film NCR1_30B_insitu was less pronounced and had peaks shifted to higher temperatures than the control and Q1_MTEtOH_insitu films. The less pronounced loss factor peaks may be a result of the restricted mobility from the incorporation of the rigid organomodified montmorillonite clay.[11] In contrast, the tan δ plot of Q1_MTEtOH_insitu had loss factor peaks were shifted to lower temperatures and were much more pronounced, another indication of the possible plasticization of the MTEtOH organic modifier on the polyester film.

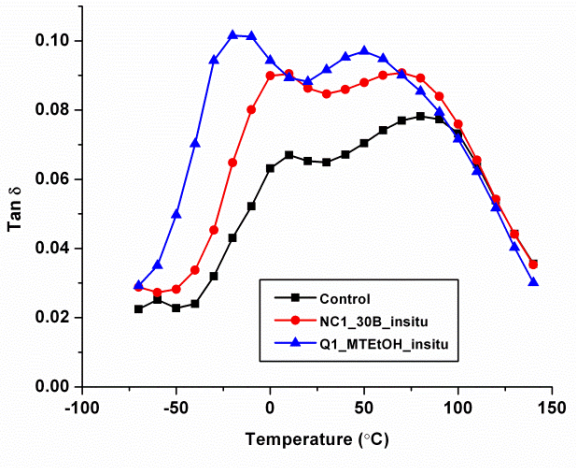

Figure 3.4: Representative tan δ plots from dynamic mechanical analysis demonstrating the impact of the MTEtOH quaternary alkylammonium organic modifiers on mechanical properties.

3.3.4. Thermal stability and optical clarity – Thermogravimetric analysis and UV-visible spectroscopy

The MTEtOH and CTAB organic modifiers did not influence the thermal stability of the coatings systems to the same extent as the mechanical properties. The TGA degradation curves are displayed in Figure 3.5, and the temperature at 10% weight loss (T_{10}%) is reported in Table 3.3.

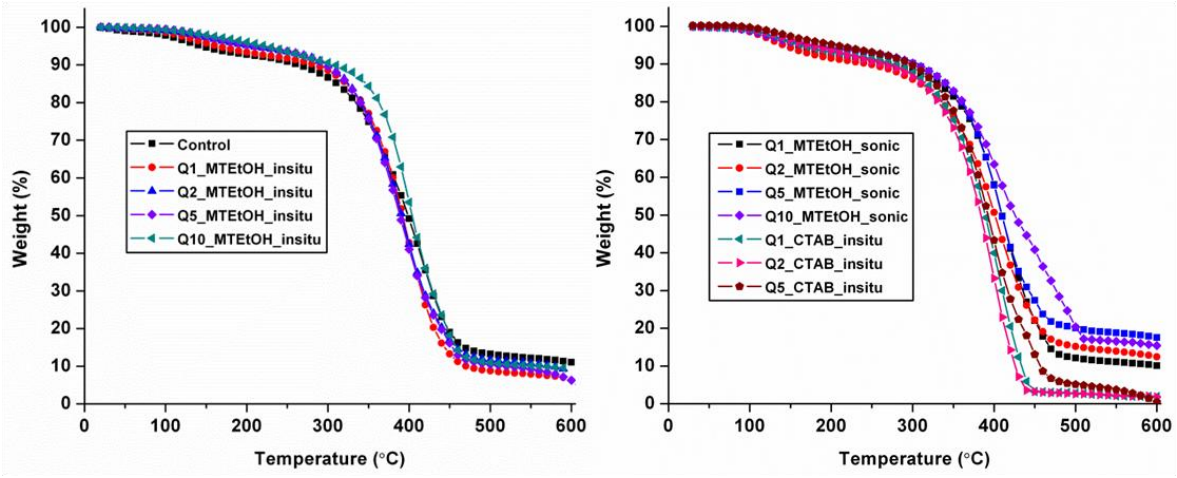

(a) **(b)**

Figure 3.5: TGA degradation curves for (a) in situ preparation MTEtOH-containing coatings and (b) sonication MTEtOH-containing coatings and in situ preparation CTAB-containing coatings.

Each MTEtOH-containing and CTA-containing coating had a T_{10}% at approximately 300 °C, except for Q5_MTEtOH_sonic and Q10_MTEtOH_sonic. These two coatings had noticeable decreases in T_{10}%, up to 50 °C. Again, once the higher concentrations of MTEtOH were incorporated into the coating, diminishing thermal stability was observed. Comparisons of the nanocomposite degradation temperature to the organic modifier-containing coating of equivalent organic modifier concentration did not demonstrate any significant decreases in

thermal stability. From this thermogravimetric analysis, the organic modifier does not appear to greatly impact the thermal stability of these coatings systems.

Coating optical clarity was not affected by the incorporating the MTEtOH and CTAB organic modifiers into polyester resins (Table 3.3). With the clay-containing nanocomposites, significant decreases in the transmittance were observed with 5 – 10 wt.% clay loading, a trend not repeated with the organic modifier-containing coatings. The transmittance values of the organic modifier-containing coatings ranged from 93 – 99%. Neither the MTEtOH nor CTAB organic modifier decreased the optical clarity of these coatings. Therefore, the decreases in the optical clarity observed with the nanocomposite samples may be a direct result of the distribution of nanoclays within the coating, where less dispersed silicates diminished the transmittance of the nanocomposite films.

3.4. Conclusions

The structure and concentration of layered silicate alkylammonium organic modifiers MTEtOH and CTAB had a significant impact on both polyester resin and coating properties. MTEtOH-containing polyester molecular weight, viscosity, and T_g were all lower than their Cloisite® 30B clay-containing polyester counterpart regardless of organic modifier dispersion technique. These low viscosity systems directly influenced the overall conversion of the UV-curable coatings systems, where the final conversion was approximately equivalent to the control coating. The higher viscosity CTAB-containing polyesters produced higher conversions. Coatings prepared from the MTEtOH-containing polyesters demonstrated profound decreases in the mechanical performance, particularly storage moduli and

crosslink density at high organic modifier concentrations (5 – 10 wt.%). As similar trends in mechanical performance were observed in our previous studies with 5 – 10 wt.% Cloisite® 30B clay, there seems to be a viable contribution of the MTEtOH structure and concentration to the final coating properties. Although coating mechanical properties were greatly affected by the organic modifiers, thermal stability and optical clarity of the coatings were relatively unaffected. This study demonstrates the impact of the organic modifier, without silicate filler, on the properties of polymer and coatings systems in which they are incorporated.

3.5. References

1. Miyagawa, H.; Rich, M. J.; Drzal, L. T., *Polymer Composites* **2005,** *26* (1), 42-51.

2. Shah, R. K.; Paul, D. R., *Polymer* **2006,** *47* (11), 4075-4084.

3. Cervantes-Uc, J. M.; Cauich-Rodríguez, J. V.; Vázquez-Torres, H.; Garfias-Mesías, L. F.; Paul, D. R., *Thermochimica Acta* **2007,** *457* (1-2), 92-102.

4. Pluta, M.; Jeszka, J.; Boiteux, G., *European Polymer Journal* **2007,** *43* (7), 2819-2835.

5. Fu, X.; Qutubuddin, S., *Polymer* **2001,** *42* (2), 807-813.

6. Kim, H. J.; Hwang, S. H.; Kim, J.; Huh, W.; Lee, S. W., *Journal Of Korean Industrial and Engineering Chemistry* **2004,** *15* (5), 533-536.

7. Chen, Z.; Yang, G.; Zhang, Z., *Synthetic Communications* **2003,** *33* (5), 729-734.

8. Curtis, L.; Edwards, D.; Simons, R.; Trent, P.; Von Bramer, P., *Industrial & Engineering Chemistry Product Research and Development* **1964,** *3* (3), 218-221.

9. Carothers, W. H.; Arvin, J. A., *Journal of the American Chemical Society* **1929,** *51* (8), 2560-2570.

10. Yang, Y. S.; Pascault, J. P., *Journal of Applied Polymer Science* **1997,** *64* (1), 133-145.

11. Liu, M.; Guo, B.; Du, M.; Lei, Y.; Jia, D., *Journal of Polymer Research* **2008,** *15* (3), 205-212.

CHAPTER 4. NOVEL POLYMER-CLAY NANOCOMPOSITE PREPARATION TECHNIQUE USING "REVERSE" IN SITU INTERCALATIVE POLYMERIZATION PROCESS

4.1. Introduction

Phase-separation caused by clay and polymer immiscibility typically leads to poor physical properties, such as decreases in mechanical performance and thermal stability.[1] Organic modification of hydrophilic clay surfaces may be utilized to increase the organophilicity of the inorganic fillers. Commonly, quaternary ammonium cationic surfactants are used to lower the clay surface energy and help render the clay organophilic.[2] Yang et al. reported the final dispersion of organically-modified montmorillonite clay in polyimide hybrids was enhanced depending on the chemical structure of the organic modifier.[3] Higher dispersion of the modified montmorillonite improved several hybrid properties, including decreased thermal expansion coefficient and increased thermal stability. Dasari et al. studied the wear properties of nylon 6 composites containing both organically modified and pristine clay.[4] From this study, the organomodified clay produced nanocomposites with superior wear-performance compared to the nylon 6-pristine clay composites due primarily to increased dispersion and higher interfacial interaction between the clay layers and nylon 6. Several authors have also reported the importance of organic modification of montmorillonite clay to achieve greater clay dispersion.[5-8] Utilization of in situ type polymerizations to intercalate or exfoliate layered silicates has been studied in a large variety of polymers with

various organic modifications. Messersmith and Giannelis studied the initiation and propagation mechanisms during the intercalation of layered silicates through in situ intercalative polymerization of ε-caprolactone.[9] The interlayer cation proved to be vital in the success of the ring-opening polymerization, where Cr^{3+}-modified fluorohectorite appeared to catalyze the polymerization reaction unlike Cu^{2+}, Co^{2+}, and Na^{+}. To further induce the delamination of montmorillonite, Paul et al. utilized organic modifiers bearing hydroxy-groups to graft poly(L,L-lactide) to the modified clays to create exfoliated nanocomposites via ring-opening in situ intercalative polymerization.[10] Exfoliated poly(ε-caprolactone) nanocomposites were also prepared with hydroxy-functional alkylammonium organic modifiers by first activating the hydroxy groups with tin (IV) dialkoxide, which in turn initiated the in situ intercalative lactone polymerization.[11] Through this in situ technique, nanocomposites with increased thermal stability were obtained compared to unmodified clay-containing nanocomposites. Apart from polyesters, similar in situ intercalative polymerization research utilizing hydroxy-functional organic modifiers have been reported in the production of several polymer-clay nanocomposite systems including polyethers[12], polyurethanes[13-14], phenolic resins[15], and acrylic resins[16].

Previously, the development of UV-curable polyester nanocomposite films through a novel in situ preparation technique was reported in Chapter 2. Liquid monomer diethylene glycol and Cloisite® 30B, a commercially-available hydroxy-functional montmorillonite clay, were dispersed at high shear, followed by synthesis of unsaturated polyester resins containing 1 – 10 wt.% clay. UV-curable

nanocomposite films were formed utilizing donor-acceptor chemistry to produce intercalated and exfoliated coatings with increased conversion, water vapor barrier protection, and mechanical performance. Particularly, coatings containing 1 – 2 wt.% Cloisite® 30B produced exfoliated nanocomposites, whereas higher clay loading (5 – 10 wt.%) led to primarily intercalated morphologies. To elucidate the influence of the Cloisite® 30B organic modifier on the UV-curable film properties, the impact of the alkylammonium organic modifier MTEtOH by modifying the novel in situ process previously developed by synthesis polyesters in the presence of only the MTEtOH modifier, without montmorillonite clay, was investigated in Chapter 3. Higher levels of MTEtOH loading diminished both mechanical and thermal properties, suggesting possible plasticization of the MTEtOH organic modifier on the polyester resin.

Based on the success of obtaining high clay dispersion in a precursor resin with the in situ polymerization technique, this study explored a novel in situ technique to further increase clay dispersion. Typically, in situ intercalative polymerizations involve creating a precursor dispersion of organomodified clay and monomer, followed by polymerization to induce delamination of the clay platelets by the increased volume of the polymer chains between clay platelets. In stark contrast, this novel “reverse” in situ polymerization technique is characterized by the addition of unmodified montmorillonite clay *during* polyesterification to a reaction mixture already containing MTEtOH, the hydroxy-functional alkylammonium organic modifier of Cloisite® 30B. Through this process, the unmodified clay may undergo an in situ ion exchange reaction with the alkylammonium surfactant, and

disperse uniformly throughout the polyester resin. A unique feature of this novel in situ intercalative polymerization is the simultaneous polyesterification and ion exchange reaction between the MTEtOH organic modifier and unmodified Cloisite® Na^+ clay. By using this reverse in situ polymerization process, the goal is to disrupt the clay order and produce highly dispersed clays in the precursor polyester. The reverse in situ technique was compared to a clay dispersion technique of mixing and sonication to study the impact of the dispersion route.

4.2. Experimental

4.2.1. Materials

Monomers 1,6-hexanediol, maleic anhydride, and diethylene glycol were obtained from Sigma Aldrich (Milwaukee, WI) along with reactive diluent tri(ethylene glycol) divinyl ether and iodomethane. Monomer 1,4-cyclohexanedicarboxylic acid was obtained from Eastman Chemical Company (Kingsport, TN). The photoinitiator Darocur® 1173, 2-hydroxy-2-methyl-1-phenyl-propan-1-one, was obtained from CIBA (Basel, Germany). Ethomeen T/12, a bis(2-hydroxyethyl) tallow alkyl amine, was generously supplied from AkzoNobel (Houston, TX). Cloisite® Na^+, a naturally-occurring montmorillonite clay, was obtained from Southern Clay Products (Gonzales, TX). All reagents were used as received without further purification.

4.2.2. Organic modifier preparation

The procedure for the preparation of MTEtOH, the organic modifier of Cloisite® 30B, has been reported earlier in Chapter 3. Briefly, Ethomeen T/12

(10.00 g) was quaternized with iodomethane (11.95 g) in dimethylsulfoxide at 23 °C, precipitated, and dried in a vacuum oven at room temperature.

4.2.3. "Reverse" in situ intercalative polymerization technique

The unsaturated polyester resins were synthesized from a modification to a standard melt polyesterification process to create a "reverse" in situ intercalative polymerization technique. First, liquid monomer diethylene glycol and MTEtOH were homogenized at high shear, then mixed overnight via magnetic stir bar. The monomer-organic modifier solution was weighed with the remaining monomers and added to a 250 mL 3-neck RBF equipped with a temperature probe/controller, mechanical stirrer, nitrogen inlet, condenser, heating mantle, and water collection flask according to the previous study in Chapter 2. The monomer composition was constant for each polyesterification (moles indicated in parentheses): maleic anhydride (1.000), diethylene glycol (0.824), 1,6-hexanediol (0.625), and 1,4-CHDA (0.172). The reaction mixture was carefully ramped to 60, 120, and 180 °C under a N_2 atmosphere to prevent side reactions such as oxidation of double bonds. When the reaction mixture stabilized at 120 °C, the unmodified Cloisite® Na^+ was added to the reaction flask. The polyester polymerization continued until an acid number of approximately 20 mg KOH/gram of resin was achieved, as determined by titration. The MTEtOH and Cloisite® Na^+ weights were based on the Cloisite® 30B clay organic modifier content (30 wt.%), and the desired clay loading in the final nanocomposite (1, 2, 5, and 10 wt.%). For example, 1 wt.% Cloisite® 30B clay with this in situ process would be 1.20 g (based on ≈ 120 g of monomer). Therefore, 0.36 g of MTEtOH and 0.84 g of Cloisite® Na^+ was used to

achieve organically-modified clay loading similar to the loading of Cloisite® 30B clay.

4.2.4. Sonication dispersion technique

With the sonication dispersion route, unsaturated polyesters were synthesized as described in Section 4.2.3, but the unmodified clay was not added during the polyesterification reaction. Instead, Cloisite® Na^+ was added to the polyester resin after polymerization, mixed to uniformity, and sonicated for eight hours with an ultrasonic bath. Again, the desired clay loading for this technique was 1, 2, 5, and 10 wt.%.

4.2.5. UV-curable nanocomposite coating preparation

Nanocomposite coatings were formulated based on a 1:1 stoichiometric ratio between the maleate and vinyl ether functional groups from the unsaturated polyester and TEGDVE, respectively. Photoinitator Darocur® 1173, 2-hydroxy-2-methyl-1-phenyl-propan-1-one, was added to the unsaturated polyester and reactive diluent mixture based on 6 wt.% of the polyester, diluent, and clay weight. The formulation was mixed to uniformity with a hand spatula, left undisturbed for 1-2 hours for air bubble dissipation, and then deposited onto glass and aluminum substrates with a Gardco bar-coater with five mil wet clearance (final film thickness ≈ 85 μm). The coated substrates were subjected to UV-irradiation (Dymax 200 EC silver lamp, UV-A, 365 nm, intensity ≈ 40 mW/cm^2) until the nanocomposite coatings were tack-free (approximately 60 seconds). The films were allowed to equilibrate for 24 hours at room temperature before testing.

4.2.6. Nomenclature

The unsaturated polyesters were named based on the wt.% organically-modified clay and the clay dispersion technique. The polyester name is as follows: wt.% MTEtOH-modified clay_dispersion method. For example, R1_insitu denotes the polyester containing 1 wt.% MTEtOH-modified clay prepared through the reverse in situ technique. The prefix “R” is used to distinguish the reverse in situ or sonication clay dispersion route was utilized in this study. The coatings were named similarly, but have a “NC” prefix to specify the nanocomposite derived from a particular polyester.

4.2.7. Characterization

The polyester resin molecular weight, viscosity, glass transition temperature (T_g), and backbone isomerization were characterized prior to film formation. Molecular weight was determined using a Waters 2410 Gel Permeation Chromatograph equipped with a refractive index detector. A 1% sample solution was created by dissolving the polymer sample in solvent tetrahydrofuran (THF). The flow rate was 1 mL/min, and calibration was performed with polystyrene standards. The polyester viscosity was determined from an ICI cone and plate viscometer at 100 °C. Differential scanning calorimetry was employed to measure the polyester T_g using a TA Instruments Q1000 Series DSC. The heat-cool-heat test method was applied, where polyester samples were first equilibrated at -90 °C, heated to 100 °C at a rate of 10 °C/min, cooled to -90 °C at a rate of 10 °C/min, then heated once again to 100 °C at a rate of 10 °C/min. The polyester T_g was determined from the inflection point in the second heating cycle. Maleate-fumarate

isomerization of the polyester backbones were determined from ^{1}H nuclear magnetic resonance (NMR) spectroscopy using a JEOL ECA Series 400 MHz NMR spectrometer using a procedure from Curtis et al.[17]

Real-time infrared spectroscopy measurements were performed using a Thermo Nicolet Magna-IR 850 spectrometer with detector type DTGS KBr to study cure characteristics of the nanocomposite systems. The UV-irradation source for curing the samples was a LESCO Super Spot MK II UV-curing lamp equipped with a fiber-optic light guide. Each nanocomposite formulation was spin-coated onto a KBr window at 3000 RPM, placed in the spectrometer chamber, and was simultaneously exposed to UV and infrared irradiation. The coated KBr windows were approximately 20 mm from the fiber-optical cable (light intensity ≈ 10 mW/cm^2). The degree of conversion was determined from the disappearance of the vinyl ether double bonds (1639 cm^{-1}). The conversion was calculated from equation (4.1) where $(A_{1639})_0$ is the absorbance at time=0 and $(A_{1639})_t$ is the absorbance at time=t.

$$\%\, conversion = \{[(A_{1639})_0 - (A_{1639})_t]/(A_{1639})_0\} \times 100 \qquad (4.1)$$

Nanocomposite morphology was characterized by X-ray diffraction. X-ray powder diffraction was collected using a Bruker AXS' D8 Discover diffractometer in Bragg-Brentano geometry, using Cu Kα radiation with a wavelength of 1.5406 Å. ASTM E96, “Standard Test Methods for Water Vapor Transmission, Water Method,” was employed for characterizing the barrier performance of the nanocomposite films. Samples were placed inside a controlled humidity chamber with conditions of 70% ± 2% relative humidity and 20 °C ± 2 °C. Under steady

state conditions, the mass loss over time correlated with water vapor transmission and permeance under steady state conditions, and duplicate samples were tested to verify these results. The viscoelastic properties were tested by dynamic mechanical analysis using a TA Instruments Q800 Dynamic Mechanical Analyzer in tensile mode. Nanocomposite free films, approximately 15 mm in length, 5 mm in width, and 0.070 – 0.080 mm in thickness, were measured using 1 Hz frequency, constant strain of 0.05%, and a heating rate of 5 °C/min over a temperature range of -50 °C to 200 °C. Thermogravimetric analysis was employed to study nanocomposite thermal stability using a TA Instruments Q500 Thermogravimetric Analyzer. Nanocomposite samples were heated in a nitrogen atmosphere from ambient temperatures to 600 °C at a rate of 20 °C/min. The optical clarity of each cured film was measured by a Varian Cary 5000 UV-Vis Spectrometer by determining transmittance at 400 nm.

4.3. Results and discussion

4.3.1. "Reverse" in situ intercalative polymerization technique

In Chapter 2, in situ intercalative polymerization was employed to generate highly disperse hydroxy-functional montmorillonite clay in a precursor polyester resin. Through this technique, exfoliated nanocomposite films were produced at low levels of clay loading (1 -2 wt.%). The in situ process was slightly modified in this study to produce a novel "reverse" in situ polymerization technique to explore the ability to further induce clay exfoliation in a precursor resin. Scheme 4.1 illustrates the steps involved to induce clay dispersion during polyesterification. The first step of the reverse in situ technique is to create a homogenous dispersion

of MTEtOH and diethylene glycol to be used in the unsaturated polyester synthesis reaction.

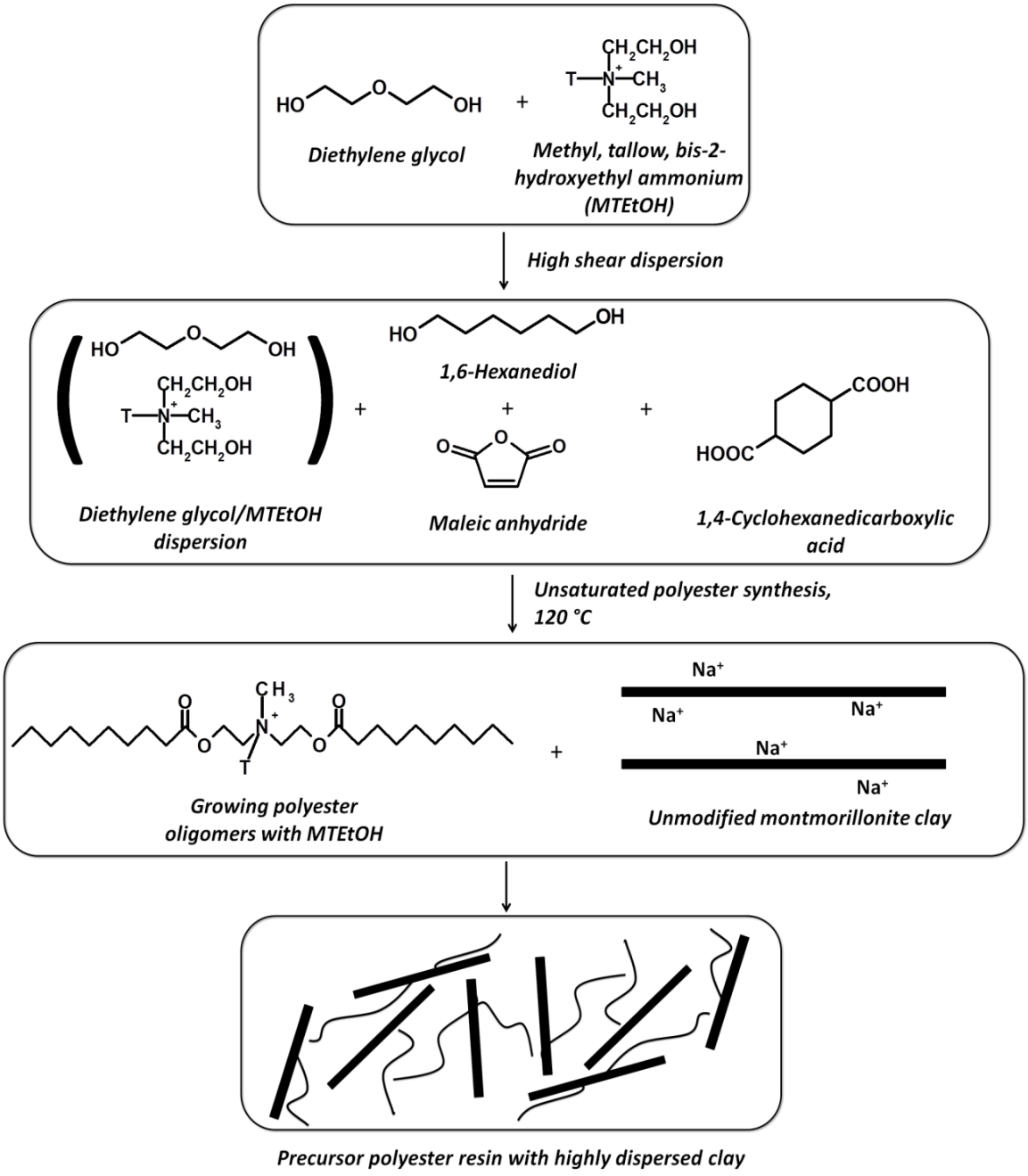

Scheme 4.1: "Reverse" in situ polymerization technique to produce highly dispersed, functionalized-clay within a polyester resin by undergoing an in situ ion exchange reaction.

Once the homogenous dispersion is achieved, the additional monomers (maleic anhydride, 1,6-hexanediol, and 1,4-CHDA) are added to the diethylene glycol-MTEtOH dispersion. The unmodified clay (Cloisite® Na^+) was added to the reaction mixture during polyesterification once the temperature was ramped to 120 °C. The temperature for the unmodified clay addition was chosen to be in excess of 100 °C to ensure the reaction mixture had low viscosity to aid in the dispersion of the unmodified clays. Through this reverse in situ polymerization method, the goal was to perform an in situ ion exchange reaction to attach the organic modifier MTEtOH to the unmodified clay. If the MTEtOH organic modifier achieves a high degree of dispersion within the reaction medium, then the unmodified clay may also be highly dispersed in the final polyester resin. In addition, the hydroxy-functionality of the MTEtOH organic modifier will also help in the exfoliation of clay throughout the polyester resin by reacting with acid functional monomers. If the MTEtOH reaction occurs after the in situ ion exchange with the unmodified clay, the growing volume of the polyester oligomers may also increase the distance between clay layers. The final polyester resin containing MTEtOH-modified clay may then serve as a precursor system to creating nanocomposite films with exfoliated morphologies.

4.3.2. Unsaturated polyester properties

The polyester resins were fully characterized prior to coating formation as their physical properties have a profound impact on many of the nanocomposite film properties, including morphology, conversion, and mechanical performance. A summary of the unsaturated polyester properties are located in Table 4.1.

TABLE 4.1
Properties of unsaturated polyesters prepared through the "reverse" in situ intercalative polymerization and sonication techniques

Polyester Name	Acid value	M_n (g/mol)	M_w (g/mol)	PDI	Viscosity (Poise)	T_g (°C)	% Fumarate
Control	21	1100	2400	1.9	2.4	-42	33
R1_insitu	19	1400	2900	2.1	3.2	-35	37
R2_insitu	21	1600	3200	2.0	3.4	-37	40
R5_insitu	22	1700	4100	2.4	7.2	-32	52
R10_insitu	21	1600	4100	2.6	8.8	-34	55
R1_sonic	21	1600	2900	1.8	2.6	-42	38
R2_sonic	22	1700	3100	1.9	3.2	-41	38
R5_sonic	21	1600	3000	1.9	4.0	-38	39
R10_sonic	21	1700	3400	2.0	5.4	-37	37

The target acid value was approximately 20 mg KOH/g of polyester; careful monitoring of the acid values of each polyester resin was important to maintain equivalent degrees of polymerization.[18] Consistent acid number values were obtained between each polyester synthesis by being maintained between 19 – 21 mg KOH/g of polyester. The incorporation of the MTEtOH modifier and clay into the polyester matrix increased molecular weight and PDI values for both the "reverse" in situ polymerization and sonication clay dispersion routes. As determined by GPC, the M_n for each polyester resin was slightly increased from the control sample, approximately 1600 g/mol, regardless of clay loading or dispersion technique. More dramatic increases in the M_w and PDI were observed, particularly with higher levels of clay loading (5 – 10 wt.%). Polyesters R5_insitu and R10_insitu each had M_w of 4100 g/mol, almost twice the value of the control polyester (2400 g/mol). The polyesters prepared through the sonication dispersion technique had M_w values ranging from 2900 – 3400 g/mol. The wt.% clay

appeared to have a direct correlation to the M_w, where higher clay loading increased M_w. The elevated molecular weights may be attributed to the higher hydrodynamic volume of the polyester resins containing clay as the polyester was passed through the GPC column without clay removal.

Clay incorporation had a profound impact of the rheological properties of the polyester resins: higher clay content produced significantly higher viscosity systems. As expected, the control polyester was lowest in viscosity (2.4 Poise) compared to the clay-containing resins. Low levels of clay loading (1 – 2 wt.%) increased the polyester viscosity slightly, whereas the higher levels of clay content (5 – 10 wt.%) produced much more viscous resins. Polyesters R5_insitu and R10_insitu had the highest viscosities at 7.2 and 8.8 Poise, respectively. The rheological properties of each polyester resin were directly affected by not only the clay content but also the dispersion route. Interestingly, the reverse in situ technique generated higher viscosity polyesters than the sonication clay dispersion route for equivalent clay content. As the reverse in situ synthesis technique produced higher viscosity resins, the dispersion of clay within the polyester may be a contributing factor to the final resin viscosity.

The reverse in situ synthesis technique created polyester resins with higher T_g values than the sonication dispersion route. Each polyester prepared by the reverse in situ technique had T_g values 5 – 10 °C higher than the control polyester (-42 °C). Once again, the higher clay content (5 – 10 wt.%) led to more significant increases in the T_g than the lower clay loading (1 -2 wt.%). The increased T_g may be a reflection of decreased mobility of polyester chains due to confinement from

the clay platelets. As more clay filler is incorporated into the matrix, the mobility decreases further, resulting in the polyesters with higher clay content having the highest T_g values. Although the same trend is observed with the sonication dispersion route, the T_g increases were not as significant. The T_g value of polyester R10_sonic (-37 °C) was 5 °C higher than the control resin, which was the most dramatic increase observed with the sonication dispersion route. When comparing T_g values of polyesters with equivalent clay loading, the reverse in situ process had consistently higher thermal transitions. Once again, the final clay dispersion within the polyester resin may be causing the disparities in T_g, where the higher degree of clay dispersion may be impacting the polyester chain mobility to a greater extent through the reverse in situ process.

Higher maleate-fumarate isomerization of the unsaturated polyester backbone was observed with the reverse in situ technique as determined by ^{1}H NMR spectroscopy. Steric hindrance has been shown to influence the degree of cis to trans isomerization in unsaturated polyesters, where steric hindrance increases the likelihood of monomers to react with the trans isomer.[17] With the reverse in situ polymerization technique, the fumarate isomerization increased to 55% for R10_insitu. Continually, increased levels of clay loading led to further increases in the fumarate isomer. These trends may be a reflection of the degree of clay dispersion and clay volume fraction in the polymer matrix. The incorporation of the clay fillers into the polyester resin was directly correlated to the increased amount of fumarate isomers. Conversely, the sonication dispersion route did not

influence the final isomerization of the polyester backbone, where each resin ranged between 37 – 39%.

4.3.3. Cure characteristics – Real-time infrared spectroscopy

Donor-acceptor chemistry was employed to create UV-curable nanocomposite coatings derived from the unsaturated polyester resins and reactive diluent TEGDVE, based on a 1:1 stoichiometric ratio of maleate to vinyl ether functionality. Large increases in the final conversion of the UV-curable coatings were observed by monitoring the disappearance of the reactive diluent vinyl ether double bonds at 1639 cm^{-1} (Table 4.2) to determine the extent of the maleate-vinyl ether reaction. Each clay-containing formulation, regardless of dispersion technique, had final conversions up to 15% higher than the control formulation containing no clay (72% final conversion). The reverse in situ preparation technique produced coatings with higher conversions ranging from 78 – 87%, where by comparison, the sonication dispersion route coatings had slightly reduced final conversions of 74 – 82%. Figure 4.1 demonstrates the dramatic final conversion increase with the incorporation of just 1 wt.% clay. The highest conversion was the coating formulation containing polyester R2_insitu with a final conversion of 87%. Increased final conversions of the clay-containing formulations may directly correlate to the polyester viscosities. With coating formulation viscosity increases from the high viscosity polyesters, reactive chain ends have more difficulty diffusing through the coatings system, thereby decreasing the rate of termination. If the lower molecular weight reactive diluent can still freely diffuse through the coatings system, the final conversion increases from an

autoacceleration effect. The same trend was observed in our previous nanocomposite study, where increased viscosity from the clay-containing polyesters produced final conversions 10 – 15% higher than the control formulation.

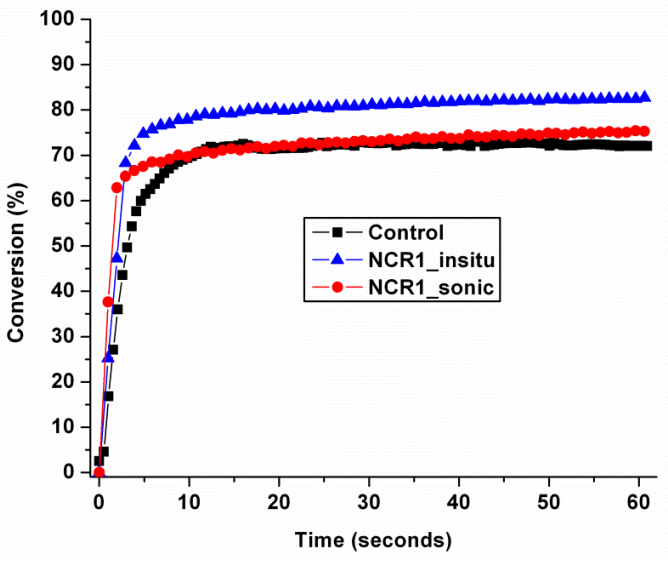

Figure 4.1: Final conversion of control, NCR1_insitu, and NCR1_sonic coatings systems determined by disappearance of vinyl ether double bond (1639 cm^{-1}) via RTIR spectroscopy with 60 seconds of UV-irradiation.

TABLE 4.2
UV-curable nanocomposite coating cure, morphological, mechanical, thermal, and optical clarity property data

Nanocomposite Name	Conver-sion (%)	*d*-spacing (nm)	*E'* (MPa, 25°C)	Crosslink density (mol/cm^3)	T_{10} % (°C)	Transmitt-ance (%)
Control	72	----*	370	0.022	240	98
NCR1_insitu	82	----	425	0.015	300	99
NCR2_insitu	87	----	460	0.023	300	93
NCR5_insitu	82	----	510	0.019	290	91
NCR10_insitu	78	----	270	0.016	270	70
NCR1_sonic	74	----	535	0.037	300	96
NCR2_sonic	80	----	525	0.032	290	92
NCR5_sonic	82	1.96	515	0.025	285	82
NCR10_sonic	82	1.88	420	0.016	290	60

*Indicates no XRD diffraction peak observed

4.3.4. Nanocomposite morphology – X-ray diffraction and transmission electron microscopy

Clay dispersion within polymer-clay nanocomposites are typically characterized by two techniques: XRD and TEM. XRD may indicate the final degree of clay dispersion based on diffraction peaks occurring between 2 – 9 2θ. From the maximum value of the diffraction peaks in this range, the *d*-spacing, or interlayer distance between clay platelets, can be calculated from Bragg's Law. Figure 4.2 displays the XRD scans for the pristine clays and nanocomposite films, and *d*-spacing values are reported in Table 4.2. The *d*-spacing of pristine Cloisite® 30B and Cloisite® Na^+ montmorillonite clays were determined to be 1.84 nm and 1.09 nm, respectively. While the two pristine clays had sharp, prominent diffraction peaks, the nanocomposite samples had significantly lower intensities when diffraction peaks were resolved. No diffraction peaks for each nanocomposite that was formulated with the polyesters prepared through the reverse in situ technique (1 – 10 wt.%) were observed in the low 2θ range an indicator of high clay dispersion with possible clay delamination. Conversely, the nanocomposites containing 5 – 10 wt.% clay prepared through the mixing-sonication dispersion technique had small, wide diffraction peaks. Nanocomposites NCR5_sonic and NCR10_sonic had *d*-spacing values of 1.96 and 1.88 nm, respectively. As these *d*-spacing values were much greater than the pristine Cloisite® Na^+ clay, the formation of nanocomposites with intercalated morphologies is indicated. Based on XRD analysis, the level of clay loading and dispersion technique had a significant impact on the final degree of clay dispersion. The reverse in situ preparation

technique appeared to result in a higher degree of clay dispersion throughout the UV-curable nanocomposite network as no diffraction peaks were observed in the low 2θ range. The mixing-sonication dispersion technique produced nanocomposites with diffraction peaks at higher levels of clay loading (5 – 10 wt.%), indicating an intercalated, not exfoliated, nanocomposite morphology.

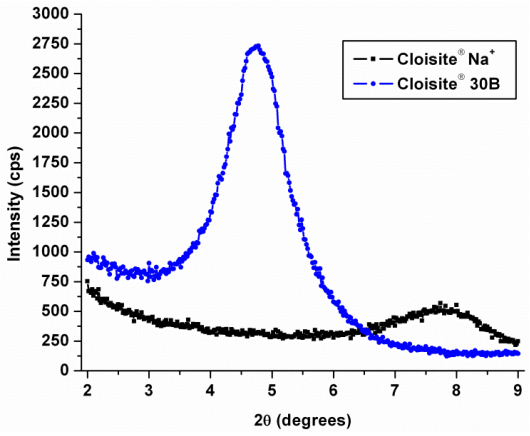

(a)

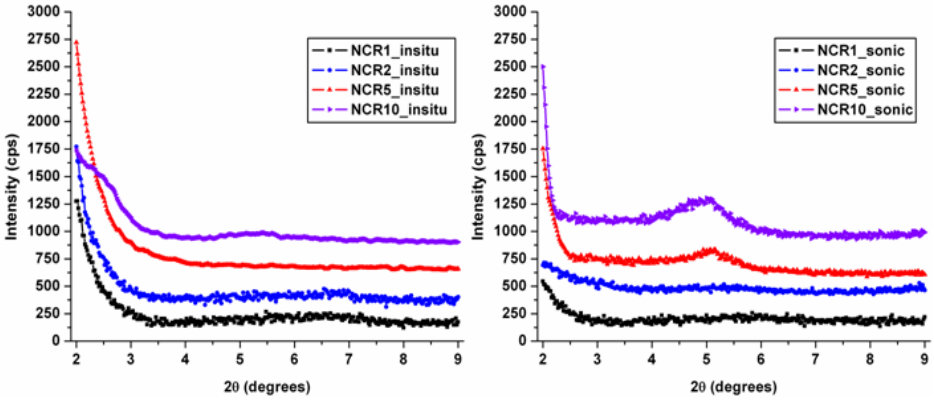

(b)

Figure 4.2: XRD scans of (a) the pristine Cloisite® Na^+ and Cloisite® 30B clays and (b) the nanocomposites prepared by the in situ and mixing-sonication dispersion techniques.

Although XRD can be an excellent indicator of nanocomposite morphology and *d*-spacing determination, proper morphological classification must be done in

conjunction with TEM.[19] Figure 4.3 displays the TEM micrographs for the nanocomposites prepared by both the reverse in situ and sonication techniques.

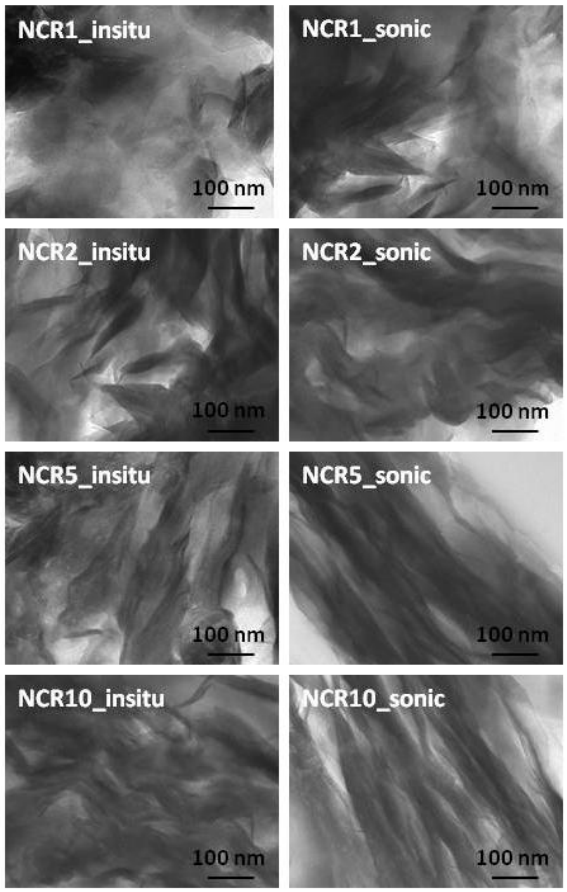

Figure 4.3: Transmission electron micrographs of the UV-curable nanocomposite films.

The dark lines in the micrographs are cross-sections of the layered silicates dispersed throughout the polyester matrix. From TEM analysis, primarily exfoliated morphologies were obtained for nanocomposites prepared with the reverse in situ method with 1 – 2 wt.% clay. Once the clay loading was increased higher than 2 wt.% clay, the morphology shifted from exfoliated to a mixture of exfoliation and intercalation. Nanocomposites prepared through the mixing and sonication dispersion route were classified as primarily intercalated with portions of phase

separation, except for NCR1_sonic, which was classified as partially exfoliated and intercalated. The TEM results obtained correlate to the XRD analysis.

4.3.5. Barrier properties – Water vapor transmission and permeability

Nanocomposite formation led to reductions in water vapor transmission (WVT) and water vapor permeability (WVP) compared to the control coating. Figures 4.4 and 4.5 display the trends in WVT and WVP with increased clay loading, and WVT and WVP data results are reported in Table 4.3. ASTM E96 was employed to measure the nanocomposite barrier properties of free films with comparable thickness (86 ± 8 μm). While each nanocomposite film decreased both WVT and WVP, the clay dispersion technique applied in the preparation of each nanocomposite as well as the final clay volume fraction greatly dictated the final barrier properties.

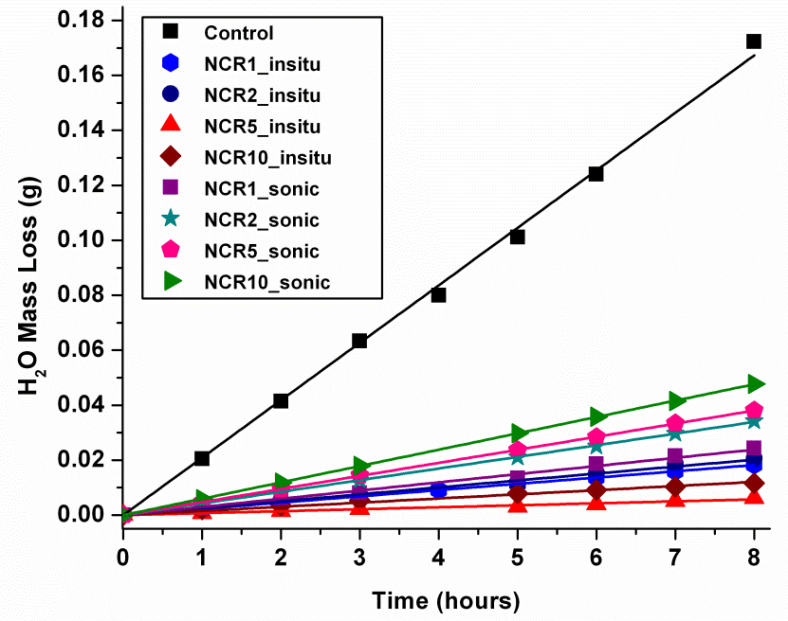

Figure 4.4: Water vapor transmission (WVT) according to ASTM E96 of UV-curable nanocomposite free films.

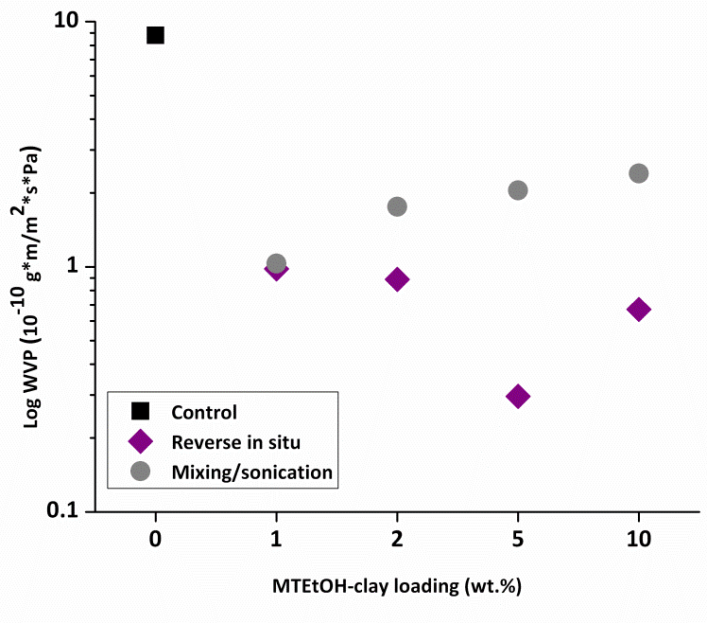

Figure 4.5: Water vapor permeability (WVP) according to ASTM E96 of UV-curable nanocomposite free films.

Two striking trends appeared in the analysis of the nanocomposite barrier results. First, the reverse in situ technique produced better barrier films compared to the mixing and sonication clay dispersion route. With the incorporation of just 1 wt.% clay, the WVP of nanocomposite NCR1_inistu (9.18E-11 g·m/m^2·s·Pa) was one magnitude lower in permeability than the control film (8.79E-10 g·m/m^2·s·Pa). Further increases in the clay loading produced lower WVP readings, where nanocomposite NCR5_insitu recorded the lowest WVP (2.96E-11 g·m/m^2·s·Pa) for the coatings prepared through the reverse in situ process. Although nanocomposite NCR10_inistu had the highest clay volume fraction throughout the polymer matrix, the WVP increased slightly compared to NCR5_insitu (6.70E-11 g·m/m^2·s·Pa). The dramatic reductions in the nanocomposite WVT and WVP may be attributed to the dispersion of the nanoscale clay fillers throughout the polymer

film, where a highly tortuous diffusion path may form from the incorporation of the impermeable clay platelets.

The uniformity of clay dispersion also affects the final barrier performance of the nanocomposite films. The second striking trend observed in the nanocomposite barrier properties is the mixing and sonication dispersion technique produced nanocomposites with increasing WVT and WVP for increased clay loading, an opposite trend than the reverse in situ preparation method. Nanocomposite NCR1_sonic measured the lowest WVP (1.03E-11 g·m/m^2·s·Pa) of the four nanocomposites prepared through the mixing and sonication technique. Although the remaining nanocomposites of the sonication dispersion route measured WVT and WVP lower than the control coating, the barrier properties diminished when the clay loading was increased from 2 to 10 wt.% clay. Based on the TEM micrographs and XRD analysis, the dispersion of clay within the cured film may be contributing to the increases in both WVT and WVP. While the incorporation of clay typically improves the barrier properties of polymeric materials by introducing a tortuous diffusion path, high uniformity of the clay distributed throughout the polymer matrix is essential to optimize the incorporation of the impermeable clay fillers. As seen with the TEM micrographs, the reverse in situ preparation led to a greater dispersion of the layered silicates within the polymer matrix, particularly with 1 – 5 wt.% clay loading. By improving the clay dispersion, the tortuous diffusion path of the permeating water vapor molecules may be significantly increased, leading to lower WVP results of the reverse in situ method over the sonication preparation technique.

TABLE 4.3
UV-curable nanocomposite water vapor transmission and permeability results as determined by ASTM E96

Nanocomposite Name	Mass loss/time (g/hr)	WVT ($g/m^2/s$)	Thick-ness (μm)	WVP ($g \cdot m/m^2 \cdot s \cdot Pa$)
Control	2.15 E-02	5.97E-03	86	8.79E-10
NCR1_insitu	2.30E-03	6.39E-04	84	9.18E-11
NCR2_insitu	2.40E-03	6.67E-04	78	8.90E-11
NCR5_insitu	7.00E-04	1.94E-04	89	2.96E-11
NCR10_insitu	1.50E-03	4.17E-04	94	6.70E-11
NCR1_sonic	2.70E-03	7.50E-04	80	1.03E-10
NCR2_sonic	4.20E-03	1.17E-03	88	1.76E-10
NCR5_sonic	4.80E-03	1.33E-03	90	2.05E-10
NCR10_sonic	5.80E-03	1.61E-03	87	2.40E-10

4.3.6. Mechanical properties – Dynamic mechanical analysis

Nanocomposite viscoelastic properties, as determined by dynamic mechanical analysis (DMA), were greatly influenced by the differing clay dispersion techniques. The trends observed in the barrier performance of the nanocomposite films was repeated in the mechanical performance of these coatings: the reverse in situ technique increased storage moduli with increased clay loading, while the mixing and sonication dispersion method decreased the mechanical properties with higher clay content. The DMA storage modulus plots are shown in Figure 4.6, and storage moduli and crosslink density data is compiled in Table 4.2. Nanocomposite preparation from the reverse in situ technique led to increased storage moduli up to 5 wt.% clay loading. The control coating containing no clay filler recorded a storage modulus at room temperature of 370 MPa. By introducing 1 wt.% clay into the polymer matrix, the storage modulus of NCR1_inistu increased to 425 MPa. Further increasing the clay loading to 2 and 5 wt.% produced even

higher storage moduli, where NCR2_inistu and NCR5_insitu had values of 460 and 510 MPa, respectively.

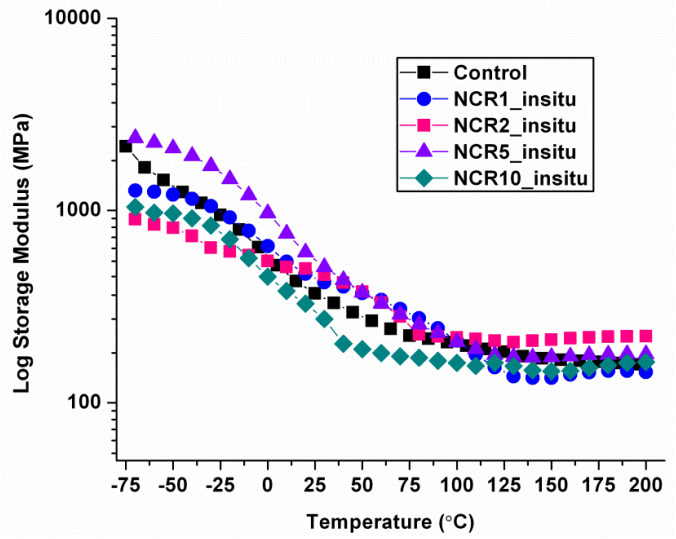

(a)

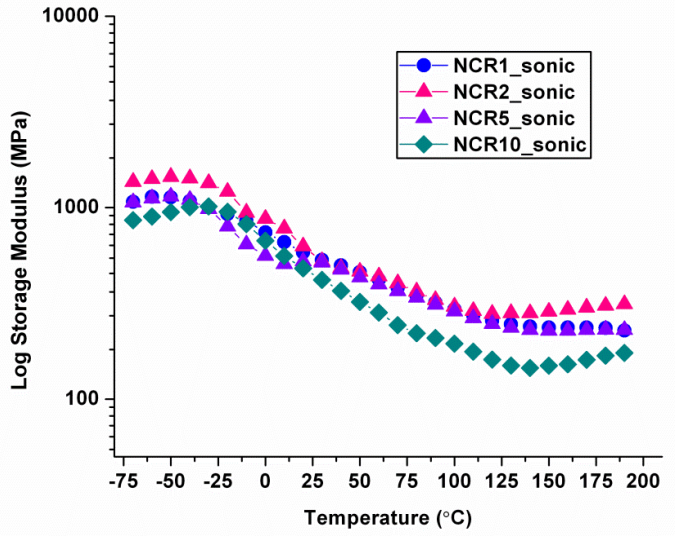

(b)

Figure 4.6: DMA storage modulus plots for UV-curable nanocomposites prepared by the (a) reverse in situ technique and (b) mixing and sonication dispersion route.

Once the clay loading reached 10 wt.%, dramatic reductions in the storage moduli were observed as NCR10_insitu had a storage modulus 100 MPa lower than the control coating at 270 MPa. Increased crosslink density was observed

when the clay loading was increased to 2 wt.% clay (0.023 mol/cm^3), but higher clay content (5 – 10 wt.%) resulted in crosslink densities lower than the control coating (0.016 – 0.019 mol/cm^3). From these results, the peak mechanical performance of the nanocomposites prepared through the reverse in situ process falls with clay loading between 2 – 5 wt.%.

The mixing and sonication clay dispersion route produced nanocomposite films with diminishing mechanical properties as clay loading is increased, a trend similar to the barrier properties observed by water vapor transmission testing. Nanocomposite NCR1_sonic measured a storage modulus of 535 MPa at room temperature, but higher clay content continually reduced the storage modulus. When the clay loading reached 10 wt.%, the storage modulus of nanocomposite NCR10_sonic was 420 MPa, over 100 MPa lower than NCR1_sonic. Continually, the same trend was observed with crosslink density, where NCR1_sonic had the highest crosslink density, of the mixing and sonication dispersion technique, at 0.037 mol/cm^3, and NCR10_sonic had the lowest value (0.016 mol/cm^3). Similar trends in the mechanical performance were observed with the original in situ preparation of UV-curable nanocomposites, where increased clay content decreased storage moduli and crosslink densities. To better understand this peculiar behavior, the impact of the organic modifier structure and concentration on the polymer and coating properties was studied (Chapter 3). From this research, we determined the organic modifier, particularly the Cloisite® 30B organic modifier, may plasticize the polymer matrix when at high concentrations, leading to reductions in mechanical performance among other material properties.

Based on the mechanical performance of the nanocomposites in this study, it appears a similar phenomenon may have occurred. In addition to plasticization from the organic modifier, the degree of clay dispersion, particularly the uniformity, may be impacting the final film properties. Because the reverse in situ method led to a much higher degree of clay dispersion than the mixing and sonication method, the clay fillers of the nanocomposites prepared through the reverse in situ method may be reinforcing the polymer matrix, and thus improving the mechanical properties. Conversely, the sonication preparation method, producing primarily intercalated morphologies with some phase-separation, may not improve the mechanical properties due to poorer clay dispersion.

4.3.7. Thermal stability and optical clarity – Thermogravimetric analysis and UV-visible spectroscopy

Large increases in thermal stability were recorded by the formation of nanocomposites with clay incorporation through both the reverse in situ and mixing/sonication dispersion techniques. The TGA degradation curves shown in Figure 4.7 and the temperature at 10% weight loss (T_{10}%) in Table 4.2 display the dramatic improvements in thermal stability by nanocomposite creation. Both dispersion techniques increased the T_{10}% values. The control coating recorded a T_{10}% of 240 °C, whereas for the nanocomposites, this value increased to 300 °C with nanocomposites NCR1_insitu, NCR2_insitu, and NCR1_sonic. The thermal stability declined slightly as the clay loading increased, but the nanocomposite films maintained T_{10}% values at least 30 °C higher than the control film. From this

thermal analysis, nanocomposites with higher clay loading had somewhat diminished thermal stability compared to nanocomposites with 1 – 2 wt.% clay loading. Once again, the impact of the clay volume fraction drastically influences the nanocomposite material properties.

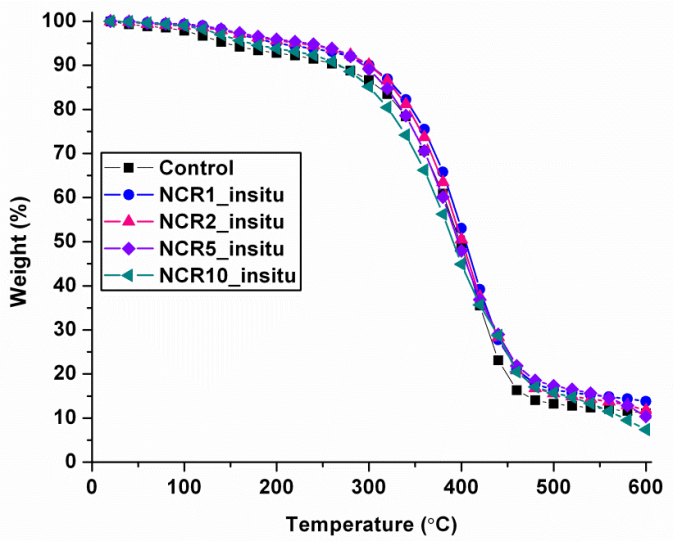

(a)

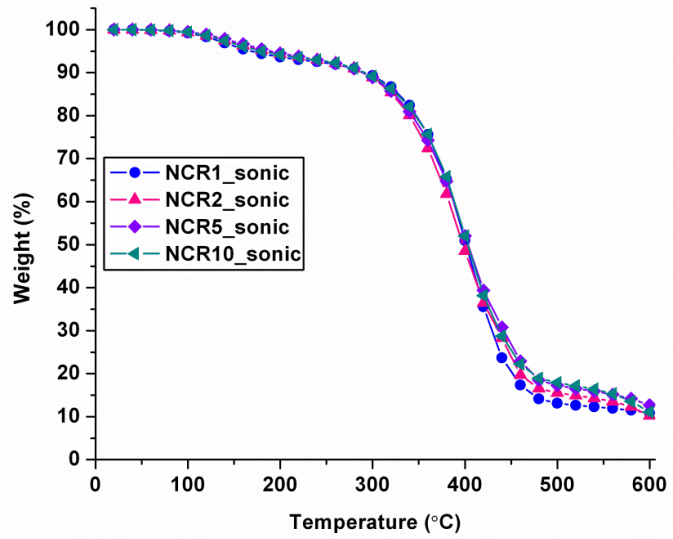

(b)

Figure 4.7: TGA plots for UV-curable nanocomposites prepared by the (a) reverse in situ technique and (b) mixing and sonication dispersion route.

Two main trends were observed when examining nanocomposite optical clarity: increased clay loading decreased transmittance and the reverse in situ technique had higher transmittance values than the mixing and sonication dispersion route for equivalent clay content. Figure 4.8 displays the reductions in transmittance at higher clay loading, and Table 4.2 reports the percent transmittance at 400 nm as determined by UV-visible spectroscopy.

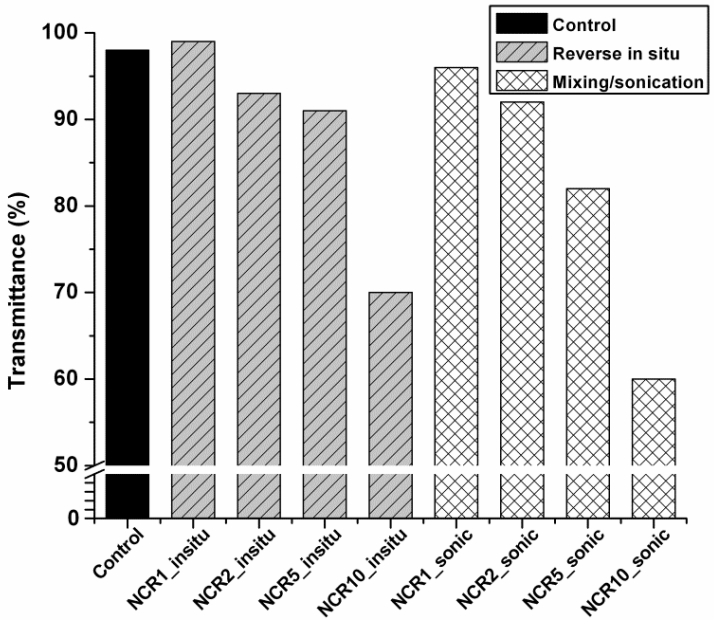

Figure 4.8: Optical clarity of UV-curable nanocomposite films as determined by percent transmittance at 400 nm from UV-visible spectroscopy.

Nanocomposites prepared from the reverse in situ process maintained high levels of optical clarity (91 – 99 %) with up to 5 wt.% clay loading. High transmittance values through these films represent a high degree of uniform clay dispersion throughout the polymer matrix. However, once 10 wt.% clay was incorporated into the polymer matrix, the transmittance decreased dramatically to 70% for nanocomposite NCR10_insitu which indicates reductions in homogenous

clay dispersion. Nanocomposite preparation through the mixing and sonication dispersion route maintained high optical clarity (92 – 96%) up to 2 wt.% clay loading, but higher clay content (5 – 10 wt.%) reduced film transmittance. Nanocomposite NCR10_sonic had the lowest transmittance of any nanocomposite prepared in this study at 60%. Since the reverse in situ process had higher transmittance values than the sonication dispersion technique for equivalent clay loading, the clarity of these nanocomposites indicated the reverse in situ process produced nanocomposites with better clay dispersion.

4.4. Conclusions

Enhanced cure, barrier, mechanical, and thermal properties were observed with the formation of polymer/clay nanocomposites through a novel “reverse” in situ intercalative technique. Unmodified clay was incorporated into a polyester reaction mixture containing MTEtOH during polyesterification to induce an in situ ion exchange reaction and creating a precursor resin with highly dispersed, organically-modified layered silicates. Polyester characterization demonstrated the impact of clay loading and dispersion on the resin physical properties, where higher clay volume fractions increased resin viscosity, backbone isomerization, and M_w while decreasing the T_g. The formation of UV-curable coatings based on donor-acceptor chemistry by reacting the electron-poor sites of unsaturation in the polyester resin with the electron-rich vinyl ether groups of reactive diluent TEGDVE. The reverse in situ synthesis technique improved material film properties, such as increasing conversion up to 15% and decreasing both WVT and WVP. The optimal clay loading was determined to be between 2 -5 wt.% to

obtain peak mechanical performance and highest thermal stability. When comparing the nanocomposites prepared through the reverse in situ technique to the clay dispersion technique of mixing and sonication, the reverse process generated nanocomposites with significantly better barrier performance. The improvement in the barrier properties was attributed to much better clay dispersion than the sonication preparation route, as the morphology was classified as primarily exfoliated for 1 – 2 wt.% clay, and a mixture of exfoliation and intercalation for higher clay loading (5 – 10 wt.%).

4.5. References

1. Sinha Ray, S.; Okamoto, M., *Progress in Polymer Science* **2003,** *28* (11), 1539-1641.

2. Fornes, T. D.; Hunter, D. L.; Paul, D. R., *Macromolecules* **2004,** *37* (5), 1793-1798.

3. Yang, Y.; Zhu, Z.-k.; Yin, J.; Wang, X.-y.; Qi, Z.-e., *Polymer* **1999,** *40* (15), 4407-4414.

4. Dasari, A.; Yu, Z.-Z.; Mai, Y.-W.; Hu, G.-H.; Varlet, J., *Composites Science and Technology* **2005,** *65* (15-16), 2314-2328.

5. Davis, C. H.; Mathias, L. J.; Gilman, J. W.; Schiraldi, D. A.; Shields, J. R.; Trulove, P.; Sutto, T. E.; Delong, H. C., *Journal of Polymer Science Part B: Polymer Physics* **2002,** *40* (23), 2661-2666.

6. Marras, S.; Tsimpliaraki, A.; Zuburtikudis, I.; Panayiotou, C. In *Surfactant-induced morphology and thermal behavior of polymer layered silicate nanocomposites*, IOP Publishing: 2007; p 1366.

7. Litchfield, D. W.; Baird, D. G.; Rim, P. B.; Chen, C., *Polymer Engineering & Science* **2010,** *50* (11), 2205-2215.

8. Wang, Z. M.; Nakajima, H.; Manias, E.; Chung, T. C., *Macromolecules* **2003,** *36* (24), 8919-8922.

9. Messersmith, P. B.; Giannelis, E. P., *Chem. Mat.* **1993,** *5* (8), 1064-1066.

10. Paul, M.-A.; Delcourt, C.; Alexandre, M.; Degée, P.; Monteverde, F.; Rulmont, A.; Dubois, P., *Macromolecular Chemistry and Physics* **2005,** *206* (4), 484-498.

11. Pantoustier, N.; Lepoittevin, B.; Alexandre, M.; Dubois, P.; Kubies, D.; Calberg, C.; Jérôme, R., *Polymer Engineering & Science* **2002,** *42* (9), 1928-1937.

12. Tasdelen, M. A.; Van Camp, W.; Goethals, E.; Dubois, P.; Du Prez, F.; Yagci, Y., *Macromolecules* **2008,** *41* (16), 6035-6040.

13. Kim, D. S.; Kim, J.-T.; Woo, W. B., *Journal of Applied Polymer Science* **2005,** *96* (5), 1641-1647.

14. Choi, M. Y.; Anandhan, S.; Youk, J. H.; Baik, D. H.; Seo, S. W.; Lee, H. S., *Journal of Applied Polymer Science* **2006,** *102* (3), 3048-3055.

15. Rivero, G.; Vázquez, A.; Manfredi, L. B., *Journal of Applied Polymer Science* **2009,** *114* (1), 32-39.

16. Nikolaidis, A. K.; Achilias, D. S.; Karayannidis, G. P., *Industrial & Engineering Chemistry Research* **2010,** *50* (2), 571-579.

17. Curtis, L.; Edwards, D.; Simons, R.; Trent, P.; Von Bramer, P., *Industrial & Engineering Chemistry Product Research and Development* **1964,** *3* (3), 218-221.

18. Carothers, W. H.; Arvin, J. A., *Journal of the American Chemical Society* **1929,** *51* (8), 2560-2570.

19. Morgan, A. B.; Gilman, J. W., *Journal of Applied Polymer Science* **2003,** *87* (8), 1329-1338.

CHAPTER 5. INTRODUCTION: ORGANIC-INORGANIC HYBRID SOL-GEL MATERIALS

5.1. Introduction

Similar to polymer-clay nanocomposite technology, the preparation of organic-inorganic hybrid materials via sol-gel processing incorporates the advantageous physical properties of organic and inorganic precursors into a single system that may be uniquely tailored to a wide variety of applications. Currently, sol-gel technology is employed in the fields of electronics,[1-3] chemistry,[4-6] polymers,[7-8] biochemistry,[9-10] and engineering[11-12] among others. The popularity of sol-gel preparation methods are primarily due to many favorable processing conditions including mild reaction temperatures, highly pure products, relatively easy control of reaction kinetics, and control of the final sol-gel structure.[13] As also observed with polymer-clay nanocomposites, 1 – 100 nm inorganic domains manifest throughout a polymer matrix in sol-gel prepared organic-inorganic hybrids, thus producing mechanical, thermal, and optical properties not otherwise obtainable by micro- or macro-composite systems.[14]

The sol-gel process, composed primarily of inorganic polymerization reactions, was initially utilized in the preparation of ceramic binders in the precursor materials for brick and porcelain applications in the mid 1800s.[15] Although originally used for primarily decorative materials, W.A. Patrick catalyzed sol-gel research in the 1920s when he produced porous silica films by applying high temperatures to silica gels and demonstrated the facile nature of sol-gel processing and the ability to tailor hybrid materials by varying the organic-inorganic

ratio.[16-18] Recently, sol-gel processing has been utilized to create a new class of nanocomposites referred to as organic-inorganic hybrids.

5.2. Sol-gel chemistry and processing

The formation of organic-inorganic hybrids via sol-gel chemistry proceeds by simultaneous chemical reactions to form an inorganic network throughout an organic polymer matrix. The sol, or precursor colloidal suspension, converts to a solid material through simultaneous hydrolysis and condensation reactions to form a viscous gel, followed by aging and densification to create a non-porous hybrid network. Although many stages of the organic-inorganic hybrid formation happen concurrently, the sol-gel process will be presented separately. A schematic representation of the sol-gel process is shown in Figure 5.1.

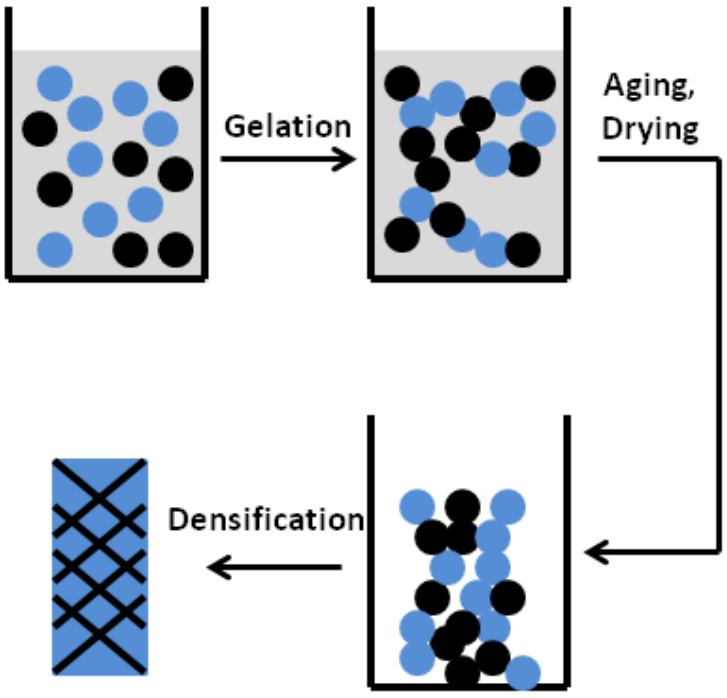

Figure 5.1: Schematic illustration of sol-gel processing [adapted from Ref. 15] including the gelation, aging, drying, and densification stages.

5.2.1. Hydrolysis

The first stage of organic-inorganic hybrid formation by sol-gel methods is alkoxide hydrolysis to produce hydroxy groups. The hydrolysis reaction, a nucleophilic substitution, proceeds by three steps: nucleophilic addition, proton transfer, and removal of protonated species (water or alcohol).[19] With silicon-based alkoxides, the hydrolysis reaction proceeds through acid or base catalysis (Scheme 5.1); therefore, the pH of the reaction medium has a strong impact on the hybrid network formation and structure. As expected, pH levels near the isoelectric point, or where the species net charge is zero, have lower hydrolysis rates and the time to gelation (t_{gel}) increases.[20] The selection of an acidic or basic reaction environment will help dictate the network structure. Silicon-based alkoxide precursor hydrolysis rates are higher than condensation rates in acidic environments leading to more linear or polymeric-type network formations.[21] Base catalyzed hydrolysis produces more colloidal, particulate type networks. Additionally, base catalyzed hydrolysis rates are higher than acid catalyzed systems due to electronic effects. Because alkoxy groups are more electron donating than hydroxy groups, the positively-charged transition state in acid catalyzed hydrolysis is destabilized by the conversion of alkoxy to hydroxy groups and the hydrolysis rate decreases.[13] Conversely, the negatively-charge base catalyzed transition state is further stabilized by the hydroxy groups and the hydrolysis rate increases. The likelihood of the reverse esterification reaction will also be influenced by the pH of the reaction medium, where acidic conditions increase the possibility of esterification by stabilizing the transition state.

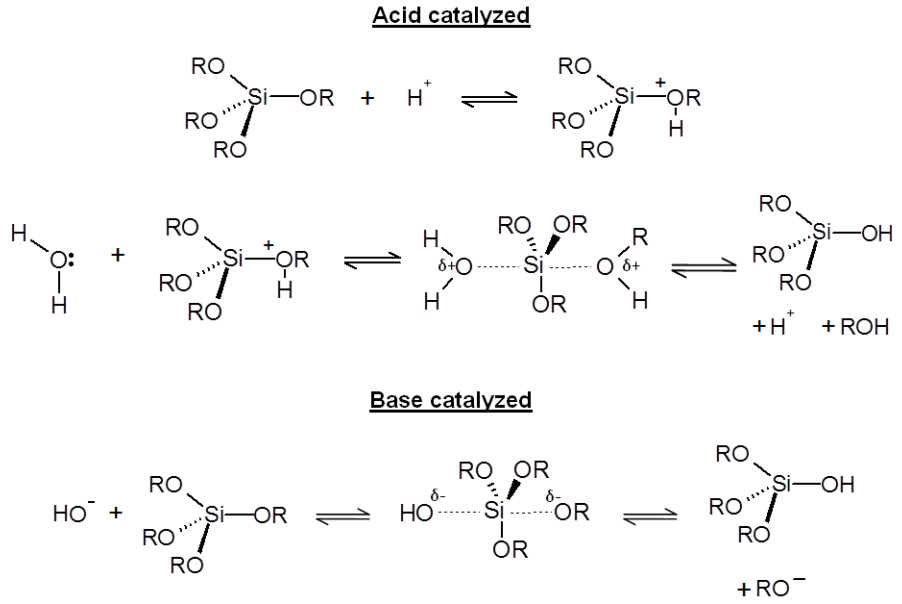

Scheme 5.1: Sol-gel reaction mechanism for acid and base catalyzed hydrolysis.

5.2.2. Condensation

Sol-gel condensation reactions, occurring simultaneously with hydrolysis, also proceed by acid and base catalysis for silicon-based alkoxide precursors (Scheme 5.2). With both types of catalysis, the charged intermediate is rapidly formed when the hydroxy group reacts with either a proton or hydroxide ion. The addition of a second, neutral alkoxide species to form Si-O-Si linkages is significantly slower. The condensation rates of the sol-gel process will impact the final hybrid network formation and are directly related to the rate of hydrolysis.

With acid catalyzed sol-gel chemical reactions, the extent of hydrolysis will affect the rate of condensation. Because the acid catalyzed hydrolysis reaction intermediate is less stable as more electron withdrawing hydroxy groups replace electron donating alkoxide groups, the intermediate $(RO)_3SiOH$ will condense quicker than $(RO)_2Si(OH)_2$ and $(RO)Si(OH)_3$, initially producing an open network.[22]

With subsequent hydrolysis and condensation, the network densifies significantly. With base catalyzed sol-gel reactions, a fully hydrolyzed silicon precursor will undergo faster hydrolysis and condensation as the electron withdrawing hydroxy groups stabilize the negative reaction intermediate. Due to the rapid hydrolysis and condensation, the final hybrid network structure has a mixture of highly dense, discrete particulates and large pores from high t_{gel} values.[23]

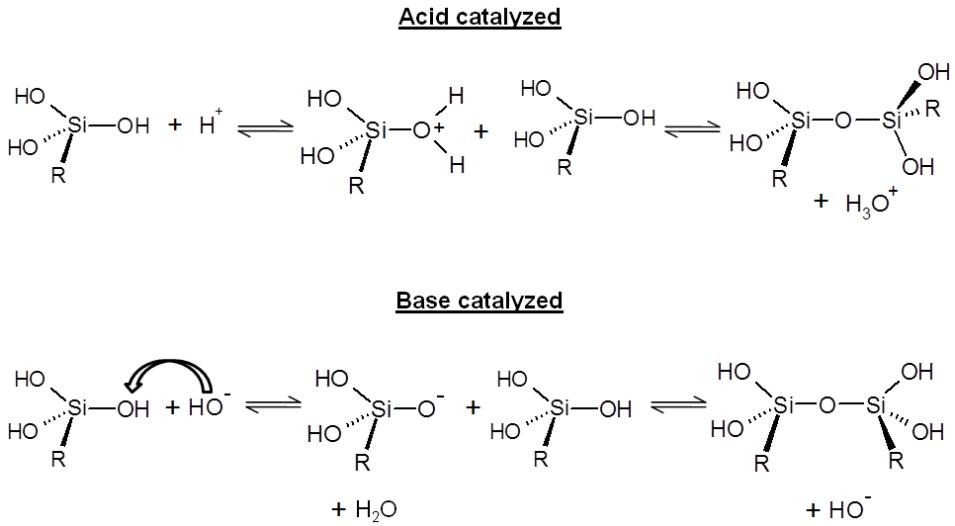

Scheme 5.2: Sol-gel reaction mechanism for acid and base catalyzed condensation.

5.2.3. Gelation

With time and concurrent hydrolysis and condensation reactions of the alkoxide precursors, gelation will occur and produce a three-dimensional network of linked sol macroparticles. The gel network formation will be dependent on the degree of crosslinking prior to gelation and the size of the precursor sol particulates.[24] With gelation, the system experiences dramatic changes in physical properties as the system begins to solidify. The onset of gelation has a

characteristic spike in viscosity, forms to the shape of its mold or container, and supports stress elastically.[25] Although the onset of gelation may be easily defined qualitatively, the analytical determination of gelation is much more difficult as no endotherm, exotherm, or significant chemical change occurs.[26]

Sacks and Sheu characterized the t_{gel} of sol-gel systems by measuring the viscoelastic response as a function of shear rate.[27] First, the complex shear modulus G was measured by a narrow gap viscometer, assuming the sol oscillates at a frequency ω. Next, the complex shear modulus was defined in terms of storage modulus and loss modulus in equation (5.1), where G' is the storage modulus and G" is the loss modulus.

$$G = G'(\omega) + iG"(\omega) \tag{5.1}$$

The elastic component of the sol is represented by the storage modulus, whereas the viscious component is represented by the loss modulus. The sol-gel storage moduli increased dramatically once t_{gel} was reached, a consequence of the interconnected sol particles ability to elastically support a load. Because t_{gel} is not an intrinsic material property, determination of t_{gel} will depend on the size of the container or mold supporting the sol-gel sample. Several additional factors will impact t_{gel} including pH, hydrolysis and condensation rates, temperature, solvent choice, and solvent removal.

The considerable spike in viscosity associated with gelation is expected due to the interconnection of sol particles to form a three-dimensional network spanning the container or mold.[28] Figure 5.2 demonstrates the characteristic viscosity increase associated with the onset of gelation. Time and sol particle size

represent the two reaction variables contributing most significantly to higher viscosities of sol-gel systems, thus affecting t_{gel}. The selection of acid or base catalysis for the hydrolysis and condensation of the sol-gel systems impacts the size of the sol particles. Typically, acid catalyzed sol-gel chemical reactions induce large sol particles, leading to higher viscosities than base catalyzed sol-gel reactions.[29] The concentration of sol-gel solvents, primarily alcohols and water, has a complex relationship with the sol-gel viscosity. When solvent concentration is raised from small amounts, sol-gel viscosity increases by raising the hydrolysis and condensation rates. Once the solvent concentration increases further to severely dilute the sol-gel system, viscosity decreases are observed.

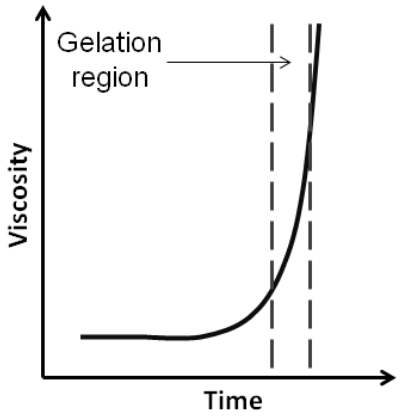

Figure 5.2: Characteristic viscosity increase indicative of gelation in sol-gel systems [adapted from Ref. 13].

5.2.4. Aging, drying, and densification

The final sol-gel processing steps (aging, drying, and densification) convert the porous gels to highly crosslinked, solid materials and impact the final degree of network porosity. Aging occurs after the onset of gelation, and is defined by maintaining the gel for a set period of time to allow for further condensation and

porosity reduction.[25] The aging sol-gel processing step may be the most important to achieving the desired final material properties as the extent of crosslinking is strongly dictated by the aging time. Three distinct processes may occur during the aging stage: condensation, syneresis, and coarsening.[30] When the gelled product is maintained within the original solvent (typically water), trans-pore condensation reactions may manifest between neighboring silanol groups. During aging, sample shrinkage is common as the degree of crosslinking increases from continued condensation. Increasing the sol-gel environmental temperature may further induce crosslinking and shrinkage by elevating the rate of the condensation reactions.[31]

Syneresis describes the shrinkage of the gelled material coupled with expulsion of the water and alcohol from the gel pores, thus transforming the gel to a solid material. The gel network contraction has been attributed to both the condensation reaction as well as the tendency to reduce the interfacial interactions between the solid and liquid. The rate of syneresis may be controlled by the reaction variables to tailor the degree of crosslinking and porosity. The syneresis process slows when the pH approaches the isoelectric point as a result of reducing the condensation rate.[32] The presence of organic solvents may also reduce the rate of syneresis if hydrogen bonding occurs between the organic solvent and silanol groups. In addition to condensation and syneresis, coarsening is an additional aging step characterized by the precipitation of dissolved gel into the curvatures surrounding particulates.[33] The small “necks” between particles have

low solubility and will preferentially accumulate dissolved sol-gel materials, thus strengthening the gel network and altering the size of network pores.

The drying stage of sol-gel processing describes the removal of liquid from the pores of the interconnected gel network. Initially, the volume reduction of the gel network associated with shrinkage will be equivalent to the volume of liquids expelled from the gel, and a constant rate of drying will occur if the network still maintains considerable flexibility.[34] With continued liquid evaporation, the gelled network reaches a critical point of drying where the system cannot undergo further shrinkage due to increased stiffness. Once the critical point is reached, liquid retreats to the porous sections of the gelled network and large pressure differences arise across the curved pore interfaces. If the gel network has not undergone proper aging, the interconnected network may crack due to the capillary stress.[35] Several techniques have been researched to deter network cracking including the use of supercritical drying, freeze-drying, increased aging time, and drying control additives.[30, 36-38]

Densification of the gel network is the final stage of sol-gel processing where the gelled network is subjected to a thermal treatment to simultaneously eliminate pores and increase network density. While some hybrid materials cannot withstand elevated temperatures and must be dried at room temperature, subjecting the gel to thermal treatments results in pore reduction and removal.[39] Network structural changes will be influenced by the rate of heating applied to the gel. Maintaining a consistent temperature eventually produces a steady decrease in densification with the reduction of pores and elimination of residual liquid. If the

gelled network is subjected to a fast heating rate, densification occurs much more quickly but could potentially entrap gaseous species, potentially leading to entrapment and cracking.[40]

5.2.5. Effect of reaction parameters

The complexity of the preceding sol-gel processing steps occurs as a result of the concurrent chemical reactions, network formation, liquid removal, and densification. Despite its complexity, sol-gel systems have an inherent flexibility in their production as several reaction parameters may be specifically tailored to achieve a desired final product. The structure of the precursor alkoxide-containing sol greatly impacts hydrolysis and condensation, thus contributing to the formation the gelled network. In particular, steric hindrance from the alkoxide precursor structure decreases both the hydrolysis and condensation rates.[41] Longer alkyl chain lengths and chain branching have been shown to decrease the sol-gel chemical reactions. Larger alkoxide functional groups will slow hydrolysis and condensation by crowding the transition state.[42]

The concentration of water utilized in sol-gel processing contributes to the gel network formation. Linear and branched gel networks are typically observed with lower water concentrations ($H_2O/Si < 2$) as the alkoxide groups will only partially hydrolyze.[13] With simultaneous condensation reactions, linear connections between sol particles dominate. As the water concentration increases to the range of 4 – 10 H_2O/Si, the alkoxide precursors tend to be fully hydrolyzed with acid catalyzed sol-gel systems and form gelled networks. Conversely, base catalyzed systems with increased water concentrations may phase separate as the gelation

occurs rapidly and unhydrolyzed alkoxide precursors can become entrapped within the network.[43] Further increases in the water concentration (25 – 50 H_2O/Si) hinder network formation as interconnection reactions between the alkoxide precursors are less likely from dilution and the final network structure consists of isolated, dense particles.

Due to immiscibility between hydrophobic alkoxide sol precursors and water, co-solvents may be added to sol-gel system to facilitate hydrolysis of the alkoxide functional groups.[44] The most common co-solvents to increase miscibility are alcohols,[45] but tetrahydrofuran,[46] formamide,[47] and 1,4-dioxane[48] have also been reported to successfully serve as co-solvents for sol-gel systems. Co-solvents will participate in breaking the hydrogen bonds of water, thus increasing the solvation of H^+ and OH^- ions and decrease solution acidity or basicity and diminish the hydrolysis reactions.[49] However, raising the co-solvent concentration will produce the opposite effect, raising the catalyst activity and hydrolysis rate.

5.2.6. Non-silicon sol-gel chemistry

Although silicon-based precursors are currently the most widely studied in sol-gel science, metal oxide-based sol-gel technologies may also be employed to produce gelled networks. Metal oxide sol-gel chemistry is largely dependent on the selection of the metal atom because the metal electropositive character will dictate the rates of hydrolysis and condensation. Metals used in metal oxide precursors include zirconium, titanium, and tungsten. Non-silicon metal alkoxides have higher electropositive character, leading to higher rates of nucleophilic attack compared to alkoxysilane-precursors. Metal alkoxide precursors undergo hydrolysis and

condensation both in the presence and absence of acid and base catalysts. The mechanism for hydrolysis and condensation of metal alkoxides in the absence of acid or base catalysts is shown in Scheme 5.3. The hydrolysis reaction proceeds by two steps. First, water reacts with the metal alkoxide precursor by a nucleophilic addition. Second, alcohol is generated with a proton transfer from the water to alkoxy group. Metal alkoxide condensation mechanisms proceed by three different mechanisms: alcoxolation, oxolation, and olation. Alcoxolation describes the reaction of M-OH speices with another alkoxide, oxolation describes the reaction of two M-OH species, and olation describes the reaction of M-OH with a solvated metal species. Similar to alkoxysilane precursors, metal oxide sol-gel precursors are affected by the selection of a catalyst, steric effects, and solvent choice.

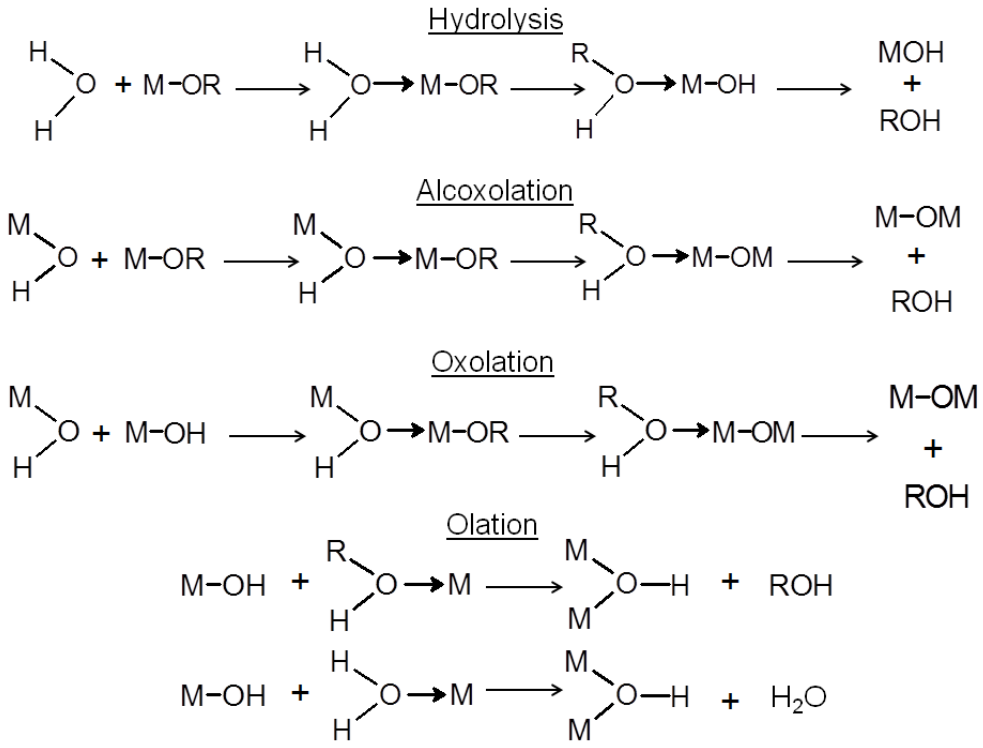

Scheme 5.3: Hydrolysis and condensation reaction mechanisms of metal alkoxide precursors.

5.3. Organic-inorganic hybrid materials

Although sol-gel chemistry has its complexities due to simultaneous reactions and sensitivity to several reaction parameters, the ability to tailor the final hybrid network to achieve unique chemical and physical properties promotes the use of sol-gel methods to create high performance materials. One particular class of sol-gel materials, organic-inorganic hybrids, has emerged as a viable alternative to traditional polymeric composites due to the nanoscale mixing between the organic and inorganic components. Organic-inorganic hybrids are continually becoming more versatile as the availability and variety of alkoxysilane organic precursors increases. Because organic-inorganic hybrids may be produced from both small monomeric species and large polymeric materials, the resulting organic-inorganic network properties will largely be a result of the precursor materials.

5.3.1. Common alkoxysilane organic precursors

Several monomeric alkoxysilane organic precursors have been utilized in sol-gel chemistry to introduce additional functionality in the crosslinked coatings. Methyl trimethoxysilane, tetramethyl orthosilicate, methyl trimethoxysilane, and tetraethyl orthosilicate are four commonly used silane crosslinking agents employed in the formation of organic-inorganic hybrids, and their structures are the building blocks of additional alkoxysilane precursors containing additional organic functional groups.[50] With multi-functional organosilanes, the alkoxide group may participate in hydrolysis and condensation reactions to create continuous inorganic linkages while possessing an organic functionality. Figure 5.3 displays several alkoxysilane organic precursors employed in the preparation of organic-inorganic

hybrids. Again, the ability to tailor the final network properties largely depend on the selection of the alkoxysilane precursor.

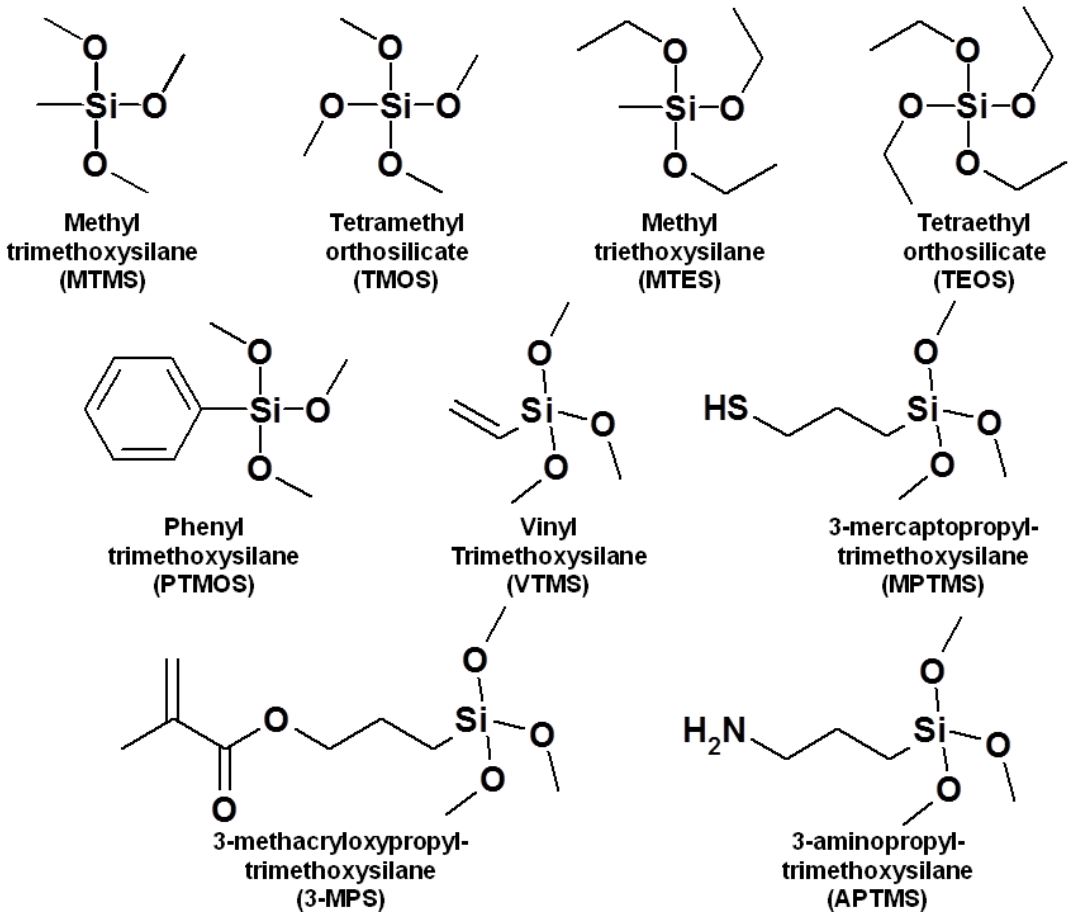

Figure 5.3: Common alkoxysilane organic precursors utilized in the production of organic-inorganic hybrids.

Two common alkoxysilane organic precursors contain both a silane functional group to undergo hydrolysis and condensation and a site of unsaturation to participate in free radical polymerizations: vinyl trimethoxysilane (VTMS) and 3-methacryloxypropyltrimethoxysilane (3-MPS). VTMS has been employed to create organic-inorganic hybrids that may undergo photopolymerization. Crivello et al.

reported the synthesis of trialkoxysilane-functional epoxides using VTMS to create silane-epoxide resins that may undergo thermal or UV-induced cationic polymerization.[51] Hydrosilation with VTMS produced multi-functional precursors bearing both trimethoxysilane and epoxy functionality for both sol-gel and cationic polymerization reactions to create organic-inorganic hybrid materials. UV-curable organic-inorganic hybrids composed of VTMS and polyurethane acrylates were studied by Choi and coworkers for the aluminum-polycarbonate interfaces of automobiles.[52]

Pellice et al. reported the development of 3-MPS-derived organic-inorganic hybrid sol by a two-step synthesis process involving sol-gel chemistry and free radical copolymerization.[53] First, 3-MPS and tetraethyl orthosilicate (TEOS) were reacted through inorganic polycondensation to create a sol precursor containing a site of unsaturation. Second, 2-hydroxyethylmethacrylate (HEMA) was copolymerized with the 3-MPS derived sol to create an organic-inorganic network. The final degree of gelation was determined to be a result of both the inorganic polycondensation and free radical copolymerization reactions. Copolymers derived from 3-MPS to create alkoxysilane-functional to potentially be used for sol-gel precursors have also been carried out using controlled free radical polymerization techniques such as atom transfer radical polymerization (ATRP)[54] and reversible addition-fragmentation chain transfer (RAFT)[55]. The alkoxysilane precursor phenyl trimethoxysilane (PTMOS) has been employed for the creation of hydrophobic organic-inorganic hybrid coatings for corrosion protection. Sol-gel derived organic-inorganic hybrids for corrosion protection of aluminum substrates were researched

by Raps et al. as viable alternatives to chromate-based aluminum pretreatments.[56] Several stoichiometric variations of alkoxysilane precursors PTMOS, 3-MPS, and TEOS were utilized to create hybrid sol-gel films containing corrosion inhibiting dopants. First, the controlled hydrolysis of the sol precursors was performed by acid catalysis with a stoichiometric ratio of 4 mol H_2O to 1 mol TEOS. Thermal free radical initiator 2,2'-azobis(2-methylbutyronitrile) was added to the sol solution, followed by free radical polymerization to create the continuous organic network. Electrochemical impedance spectroscopy (EIS) and the scanning vibrating electrode technique (SVET) measured increased barrier performance and characterized local corrosion activity for each sol-gel hybrid film. Significant improvements in barrier protection with the addition of corrosion inhibiting dopants dispersed throughout the organic-inorganic hybrid network were attributed to increased active corrosion protection from the stabilized aluminum oxide layer and self-healing properties. PTMOS-based gas separation organic-inorganic hybrid membranes were studied as permselective coatings.[57] Various proportions of alkoxysilane precursors PTMOS and TMOS were pre-hydrolyzed, cast onto polyacrylonitrile substrates, and dried for several days at room temperature. The gas flux and selectivity of the resulting hybrid membranes were measured by applying pure gases (carbon dioxide, nitrogen, and helium) to the membranes at fixed pressures of 200 and 500 kPa. The PTMOS-TMOS hybrids demonstrated higher gas selectivity due to more complete crosslinking.

The alkoxysilane precursor 3-mercaptopropyltrimethoxysilane (MPTMS) has been utilized in sophisticated applications for chromatography and mesoporous

composites. Organic-inorganic hybrid monoliths derived from sol-gel processing of MPTMS and TEOS for capillary electrochromatography use was reported by Chen and coworkers.[58] After hydrolysis of the alkoxysilane precursors, oxidation of the gelled product within a column was performed to yield sulfonic acid groups, which act as cation exchange agents and create a stabilized electroosmotic flow. The silica-based column successfully isolated natural alkaloids theophylline and caffeine additives from eight beverages (carbonated, juice, and tea) which were passed through the column, thereby providing an efficient and facile analytical approach towards determined alkaloid content in beverages. Organic-inorganic mesoporous hybrids containing MPTMS were created in a one-pot synthesis procedure by Yu et al. in the presence of sodium silicates, a inexpensive replacement material for tetraalkoxysilane precursors, with high surface area (899-1042 m^2/g) and pore volume (0.70 – 1.09 cm^3/g).[59]

Epoxy-based organic-inorganic hybrids have been crosslinked with 3-aminopropyltrimethoxysilane (APTMS) for applications in adhesives and matrix resins for composites. Canto and coworkers researched the combination of epoxies with polysiloxanes in the development of high performance organic-inorganic hybrid coatings.[60] Uncured bisphenol A epoxy resin was reacted with APTMS by an epoxy-amine addition reaction followed with hydrolysis and condensation to produce self-supported hybrid films. The resulting epoxy-amine hybrid films demonstrated high thermal stability with degradation temperatures exceeding 400 °C. A similar approach was utilized to create epoxy-silica organic-inorganic hybrid films with enhanced mechanical and thermal properties by

incorporating polysilcic acid nanoparticles into the hybrid network.[61] After the epoxy-amine crosslinking reactions between a bisphenol A epoxy resin and 3-aminopropyltriethoxysilane (APTES), polysilcic acid nanoparticles highly functionalized with silanol groups were added to the epoxy-amine mixture. Concurrent hydrolysis and condensation of the APTES and polysilcic acid produced a continuous inorganic network throughout the epoxy-amine resin to create the organic-inorganic hybrid material. Increasing the silica content produced hybrid films demonstrating enhanced tensile strength, impact strength, T_g values, and degradation temperatures.

5.3.2. Layered silicate incorporation

Although the incorporation of layered silicates into organic-inorganic hybrid materials to couple the advantageous properties of two nanocomposite classes into one network has seemingly many interesting research possibilities, very few publications have addressed this synergistic approach to high performance materials. One example of coupling layered silicates with sol-gel organic-inorganic films is the creation of polyimide-silica organic-inorganic hybrids by dispersing hydroxy-functional montmorillonite clay with two alkoxysilane precursors, as reported by Park et al.[62] Alkoxysilane terminated amide acid oligomer and TEOS were hydrolyzed and stirred for several hours, followed by mixing at high shear with a clay solution. The resulting hybrid films were primarily exfoliated, as indicated by XRD and TEM, and demonstrated high storage moduli and thermal stability than silicate-free hybrids. Additional research groups have studied the

incorporation of silica nanoparticles into organic-inorganic hybrid materials, but the utilization of clays in sol-gel based hybrid films is severely limited.

5.4. Summary

Organic-inorganic hybrid materials created by sol-gel processing techniques represent another class of nanocomposite materials as the inorganic domains may be dispersed in the nanometer range throughout a continuous organic network. The sol-gel process may be divided into several steps, although many occur simultaneously. Hydrolysis and condensation of alkoxysilane functional groups is typically acid or base catalyzed, and the rates of hydrolysis and condensation will be dependent on the catalyst selection. Therefore, network formation is greatly influenced the pH of the reaction medium. Once gelation occurs, the network undergoes aging, drying, and densification to form the organic-inorganic hybrid material. Many reaction parameters will impact the formation of the hybrid network including structure of the alkoxysilane precursor, catalyst, and concentration of water. Several monomeric alkoxysilane organic precursors are commercially-available, and possess organic functional groups apart from the silane functionality. For example, vinyl-, methacryl-, amino-, and mercapto-functionalities may participate in free radical polymerizations or crosslinking reactions. With the proper selection of the alkoxysilane precursor, hybrid films may be tailored to achieve unique chemical and physical properties.

5.5. Research scope and purpose

As previously mentioned, the coupling of polymer-clay nanocomposite technology and organic-inorganic hybrid sol-gel materials has not yet been fully

explored. The goal of this research was to develop a process for creating novel organic-inorganic hybrid films containing layered silicates, and study the impact of the polymer structure and clay loading on the hybrid network properties. First, alkoxysilane-functional copolymers were synthesized in the presence of organically-modified montmorillonite clay by an in situ intercalative polymerization technique using 3-MPS and methyl methacrylate. The resulting copolymer-clay nanocomposite materials were then crosslinked by sol-gel processing, utilizing the alkoxysilane-functional groups located on the copolymer backbone. The resulting organic-inorganic hybrid materials, containing layered silicates, were studied for their morphology as well as their barrier, mechanical, thermal, and optical properties, specifically focusing on the impact of clay loading and copolymer backbone composition. The next objective with the development of novel organic-inorganic hybrid films was to create amine-based hybrid materials to be used in carbon dioxide capture or separation technology. Two routes were explored to incorporate the amine functional groups into the final network structure. The first route was to synthesize copolymers with the monomers 2-(dimethylamino)ethyl methacrylate and 3-MPS in the presence of modified clays to incorporate both amino and alkoxysilane functionalities into the copolymer backbone. The second route was to incorporate amine-functionality in the sol-gel processing step by utilizing the alkoxysilane precursor APTMS. The final hybrid variation researched was to explore the influence of conventional free radical copolymerizations with controlled free radical copolymerizations via RAFT.

5.6. References

1. Klein, L. C., *Sol-gel technology for thin films, fibers, preforms, electronics, and specialty shapes*. William Andrew: 1988.

2. Verghese, M.; Ramanathan, K.; Ashraf, S.; Kamalasanan, M.; Malhotra, B., *Chem. Mat.* **1996,** *8* (4), 822-824.

3. Lev, O.; Wu, Z.; Bharathi, S.; Glezer, V.; Modestov, A.; Gun, J.; Rabinovich, L.; Sampath, S., *Chem. Mat.* **1997,** *9* (11), 2354-2375.

4. Livage, J., *Sol--Gel Science and Technology* **1989**, 103-152.

5. Sanchez, C.; Ribot, F.; Lebeau, B., *Journal of Materials Chemistry* **1999,** *9* (1), 35-44.

6. Letailleur, A. A.; Ribot, F.; Boissière, C.; Teisseire, J.; Barthel, E.; Desmazières, B.; Chemin, N.; Sanchez, C., *Chem. Mat.* **2011**.

7. Park, S. H.; Park, J. S.; Yim, S. D.; Lee, Y. M.; Kim, C. S., *Journal of Power Sources* **2008,** *181* (2), 259-266.

8. Shelekhov, N. S., Sol-gel-polymer nanocomposite and methods thereof. Google Patents: 2011.

9. Kang, X.; Mai, Z.; Zou, X.; Cai, P.; Mo, J., *Talanta* **2008,** *74* (4), 879-886.

10. Gupta, R.; Chaudhury, N., *Biosensors and Bioelectronics* **2007,** *22* (11), 2387-2399.

11. Reetz, M. T.; Zonta, A.; Simpelkamp, J., *Biotechnology and Bioengineering* **1996,** *49* (5), 527-534.

12. Podbielska, H.; ZA, A. U. J. A. R., *Technical Sciences* **2005,** *53* (3).

13. Wright, J. D.; Sommerdijk, N. A. J. M., *Sol-gel materials: chemistry and applications*. CRC: 2001; Vol. 4.

14. Kasemann, R.; Schmidt, H., *New Journal of Chemistry* **1994,** *18* (10), 1117-1124.

15. Brinker, C. J.; Scherer, G. W., *Sol-gel science: the physics and chemistry of sol-gel processing*. Academic Pr: 1990.

16. McGavack Jr, J.; Patrick, W., *Journal of the American Chemical Society* **1920,** *42* (5), 946-978.

17. Patrick, W.; Barclay, E., *The Journal of Physical Chemistry* **1925,** *29* (11), 1400-1405.

18. Patrick, W.; Frazer, J.; Bush, R., *The Journal of Physical Chemistry* **1927,** *31* (10), 1511-1520.

19. Corriu, R. J. P.; Leclercq, D., *Angewandte Chemie International Edition in English* **1996,** *35* (13-14), 1420-1436.

20. Pope, E.; Mackenzie, J., *Journal of Non-Crystalline Solids* **1986,** *87* (1-2), 185-198.

21. Wen, J.; Wilkes, G. L., *Chem. Mat.* **1996,** *8* (8), 1667-1681.

22. Matejka, L.; Dukh, O.; Meissner, B.; Hlavatá, D.; Brus, J.; Strachota, A., *Macromolecules* **2003,** *36* (21), 7977-7985.

23. Figus, C. Hybrid organic-inorganic materials: from self-organization to nanocrystals. University of Sassari, 2010.

24. Siouffi, A. M., *Journal of Chromatography A* **2003,** *1000* (1-2), 801-818.

25. Hench, L. L.; West, J. K., *Chemical Reviews* **1990,** *90* (1), 33-72.

26. Brinker, C.; Keefer, K.; Schaefer, D.; Ashley, C., *Journal of Non-Crystalline Solids* **1982,** *48* (1), 47-64.

27. Sacks, M.; Sheu, R. S., *Wiley, New York* **1986**, 100.

28. Brinker, C.; Hurd, A.; Schunk, P.; Frye, G.; Ashley, C., *Journal of Non-Crystalline Solids* **1992,** *147*, 424-436.

29. Klein, L., *Annual Review of Materials Science* **1985,** *15* (1), 227-248.

30. Davis, P. J.; Jeffrey Brinker, C.; Smith, D. M., *Journal of Non-Crystalline Solids* **1992,** *142*, 189-196.

31. Pope, E. J. A.; Sano, Y.; Wang, S.; Sarkar, A., Sol-gel process for glass and ceramic articles. Google Patents: 1991.

32. Dunn, B.; Zink, J. I., *Journal of Materials Chemistry* **1991,** *1* (6), 903-913.

33. Hench, L. L., *Sol-gel silica: properties, processing, and technology transfer*. William Andrew: 1998.

34. Mackenzie, J. D.; Bescher, E. P., *Accounts of Chemical Research* **2007,** *40* (9), 810-818.

35. Chiu, R.; Garino, T.; Cima, M., *Journal of the American Ceramic Society* **1993,** *76* (9), 2257-2264.

36. Yamamoto, T.; Nishimura, T.; Suzuki, T.; Tamon, H., *Journal of Non-Crystalline Solids* **2001,** *288* (1), 46-55.

37. Tamon, H.; Ishizaka, H., *Drying Technology* **1999,** *17* (7-8), 1653-1665.

38. Hench, L. L.; Orcel, G. F., Drying control chemical additives for rapid production of large sol-gel derived silicon, boron and sodium containing monoliths. Google Patents: 1989.

39. Burgos, M.; Langlet, M., *Journal of Sol-Gel Science and Technology* **1999,** *16* (3), 267-276.

40. Guglielmi, M., *Journal of Sol-Gel Science and Technology* **1997,** *8* (1), 443-449.

41. Livage, J.; Sanchez, C., *Journal of Non-Crystalline Solids* **1992,** *145*, 11-19.

42. Chambers, R. C.; Jones Jr, W. E.; Haruvy, Y.; Webber, S. E.; Fox, M. A., *Chem. Mat.* **1993,** *5* (10), 1481-1486.

43. Loy, D. A.; Baugher, B. M.; Baugher, C. R.; Schneider, D. A.; Rahimian, K., *Chem. Mat.* **2000,** *12* (12), 3624-3632.

44. Sharp, K. G., *Journal of Sol-Gel Science and Technology* **1994,** *2* (1), 35-41

45. Novak, B. M.; Davies, C., *Macromolecules* **1991,** *24* (19), 5481-5483.

46. Huang, H. H.; Orler, B.; Wilkes, G. L., *Macromolecules* **1987,** *20* (6), 1322-1330.

47. Kaji, H.; Nakanishi, K.; Soga, N., *Journal of Sol-Gel Science and Technology* **1993,** *1* (1), 35-46.

48. Gash, A. E.; Tillotson, T. M.; Satcher Jr, J. H.; Poco, J. F.; Hrubesh, L. W.; Simpson, R. L., *Chem. Mat.* **2001,** *13* (3), 999-1007.

49. Klingshirn, M. A.; Spear, S. K.; Holbrey, J. D.; Rogers, R. D., *Journal of Materials Chemistry* **2005,** *15* (48), 5174-5180.

50. Judeinstein, P.; Sanchez, C., *J. Mater. Chem.* **1996,** *6* (4), 511-525.

51. Crivello, J. V.; Song, K. Y.; Ghoshal, R., *Chem. Mat.* **2001,** *13* (5), 1932-1942.

52. Choi, H.; Lim, C.; Lee, D.; Kim, B., *Journal of Polymer Engineering* **2009,** *29* (1-3), 1-14.

53. Pellice, S. A.; Williams, R. J. J.; Sobrados, I.; Sanz, J.; Castro, Y.; Aparicio, M.; Duran, A., *Journal of Materials Chemistry* **2006,** *16* (32), 3318-3325.

54. Du, J.; Chen, Y., *Macromolecules* **2004,** *37* (17), 6322-6328.

55. Mellon, V.; Rinaldi, D.; Bourgeat-Lami, E.; D'Agosto, F., *Macromolecules* **2005,** *38* (5), 1591-1598.

56. Raps, D.; Hack, T.; Wehr, J.; Zheludkevich, M. L.; Bastos, A. C.; Ferreira, M. G. S.; Nuyken, O., *Corrosion Science* **2009,** *51* (5), 1012-1021.

57. Smaïhi, M.; Jermoumi, T.; Marignan, J.; Noble, R. D., *Journal of Membrane Science* **1996,** *116* (2), 211-220.

58. Chen, M.-L.; Zheng, M.-M.; Feng, Y.-Q., *Journal of Chromatography A* **2010,** *1217* (21), 3547-3556.

59. Yu, N.; Gong, Y.; Wu, D.; Sun, Y.; Luo, Q.; Liu, W.; Deng, F., *Microporous and Mesoporous Materials* **2004,** *72* (1-3), 25-32.

60. Canto, C. F.; Prado, L. A. S. d. A.; Radovanovic, E.; Yoshida, I. V. P., *Polymer Engineering & Science* **2008,** *48* (1), 141-148.

61. Lu, S.-R.; Zhang, H.-L.; Zhao, C.-X.; Wang, X.-Y., *Journal of Materials Science* **2005,** *40* (5), 1079-1085.

62. Park, C.; Smith Jr, J. G.; Connell, J. W.; Lowther, S. E.; Working, D. C.; Siochi, E. J., *Polymer* **2005,** *46* (23), 9694-9701.

CHAPTER 6. ORGANIC-INORGANIC HYBRID COATINGS DERIVED FROM ALKOXYSILANE-FUNCTIONAL CLAY NANOCOMPOSITES

6.1. Introduction

The combination of inorganic and organic materials to create hybrid composites via sol-gel processing has produced high-performance coatings possessing enhanced material properties. Several advantageous processing and reaction conditions for sol-gel syntheses have contributed to the increased use of sol-gel based materials, including mild reaction temperatures, highly pure products, relatively easy control of reaction kinetics, and control of the final sol-gel structure.[1] Based on these favorable attributes, sol-gel materials have been employed as protective coatings,[2-5] optical materials,[6-7] catalysts,[8-9] and sensors.[10-12] Recently, organic-inorganic hybrids have been widely studied as a relatively facile approach towards incorporating organic and inorganic domains into one system. Commonly, monomeric alkoxysilane precursors are employed to impart additional organic functional groups to the final hybrid network. These precursor materials may crosslink via sol-gel chemistry with its silane functional group while possessing additional organic functionality. Alkoxysilane precursors have been employed to undergo both free radical and UV-curing polymerizations,[13-14] to crosslink by epoxy-amine chemistry,[15] and to create acrylate-functional coatings.[16]

Another popular method of incorporating organic and inorganic materials into one hybrid system is the incorporation of nanosized layered silicate (clay) fillers into polymer matrices to form polymer/clay nanocomposites. Several

enhancements in material properties have been reported with the formation of nanocomposites containing organically modified clays including increased tensile strength,[17] thermal stability,[18-19] and barrier protection.[20-21] Organomodification of the clay platelet surfaces by cationic surfactants improves the miscibility between the hydrophilic inorganic silicates and the host organic polymer. Through this increased compatibility, the polymer chains more easily intercalate between the clay layers and enhance the polymer/clay interfacial interaction. Because of the nanoscale interactions between the reinforcing clay fillers and polymer matrix, significantly lower clay loading (1 – 5 wt.%) are needed to observe material enhancement as compared to traditional phase-separated composites (20 – 30 wt.%).[22]

Although the success of both sol-gel and polymer/clay nanocomposite organic-inorganic hybrid materials have been widely reported, the coupling of both techniques has not yet been explored. By implementing the advantageous material properties of each independent system into one network, novel hybrid materials with enhanced mechanical, thermal, and barrier properties may be formed. Therefore, this research focuses on the development of organic-inorganic hybrid sol-gel coatings derived from alkoxysilane-functional polymer/clay nanocomposites. The formation of a crosslinked polymer network with both sol-gel and nanocomposite inorganic components proceeded through a two step process. First, free radical copolymerization of 3-methacryloxypropyltrimethoxysilane (3-MPS) and methyl methacrylate (MMA) was conducted in the presence of organomodified clay to form an alkoxysilane-functional clay nanocomposite sol

precursor. Second, crosslinking agent was reacted with the silane-functional sol precursor to create continuous inorganic Si-O-Si linkages throughout the polymer matrix containing the clay fillers. The impact of the copolymer backbone was explored by varying the monomer molar ratio, and the clay loading ranged from 1 – 10 wt.%.

6.2. Experimental

6.2.1. Materials

Methyl methacrylate (MMA), tetraethyl orthosilicate (TEOS), 2-dimethylaminoethyl methacrylate (DMAEMA), 1-bromooctane, and anhydrous toluene were purchased from Sigma Aldrich (Milwaukee, WI). MMA was purified by passing through a column containing activated, basic aluminum oxide to remove the inhibitor. Monomer 3-methacryloxypropyltrimethoxysilane (3-MPS) was obtained from Gelest (Morrisville, PA), and purified by distillation under vacuum. Initiator 2,2'-azobis(2-methylbutyronitrile), "Vazo 67", was gratefully supplied by DuPont (Belle, WV). Cloisite® Na^+, an unmodified montmorillonite clay, was obtained from Southern Clay Products (Gonzales, TX). Unless specified, materials were used as received.

6.2.2. Preparation of 2-methacryloyloxyethyloctyldimethylammonium modified montmorillonite clay

The preparation of a quaternary ammonium surfactant bearing methacrylate functionality was similar to the procedure reported by Zeng and Lee.[23] DMAEMA (0.050 mol), 1-bromooctane (0.025 mol), and ethyl acetate (0.100 mol) were charged to a 3-neck, 100 mL RBF equipped with a temperature probe/controller,

magnetic stir bar, condenser, heating mantle, and stir plate. The solution was mixed for 24 hours at 60 °C under reflux to initiate a quaternization reaction (Scheme 6.1). The reaction mixture was then cooled to room temperature, and the precipitate was filtered off. The resulting 2-methacryloyloxyethyloctyldimethyl-ammonium bromide (MEOAB) product was dried in an oven at 45 °C for one hour.

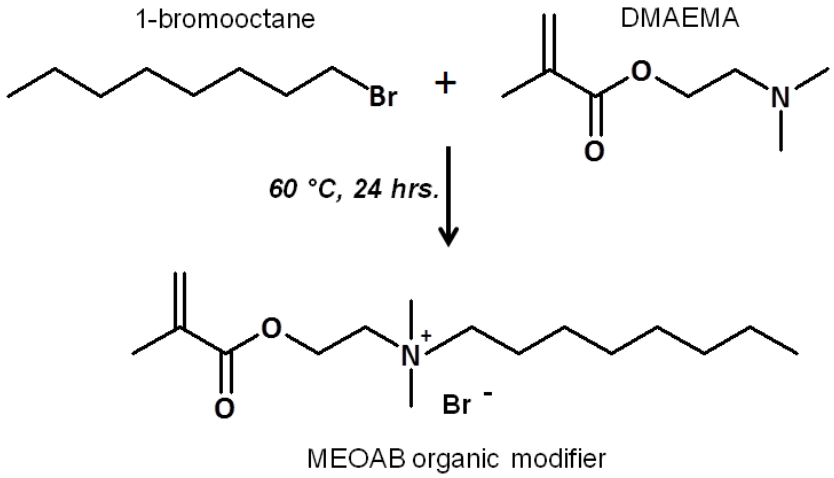

Scheme 6.1: Quaternization reaction of 1-bromooctane and 2-(dimethyl-amino)ethyl methacrylate (DMAEMA) to synthesize 2-methacryl-oyloxyethyloctyldimethylammonium bromide (MEOAB).

Next, an ion exchange reaction to functionalize the unmodified Cloisite® Na^+ montmorillonite clay with MEOAB was performed (Scheme 6.2). The unmodified clay (10.00 g) was added to a 3-neck, 1000 mL RBF with 800 mL of deionized water equipped with a mechanical stir rod, and stirred vigorously for 60 minutes at room temperature. MEOAB (5.30 g) was carefully added to the clay/H_2O solution, and the resulting mixture was stirred quickly overnight at room temperature. The solution was filtered and rinsed several times with deionized water until no bromide counterion was observed in the filtrate from 0.1 N $AgNO_3$ addition. The resulting

MEOA-clay was dried in an oven at 50 °C for several hours, then ground to a fine powder with a mortar and pestle.

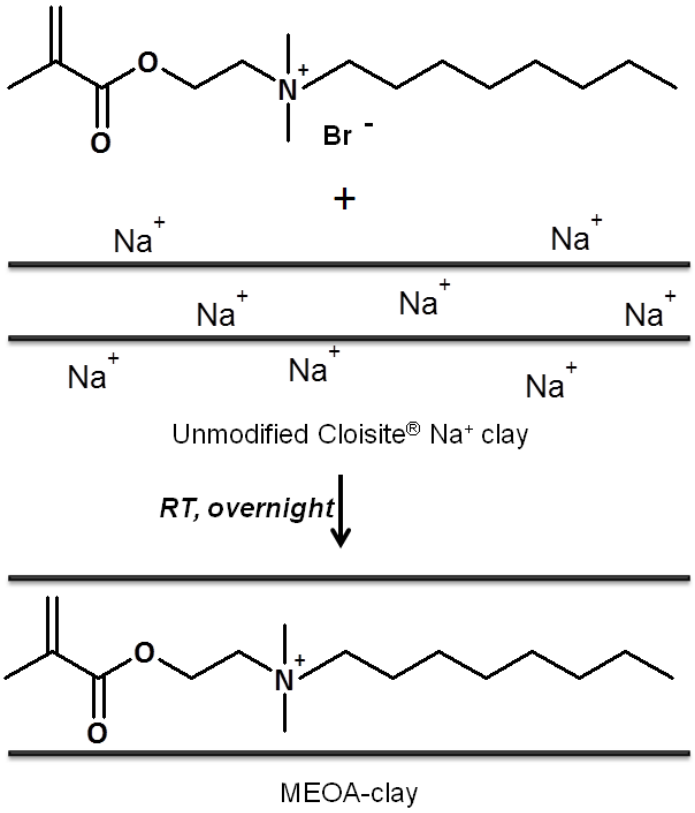

(b)

Scheme 6.2: Ion exchange reaction of MEOAB and Cloisite® Na^+ to produce methacrylate-functional organomodified montmorillonite clay.

6.2.3. Nanocomposite formation via copolymerization with organomodified clay

Copolymers of MMA and 3-MPS were prepared by conventional free radical polymerization using a semi-batch process in the presence of the MEOA-clay. Three series of the copolymer/clay nanocomposites were prepared with MMA:3-MPS molar ratios of 3:1, 2:1, and 1:1 and 0, 1, 2, 5, and 10 wt.% clay (based on total monomer weight) for a total of 15 nanocomposites (Table 6.1). Monomers

MMA and 3-MPS were added with MEOA-clay to a 1-neck, 250 mL RBF and stirred overnight. For example, the copolymer with a 3:1 molar ratio and 5 wt.% clay consisted of 15.00 g MMA (0.15 mol), 12.42 g 3-MPS (0.05 mol), and 1.37 g MEOA-clay. Toluene (40 g, 0.43 mol) and TEOS (10 g, 0.05 mol) were added to a 4-neck, 250 mL RBF equipped with a temperature probe/controller, nitrogen inlet, mechanical stirring rod, addition funnel, condenser, and heating mantle. The solvents were heated to 70 °C under reflux in a nitrogen atmosphere. Initiator 2,2'-azobis(2-methylbutyronitrile) (2.5 wt.% of total monomer weight) was added to the monomer and clay solution, stirred until dissolved, and charged to the addition funnel. The monomer solution was then slowly added dropwise to the solvent mixture at a rate of 1 mL/min. The copolymerization continued for 24 hours, and solvents were removed by a rotary evaporator.

TABLE 6.1
Alkoxysilane-functional copolymer-clay nanocomposite nomenclature and composition

MMA:3-MPS (molar ratio)	Nanocomposite Name	MEOA-clay (wt.%)
3:1 Molar Ratio	Control-3_1	0
	NC1_3-1	1
	NC2_3-1	2
	NC5_3-1	5
	NC10_3-1	10
2:1 Molar Ratio	Control-2_1	0
	NC1_2-1	1
	NC2_2-1	2
	NC5_2-1	5
	NC10_2-1	10
1:1 Molar Ratio	Control-1_1	0
	NC1_1-1	1
	NC2_1-1	2
	NC5_1-1	5
	NC10_1-1	10

6.2.4. Organic-inorganic hybrid formation via sol-gel chemistry

Once the copolymer/clay nanocomposites had been synthesized, the alkoxysilane functionality from the 3-MPS monomer was reacted via sol-gel chemistries to create a crosslinked coating with continuous inorganic linkages throughout the cured film. First, a solution composed of TEOS, deionized water, ethanol, and hydrochloric acid was mixed with the molar ratio (1:25:5:0.025), similar to a solution created by Chan et al.[24] Next, a 90:10 weight ratio of nanocomposite:TEOS solution was mixed for 1 hour at room temperature to initiate hydrolysis and condensation, then spin coated onto glass, aluminum, and porous (5-6 μm) PTFE membrane substrates (Savillex Corporation) substrates for 20 seconds at 500 RPM. The coated substrates were placed in a vacuum oven at 70 °C for three hours for a thermal treatment to complete cure and densify the networks.

6.2.5. Characterization

The nanocomposites were first characterized prior to sol-gel coating formation to study the impact of monomer molar ratio and MEOA-clay loading on the copolymer backbone and physical properties. Fourier-Transform infrared (FTIR) spectroscopy was employed to study the copolymer backbone structure using a Nicolet Magna-IR 850 spectrometer with detector type DTGS KBr, and spectra were obtained in transmittance mode between 400 and 4000 cm^{-1}. Gel permeation chromatography (GPC) was used to determine the copolymer molecular weight and polydispersity index using a Water 2410 Gel Permeation Chromatograph equipped with a refractive index detector. The copolymer samples

were dissolved in tetrahydrofuran (THF) to create a 1% solution. Calibration was performed with polystyrene standards, and a flow rate of 1 mL/min was used. The copolymer viscosity was measured from an ICI cone and plate viscometer at 75 °C.

The degree of clay dispersion within each sol-gel coating sample was determined by X-ray diffraction (XRD) using a Bruker AXS' D8 Discover diffractometer in Bragg-Brentano geometry with Cu Kα radiation at a wavelength of 1.5406 Å. Each sample was scanned from 1.5° – 50° 2θ, and the run time was 1 sec/step. Barrier properties of the sol-gel coatings were studied by employing ASTM E96, “Standard Test Methods for Water Vapor Transmission, Water Method.” Sol-gel samples coated on a porous membrane substrate were secured to a permeability cup containing distilled water, placed inside a controlled humidity chamber with conditions of 70% ± 2% relative humidity and 20 °C ± 2 °C, and mass loss was recorded over time until steady state was achieved. Duplicate samples were tested for verification. The sol-gel coating viscoelastic properties were examined by dynamic mechanical analysis using a TA Instruments Q800 Dynamic Mechanical Analyzer in tensile mode. Free films of the sol-gel coatings, approximately 15 mm x 5 mm in x 0.085 mm, were measured using 1 Hz frequency, constant strain of 0.05%, and a heating rate of 5 °C/min over a temperature range of -75 °C to 150 °C. Nanocomposite film hardness was measured with a BYK-Gardner pendulum hardness tester on aluminum substrates. Thermal stability was measured by thermogravimetric analysis using a TA Instruments Q500 Thermogravimetric Analyzer. Each nanocomposite sample was

heated from ambient temperatures to 600 °C at a rate of 20 °C/min in a nitrogen atmosphere. Nanocomposite optical clarity was determined by measuring percent transmittance at 400 nm with a Varian Cary 5000 UV-Vis Spectrometer.

6.3. Results and discussion

6.3.1. Organic-inorganic hybrid coatings derived from copolymer-clay nanocomposites

Organic-inorganic hybrid coatings have been widely studied due to the advantageous enhancements in material properties by incorporating both organic and inorganic components into one network. Both polymer/clay nanocomposites and hybrid sol-gel coatings utilize composite formation containing both organic and inorganic precursors. Despite the success of nanocomposites and sol-gel based coatings, little attention have been given to the synergistic impact of incorporating both established technologies into one hybrid coatings system. Therefore, the goal of this research is to create and study novel organic-inorganic hybrid sol-gel coatings derived from polymer/clay nanocomposite sol precursors. The development of these hybrid systems stems from two independent steps: synthesis of alkoxysilane-functional copolymer/clay nanocomposites and sol-gel coating creation using the nanocomposite precursor. Scheme 6.3 depicts the formation of the novel organic-inorganic hybrid coatings. Prior to the copolymerization reaction between MMA and 3-MPS, the unmodified Cloisite® Na^+ montmorillonite was modified with a quaternary alkylammonium cationic surfactant bearing a methacrylate functional group. Through this organomodification, the clay is rendered more organophilic, thereby increasing compatibility between the

hydrophilic clay platelets and the organic monomers. Additionally, the methacrylate-functionality provides a site of unsaturation that may participate in the copolymerization of MMA and 3-MPS. If the MEOA-clay reacts with either monomer, the copolymer chain may graft to the layered silicate surface, and the growing copolymer chains increased volume may disperse the silicates uniformly throughout the polymer matrix. Through the reaction of the 3-MPS monomer with MMA, the copolymer chains will possess alkoxysilane functional groups, which in turn may undergo hydrolysis and condensation with TEOS to organic-inorganic sol-gel coatings containing nanoclay fillers.

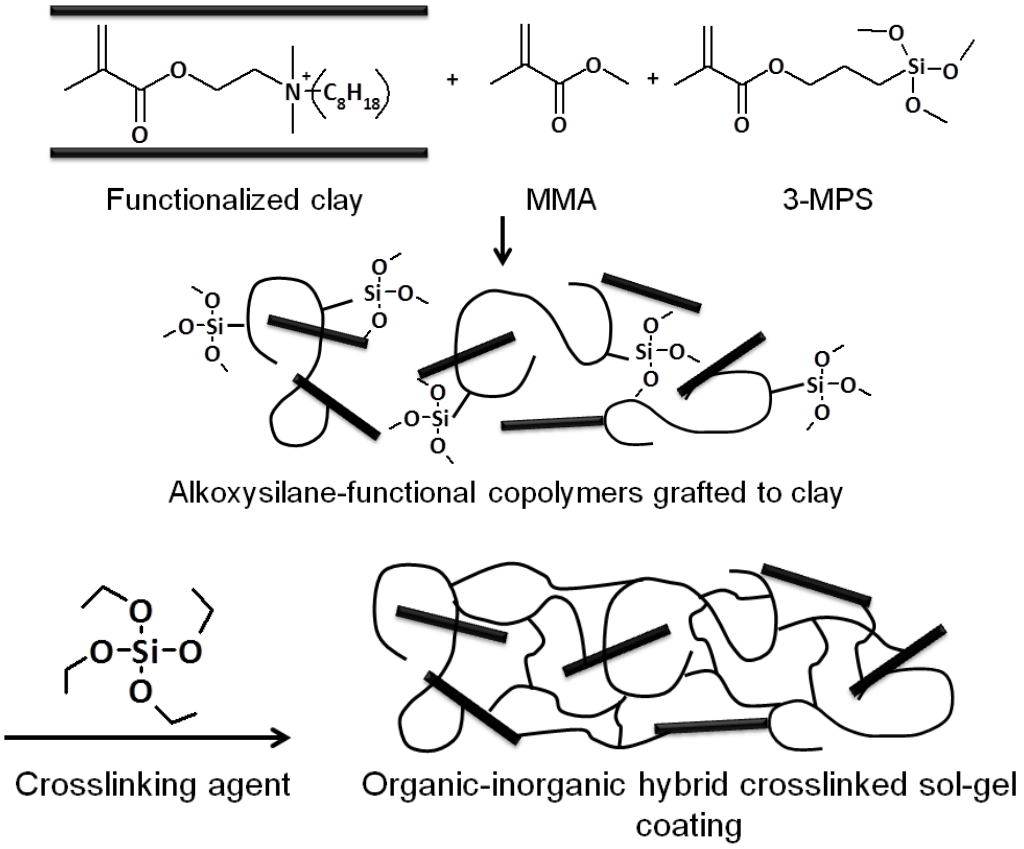

Scheme 6.3: Formation of alkoxysilane-functional copolymers grafted to organomodified clay platelets and sol-gel crosslinking reaction with tetraethyl orthosilicate (TEOS) to create organic-inorganic hybrid crosslinked coatings.

6.3.2. Copolymer-clay nanocomposite characterization

The characterization of the copolymer backbone and physical properties was performed prior to film formation to study the impact of the monomer molar ratio and the final clay content as these variables will greatly impact the properties of the hybrid coatings. Figure 6.1 displays a characteristic FTIR spectra representative of copolymers synthesized from MMA and 3-MPS. FTIR was a key analytical technique to not only confirm the conversion of the copolymer, but also ensure no premature hydrolysis or condensation of the alkoxysilane functional groups had occurred during the copolymerization reaction. The absorption band at 1635 cm^{-1}, attributed to the $CH=CH_2$ bond of the 3-MPS and MMA monomers, was not observed with the copolymer samples, indicating successful monomer to copolymer conversion.

Apart from the 1635 cm^{-1} absorption band, the remaining distinguishable absorption bands remained consistent between the 3-MPS monomer and nanocomposites. In particular, no OH bands were observed in the 3700 – 3200 cm^{-1} range, suggesting that no hydrolysis of the alkoxysilane functional groups occurred during the copolymer synthesis. The $Si-OCH_3$ absorption peak at 1080 cm^{-1} did not broaden with the copolymerization reactions indicating condensation to form siloxane Si-O-Si linkages did not occur. The strong peak observed at 1730 cm^{-1} is attributed to the C=O functionality of the 3-MPS and MMA methacrylate groups. Additional absorption peaks appearing in each copolymer sample include 2920 cm^{-1} and 2850 cm^{-1} representing CH and $O-CH_3$ functional groups, respectively.

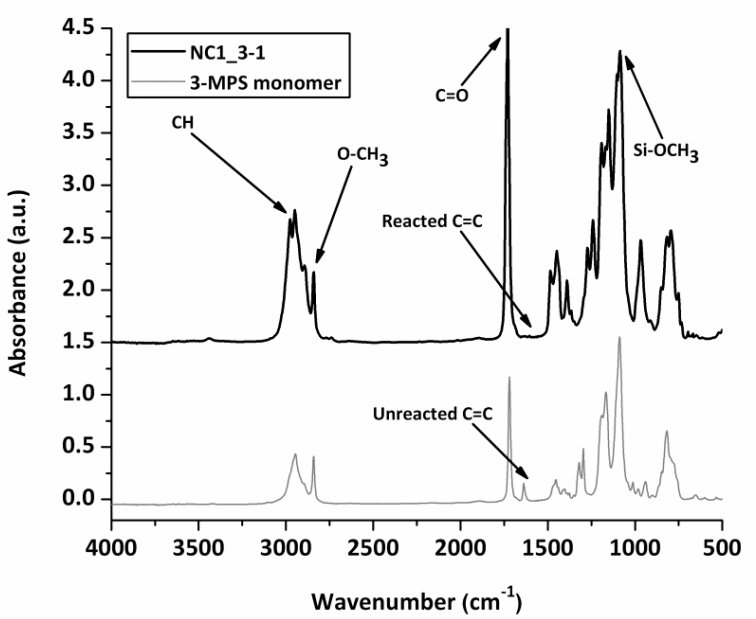

Figure 6.1: FTIR spectra of copolymer-clay nanocomposite NCR1_3-1 and 3-MPS monomer.

The methacrylate-functional MEOA-clay produced a profound impact on the molecular weight and polydispersity of each nanocomposite sample. Table 6.2 displays the molecular weight M_n and M_w values as well as the polydispersity index (PDI) as determined from GPC analysis. Two distinct trends regarding the copolymer molecular weight were observed: M_n decreased and M_w increased with higher clay weight fractions (5 – 10 wt.%). Initially, when 1 -2 wt.% MEOA-clay was incorporated into the copolymer resins, the number average molecular weight M_n values increased approximately 2,000 - 5,000 g/mol. For instance, the sample Control_3-1 had a M_n = 11,000 g/mol, and the incorporation of MEOA-clay at 1 and 2 wt.% increased the M_n to 15,700 and 14,800 g/mol, respectively. This M_n increase was also reflected in the nanocomposites with 2:1 and 1:1 monomer molar ratios. Once the clay loading reached higher fractions (5 – 10 wt.%), the M_n

decreased. For samples NC10_3-1 and NC10_1-1, the M_n was even lower than the control samples of equivalent monomer molar ratio.

TABLE 6.2
Alkoxysilane-functional copolymer-clay nanocomposite properties

Nanocomposite Name	M_n (g/mol)	M_w (g/mol)	PDI (M_w/M_n)	Viscosity (Poise)
Control-3_1	11,000	35,300	3.2	2.0
NC1_3-1	15,700	39,000	2.5	2.4
NC2_3-1	14,800	42,400	2.9	2.2
NC5_3-1	14,000	41,000	2.9	1.8
NC10_3-1	9,500	54,000	5.7	1.4
Control-2_1	9,000	27,400	3.0	1.6
NC1_2-1	10,200	36,800	3.6	1.4
NC2_2-1	10,200	43,300	4.2	1.6
NC5_2-1	9,400	48,500	5.2	1.0
NC10_2-1	8,300	50,100	6.0	0.8
Control-1_1	8,300	25,400	3.1	0.4
NC1_1-1	12,900	25,000	1.9	0.6
NC2_1-1	12,600	28,500	2.3	0.6
NC5_1-1	8,700	27,500	3.2	0.6
NC10_1-1	7,600	31,500	4.1	0.4

The observation of M_n reaching a maximum at 2 wt.% MEOA-clay loading followed by a reduction in M_n molecular weight may be attributed to the MEOA organic modifier acting as an additional site for reacting with the MMA and 3-MPS monomers. By incorporating a methacrylate-functional group to the layered silicate surface, the MEOA organic modifier may participate in the free radical copolymerization, either as a source for monomer addition or as a chain transfer agent, to initiate copolymer grafting to the layered silicate surface. Similar reductions in M_n were reported by Lepoittevin et al. when functionalized clay were used in the in situ intercalative polymerization of poly(ε-caprolactone)/clay nanocomposites.[25] The M_n values of the poly(ε-caprolactone) decreased

significantly when the volume fraction of the hydroxy-functional montmorillonite clay was increased from 1 to 10%. This phenomenon was attributed to the hydroxy-functionality acting as a co-initiator or chain transfer agent. By increasing the clay loading, the hydroxy-functional groups from the organic modification was also increased. As a result, an increased number of initiation sites for the ε-caprolactone monomer occurred.

By functionalizing the clay in this study with the MEOA organic modifier, it appears a similar phenomenon has occurred to reduce the copolymer M_n values. Expectedly, reducing the monomer molar ratio produced lower M_n values as lower concentrations of monomer were used in the nanocomposite formation. Unlike the reduced number average molecular weight M_n values, the weight average M_w grew with increased clay loading. As the clay fillers were not removed prior to samples being passed through the GPC column, higher hydrodynamic volumes from clay intercalation into the copolymer resin may have resulted in significantly increased M_w values, particularly with copolymers containing higher levels of clay loading (5 – 10 wt.% MEOA-clay). Because the GPC analysis was performed with a polystyrene calibration, the obtained molecular weight results are relative.

The copolymer/clay nanocomposite viscosities were influenced by the monomer molar ratio and clay loading. As determined by an ICI cone and plate viscometer, decreasing the monomer molar ratio from 3:1 to 1:1 reduced the nanocomposite viscosity. This reduction in viscosity also correlated with the copolymer molecular weight, where lowering the monomer molar ratio decreased the molecular weight determined from GPC analysis. By comparing each series of

varying monomer molar ratios, the 3:1 molar ratio series had the highest molecular weight values whereas the 1:1 molar ratio series recorded the lowest molecular weights. With reductions in molecular weight, few chain entanglements may occur, contributing to the reductions in viscosity. The introduction of higher MEOA-clay loading did not increase the viscosity as might be expected. Instead, small reductions in the viscosity were observed as higher clay weight fractions (5 – 10 wt.%) were included with the copolymer. If a higher degree of grafting occurred with increased MEOA-clay, reductions in molecular weight, and thus viscosity, may occur. The viscosities of the copolymer/clay nanocomposites were more greatly influenced by the copolymer molecular weight than the level of clay loading.

6.3.3. Hybrid morphology – X-ray diffraction and atomic force microscopy

After the copolymer/clay nanocomposites were characterized, organic-inorganic hybrid sol-gel coatings were created by crosslinking with alkoxysilane-functional organic precursor TEOS. Figure 6.2 displays the XRD scans of the pristine unmodified Cloisite® Na^+ and MEOA-modified pristine clays as well as each sol-gel coating to study the degree of clay dispersion in the final crosslinked film. The modification of the Cloisite® Na^+ clay produced an increase in the *d*-spacing, or the distance between clay platelets, as the diffraction peak shifted to lower 2θ values (Figure 2a). As a result, the MEOA-clay *d*-spacing increased to 1.48 nm from 1.08 nm, the *d*-spacing of the unmodified Cloisite® Na^+. From the increase in *d*-spacing, the organomodification with MEOA was effective in the displacement of the Na^+ exchangeable cations to produce methacrylate-functional layered silicates. From the XRD scans of the cured coating samples, the formation

of nanocomposites had occurred as increases in *d*-spacing values were observed when a diffraction peak was observed (Figure 2b-d). Several coatings, particularly those with 1 – 2 wt.% MEOA-clay, did not have characteristic diffraction peaks in the 2 – 9 2θ range, a possible indicator of high clay dispersion and exfoliation. Two organic-inorganic coatings, both with 10 wt.% MEOA-clay, produced diffraction peaks, and thus *d*-spacing values, in the 2 – 9 2θ range: NC10_2-1_ctg (1.51 nm) and NC10_1-1_ctg (1.55 nm). The increased *d*-spacing values from the pristine MEOA-clay suggest the intercalation of copolymer between the clay platelets. Although XRD may indicate the final degree of clay dispersion within a coatings system, the sensitivity of the instrument to small clay volume fractions and filler geometry will influence the appearance of diffraction peaks.[26]

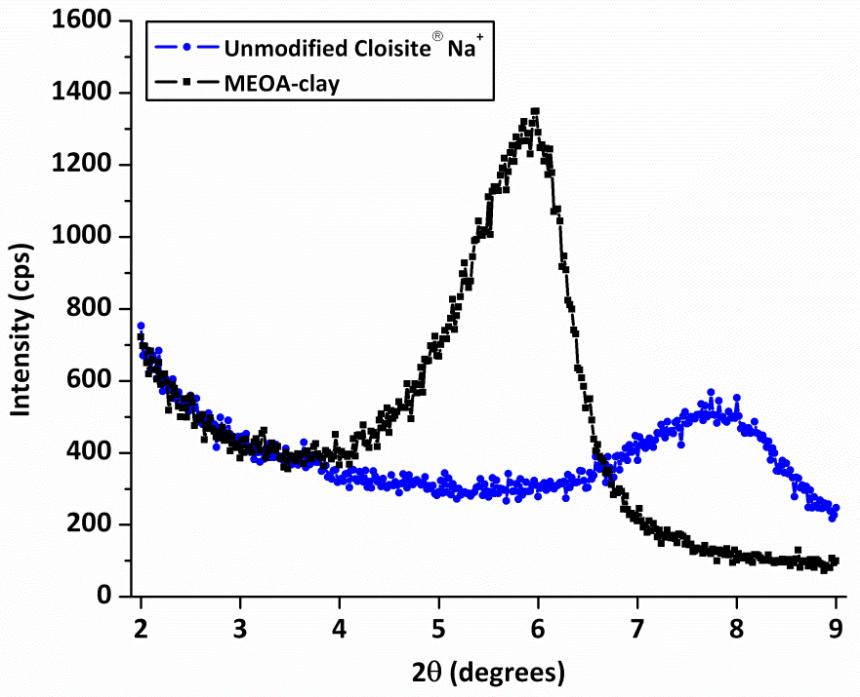

(a)

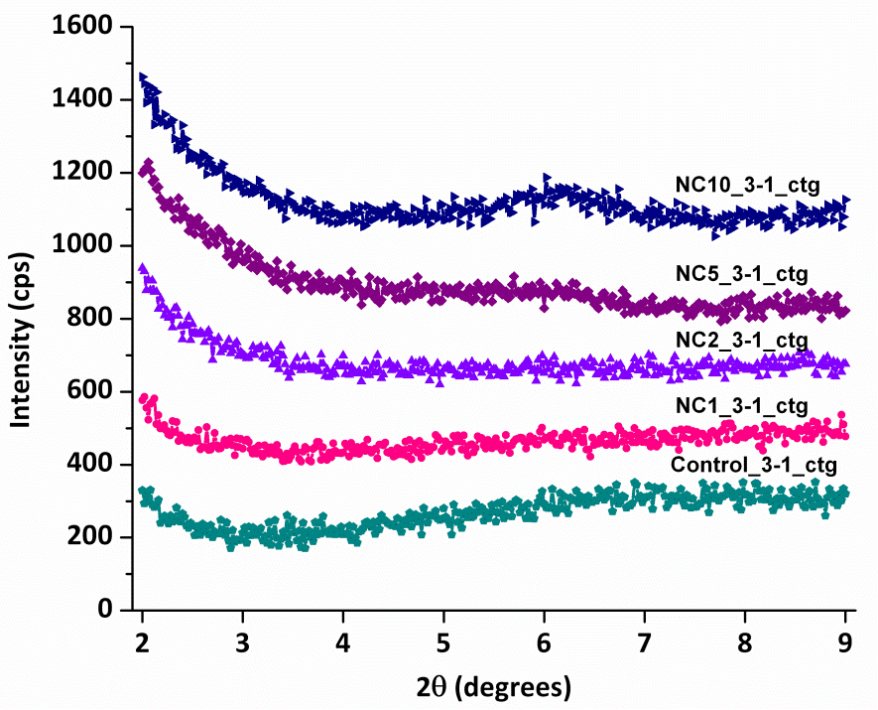
Intensity (cps)
2θ (degrees)
NC10_3-1_ctg
NC5_3-1_ctg
NC2_3-1_ctg
NC1_3-1_ctg
Control_3-1_ctg

(b)

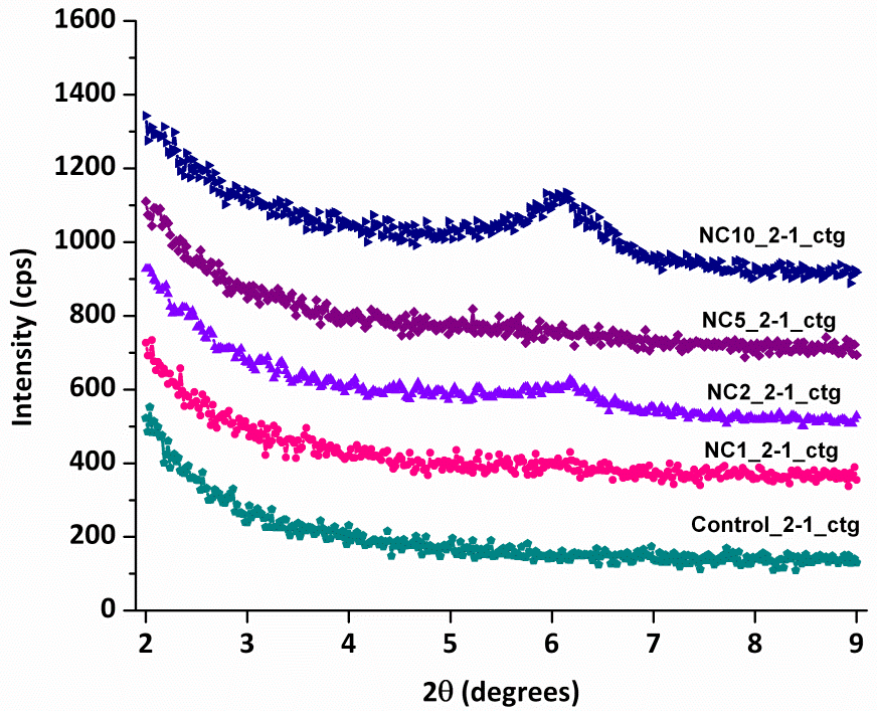
Intensity (cps)
2θ (degrees)
NC10_2-1_ctg
NC5_2-1_ctg
NC2_2-1_ctg
NC1_2-1_ctg
Control_2-1_ctg

(c)

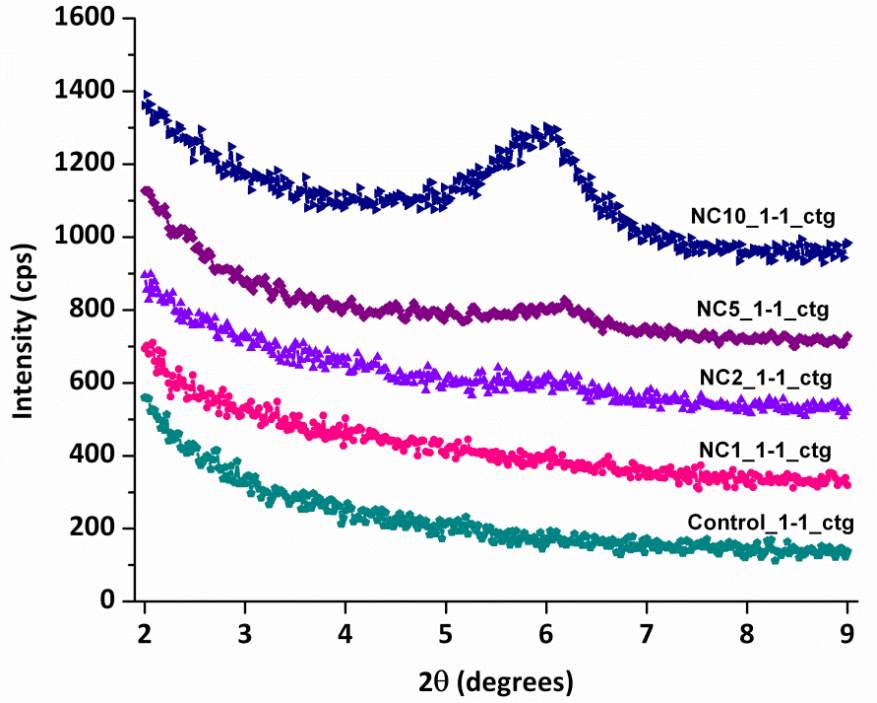

(d)

Figure 6.2: X-ray diffraction plots of (a) pristine clays and the organic-inorganic hybrid sol-gel coatings derived from the nanocomposites containing (b) 3:1, (c) 2:1, and (d) 1:1 monomer molar ratios.

Atomic force microscopy (AFM) was also employed to study the phase separation and morphology of the hybrid films containing organomodified clay. Figures 6.3 and 6.4 demonstrate the representative changes in the hybrid morphology as the clay content was increased for the nanocomposites series prepared with a sol precursor of 2:1 monomer molar ratio. The most striking observation is the distinct change in morphology when higher levels of clay (5 – 10 wt.%) are included into the hybrid network. Subtle changes in hybrid morphology were observed with 1 – 2 wt.% clay, whereas dramatic increases in roughness were exhibited with 5 – 10 wt.% clay. From the AFM analysis, it is apparent that the organomodified clay loading strongly influences the phase separation and

morphological properties of the hybrid networks, particularly as the clay loading exceeds 5 wt.%.

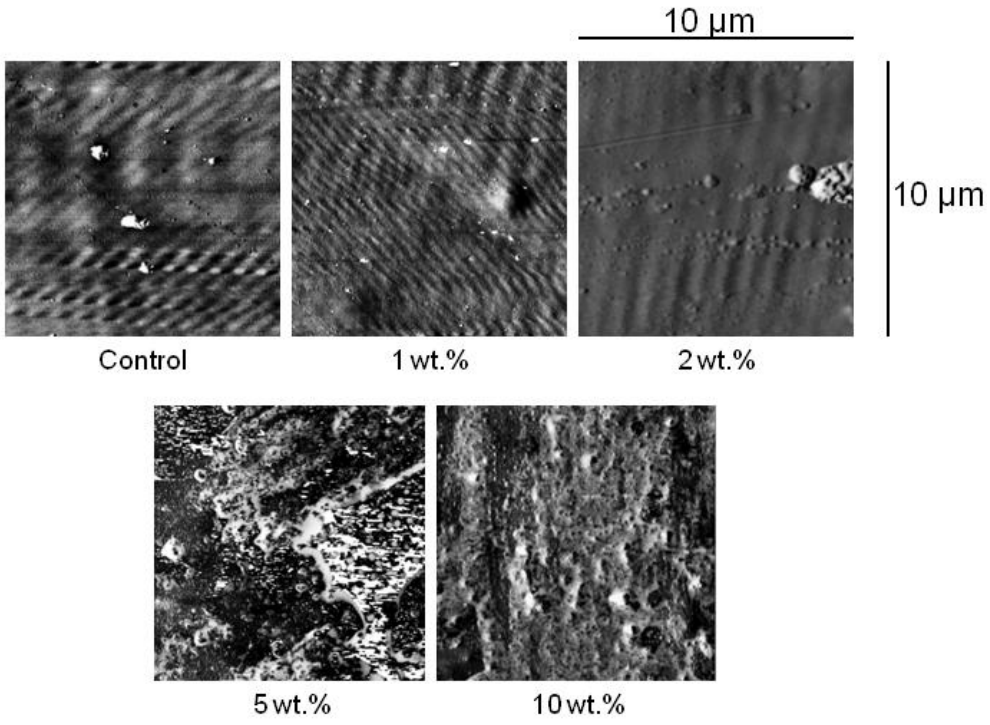

Figure 6.3: AFM regular phase detected images for organic-inorganic hybrids prepared with nanocomposite sol precursors with a 2:1 monomer molar ratio.

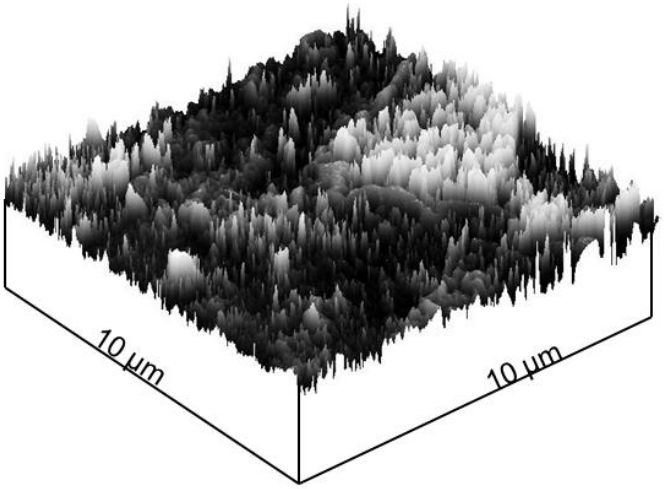

Figure 6.4: AFM three-dimensional image for hybrid NC10_2_1_ctg.

6.3.4. Barrier properties – Water vapor permeability

Over one magnitude improvement in the water vapor permeability (WVP) of the organic-inorganic hybrid coatings was measured with the incorporation of clay fillers in the formation of the crosslinked network. In accordance with ASTM E96, the organic-inorganic cured films (supported on a porous membrane substrate) were subjected to a controlled atmosphere to monitor water mass loss over time until steady state conditions were reached (typically within 72 hours). Figure 6.5 displays the impact of both the monomer molar ratio and the final clay loading on the WVP of each hybrid film, and the WVP data is reported in Table 6.3. Regardless of monomer molar ratio and the clay fraction, each hybrid sol-gel coating derived from the nanocomposites significantly decreased the WVP compared to the control films. Each control film, containing no organically-modified silicates, had the highest WVP measurement when compared to coatings of equivalent monomer molar ratio, ranging from 2.31E-10 $g \cdot m/m^2 \cdot s \cdot Pa$ for Control_3-1_ctg to 4.11E-10 $g \cdot m/m^2 \cdot s \cdot Pa$ for Control_1-1_ctg.

With the addition of just 1 wt.% MEOA-clay into the hybrid network, the resulting coatings reduced the WVP by over one magnitude. As the monomer molar ratio of the nanocomposite sol precursor was reduced from 3:1 to 1:1, the WVP also decreased for equivalent clay loadings. The reductions in WVP with decreased molar ratios may be a result of the increased crosslink density (see section 6.3.5). By increasing the crosslink density, the permeating water vapor encounters a greater concentration of impermeable inorganic linkages, thereby decreasing the WVP of the hybrid films.

A peak in the barrier performance of the organic-inorganic hybrid films occurred between 2 – 5 wt.% MEOA-clay. With the incorporation of impermeable layered silicates into the final coating network, an increased tortuous diffusion path for the permeating water vapor molecules occurred, leading to further reductions in the WVP. Once the MEOA-clay loading reached 10 wt.%, the improvements that had been observed in the WVP diminished, likely a result of the poorer clay dispersion. Continuously increasing the clay volume fraction will not directly correlate to improved barrier protection as the polymer may not fully intercalate between the increased clay filler concentration, potentially forming phase-separated agglomerates within the final crosslinked film. Diminished clay dispersion may then decrease the tortuous diffusion path compared to a well-dispersed inorganic phase within the film.

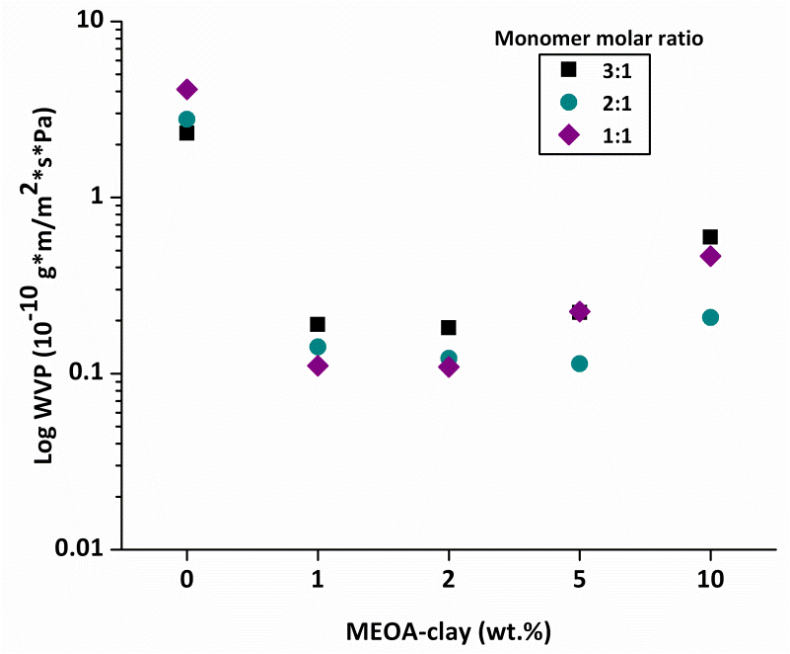

Figure 6.5: WVP results, as determined by ASTM E96, for the organic-inorganic hybrid sol-gel coatings containing MEOA-clay.

TABLE 6.3
Organic-inorganic hybrid sol-gel coating barrier, mechanical, thermal, and optical properties results

Hybrid Name	WVP (g·m/ m^2·s·Pa)	*E'* (MPa, 25°C)	XLD (mol/ cm^3)	König Hardness (sec)	T_{10} % (°C)	Char yield (%)	Transmitt-ance (%)
Control-3_1_ctg	2.31E-10	60	0.004	132	180	8	95
NC1_3-1_ctg	1.90E-11	165	0.010	152	185	11	92
NC2_3-1_ctg	1.82E-11	980	0.032	147	250	12	92
NC5_3-1_ctg	2.22E-11	2440	0.165	101	200	12	74
NC10_3-1_ctg	5.94E-11	825	0.047	98	180	20	68
Control-2_1_ctg	2.78E-10	380	0.022	104	175	4	92
NC1_2-1_ctg	1.42E-11	615	0.025	109	175	6	91
NC2_2-1_ctg	1.22E-11	1770	0.093	136	180	7	88
NC5_2-1_ctg	1.14E-11	2070	0.131	112	190	8	77
NC10_2-1_ctg	2.08E-11	835	0.032	94	220	21	69
Control-1_1_ctg	4.11E-10	1060	0.105	105	220	11	94
NC1_1-1_ctg	1.11E-11	3000	0.203	106	220	16	89
NC2_1-1_ctg	1.09E-11	3070	0.137	117	240	29	86
NC5_1-1_ctg	2.25E-11	1060	0.068	103	220	31	81
NC10_1-1_ctg	4.64E-11	800	0.058	102	170	9	58

6.3.5. Mechanical properties – Dynamic mechanical analysis and König hardness

The viscoelastic properties of the organic-inorganic hybrid sol-gel coatings, as determined by dynamic mechanical analysis (DMA), displayed a considerable dependence on both the final clay loading and the monomer molar ratio of the precursor nanocomposite sol. Figure 6.6 shows the DMA storage modulus plots of each hybrid film, and Table 6.3 reports the storage moduli (E') and crosslink density (XLD) data determined from these plots. Two noticeable trends emerged with the DMA storage moduli data. First, decreasing the monomer molar ratio from 3:1 to 1:1 produced significantly higher storage moduli values for both the control

films and the clay-containing hybrids. The impact of the monomer molar ratio is especially evidenced in the control hybrid films.

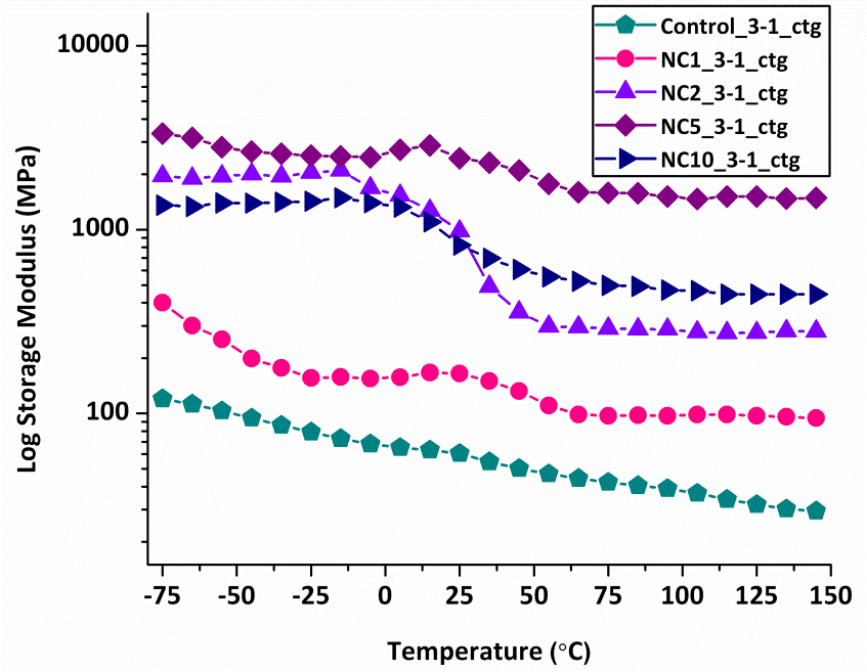

(a)

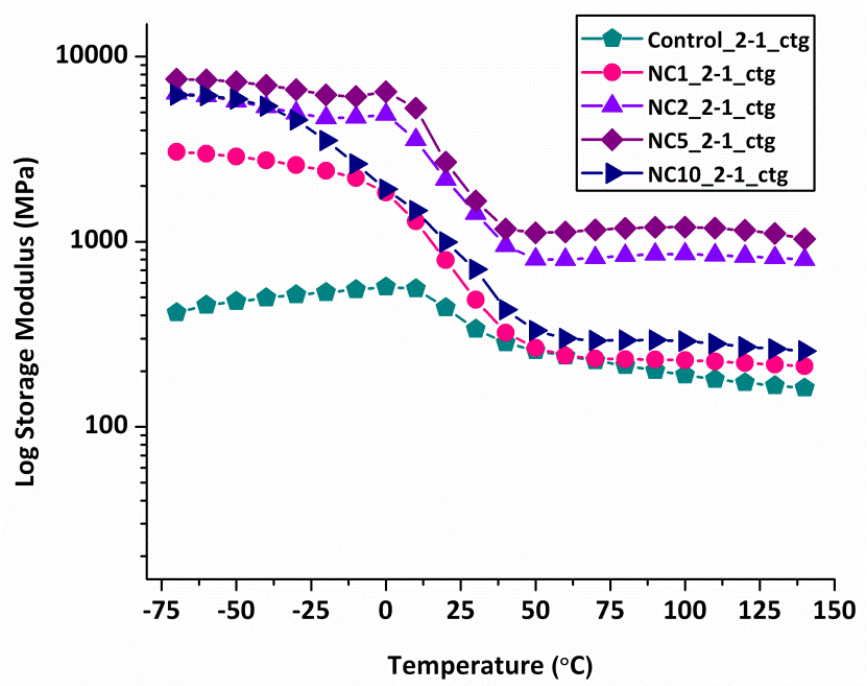

(b)

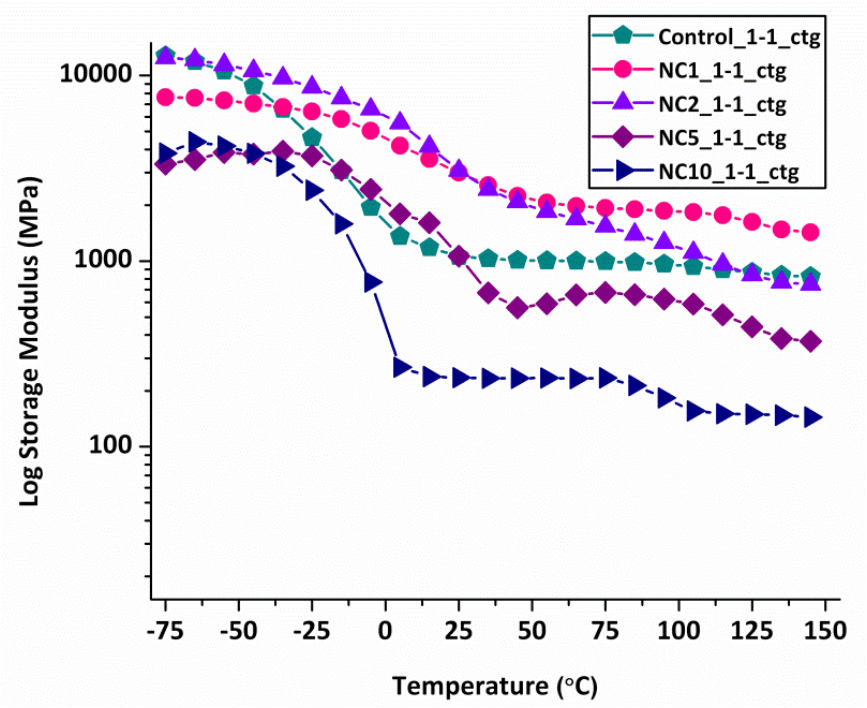

(c)

Figure 6.6: DMA storage modulus plots of the organic-inorganic hybrid sol-gel coatings derived from nanocomposites containing (a) 3:1, (b) 2:1, and (c) 1:1 monomer molar ratios.

The storage modulus at room temperature for hybrid coating Control-3-1_ctg was 60 MPa, whereas the storage moduli for Control-2-1_ctg and Control-3-1_ctg were significantly higher at 380 MPa and 1,060 MPa, respectively. Second, with the incorporation of the MEOA-clay, the resulting hybrid coatings measured additional increases in the storage moduli at room temperature with clay loadings up to 5 wt.% MEOA-clay. The highest storage moduli reported at room temperature for each series were as follows: NC5_3-1_ctg (2,440 MPa), NC5_2-1_ctg (2,070 MPa), and NC2_1-1_ctg (3,070 MPa). From these results, it is apparent the stiffness of these films dramatically increased with clay loading around 2 -5 wt.% MEOA-clay and reduced monomer molar ratios. Clay loadings of

10 wt.% MEOA-clay resulted in diminished storage moduli values compared to the 5 wt.% MEAO-clay films. This reduction in storage moduli may be a result of poorer clay dispersion, where the volume of inorganic clay filler cannot be supported by the polymer network, leading to phase separation and diminished mechanical performance.

The XLD of each organic-inorganic hybrid film displayed similar trends to the measured storage moduli, where smaller monomer molar ratios and higher clay loadings produced greater XLD values. The coatings derived from the 3:1 monomer molar ratio nanocomposites had lower XLD compared to the 2:1 and 1:1 series, an expected result as the alkoxysilane-functional groups on the copolymer backbone would be more concentrated as the MMA content is decreased. By having a greater alkoxysilane-functional group presence per copolymer chain, the overall degree of crosslinking may increase, as seen in the calculated XLD values from the DMA storage modulus plots. The volume fraction of clay and its dispersion affected the final XLD of each hybrid coating, where the highest XLD values were associated with the coatings containing 5 wt.% clay for the 3:1 and 2:1 monomer molar ratios and 1 wt.% clay for the 1:1 series. As the monomer molar ratio decreases, the increased inclusion of the inorganic clay filler may limit the degree of crosslinking, as observed with the 1:1 molar series reduced XLD with increased clay loading.

The maximum hardness of the organic-inorganic hybrid sol-gel coatings occurred between 1 – 2 wt.% MEOA-clay, as observed in Figure 6.7. The average König pendulum hardness for each coating is reported in Table 6.3. All three series

of hybrid films repeated the same hardness trends, where higher monomer molar ratios and lower clay loading produced harder films. Coatings NC1_3-1_ctg and NC2_3-1_ctg had the highest average hardness values of 152 and 147 seconds, respectively, of the fifteen hybrid coatings. The hybrid coatings derived from 2:1 and 1:1 monomer molar ratios had maximum hardness at 2 wt.% MEOA-clay with NC2_2-1_ctg and NC2_1-1_ctg recording values of 136 and 117 seconds, respectively. One trend repeated through each coating series was the diminishing coating hardness as 5 – 10 wt.% clay was included in the crosslinked network. Previous researchers have reported reductions in nanocomposite film hardness as clay loading increased and have attributed the phenomenon to clay filler inability to be well-dispersed throughout the cured film due to crowding.[27] Therefore, reductions in clay dispersion may account for the decreased film hardness.

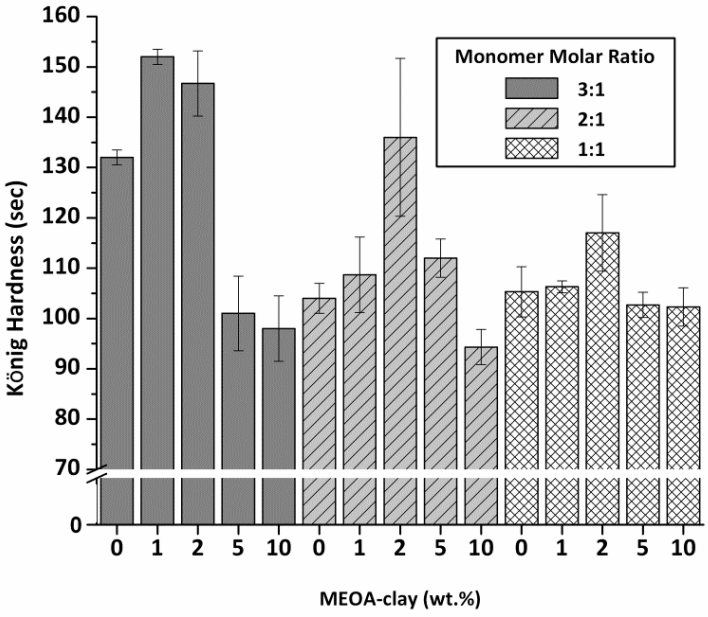

Figure 6.7: König pendulum hardness of the organic-inorganic hybrid sol-gel coatings.

6.3.6. Thermal stability and optical clarity – Thermogravimetric analysis and UV-visible spectroscopy

The thermal stability of the organic-inorganic films was examined by thermogravimetric analysis (TGA), particularly comparing the temperature at 10 wt.% loss (T_{10}%) for each coating. Figure 6.8 displays the degradation curves of each hybrid coating, and Table 6.3 reports the T_{10}% values. Increased thermal stability was observed with the incorporation of MEOA-clay into the sol-gel network. Hybrid films derived from the 3:1 monomer molar ratio nanocomposites experienced a 70 °C increase in T_{10}% with 2 wt.% MEOA-clay. Likewise, the 2:1 series also significantly enhanced the thermal stability with MEOA-clay inclusion, as the T_{10}% value increased 55 °C with NC10_2-1_ctg. The 1:1 monomer molar ratio series typically produced the highest T_{10}% for equivalent clay loadings, where the control film Control_1-1_ctg T_{10}% was 220 °C, and the introduction of MEOA-clay raised the T_{10}% 20 °C higher to 240 °C. The less dramatic increase in thermal stability with MEOA-clay may be attributed to the high crosslink density in the 1:1 monomer molar ratio series, where the high concentration of the inorganic linkages from sol-gel processing contributes more to the improved thermal stability than the incorporation of clay fillers. The coating NC10_1-1_ctg recorded a T_{10}% less than the control at 170 °C, likely a consequence of crowding and phase separation within the hybrid network. The hybrid coatings char yields increased with the higher MEOA-clay, a reflection of higher inorganic content by increasing the organomodified clay loading. The only coating to not reflect this trend was NC10_1-1_ctg, where the char yield decreased, which again may be a result of

poor clay dispersion and phase separation. The lower char yield for NC10_1-1_ctg may also contribute to the reduced thermal stability observed as the T_{10}% decreased.

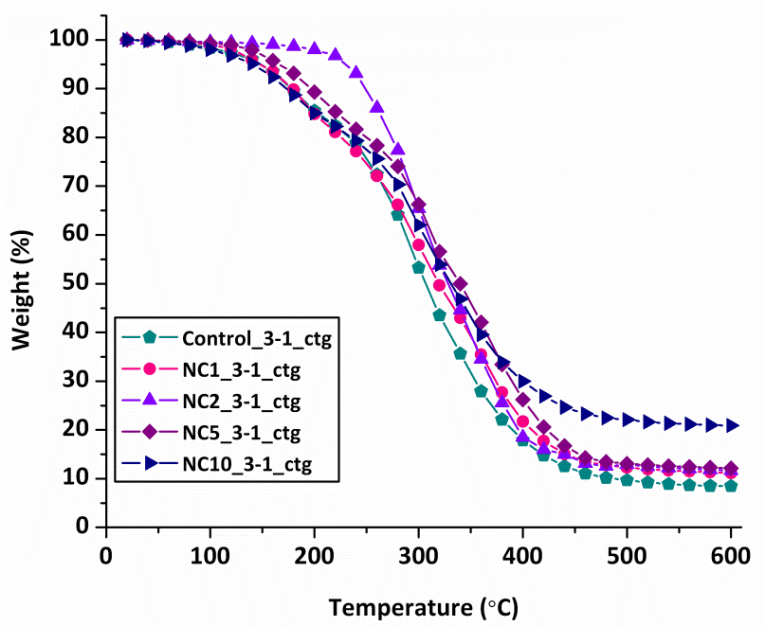

(a)

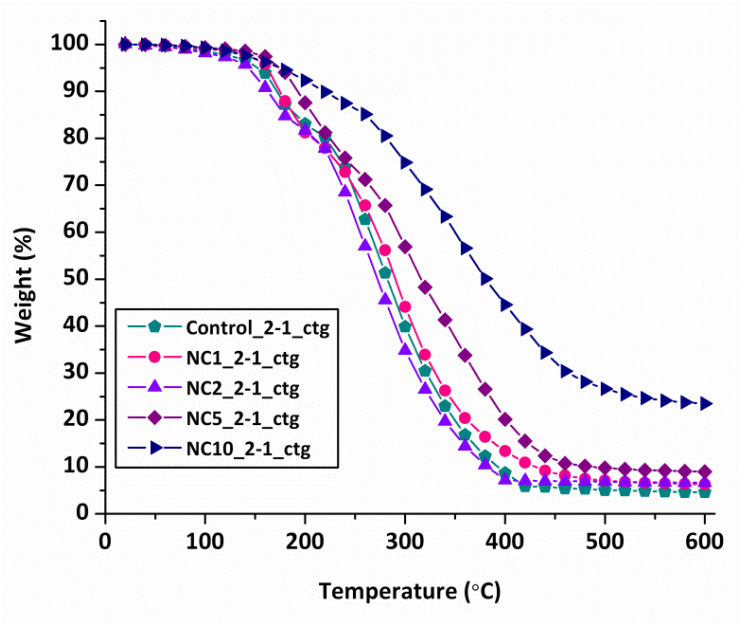

(b)

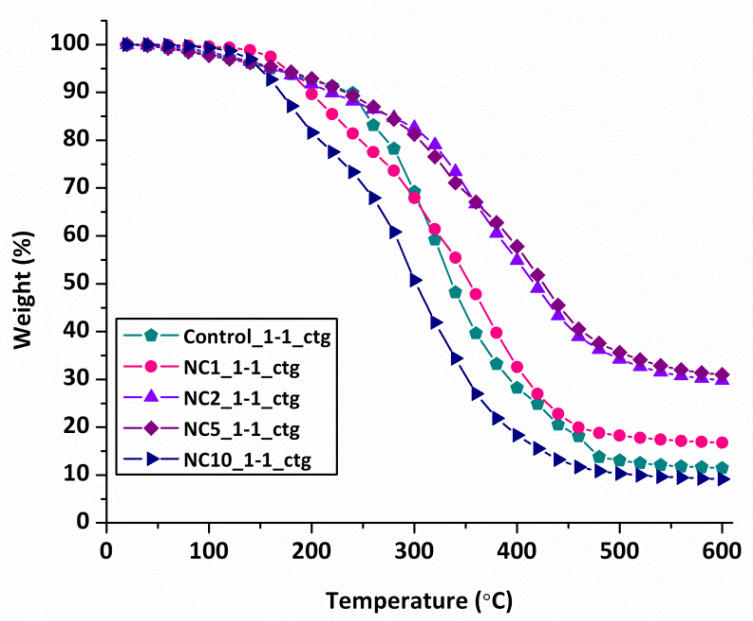

(c)

Figure 6.8: TGA degradation curves of organic-inorganic hybrid films containing nanocomposites derived from (a) 3:1, (b) 2:1, and (c) 1:1 monomer molar ratio.

Figure 6.9 and Table 6.3 display the transmittance data obtained from UV-visible spectroscopy to examine the optical clarity of each organic-inorganic hybrid film. As expected, high levels of MEOA-clay loading (5 – 10 wt.%) decreased the transmittance of each film, a consequence of higher inorganic loading and poorer clay dispersion throughout the hybrid coatings. However, low levels of clay loading maintained high clarity, where the transmittance ranged from 88 – 92%, only slightly lower than the control films (92 – 95%). Another trend occurring in the transmittance data was the reduction in transmittance as the monomer molar ratio decreased from 3:1 to 1:1, particularly with 10 wt.% clay. This large reduction may once again be attributed to the poor MEOA-clay dispersion leading to phase separation and increased turbidity.

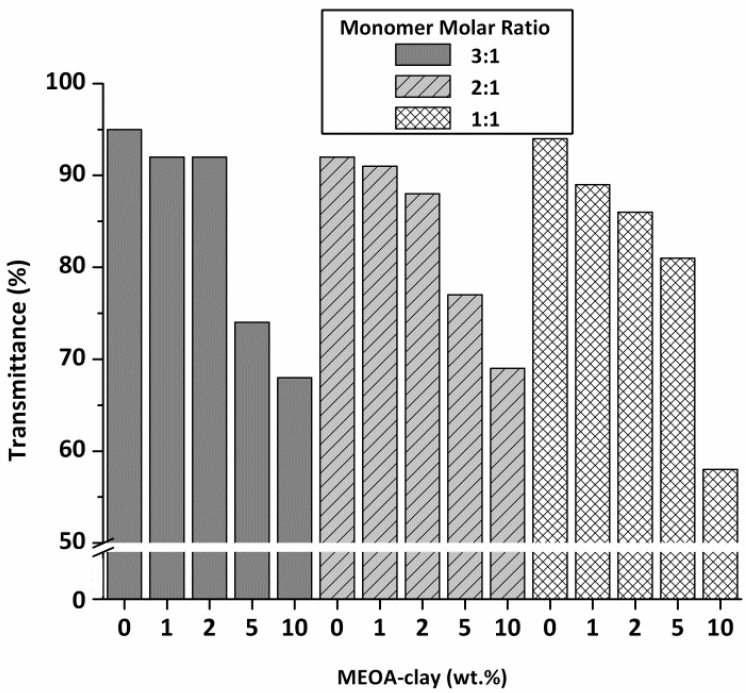

Figure 6.9: Organic-inorganic hybrid transmittance at 400 nm as determined by UV-visible spectroscopy.

6.4. Conclusions

Organic-inorganic hybrid films created from precursor alkoxysilane-functional nanocomposites were produced to study the impact of clay inclusion on a sol-gel coating network. The final copolymer structure and physical properties were directly dependent on the molar ratio of the MMA and 3-MPS monomers as well as the MEOA-clay loading. Reductions in M_n and viscosity of the nanocomposites with increased clay wt.% was attributed to the additional methacryl-functional groups on the modified clay surfaces, producing more sites for grafting and chain transfer during the copolymerization reaction. Significant improvements in barrier, mechanical, and thermal hybrid film properties were measured. Particularly, MEOA-clay incorporation reduced WVP over one magnitude. The hybrid coatings storage moduli and crosslink density dramatically

increased with up to 5 wt.% MEOA-clay. An increase in thermal stability was also observed by the incorporation of the functionalized clay. The hybrid coatings containing 2 – 5 wt.% clay demonstrated the most considerable improvements in the material properties.

6.5. References

1. Pierre, A. C., *Introduction to sol-gel processing*. Springer: 1998; Vol. 1.

2. Chen, Y.; Jin, L.; Xie, Y., *Journal of Sol-Gel Science and Technology* **1998,** *13* (1), 735-738.

3. Gallardo, J.; Galliano, P.; Durán, A., *Journal of Sol-Gel Science and Technology* **2001,** *21* (1), 65-74.

4. Zheludkevich, M. L.; Salvado, I. M.; Ferreira, M. G. S., *Journal of Materials Chemistry* **2005,** *15* (48), 5099-5111.

5. Rosero-Navarro, N. C.; Pellice, S. A.; Durán, A.; Aparicio, M., *Corrosion Science* **2008,** *50* (5), 1283-1291.

6. Jiang, H.; Yuan, X.; Yun, Z.; Chan, Y.-C.; Lam, Y.-L., *Materials Science and Engineering: C* **2001,** *16* (1-2), 99-102.

7. Orhan, J. B.; Parashar, V. K.; Sayah, A.; Gijs, M. A. M., *Microelectronic Engineering 83* (4-9), 1329-1332.

8. Lopez, T.; Gomez, R.; Sanchez, E.; Tzompantzi, F.; Vera, L., *Journal of Sol-Gel Science and Technology* **2001,** *22* (1), 99-107.

9. Backhaus-Ricoult, M.; Gu, Y., Sol-gel derived high performance catalyst thin films for sensors, oxygen separation devices, and solid oxide fuel cells. US Patent App. 20,090/297,923: 2008.

10. Dave, B. C.; Dunn, B.; Valentine, J. S.; Zink, J. I., *Analytical Chemistry* **1994,** *66* (22), 1120A-1127A.

11. Zou, Y.; Xiang, C.; Sun, L.-X.; Xu, F., *Biosensors and Bioelectronics* **2008,** *23* (7), 1010-1016.

12. Ju, H.; Zhang, X.; Wang, J., Biosensors Based on Sol–Gel Nanoparticle Matrices Springer New York: 2011; pp 305-332.

13. Crivello, J. V.; Song, K. Y.; Ghoshal, R., *Chemistry of Materials* **2001,** *13* (5), 1932-1942.

14. Choi, H.; Lim, C.; Lee, D.; Kim, B., *Journal of Polymer Engineering* **2009,** *29* (1-3), 1-14.

15. Vreugdenhil, A. J.; Woods, M. E., *Progress in Organic Coatings* **2005,** *53* (2), 119-125.

16. Pellice, S. A.; Williams, R. J. J.; Sobrados, I.; Sanz, J.; Castro, Y.; Aparicio, M.; Duran, A., *Journal of Materials Chemistry* **2006,** *16* (32), 3318-3325.

17. Kawasumi, M.; Hasegawa, N.; Kato, M.; Usuki, A.; Okada, A., *Macromolecules* **1997,** *30* (20), 6333-6338.

18. Gilman, J. W., *Applied Clay Science* **1999,** *15* (1-2), 31-49.

19. Zhu, J.; Start, P.; Mauritz, K. A.; Wilkie, C. A., *Polymer Degradation and Stability* **2002,** *77* (2), 253-258.

20. Meneghetti, P.; Qutubuddin, S., *Thermochimica Acta* **2006,** *442* (1-2), 74-77.

21. Urresti, O.; González, A.; Fernández-Berridi, M. J.; Iruin, J. J.; Irusta, L., *Journal of Membrane Science* **2011,** *373* (1-2), 173-177.

22. Bharadwaj, R. K.; Mehrabi, A. R.; Hamilton, C.; Trujillo, C.; Murga, M.; Fan, R.; Chavira, A.; Thompson, A. K., *Polymer* **2002,** *43* (13), 3699-3705.

23. Zeng, C.; Lee, L. J., *Macromolecules* **2001,** *34* (12), 4098-4103.

24. Chan, C. K.; Peng, S. L.; Chu, I., *Polymer* **2001,** *42* (9), 4189-4196.

25. Lepoittevin, B.; Pantoustier, N.; Devalckenaere, M.; Alexandre, M.; Kubies, D.; Calberg, C.; Jérôme, R.; Dubois, P., *Macromolecules* **2002,** *35* (22), 8385-8390.

26. Morgan, A. B.; Gilman, J. W., *Journal of Applied Polymer Science* **2003,** *87* (8), 1329-1338.

27. Ravindran, N.; Vora, A.; Webster, D. C., *Journal of Applied Polymer Science* **2007,** *105* (6), 3378-3390.

CHAPTER 7. NOVEL PREPARATION OF AMINE-BASED ORGANIC-INORGANIC HYBRIDS FOR CO_2 CAPTURE AND SEPARATION MEMBRANE APPLICATIONS

7.1. Introduction

By combining the high strength and hardness of inorganic domains with the flexibility of primarily organic polymers, hybrid materials with enhanced mechanical, thermal, and barrier properties may be obtained.[1] The utilization of sol-gel chemistry to prepare organic-inorganic hybrids has widely been employed due to several advantageous processing conditions, including ambient temperature reactions and high purity products, in electrical,[2-3] biochemical,[4-5] and optical coating[6-7] applications. In addition to providing silane functionality to participate in sol-gel chemical reactions, organic alkoxysilane precursors introduce additional functionalities to the hybrid network. In particular, the monomer 3-methacryloxypropyltrimethoxysilane (3-MPS) has both alkoxysilane- and methacrylate-functional groups that may undergo inorganic and free radical polymerizations, respectively. Abe et al. reported the preparation of organic-inorganic hybrids derived from the free radical polymerization of 3-MPS, followed by subsequent hydrolytic polycondensation.[8] In the preparation of these hybrids, 3-MPS was free radically polymerized with initiator t-butyl peroxide. Next, the resulting alkoxysilane-functional polymer was crosslinked via acid catalyzed sol-gel chemistry to create organic-inorganic gelled films. The mechanical performance of the hybrid films was directly dependent on the degree of polymerization. As the degree of polymerization for the alkoxysilane-functional 3-MPS polymer was

increased, the hybrid films shifted from tough and rigid to rubbery hybrids. 3-MPS has also been utilized as a co-monomer in the synthesis of alkoxysilane-functional copolymers. Costa and Vasconcelos researched the copolymerization of 3-MPS and 2-hydroxyethyl methacrylate (HEMA) to understand structural control of organic-inorganic hybrids based on interactions between organic and inorganic components.[9] 3-MPS and HEMA were copolymerized in a solvent mixture of ethanol and tetramethyl orthosilicate (TMOS), then crosslinked with additional TMOS and water. The resulting hybrid films were aged initially at room temperature, and then subjected to elevated temperatures (50 – 80 °C) to promote further drying and densification. The incorporation of 3-MPS into the precursor polymerization material prevented the formation of cracks and macrophase separation, both of which were observed with the HEMA-hybrids. The utilization of 3-MPS to create alkoxysilane-functional copolymers has also been reported with co-monomers methyl methacrylate,[10] vinylimidazole,[11] and tetraethyleneoxidedimethacrylate.[12]

Recently, interest in developing technologies for the separation and capture of carbon dioxide (CO_2) by-products from power plants has increased to help in controlling the emissions of greenhouse gases. Several different physical and chemical processes are currently employed to study CO_2 separation and capture including absorption, adsorption, and membranes.[13] Of these techniques, amine-based CO_2 absorption technologies have been the most widely developed. Amine-functional solvents, such as monoethanolamine (MEA), will absorb CO_2 and produce ammonium carbamate species under anhydrous conditions or ammonium

bicarbonate and carbonate species in the presence of water.[14] However, the use of liquid alkanoamines has distinct disadvantages such as solvent regeneration, high energy consumption, and the large quantities of water needed corrosion and viscosity control. An alternative approach to amine-based CO_2 separation is the attachment of amine groups to high surface area solids. Several studies have reported the production of solid, amine-based mesoporous hybrid materials using alkoxysilane organic precursors for potential CO_2 separation and capture applications.[15-19]

In Chapter 6, a novel, two-step process for the preparation of organic-inorganic hybrids derived from alkoxysilane-functional polymer-clay nanocomposites was developed. First, alkoxysilane-functional copolymers were synthesized in the presence of organomodified montmorillonite clay. Second, the alkoxysilane-functional groups were crosslinked with an additional silane coupling agent to create a crosslinked organic-inorganic hybrid containing layered silicates. Based on the success of this hybrid formation process, we adopted the same preparation procedure to develop amine-based organic-inorganic hybrids for potential CO_2 capture and separation membranes. With this current study, the copolymer backbone composition was modified. Monomers 3-MPS and 2-(dimethylamino)ethyl methacrylate (DMAEMA), in the presence of organomodified clay, were copolymerized by a semi-batch, conventional free radical copolymerization to obtain amino- and alkoxysilane-functional copolymers, and then crosslinked via sol-gel processing to obtain an amine-based hybrid film. The resulting amine-based organic-inorganic hybrid film incorporates the advantageous

properties associated with nanocomposite formation from both layered silicates and sol-gel processing as well as imparting amine functionality for possible CO_2 absorption.

7.2. Experimental

7.2.1. Materials

2-(dimethylamino)ethyl methacrylate (DMAEMA), tetraethyl orthosilicate (TEOS), ethanol, ethyl acetate, and 1-bromooctane were purchased from Sigma Aldrich (Milwaukee, WI). 3-methacryloxypropyltrimethoxysilane (3-MPS) was obtained from Gelest (Morrisville, PA). Monomers DMAEMA and 3-MPS were purified by distillation under vacuum and stored at 0 °C prior to copolymerization. Initiator 2,2'-azobis(2-methylbutyronitrile), "Vazo 67", gratefully supplied by DuPont (Belle, WV), was re-crystallized in ethanol prior to use. Cloisite® Na^+, a commercially-available unmodified montmorillonite clay, was obtained from Southern Clay Products (Gonzales, TX). Unless specified, all materials were used as received.

7.2.2. Clay functionalization with 2-methacryloyloxyethyloctyldimethyl-ammonium bromide

The preparation of 2-methacryloyloxyethyloctyldimethylammonium bromide (MEOAB), a quaternary ammonium surfactant with methacrylate functionality, was repeated from our previous study using a procedure reported by Zeng and Lee.[20] Briefly, DMAEMA (0.050 mol) was quaternized with 1-bromooctane (0.025 mol) in ethyl acetate (0.100 mol) at 60 °C for 24 hours. Next, an ion exchange reaction was performed with the unmodified Cloisite® Na^+ montmorillonite clay (10.00 g)

and the MEOAB product (5.30 g) in distilled water at room temperature for 24 hours. The functionalized clay, herein referred to as MEOA-clay, was filtered and rinsed with distilled water until no bromide ion was detected by 0.1 N $AgNO_3$. Once dried, the MEOA-clay was ground to a fine powder with a mortar and pestle.

7.2.3. Nanocomposite formation via copolymerization with MEOA-clay

Copolymers of 3-MPS and DMAEMA were synthesized in the presence of MEOA-clay by conventional free radical copolymerization, using a semi-batch process, to prepare copolymer-clay nanocomposites via in situ intercalative polymerization. Monomers DMAEMA (0.08 mol) and 3-MPS (0.02 mol) were mixed with MEOA-clay overnight via magnetic stir bar to achieve a homogenous dispersion. The DMAEMA:3-MPS monomer molar ratio was maintained at 4:1 with loadings of 1, 2, 5, and 10 wt.% MEOA-clay (based on total monomer weight). Ethanol (0.30 mol) and TEOS (0.10 mol) were added to a reaction flask equipped with a temperature probe/controller, nitrogen inlet, magnetic stirrer, addition funnel, condenser, heating mantle, and stir plate. The solvent solution was heated to 70 °C in a nitrogen atmosphere. Meanwhile, initiator 2,2'-azobis(2-methylbutyronitrile) was added to the monomer-clay solution at 2.5 wt.% of the total monomer weight and mixed until dissolved. The resulting monomer solution was charged to the addition funnel, and slowly added dropwise to the solvent mixture at a rate of approximately 1 mL/min. The copolymerization reaction continued for 6 hours. A control reaction was also conducted with no MEOA-clay for a total of five copolymer products.

7.2.4. Amine-based organic-inorganic hybrid coating formation via sol-gel chemistry

The resulting amine- and alkoxysilane-functional copolymer-clay nanocomposites were crosslinked using sol-gel chemistries to create organic-inorganic hybrid films. The silane crosslinking agent, TEOS, was first mixed with deionized water, ethanol, and hydrochloric acid (molar ratio of 1:25:5:0.025) according to Chen and coworkers.[21] After the TEOS solution was mixed at room temperature for several minutes, a 90:10 weight ratio of the copolymer-clay nanocomposite:TEOS solution was stirred for 1 hour at room temperature to initiate hydrolysis and condensation. The resulting mixture was cast onto glass, aluminum, and porous (5-6 μm) PTFE membrane substrates (Savillex Corporation) substrates by spin-coating for 20 seconds at 500 RPM and then cured in a vacuum oven at 70 °C to dry and densify the organic-inorganic hybrid network.

7.2.5. Characterization

Prior to hybrid film formation, the amine- and alkoxysilane-functional copolymer-clay nanocomposites were characterized to study the copolymer backbone and physical properties. The copolymer backbone structure was analyzed with Fourier-Transform infrared spectroscopy (FTIR) using a Nicolet Magna-IR 850 spectrometer with detector type DTGS KBr. The spectra were recorded in transmittance mode between 400 and 4000 cm^{-1}. The molecular weight and polydispersity index (PDI) of the copolymers were characterized by gel permeation chromatography (GPC). GPC analysis was performed using a Water 2410 Gel Permeation Chromatograph equipped with a refractive index detector.

Each copolymer sample was dissolved in the solvent tetrahydrofuran (THF) to create approximately a 1% solution. Calibration of the chromatograph was done using polystyrene standards, and the flow rate was 1 mL/min. The viscosity of each copolymer sample was measured from an ICI cone and plate viscometer, once solvents were removed by a rotary evaporator, at 75 °C.

X-ray diffraction (XRD) was employed to study the dispersion of the MEOA-clay within the cured organic-inorganic hybrid films. XRD was conducted using a Bruker AXS' D8 Discover diffractometer in Bragg-Brentano geometry with Cu Kα radiation at a wavelength of 1.5406 Å. Each hybrid film was scanned from 1.5° – 50° 2θ, and the run time was 1 sec/step. The barrier properties of each hybrid film were characterized by employing ASTM E96, “Standard Test Methods for Water Vapor Transmission, Water Method.” The cured hybrid films, coated on a porous membrane substrate, were attached to a permeability cup containing distilled water, and placed into a controlled atmospheric chamber. The conditions of the chamber were maintained at 75 ± 2% relative humidity and 20 °C ± 2 °C. The mass loss was recorded over time until a steady state of water vapor transmission was reached. Duplicate tests were performed for verification. The mechanical performance of each hybrid film was explored by studying their viscoelastic properties via dynamic mechanical analysis (DMA). The DMA testing was conducted using a TA Instruments Q800 Dynamic Mechanical Analyzer in tensile mode. Free films of the cured organic-inorganic hybrid, with dimensions of approximately 15 mm x 5 mm x 0.80 mm, were measured with a 1 Hz frequency, constant strain of 0.05%, and a heating rate of 5 °C/min. The temperature range

was -75 °C to 200 °C. The hybrid film hardness with determined by a BYK-Gardner pendulum hardness tester using the coated aluminum substrates. The thermal stability of the hybrids was determined by thermogravimetric analysis (TGA) using a TA Instruments Q500 Thermogravimetric Analyzer. The hybrid samples were heated from ambient temperatures to 600 °C at a rate of 20 °C/min under an inert (N_2) atmosphere. The optical clarity of the hybrid films was characterized by measuring percent transmittance at 400 nm with a Varian Cary 5000 UV-Vis Spectrometer.

7.3. Results and discussion

In this study, the preparation of amine-based organic-inorganic hybrid films was explored through a two-step process to create high performance materials for potential applications in CO_2 separation and capture technologies. The first part of the hybrid film preparation was to synthesize copolymers from 3-methacryloxypropyltrimethoxysilane (3-MPS) and 2-(dimethylamino)ethyl methacrylate (DMAEMA) to create amine- and alkoxysilane-functional copolymers. The copolymerization reactions were performed using an in situ intercalative polymerization technique to incorporate organomodified clays. The second step in the hybrid preparation was to crosslink the resulting amine- and alkoxysilane-functional copolymer-clay nanocomposites with the silane coupling agent tetraethyl orthosilicate (TEOS) to create amine-based organic-inorganic hybrid films. Through this novel preparation technique, the hybrid films contain both inorganic linkages from the sol-gel processing throughout the hybrid network the inorganic

layered silicates dispersed throughout the organic copolymer to serve as barriers while providing amine functionality from the copolymer backbone.

7.3.1. Amine- and alkoxysilane-functional copolymer-clay nanocomposite characterization

Before the formation of the organic-inorganic hybrid films, the amine- and alkoxysilane-functional copolymer-clay nanocomposites were characterized to explore the impact of the MEOA-clay loading on formation of the copolymer backbone and physical properties. Additionally, the copolymer-clay nanocomposites will greatly influence the material properties of the hybrid films, so their characterization prior to hybrid film formation is necessary. FTIR spectroscopy was employed to study the copolymer backbone composition, conversion of the monomeric species, and to determine whether premature hydrolysis and condensation of the alkoxysilane-functional groups had occurred during copolymerization. Figure 7.1 displays representative FTIR spectra for the copolymers synthesized from the 3-MPS and DMAEMA monomers compared to the 3-MPS and DMAEMA monomers. The successful conversion of the two monomers to copolymer was indicated by the disappearance of the absorption band at 1635 cm^{-1}, attributed to the $CH=CH_2$ double bonds from monomers 3-MPS and DMAEMA. Apart from the 1635 cm^{-1} absorption band, the remaining prominent absorption bands of the copolymer spectra were identical to that of the 3-MPS and DMAEMA spectra. With the copolymer spectra, no OH bands were observed in the 3700 – 3200 cm^{-1} range, indicating no premature hydrolysis of the alkoxysilane functional groups had occurred during copolymerization. The

broadening of the Si-OCH_3 band from the 3-MPS monomer at 1080 cm^{-1-} indicates the formation of Si-O-Si linkages, or the onset of condensation between alkoxysilane groups. Because the 1080 cm^{-1} band did not broaden during copolymerization, no premature condensation reactions of the alkoxysilane groups appeared to have occurred during copolymerization. Additional prominent bands associated with the other functionalities of the copolymer backbone include 2920 cm^{-1} (CH), 2850 cm^{-1} (O-CH_3), and 1730 cm^{-1} (C=O).

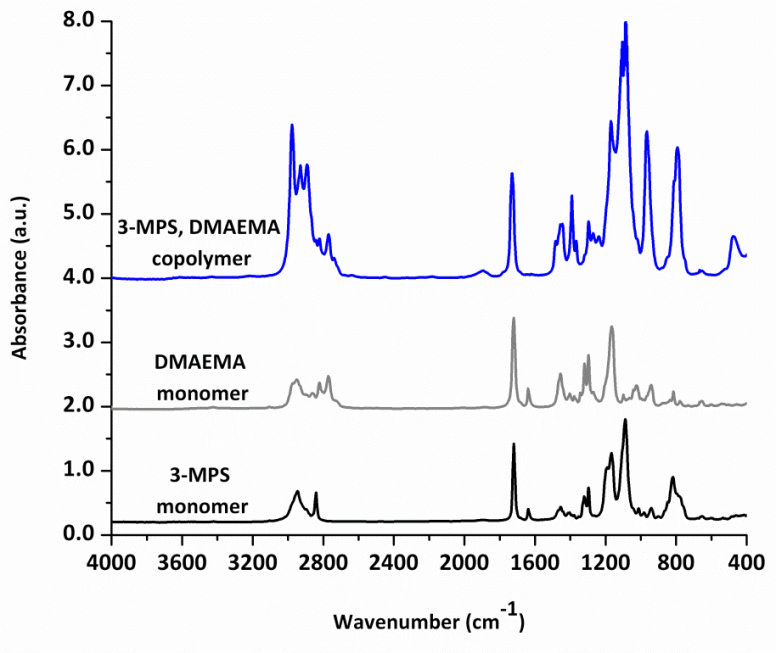

Figure 7.1: FTIR spectra results comparing monomers 3-methacryloxypropyltri-methoxysilane (3-MPS) and 2-(dimethylamino)ethyl methacrylate (DMAEMA) to the copolymer.

The addition of MEOA-clay had a profound impact on the molecular weight and viscosities of the copolymer-clay nanocomposite samples. Table 7.1 reports the molecular weight and polydispersity index (PDI) as determined by GPC analysis, and the copolymer viscosity determined from an ICI cone and plate viscometer. The first trend observed with regard to the copolymer molecular weight

was the decrease in M_n, the number average molecular weight, as the MEOA-clay loading increased to higher levels (5 – 10 wt.%). The copolymers containing 1 and 2 wt.% clay had M_n values of 9,600 and 8,700 g/mol, respectively, which was slightly higher than the control copolymer sample (8,400 g/mol). The inclusion of higher MEOA-clay loading to the copolymer samples reduced the M_n value to 7,800 g/mol for 5 wt.% clay and 5,500 g/mol for 10 wt.% clay.

TABLE 7.1
Amine- and alkoxysilane-functional copolymer-clay nanocomposite properties

MEOAB-clay loading	M_n (g/mol)	M_w (g/mol)	PDI (M_w/M_n)	Viscosity (Poise)
Control	8,400	13,000	1.5	0.4
1 wt.%	9,600	13,400	1.4	0.6
2 wt.%	8,700	17,800	2.0	1.0
5 wt.%	7,800	24,600	3.2	1.6
10 wt.%	5,500	19,800	3.6	1.8

Much more dramatic changes in the molecular weight were observed when examining the weight average molecular weight, M_w. The addition of 2 – 10 wt.% clay increased the M_w approximately 5,000 – 12,000 g/mol higher than the control M_w (13,000 g/mol). The copolymer containing 5 wt.% MEOA-clay had the largest M_w at 24,600 g/mol. The observation of these two distinct trends is a reflection of several factors. Because the clay was modified with MEOAB, the organic modifier may serve as an additional site for reacting with the 3-MPS and DMAEMA monomers. Therefore, the MEOA-clay may participate during the copolymerization reaction by acting as a chain transfer agent or supply an alternate location for monomer addition. The increased loading of MEOA-clay provides more sites for reactions with the 3-MPS and DMAEMA monomers, and may be partially

responsible for the reduction in M_n observed with higher clay loading. Increased M_w values were observed as the clay loading was increased, the opposite trend observed with the copolymer M_n values. The GPC analysis of the copolymers was performed without the removal of clay prior to each sample being passed through the column. Therefore, the inclusion of MEOA-clay may have increased the hydrodynamic volume and resulted in higher M_w values, as evidenced with the copolymers containing 5 and 10 wt.% MEOA-clay with M_w values of 24,600 and 19,800 g/mol, respectively.

The viscosity of the amine- and alkoxysilane-functional copolymer-clay nanocomposites directly correlated to the copolymer M_w. The control copolymer sample had the lowest viscosity at 0.4 Poise, and the introduction of MEOA-clay increased the copolymer viscosity slightly. As expected, the copolymers containing the highest level of MEOA-clay (5 – 10 wt.%) had the highest viscosities at 1.6 and 1.8 Poise, respectively. By raising the level of MEOA-clay within the copolymer sample, the movement of the copolymer chains may become more restricted, thereby reducing mobility and increasing the copolymer viscosity.

7.3.2. Hybrid morphology – X-ray diffraction

Once the amine- and alkoxysilane-functional copolymer-clay nanocomposites were characterized, the copolymers were crosslinked with silane coupling agent tetraethyl orthosilicate (TEOS) to create organic-inorganic hybrid films. The dispersion of MEOA-clay within the hybrid network was characterized using XRD analysis, specifically focusing on the 2 – 9 2θ range to quantify the *d*-spacing, or distance between the clay platelets. Figure 7.2 displays the XRD scans

for the pristine unmodified Cloisite® Na^+ and modified MEOA-clay as well as the five hybrid films.

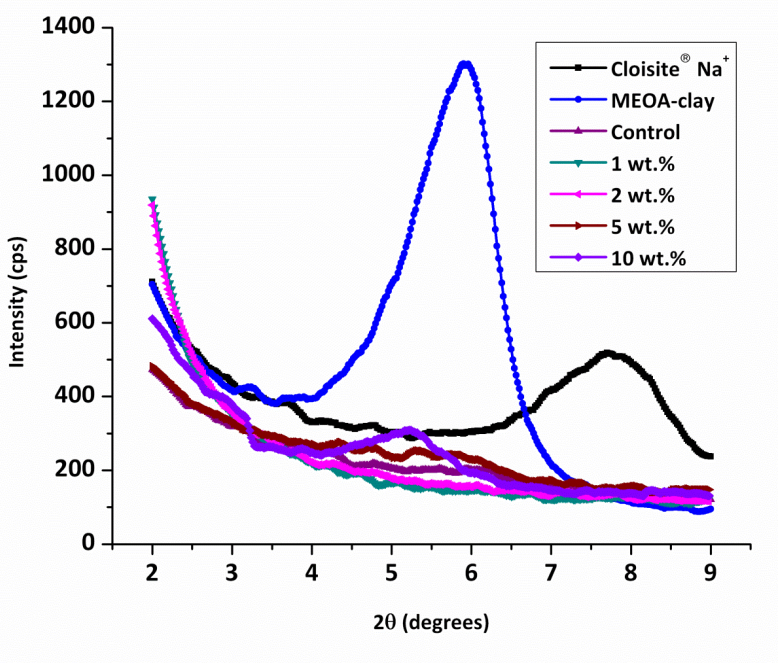

Figure 7.2: XRD scans of pristine clays and amine-based organic-inorganic hybrid films containing 0 – 10 wt.% MEOA-clay.

The diffraction peak for the MEOA-clay shifted to a lower 2θ value, indicating an increase in *d*-spacing. Using Bragg's law, the *d*-spacing for the modified clay was determined to be 1.48 nm, increased from the Cloisite® Na^+ *d*-spacing value of 1.08 nm, and demonstrates the success of the organomodification performed by the ion exchange reaction between the Na^+ exchangeable cations and the MEOAB organic modifier. The hybrids containing 1 and 2 wt.% MEOA-clay did not produce a diffraction peak in the low 2θ range, indicating the clay may be well-dispersed and potentially exfoliated throughout the hybrid network. However, the small concentration of clay included in the formation of the hybrid films may not be detected, depending on the sensitivity of the XRD

instrument or the clay geometry.[22] Diffraction peaks were observed for the hybrids containing higher levels of MEOA-clay loading (5 – 10 wt.%). The *d*-spacing was determined to be 1.54 and 1.58 nm for the 5 and 10 wt.% MEOA-clay hybrids, respectively. As the clay interlayer distance did increase from the pristine MEOA-clay, the XRD analysis indicates copolymerization did occur between the clay platelets and the final hybrid network had an intercalated morphology.

7.3.3. Barrier properties – Water vapor permeability

The inclusion of MEOA-clay into the organic-inorganic hybrid networks decreased the water vapor permeability up to 80%, in accordance with water vapor transmission testing with ASTM E96 “Standard Test Methods for Water Vapor Transmission, Water Method.” By utilizing the inorganic linkages from the sol-gel reactions to create the hybrid films as well as the incorporation of impermeable clay fillers, the organic-inorganic hybrid films employ two routes towards decreasing water vapor permeation, thus improving the barrier properties. As expected, the incorporation of the nanosized-clay fillers increased the barrier protection of the hybrid networks compared to the control film without MEOA-clay. Figure 7.3 plots the WVP, as determined by the hybrid network water vapor transmission rate (WVTR), and Table 7.2 reports each hybrid WVP. Comparing the neat organic-inorganic film to those containing MEOA-clay, the improvement in barrier protection with the inclusion of MEOA-clay was observed. The WVP of the hybrid film containing 1 wt.% MEOA-clay decreased to 6.10E-11 $g \cdot m/m^2 \cdot s \cdot Pa$, over a 50% reduction from the control hybrid film (1.14E-10 $g \cdot m/m^2 \cdot s \cdot Pa$). A maximum in barrier performance was seen with MEOA-clay loading between 2 – 5

wt.%, a similar trend observed in Chapters 2, 4, and 6. By incorporating the impermeable MEOA-clay into the hybrid network, the permeating water vapor molecules must adopt a tortuous path through the polymeric matrix and thus increase the overall diffusion path length.

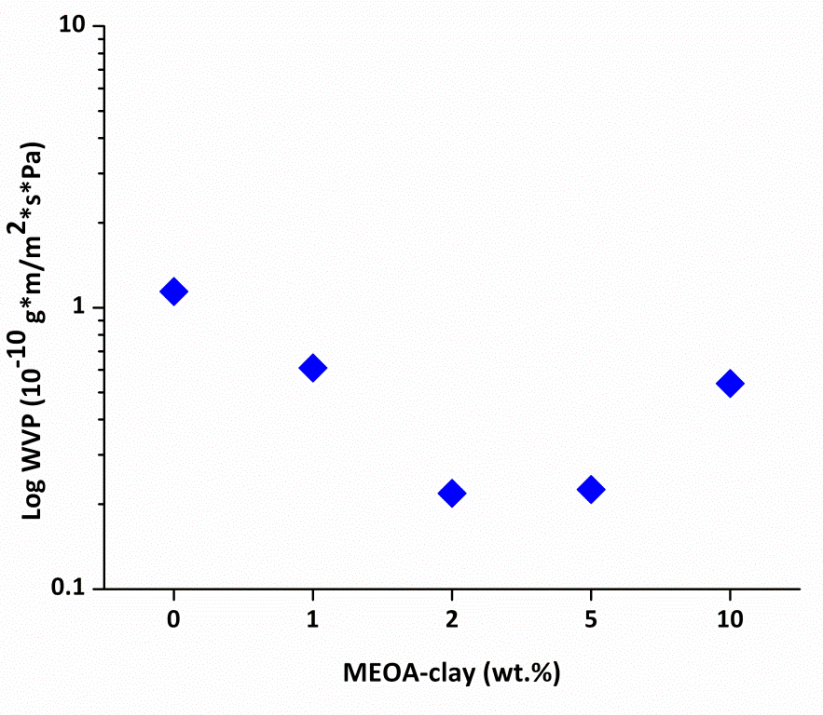

Figure 7.3: Water vapor permeability (WVP), as determined by ASTM E96, of amine-based organic-inorganic hybrids containing 0 – 10 wt.% MEOA-clay.

TABLE 7.2
Amine-based organic-inorganic hybrid films
barrier, thermal, and optical properties characterization

MEOA-clay wt.%	WVP ($g \cdot m/m^2 \cdot s \cdot Pa$)	T_{10}% (°C)	Char yield (%)	Transmittance (%)
Control	1.14E-10	160	8	94
1	6.10E-11	180	12	93
2	2.19E-11	190	28	83
5	2.26E-11	175	30	52
10	5.37E-11	175	35	44

7.3.4. Thermal stability and optical clarity – Thermogravimetric analysis and UV-visible spectroscopy

Thermal stability of the hybrid films was characterized by thermogravimetric analysis (TGA), specifically measuring the temperature at 10 wt.% loss (T_{10}%) and char yield at 600 °C. The degradation curves are displayed in Figure 7.4, and T_{10}% and char yield are reported in Table 7.2.

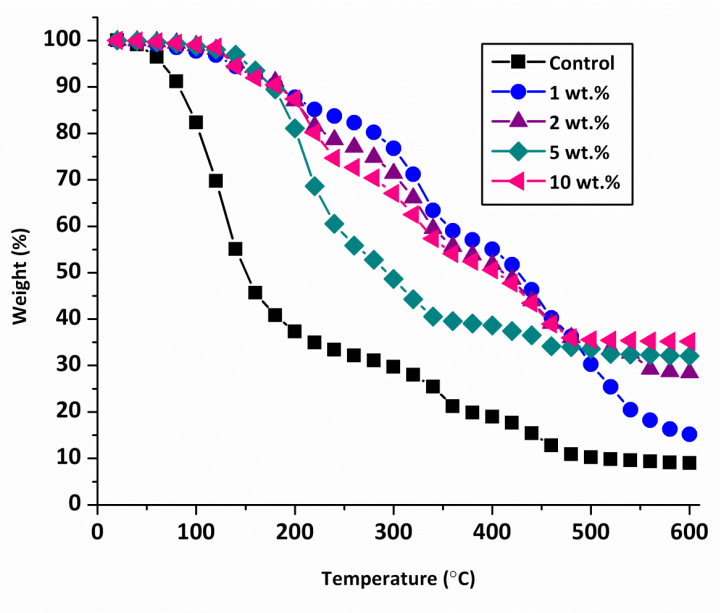

Figure 7.4: Degradation curves of the amine-based organic-inorganic hybrid films determined by thermogravimetric analysis.

With the incorporation of MEOA-clay into the amine-based hybrid network, the T_{10}% values increased up to 30 °C higher than the control hybrid network. The hybrid networks containing 1 and 2 wt.% MEOA-clay had the highest measured T_{10}% values at 180 and 190 °C, respectively. Further increases in clay loading slightly diminished the improved thermal stability to a T_{10}% value of 175 °C for the hybrids containing 5 and 10 wt.% MEOA-clay. The improvement in thermal stability

with layered silicate incorporation may be attributed to higher inorganic content. With the inclusion of the organomodified clay, the degradation of the hybrid films is slowed when the layered silicates act as a barrier. Higher levels of MEOA-clay may display somewhat reduced thermal stability as a consequence of layered silicate crowding or possibly the organic modifier acting as a plasticizer at elevated temperatures. The char yield also reflected the contribution of the layered silicates to increasing the hybrid network thermal stability. The char yield of the control hybrid film was 8%, a reflection of the inorganic Si-O-Si network formed in the organic-inorganic hybrid sol-gel system. A direct correlation between char yield and clay loading was observed: higher levels of MEOA-clay led to increased chair yield. The hybrid film containing 10 wt.% clay had a char yield of 35%, over 4 times the value obtained with the control hybrid film.

The optical clarity of the organic-inorganic hybrid films was quantitatively measured with UV-vis spectroscopy by examining the percent transmittance through the films at 400 nm (values reported in Table 7.2). The control hybrid film had high optical clarity, measuring a 94% transmittance. The inclusion of MEOA-clay into the network reduced the transmittance once the loading was increased to the 2 – 10 wt% range. The hybrid coating containing 2 wt.% clay maintained somewhat high optical clarity with 83% transmittance, but the inclusion of higher clay content drastically diminished the clarity of these hybrid films. Poorer transparency of the hybrid films containing high clay content is most likely a consequence of poorer clay dispersion throughout the network, thereby increasing the scattering of the organomodified clay.

7.3.5. Mechanical properties – Dynamic mechanical analysis and König hardness

The viscoelastic properties of the organic-inorganic hybrid films, measured by dynamic mechanical analysis (DMA), were significantly influenced by the quantity of MEOA-clay dispersed throughout the hybrid network. Figure 7.5 shows the storage modulus plots of the organic-inorganic hybrid films, and Table 7.3 reports the data obtained from these plots.

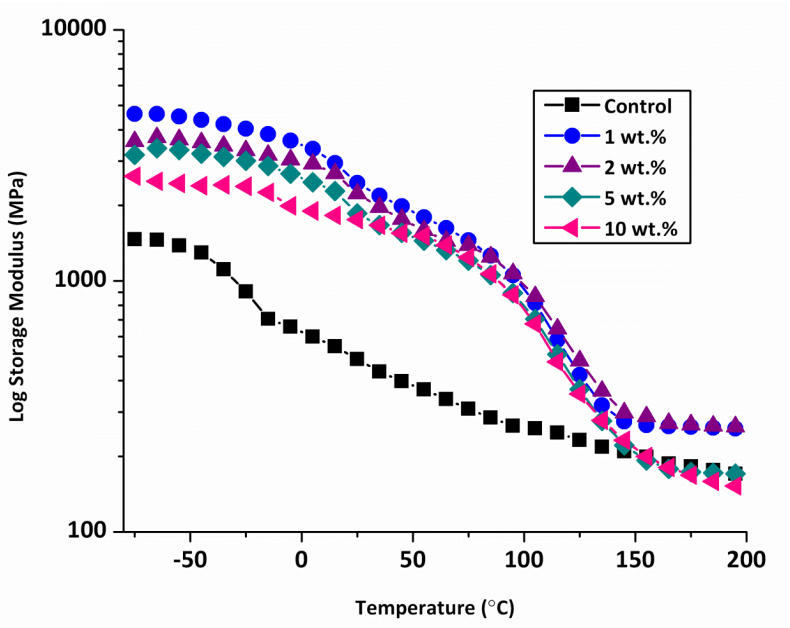

Figure 7.5: Storage modulus plots of amine-based organic-inorganic hybrid films from dynamic mechanical analysis.

The inclusion of MEOA-clay in the hybrid films greatly increased the storage moduli values in the glassy and glass-rubber transition states. As determined by dynamic mechanical thermal analysis, the storage moduli (E') of the control hybrid film was 490 at room temperature. By introducing just 1 wt.% MEOA-clay into the hybrid network, the E' increased approximately five times to 2455 MPa. Further increases in MEOA-clay loading also produce E' values higher than the control

hybrid films; however, higher clay content led to reductions in E' compared to the hybrid film containing 1 wt.% MEOA-clay. The hybrid film containing 2 wt.% MEOA-clay was comparable in E' to 1 wt.% MEOA-clay, recording a E' value of 2225 MPa at room temperature. Hybrids containing 5 and 10 wt.% MEOA-clay measured E' values of 1850 and 1755 MPa, respectively. By incorporating the organomodified clays into the hybrid networks, the reinforcing impact of layered silicates was observed.

The diminishing E' values with higher levels of clay loading may be a consequence of crowding in the network, reducing the ability of the layered silicates to mechanically support the hybrid network. This trend was also reflected in the glass transition temperature (T_g) of the hybrid films, determined by the peak in the tan δ plot. The control hybrid film measured a T_g of 94 °C, and the introduction of MEOA-clay into the hybrid networks produced higher T_g values, which was attributed to the reduction in chain mobility with the reinforcing organomodified clays. The hybrid film producing the highest T_g was with the incorporation of 2 wt.% MEOA-clay, recording a T_g of 120 °C. Higher levels of MEOA-clay loading (5 – 10 wt.%) reduced the T_g slightly to the range of 110 – 115 °C, most likely a consequence of poorer clay dispersion throughout the hybrid network.

The crosslink density (XLD) of the organic-inorganic hybrid films, as determined by E' in the rubbery plateau region, revealed the impact of clay loading on the mechanical properties of these films. The XLD of the control film was determined to be 0.014 mol/cm^3. The incorporation of lower levels of MEOA-clay (1

– 2 wt.%) increased the XLD to 0.022 mol/cm^3. Once higher levels of MEOA-clay were introduced into the network (5 – 10 wt.%), the XLD decreased to approximately the same value of the control film. The introduction of the MEOA-clay showed an increase in the XLD for lower levels of clay loading as the organomodified clay may act like a physical crosslink when interacting with polymer chains, and thus increasing the effective XLD. However, further increases in the clay fraction typically result in poorer clay dispersion, thereby reducing the ability of the clay fillers to act as crosslink and diminishing the XLD. Based on the mechanical properties of the hybrid films from DMA, the peak in mechanical performance occurred approximately at 2 wt.% MEOA-clay loading.

TABLE 7.3
Amine-based organic-inorganic hybrid mechanical properties characterization

MEOA-clay wt.%	*E'* (MPa,25°C)	T_g (°C)	XLD (mol/cm^3)	Hardness (sec)
Control	490	94	0.014	65
1	2455	116	0.022	162
2	2225	120	0.022	134
5	1850	115	0.014	95
10	1755	111	0.013	96

The König pendulum hardness results of the organic-inorganic hybrid films also demonstrated the significant impact small amounts of organomodified clay may have on the mechanical properties of these hybrids (Figure 7.6). The control hybrid film, containing no MEOA-clay, had the lowest hardness of the five hybrid films at 65 sec. Dramatic increases in the hardness were observed with the 1 and 2 wt.% MEOA-clay hybrid films with hardness values of 162 and 134 sec, respectively. Once again, higher levels of MEOA-clay incorporation in the hybrid

network diminished the mechanical properties, as the hardness decreased with clay loading ranging from 5 – 10 wt.%. The trends observed in the hardness of these hybrid films was consistent with the trends observed in mechanical properties obtained from DMA.

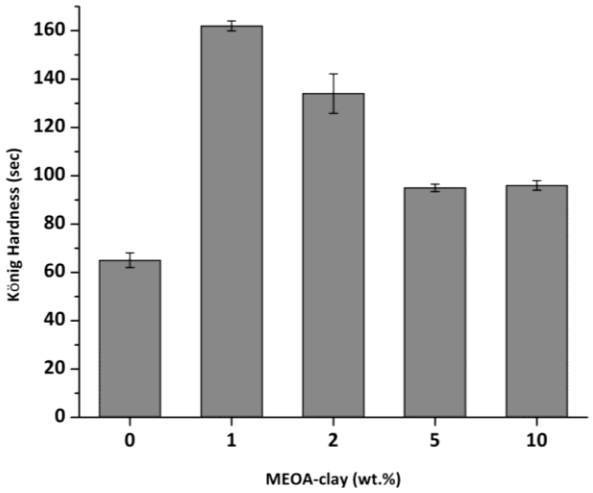

Figure 7.6: Average König pendulum hardness of amine-based organic-inorganic hybrid films on aluminum substrates.

7.4. Conclusions

Organic-inorganic hybrid films were prepared using a two-step process where precursor amine- and alkoxysilane-functional copolymer-clay nanocomposites were crosslinked via sol-gel processing to create a hybrid network containing organomodified clay. The copolymers, composed of monomers 3-methacryloxypropyltrimethoxysilane and 2-(dimethylamino)ethyl methacrylate, were copolymerized in the presence of methacrylate-functional, quaternary ammonium modified (MEOA) montmorillonite clay. The conversion of the monomers to copolymer was confirmed by FTIR spectroscopy, and the physical properties were dependent on the level of clay incorporated into the

nanocomposite sample. The crosslinked organic-inorganic hybrid films containing MEOA-clay demonstrated superior barrier, mechanical, and thermal properties compared to the neat hybrid film. The MEOA-clay containing hybrids decreased the water vapor permeability up to 80%, and demonstrated the best barrier protection with 2 – 5 wt.% clay loading. Future studies will further explore the feasibility of utilizing the amine-based organic-inorganic hybrids containing organomodified clay as potential applications for CO_2 capture and separation.

7.5. References

1. Wright, J. D.; Sommerdijk, N. A. J. M., *Sol-gel materials: chemistry and applications*. CRC: 2001; Vol. 4.

2. Klein, L. C., *Sol-gel technology for thin films, fibers, preforms, electronics, and specialty shapes*. William Andrew: 1988.

3. Lev, O.; Wu, Z.; Bharathi, S.; Glezer, V.; Modestov, A.; Gun, J.; Rabinovich, L.; Sampath, S., *Chemistry of Materials* **1997,** *9* (11), 2354-2375.

4. Kang, X.; Mai, Z.; Zou, X.; Cai, P.; Mo, J., *Talanta* **2008,** *74* (4), 879-886.

5. Gupta, R.; Chaudhury, N., *Biosensors and Bioelectronics* **2007,** *22* (11), 2387-2399.

6. Klein, L. C., *Sol-gel optics: processing and applications*. Springer: 1994.

7. Chen, D., *Solar Energy Materials and Solar Cells* **2001,** *68* (3-4), 313-336.

8. Abe, Y.; Honda, Y.; Gunji, T., *Applied Organometallic Chemistry* **1998,** *12* (10-11), 749 - 753.

9. Costa, R. O. R.; Vasconcelos, W. L., *Journal of Non-Crystalline Solids* **2002,** *304* (1-3), 84-91.

10. Mellon, V.; Rinaldi, D.; Bourgeat-Lami, E.; D'Agosto, F., *Macromolecules* **2005,** *38* (5), 1591-1598.

11. Chang, T.; Yeh, T.; Yang, C.; Hong, Y.; Wu, T., *Polymer* **2001,** *42* (21), 8565-8570.

12. Becker, C.; Krug, H.; Schmidt, H., *Journal of Sol-Gel Science and Technology* **1997,** *8* (1), 625-627.

13. Rao, A. B.; Rubin, E. S., *Environmental Science & Technology* **2002,** *36* (20), 4467-4475.

14. Yang, H.; Xu, Z.; Fan, M.; Gupta, R.; Slimane, R. B.; Bland, A. E.; Wright, I., *Journal of Environmental Sciences* **2008,** *20* (1), 14-27.

15. Hiyoshi, N.; Yogo, K.; Yashima, T., *Microporous and Mesoporous Materials* **2005,** *84* (1-3), 357-365.

16. Zelenak, V.; Halamova, D.; Gaberova, L.; Bloch, E.; Llewellyn, P., *Microporous and Mesoporous Materials* **2008,** *116* (1-3), 358-364.

17. Sakamoto, Y.; Nagata, K.; Yogo, K.; Yamada, K., *Microporous and Mesoporous Materials* **2007,** *101* (1-2), 303-311.

18. Franchi, R. S.; Harlick, P. J. E.; Sayari, A., *Industrial & Engineering Chemistry Research* **2005,** *44* (21), 8007-8013.

19. Harlick, P. J. E.; Sayari, A., *Industrial & Engineering Chemistry Research* **2006,** *45* (9), 3248-3255.

20. Zeng, C.; Lee, L. J., *Macromolecules* **2001,** *34* (12), 4098-4103.

21. Chan, C. K.; Peng, S. L.; Chu, I., *Polymer* **2001,** *42* (9), 4189-4196.

22. Morgan, A. B.; Gilman, J. W., *Journal of Applied Polymer Science* **2003,** *87* (8), 1329-1338.

CHAPTER 8. CO_2 CAPTURE AND SEPARATION MEMBRANES DERIVED FROM 3-AMINOPROPYLTRIMETHOXYSILANE-BASED ORGANIC-INORGANIC HYBRIDS

8.1. Introduction

Organic-inorganic hybrids prepared by sol-gel processing have garnered significant attention due to the improvements in material properties by incorporating the advantageous properties of organic and inorganic species into one network. Through sol-gel chemistry, nanometer-sized inorganic domains dispersed throughout an organic matrix have produced hybrid films with enhanced properties, including thermal stability and mechanical performance.[1-4] The use of sol-gel chemistry to produce organic-inorganic films is motivated by the advantageous processing conditions including mild reaction conditions, control over reaction kinetics and film morphology, and pure products.[5] The ability to tailor organic-inorganic hybrid networks to achieve unique properties is supported by the wide-availability of alkoxysilane organic precursors, or organic molecules possessing alkoxysilane-functional groups for sol-gel chemistry in addition to other organic functionalities such as vinyl,[6-7] methacrylate,[8-10] epoxy,[11-12] and phenyl[13] functional groups.

In recent years, amine-functional alkoxysilane organic precursors have been utilized to prepare organic-inorganic films for carbon dioxide (CO_2) capture applications to replace liquid alkanoamine usage in CO_2 absorption technologies due to the high energy consumption and solvent regeneration issues.[14] Amine-functional alkoxysilane precursors may act as a viable alternative to the traditional

liquid amine CO_2 absorption technologies[15], and several research groups have reported the production of amine-based mesoporous hybrid materials from amine-functional organic alkoxysilane precursors. Hiyoshi et al. reported the development or amine-functional mesoporous materials by grafting aminosilanes to mesoporous silica (SBA-15) for CO_2 absorption applications.[16] Aminosilanes 3-aminopropyltriethoxysilane, *N*-(2-aminoethyl)-3-aminopropyl-triethoxysilane, and 3-(trimethoxysilylpropyl)-diethylenetriamine were grafted onto mesoporous SBA-15 by refluxing in dehydrated toluene for 24 hours at 110 °C. The CO_2 absorbance increased as the amine content in the aminosilane grafting agent was increased, which was attributed to higher amine efficiency as the absorption of CO_2 proceeded through the conversion of the amine to an ammonium carbonate group. In addition to SBA-15, a two-dimensional structure, three-dimensional mesoporous silica precursors were utilized to develop amine-modified CO_2 separation membranes with an aminosilane grafting agent.[17] Huang et al. reported the development of CO_2 sorbent materials with the aminosilane 3-aminopropyltriethoxysilane. The basic amine groups grafted to the mesoporous MCM-48 silica function as a sorbent for the separation of acidic CO_2 gas, leading to high CO_2 absorption efficiency.

Previously, the novel development of organic-inorganic hybrid films from an organomodified clay sol precursor material was reported in Chapter 6. The hybrid films were prepared based on a two step process. First, copolymers of 3-methacryloxypropyltrimethoxysilane (3-MPS) and methyl methacrylate (MMA) were synthesized in the presence of organomodified clay by an in situ intercalative

polymerization technique to create an alkoxysilane-functional copolymer-clay nanocomposite sol precursor. Next, the nanocomposite sol was crosslinked with silane coupling agent tetraethyl orthosilicate (TEOS) to produce organic-inorganic hybrid films with organomodified clay dispersed throughout the network. By coupling the advantageous nanocomposite properties from clays and organic-inorganic hybrids into one system, improvements in mechanical, thermal, and barrier properties were observed compared to a neat organic-inorganic hybrid prepared in the absence of the organomodified clay.

Using the same hybrid preparation process to research the production of CO_2 capture and separation membranes, amine-based hybrid films were prepared in Chapter 7 by copolymerizing 2-(dimethylamino)ethyl methacrylate with 3-MPS to create amine- and alkoxysilane-functional copolymer-clay nanocomposites that may undergo sol-gel reactions. The resulting amine-based hybrids demonstrated enhanced material properties, such as increased thermal stability, but the films were brittle and difficult to handle. To overcome the brittleness of the amine-functional hybrid films derived from copolymers containing DMAEMA, an alternative method to produce amine-based hybrids is detailed in this study. The two-step hybrid preparation process was once again utilized. Copolymers of MMA and 3-MPs were synthesized in the presence of organomodified clay, and then crosslinked with amine-functional alkoxysilane precursor 3-aminopropyltrimethoxysilane (APTMS). Through this novel preparation process, the resulting APTMS-based organic-inorganic hybrid films contain amine-functionality for possible CO_2 capture along with organomodified clay to enhance

the material properties of the neat hybrid networks. The APTMS content and loading of MEOA-clay was varied to create a total of fifteen organic-inorganic hybrid film compositions.

8.2. Experimental

8.2.1. Materials

Methyl methacrylate (MMA), 2-(dimethylamino)ethyl methacrylate (DMAEMA), anhydrous toluene, 1-bromooctane, tetraethyl orthosilicate, and ethanol were obtained from Sigma Aldrich (Milwaukee, WI). To remove the inhibitor, MMA was passed through an activated basic column and stored at 0°C prior to use. The monomer 3-methacryloxypropyltrimethoxysilane (3-MPS) was purchased from Gelest (Morrisville, PA) and purified by vacuum distillation. The initiator 2,2'-azobis(2-methylbutyronitrile), "Vazo 67", gratefully supplied by DuPont (Belle, WV), was re-crystallized in ethanol. The unmodified montmorillonite clay Cloisite® Na^+ was obtained from Southern Clay Products (Gonzales, TX). Unless noted, all materials were used as received.

8.2.2. Clay functionalization with 2- methacryloyloxyethyloctyldimethyl-ammonium bromide

The unmodified montmorillonite clay, Cloisite® Na^+, was functionalized with a methacrylate-functional quaternary ammonium surfactant, 2-methacryl-oyloxyethyloctyldimethylammonium bromide (MEOAB). The preparation of MEOAB was repeated from the procedure detailed by Zeng and Lee. Briefly, 1-bromooctane (0.025 mol) was employed to quaternized DMAEMA (0.050 mol) in ethyl acetate at 60 °C for 24 hours. The quaternized product, MEOAB, was

functionalized onto Cloisite® Na^+ by an ion exchange reaction in distilled water. The functionalized clay, herein referred to as MEOA-clay, was dried and ground with a mortar and pestle.

8.2.3. In situ intercalative copolymerization with functionalized clay

Alkoxysilane-functional copolymers were synthesized with monomers methyl methacrylate (MMA) and 3-methacryloxypropyltrimethoxysilane (3-MPS) in the presence of MEOA-clay in accordance Chapter 6. The conventional free radical copolymerization of MMA and 3-MPS was employed using a semi-batch process. First, MMA (0.05 mol) and 3-MPS (0.05 mol) were mixed with MEOA-clay at 1, 2, 5, and 10 wt.% MEOA-clay (based on total monomer weight) overnight via magnetic stirrer. Toluene (0.43 mol) and TEOS (0.05 mol) were added to a 4-neck, 250 mL round bottom flask equipped with a temperature controller/probe, mechanical stirrer, nitrogen inlet, addition funnel, and heating mantle, then heated to 70 °C under a nitrogen atmosphere. Meanwhile, initiator 2,2'-azobis(2-methylbutyronitrile) was added at 2.5 wt.% of the total monomer weight to the monomer-clay mixture.

Once the toluene and TEOS solution reached 70 °C, the monomer-clay mixture was added slowly dropwise through the addition funnel. The rate of monomer solution addition was approximately 1 mL/minute. The copolymerization reaction proceeded for 24 hours, and then solvents were removed by a rotary evaporator. In addition to the MEOA-clay containing copolymers, a control copolymer reaction was performed containing no clay for a total of five copolymers with clay loading of 0, 1, 2, 5, and 10 wt.% clay.

8.2.4. APTMS-based organic-inorganic hybrid formation via sol-gel chemistry

The alkoxysilane-functional copolymer-clay nanocomposites were utilized as a precursor sol to create organic-inorganic hybrid films via sol-gel chemistry. The silane crosslinking agent, 3-aminopropyltrimethoxysilane (APTMS) was combined with ethanol, deionized water, and hydrochloric acid with a molar ratio of 1:5:25:0.025, similar to Chen et al, and stirred vigorously at room temperature. Three organic-inorganic hybrid formulations were created for each alkoxysilane-functional copolymer-clay nanocomposite with weight ratios of 90:10, 80:20, and 70:30 (copolymer:APTMS solution) for a total of fifteen hybrid formulations (Table 8.1).

TABLE 8.1
APTMS-based organic-inorganic hybrid film composition

Copolymer: APTMS (wt. ratio)	MEOA-clay (wt.%)	Hybrid name
90:10	0	Control_APTMS10
80:20		Control_APTMS20
70:30		Control_APTMS30
90:10	1	1_APTMS10
80:20		1_APTMS20
70:30		1_APTMS30
90:10	2	2_APTMS10
80:20		2_APTMS20
70:30		2_APTMS30
90:10	5	5_APTMS10
80:20		5_APTMS20
70:30		5_APTMS30
90:10	10	10_APTMS10
80:20		10_APTMS20
70:30		10_APTMS30

Each formulation was mixed at room temperature via magnetic stirring for one hour, coated onto glass and aluminum substrates by spin coating at 500 RPM for 20 seconds, and cured in a vacuum oven at 70 °C for further drying and network densification (film thickness ≈ 20 μm). A small portion of the hybrid formulation was transferred to a plastic container, aged for three days at room temperature, and transferred to a vacuum oven at 40 °C for several hours to complete network densification (thickness ≈ 120 μm).

8.2.5. Characterization

The five copolymer products used in this study were previously characterized in Chapter 6. The morphological, barrier, mechanical, thermal, and optical properties of the fifteen resulting organic-inorganic hybrid coatings were studied to explore the impact of the amine-functional crosslinker content and clay loading. X-ray diffraction was employed to study the degree of organomodified clay dispersion throughout the hybrid network. XRD results were obtained from a Bruker AXS' D8 Discover diffractometer in Bragg-Brentano geometry using Cu Kα radiation at a wavelength of 1.5406 Å. The hybrid films were scanned from 2° - 60° 2θ and the run time was 1 sec/step. The hybrid film barrier properties were measured by employing ASTM E96 "Standard Test Methods for Water Vapor Transmission, Water Method." The thicker hybrid film samples (≈120 μm) were attached to a 10 cm^2 permeability cup containing distilled water and placed into a controlled atmospheric chamber. The temperature of the atmospheric chamber was maintained at 20 ± 2 °C, and the relative humidity was maintained at 75 ± 2% with concentrated sodium chloride solutions. The permeability cups were weighed

over time until a steady state of mass loss was achieved. Duplicate samples were tested to verify the water vapor transmission results. The hybrid film viscoelastic properties were studied by dynamic mechanical analysis (DMA) with a TA Instruments Q800 Dynamic Mechanical Analyzer in tensile mode. Free films of the cured organic-inorganic hybrids were cut to dimensions of approximately 15 mm x 5 mm x 20 mm. Testing was conducted with a 1 Hz frequency, constant strain of 0.05%, and a heating rate of 5 °C/minute. The temperature range for testing was -80 °C – 200 °C. The film hardness of the organic-inorganic hybrids was determined by a BYK-Gardner pendulum hardness tester using the films coated onto aluminum substrates. The hybrid thermal stability was determined by thermogravimetric analysis (TGA) with a TA Instruments Q500 Thermogravimetric Analyzer by heating each hybrid sample from room temperature to 600 °C at a rate of 20 °C/minute under a nitrogen atmosphere. The hybrid film optical clarity was measured by determining the percent transmittance at 400 nm using a Varian Cary 5000 UV-Vis Spectrometer.

8.3. Results and discussion

In Chapter 6, a method was developed for preparing high performance, organic-inorganic hybrid films by crosslinking alkoxysilane-functional copolymer-clay nanocomposites with silane crosslinking agents to create novel hybrid networks. Methyl methacrylate (MMA) and 3-methacryloxypropyltrimethoxysilane (3-MPS) were copolymerized in the presence of organomodified clay to create alkoxysilane-functional copolymers grafted to clay platelets, followed by crosslinking via sol-gel chemistry to create organic-inorganic hybrids dispersed in

throughout the network. To introduce amine functionality through a similar preparation route, copolymers of 2-(dimethylamino)ethyl methacrylate (DMAEMA) and 3-MPS were synthesized in the presence of organomodified clay in Chapter 7, and crosslinked with tetraethyl orthosilicate (TEOS) to create novel amine-based hybrid films. The resulting amine-based films derived from the DMAEMA and 3-MPS copolymers containing clay demonstrated improved barrier, mechanical, and thermal properties, but were brittle. To overcome the brittleness of these amine-based films, an alternative method was developed to introduce amine-functionality into the hybrid film. In this study, the development of novel amine-based organic-inorganic hybrid films was explored by employing 3-aminopropyltrimethoxysilane (APTMS) as a silane agent to crosslink the alkoxysilane-functional copolymer-clay nanocomposites. Copolymers of methyl methacrylate (MMA) and 3-methacryloxypropyltrimethoxysilane (3-MPS) were synthesized in the presence of methacrylate-functional organomodified montmorillonite clay (0 – 10 wt.%) by in situ intercalative polymerization. The resulting alkoxysilane-functional copolymer-clay nanocomposites were crosslinked with APTMS at 90:10, 80:20, and 70:30 weight ratios to create the amine-based hybrids with organomodified clay dispersed throughout the network. By incorporating the amine functionality after copolymerization, the amine-based organic-inorganic films demonstrated much more flexibility and improved barrier properties.

8.3.1. Hybrid morphology – X-ray diffraction

X-ray diffraction (XRD) was employed to characterize the degree of MEOA-clay dispersion throughout the APTMS-based organic-inorganic hybrid films. As

seen from the XRD scans displayed in Figures 8.1 – 8.3, dramatic differences occurred in the hybrid diffraction peaks compared to the pristine Cloisite® Na^+ and organomodified clays. The *d*-spacing, calculated from Bragg's Law, of the unmodified Cloisite® Na^+ was determined to be 1.08 nm. By functionalizing the unmodified clay, the *d*-spacing increased to 1.48 nm, demonstrating the successful intercalation of the methacrylate-functional quaternary ammonium surfactant into the clay layers through an ion exchange reaction. The control hybrid films as well as the hybrids containing 1 and 2 wt.% MEOA-clay did not produce a diffraction peak within the 2° – 9° 2θ range. The absence of diffraction peaks at low 2θ angles indicates the possibility of high clay dispersion due to disruption of the functionalized clay well-ordered arrangement. However, poor instrument sensitivity and the geometry of testing may also contribute to an absence of diffraction peaks at low 2θ.

The APTMS-based hybrids containing higher levels of MEOA-clay (5 – 10 wt.%) produced diffraction peaks in the 2° - 9° 2θ range (*d*-spacing values are reported in Table 8.2). Each diffraction peak produced was shifted to lower 2θ angles than the pristine unmodified and functionalized clays, indicating copolymerization occurred between the clay layers as the growing volume from the propagating copolymer chain would necessitate an increase in volume between the modified clay platelets. The *d*-spacing increased from 1.48 nm for the functionalized clay to approximately 1.70 – 1.80 nm for the MEOA-clay containing hybrid films, suggesting an intercalated nanocomposite morphology.

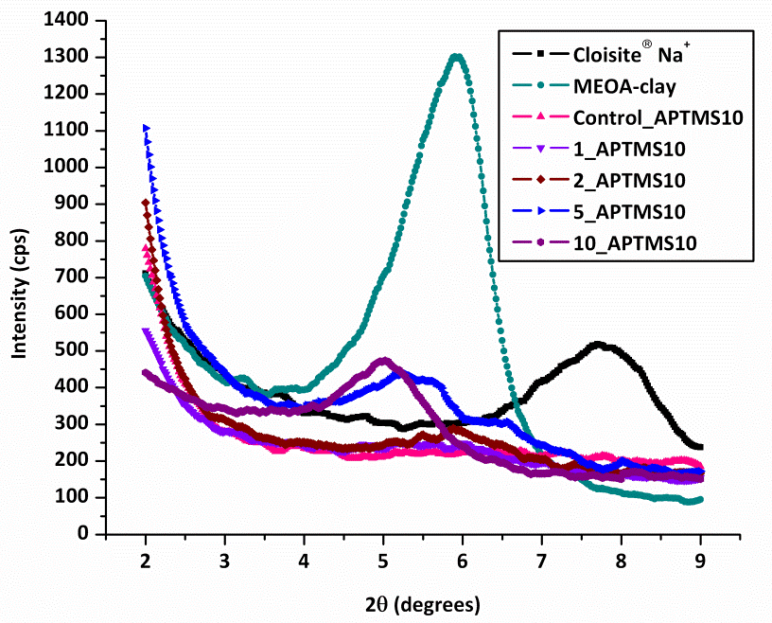

Figure 8.1: XRD scans for APTMS-based organic-inorganic hybrids formulated based on a 90:10 weight ratio.

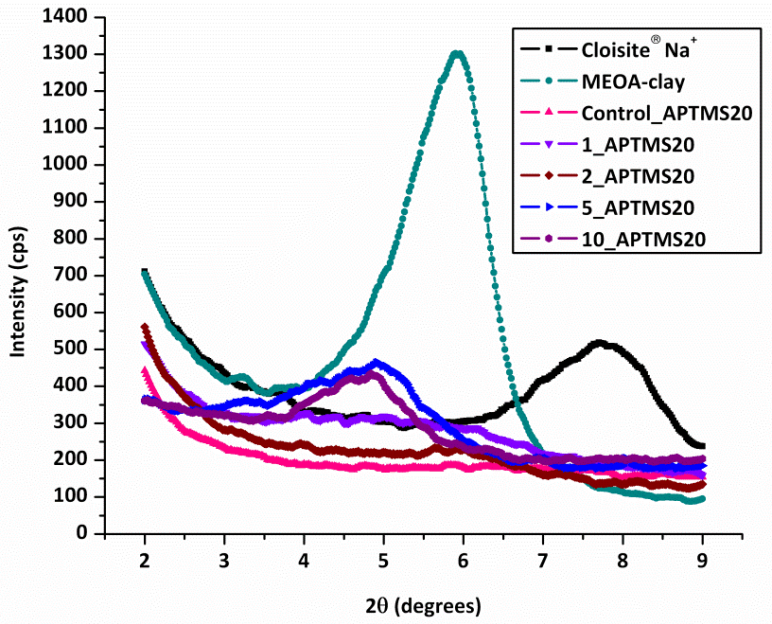

Figure 8.2: XRD scans for APTMS-based organic-inorganic hybrids formulated based on an 80:20 weight ratio.

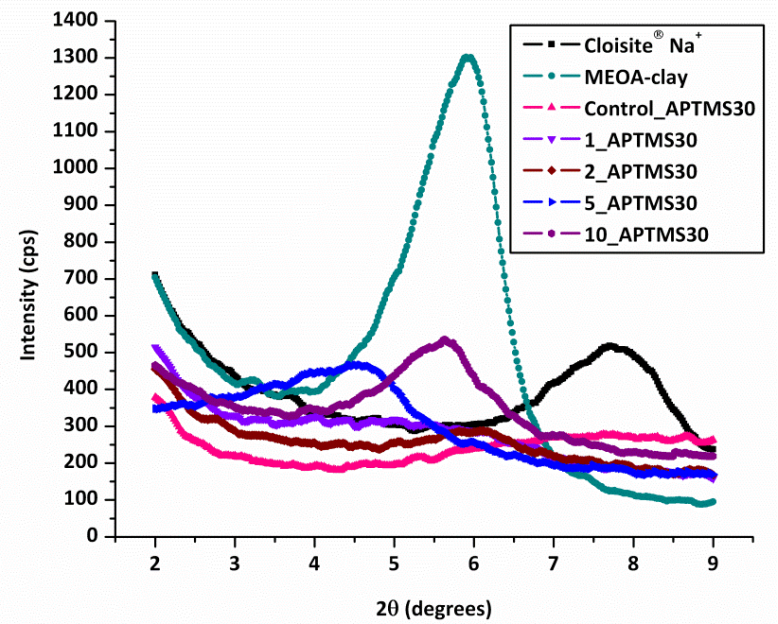

Figure 8.3: XRD scans for APTMS-based organic-inorganic hybrids formulated based on a 70:30 weight ratio.

TABLE 8.2
APTMS-based organic-inorganic hybrid films
barrier, thermal, and optical properties characterization

Hybrid Name	*d*-spacing* (nm)	WVP ($g \cdot m/m^2 \cdot s \cdot Pa$)	T_{10}% (°C)	Char yield (%)	Transmit-tance (%)
Control_APTMS10	----	2.50E-10	190	15	80
1_APTMS10	----	5.01E-11	210	15	81
2_APTMS10	----	4.36E-11	220	16	75
5_APTMS10	1.77	3.52E-11	200	23	62
10_APTMS10	1.69	4.02E-11	180	15	38
Control_APTMS20	----	5.55E-11	195	19	75
1_APTMS20	----	4.43E-11	230	29	76
2_APTMS20	----	3.30E-12	230	32	71
5_APTMS20	1.77	8.51E-13	285	38	33
10_APTMS20	1.77	2.05E-11	195	29	23
Control_APTMS30	----	2.10E-12	190	20	52
1_APTMS30	----	6.90E-13	245	37	54
2_APTMS30	----	1.61E-13	265	39	52
5_APTMS30	1.81	2.27E-13	325	47	11
10_APTMS30	1.52	4.30E-13	240	33	10

* ----- indicates no diffraction peak was observed by XRD

8.3.2. Barrier properties – Water vapor permeability

Striking improvements in the APTMS-based organic-inorganic hybrid barrier properties were observed with increasing both the APTMS and MEOA-clay content (Table 8.2). Without the contribution of the MEOA-clay to improve the barrier properties, increasing the APTMS crosslinker content decreased the WVP of the control hybrid films approximately two magnitudes. The hybrid Control_APTMS10 had a WVP of 2.50E-10 g·m/m^2·s·Pa, the highest of any hybrid film, which was attributed to having a lower degree of crosslinking compared to the other two control hybrid films. Increasing the APTMS content significantly reduced the WVP, as Control_APTMS20 had a WVP of 5.55E-11 g·m/m^2·s·Pa and the WVP of Control_APTMS30 was 2.10E-12 g·m/m^2·s·Pa.

The inclusion of MEOA-clay into the hybrid networks led to even further WVP reductions, even exceeding a three order of magnitude reduction compared to the control hybrid films. One significant trend was observed when comparing the APTMS-based hybrids with MEOA-clay dispersed throughout the network: increasing the APTMS content decreased the WVP for equivalent levels of MEOA-clay loading. As seen in Figure 8.4, hybrids formulated with the 70:30 weight ratio measured the lowest WVP for each level of MEOA-clay loading. Comparing the hybrids containing 2 wt.% MEOA-clay exemplifies this trend, as the hybrid 2_APTMS30 measured a WVP over two magnitudes lower than the hybrid 2_APTMS10. The reductions in WVP for each series of hybrid films occurred between 2 – 5 wt.% MEOA-clay loading. Increasing the loading up to 10 wt.% MEOA-clay diminished the WVP slightly for each series, most likely a

consequence of poorer clay dispersion. The dramatic WVP reductions with the inclusion of MEOA-clay into the APTMS-based organic-inorganic hybrids were a result of several factors. By increasing the APTMS content, the concentration of inorganic linkages increased. Because the inorganic Si-O-Si linkages can serve as a barrier, increasing the inorganic crosslinks improved the barrier protection of the hybrid films. The creation of a tortuous diffusion path was achieved by incorporating the organomodified clay into the hybrid network, as evidenced in the significant reductions as the clay loading was increased up to 2 – 5 wt.%. By creating a tortuous diffusion path, the path length of permeating water vapor molecules increased, and thereby increasing the time for water vapor molecules to permeate throughout the hybrid network. By coupling the barrier protection afforded from inorganic crosslinks and impermeable clay fillers, dramatic reductions in WVP of the APTMS-hybrid films was achieved.

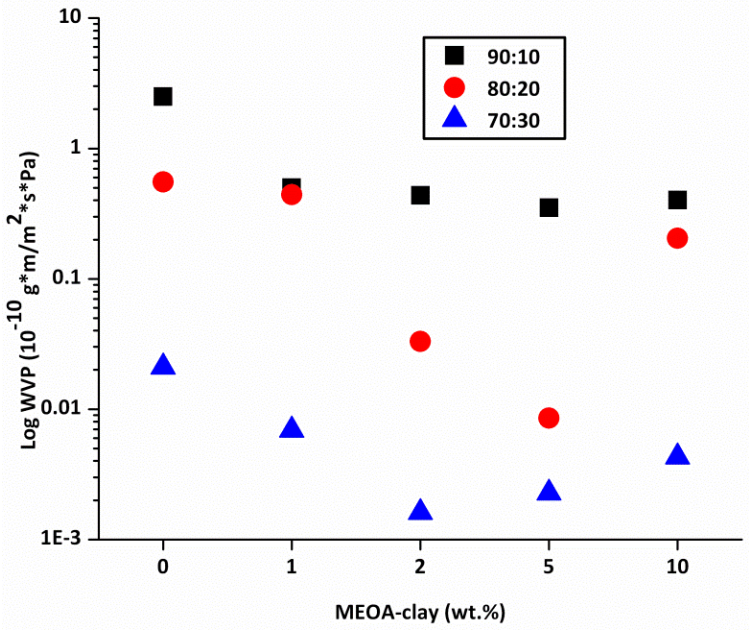

Figure 8.4: Water vapor permeability (WVP) results for APTMS-based organic-inorganic hybrids.

8.3.3. Thermal stability and optical clarity – Thermogravimetric analysis and UV-visible spectroscopy

Thermogravimetric analysis (TGA) was employed to explore the thermal stability of the APTMS-based organic-inorganic hybrid films. Figures 8.5 – 8.7 displays the TGA degradation curves of the hybrids, and Table 8.2 reports the temperature at 10 wt.% loss (T_{10}%) and char yield, or the wt.% at 600 °C. Two main trends were reflected in the thermal analysis of the hybrid films. First, raising the APTMS content within the hybrid films increased the thermal stability. When comparing the T_{10}% value for each hybrid film containing the same level of MEOA-clay loading, the 70:30 weight ratio hybrids consistently measured the highest T_{10}%. This trend is especially evidenced when comparing the hybrids containing 5 wt.% MEOA-clay. The hybrid 5_APTMS10 measured a T_{10}% of 200 °C, where 5_APTMS20 and 5_APTMS30 measured T_{10}% values of 285 and 325 °C, respectively. By increasing the concentration of the APTMS alkoxysilane crosslinker, the thermal stability rose, which was attributed to the increase in inorganic crosslinks throughout the hybrid network. The increase in thermal stability as the APTMS concentration increased directly correlated to the char yield. The hybrids formulated from the 90:10 weight ratio had consistently lower char yield (15 – 23%) than the 80:20 weight ratio (19 – 38%) and the 70:30 weight ratio (20 – 47%). The second trend observed with the thermal analysis of APTMS-based hybrids was the dependence of the thermal stability of the level of MEOA-clay loading. Each weight ratio series (90:10, 80:20, 70:30) demonstrated an increase in the thermal stability with the inclusion of MEOA-clay into the hybrid

network. The improvement in thermal stability may possibly be a result of the impermeable organomodified clay serving as a barrier to the degradation by-products, thus increasing the T_{10}% values recorded and the thermal stability of the amine-based hybrids. Dramatic increases were observed with the inclusion of MEOA-clay, particularly in the 2 – 5 wt.% range. The hybrids formulated from the 90:10 weight ratio improved the T_{10}% to approximately 30 °C higher than Control_APTMS10. The 80:20 weight ratio hybrids containing MEOA-clay increased the T_{10}% approximately 90 °C higher than Control_APTMS20, and the 70:30 hybrids recorded even higher increases in the T_{10}% compared to Control_APTMS30, approximately 135 °C higher. The significant improvements in thermal stability from the formation the APTMS-based hybrids containing organomodified clay demonstrate the ability of these hybrid systems to couple the inorganic linkages from sol-gel processing and inorganic fillers from the MEOA-clay to advantageously improve the hybrid thermal stability.

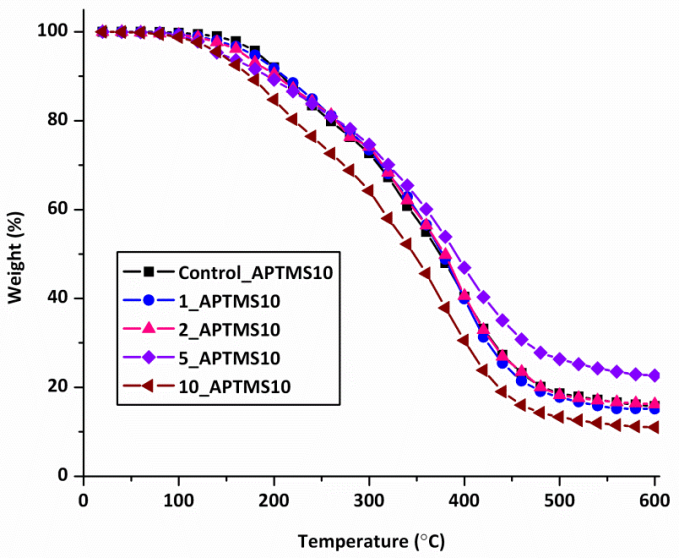

Figure 8.5: TGA degradation curves for APTMS-based organic-inorganic hybrids formulated based on a 90:10 weight ratio.

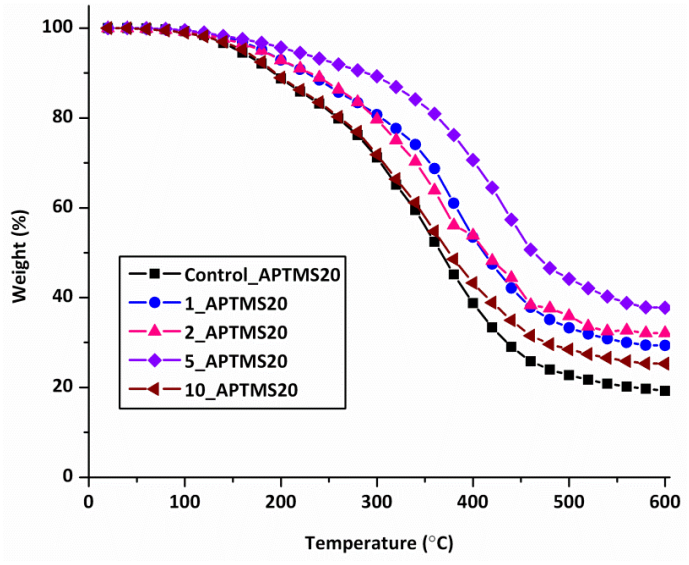

Figure 8.6: TGA degradation curves for APTMS-based organic-inorganic hybrids formulated based on an 80:20 weight ratio.

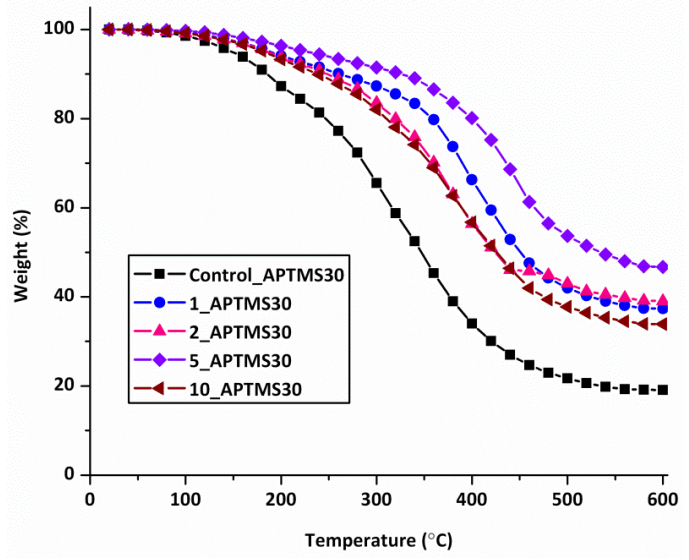

Figure 8.7: TGA degradation curves for APTMS-based organic-inorganic hybrids formulated based on a 70:30 weight ratio.

Similar to the hybrid thermal stability, the optical clarity of the APTMS-based hybrids was dependent on the APTMS weight and the level of MEOA-clay. Increasing the weight ratio of the APTMS crosslinked diminished the optical clarity

of the hybrid films (Figure 8.8). The transmittance of Control_APTMS10 was 80%, which decreased to 75% and 52% for Control_APTMS20 and Control_APTMS30. Without the contribution of the MEOA-clay to decrease the transmittance, it is evident that increasing the concentration of the APTMS crosslinker reduced the hybrid film optical clarity, likely a result of the increased inorganic crosslink density scattering light. The hybrid films containing the MEOA-clay demonstrated even further reductions in the optical clarity, particularly with the hybrids formulated with the 70:30 weight ratio. By increasing the MEOA-clay content to 2 – 10 wt.%, the transmittance of the films decreased up to 35 – 50%. The reduction in the hybrid film clarity is a result of degree of clay dispersion within the hybrid network. When the clay content is increased, high dispersion decreases, thereby increasing the likelihood of light-scattering phases from poorer clay dispersion.

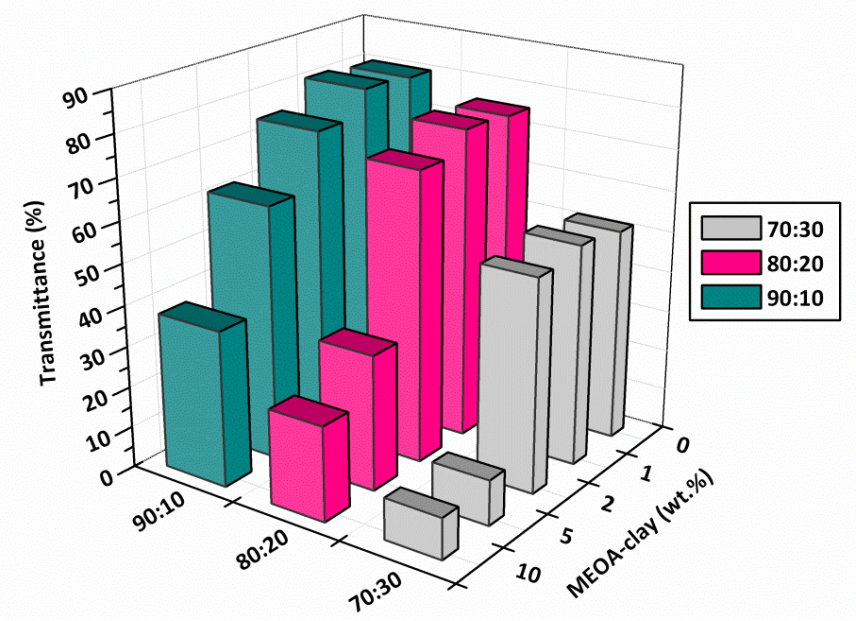

Figure 8.8: Transmittance at 400 nm of the APTMS-based organic-inorganic hybrids.

8.3.4. Mechanical properties – Dynamic mechanical analysis and König hardness

The viscoelastic properties of the APTMS-based organic-inorganic hybrids were studied by dynamic mechanical analysis (DMA). Figure 8.9 – 8.11 display the storage modulus plots of each hybrid film, and Table 8.3 reports the storage modulus (E') at room temperature, glass transition temperature (T_g) determined from the tan δ peak, and the crosslink density (XLD). The first striking trend observed in the mechanical analysis of the hybrid films is the correlation between the E' and APTMS content. From the E' values at room temperature reported in Table 8.3, it is apparent that increasing the APTMS content led to consistently higher E'. The hybrid film Control_APTMS10 measured a E' value of 105 MPa. Increasing the APTMS concentration of the control films led to significantly higher E' values as Control_APTMS20 recorded a E' value of 415 MPa and Control_APTMS30 was even higher at 765 MPa. By comparing the three control hybrid films containing no organomodified clay, it is apparent that the higher concentration of the APTMS crosslinker did indeed increase the crosslink density of the films.

With the inclusion of MEOA-clay into the hybrid network, dramatic increases in E' values were observed. As seen with the control hybrid films, increasing the APTMS content in the MEOA-clay containing hybrids also increased the E'. For example, 5_APTMS10 measured a E' of 480 MPa, whereas 5_APTMS20 and 5_APTMS30 measured E' values of 655 and 1120 MPa, respectively. Increased E' values with increasing MEOA-clay content is attributed

to the reinforcing effect of the inorganic clay fillers to improve the mechanical properties of the hybrid films. For the three hybrid series of varying APTMS content, a peak in E' occurred at 5 wt.% MEOA-clay loading. Hybrids containing 10 wt.% MEOA-clay recorded somewhat diminished E' values, likely a result of poorer clay dispersion and a decrease in the clay reinforcing effect.

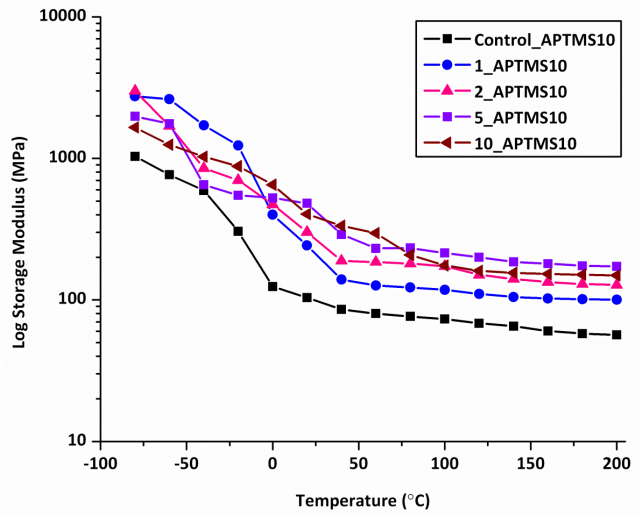

Figure 8.9: DMA storage modulus plots for APTMS-based organic-inorganic hybrids formulated based on a 90:10 weight ratio.

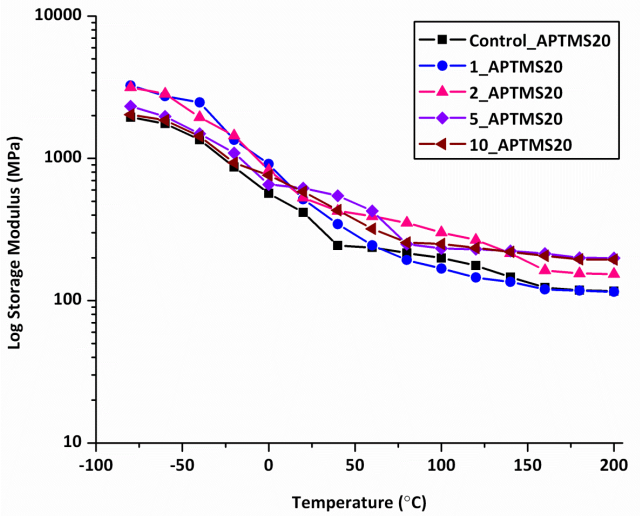

Figure 8.10: DMA storage modulus plots for APTMS-based organic-inorganic hybrids formulated based on an 80:20 weight ratio.

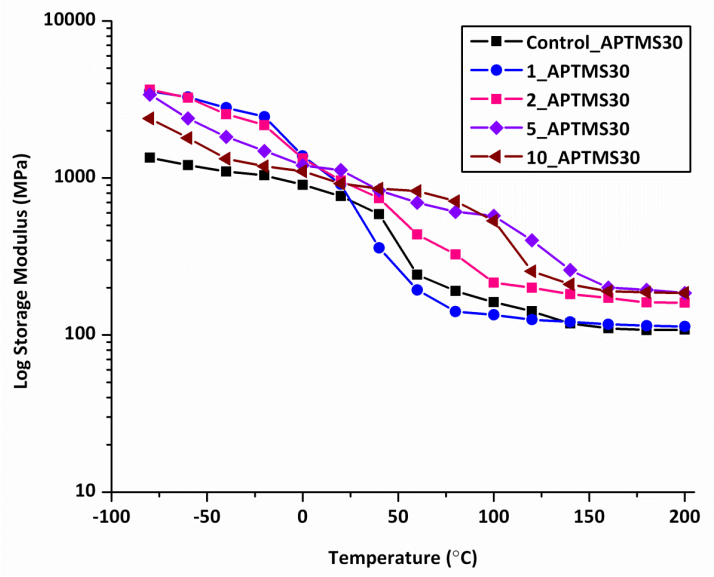

Figure 8.11: DMA storage modulus plots for APTMS-based organic-inorganic hybrids formulated based on a 70:30 weight ratio.

TABLE 8.3
APTMS-based organic-inorganic hybrid films mechanical properties characterization

Hybrid Name	*E'* (MPa, 25°C)	T_g (°C)	XLD (mol/ cm^3)	Hardness (sec)
Control_APTMS10	105	52	0.005	114
1_APTMS10	245	55	0.008	125
2_APTMS10	300	68	0.011	125
5_APTMS10	480	75	0.014	116
10_APTMS10	405	63	0.013	114
Control_APTMS20	415	61	0.009	115
1_APTMS20	515	67	0.010	132
2_APTMS20	530	76	0.013	130
5_APTMS20	655	83	0.017	134
10_APTMS20	585	71	0.017	115
Control_APTMS30	765	69	0.010	118
1_APTMS30	915	74	0.010	166
2_APTMS30	965	87	0.014	154
5_APTMS30	1120	103	0.016	140
10_APTMS30	920	83	0.016	124

Similar to the correlations between the E' and hybrid composition, the T_g and XLD of the hybrid films was also dependent on the APTMS and MEOA-clay content. The T_g, as determined by the peak in the tan δ plot, was highest for the hybrids containing the higher levels of APTMS and MEOA-clay. The control films of the 90:10, 80:20, and 70:30 weight ratio hybrids had T_g values of 52 °C, 61 °C, and 69 °C, respectively, likely a result of a higher inorganic crosslinks from higher APTMS content restricting polymer chain mobility. The inclusion of MEOA-clay led to further T_g increases for each hybrid series, as would be expected by incorporating an inorganic filler to further restrict the mobility of the copolymer backbone within the hybrid network. Interestingly, the T_g values diminished somewhat with 10 wt.% MEOA-clay, a trend similar to the decreased E' at the same clay loading. Again, poorer clay dispersion may create more phase separated MEOA-clay domains throughout the network, thereby increasing the mobility of some copolymer chains not surrounded by the organomodified clay. Continually, XLD increases were observed when the APTMS and MEOA-clay content was increased. Although small XLD increases were observed when comparing the control hybrid films, the inclusion of MEOA-clay into the hybrids led to more significant changes in the calculated XLD.

The APTMS-based hybrid film hardness directly correlated to the mechanical properties measured from DMA testing (values reported in Table 8.3). The hardness of the three control films was approximately equivalent; therefore, the level of MEOA-clay dictated the hardness of each hybrid coating. A similar trend in film hardness was observed with hybrids formulated from the 90:10 and

80:20 weight ratios. Hybrid films containing 1 – 5 wt.% organomodified clay increased the film hardness, whereas hybrids containing 10 wt.% clay had a comparable hardness to the control films. The 70:30 weight ratio hybrids demonstrated a distinctly different trend. The inclusion of just 1 wt.% MEOA-clay drastically increased the film hardness. Further increases in the MEOA-clay loading diminished the film hardness, but each clay-containing hybrid film was still harder than the control film. The trends observed in the film hardness were a consequence of both the crosslink density and clay dispersion. The initial increases in the film hardness with lower levels of MEOA-clay loading were likely a result of increased crosslink density. Once the clay content was raised to the 10 wt.% range, the contribution of higher crosslink density appeared to be overcome by clay crowding and phase separation, leading to a decreased film hardness.

8.4. Conclusions

In the present study, amine-functional organic-inorganic hybrid films were prepared for potential applications in CO_2 capture and separation membrane technology. Alkoxysilane-functional copolymer-clay nanocomposites were crosslinked with amine-functional silane coupling agent APTMS to create high performance hybrid films with superior barrier properties and thermal stability. By systematically varying the APTMS content and organomodified clay loading in the hybrid network, drastic changes to the barrier, mechanical, thermal, and optical properties were observed. One of the most striking results of increasing the APTMS content and clay loading was the dramatic reduction in WVP – over three orders of magnitude lower than a control hybrid film containing no organomodified

clay. The hybrid films containing the highest APTMS content reported the highest storage moduli, glass transition temperatures, and crosslink densities. The high APTMS content also resulted in the greatest improvement in the thermal stability of the hybrid films.

8.5. References

1. Yano, S.; Iwata, K.; Kurita, K., *Materials Science and Engineering: C* **1998,** *6* (2-3), 75-90.

2. Mammeri, F.; Bourhis, E. L.; Rozes, L.; Sanchez, C., *Journal of Materials Chemistry* **2005,** *15* (35-36), 3787-3811.

3. Ni, Y.; Zheng, S.; Nie, K., *Polymer* **2004,** *45* (16), 5557-5568.

4. Agag, T.; Tsuchiya, H.; Takeichi, T., *Polymer* **2004,** *45* (23), 7903-7910.

5. Wright, J. D.; Sommerdijk, N. A. J. M., *Sol-gel materials: chemistry and applications*. CRC: 2001; Vol. 4.

6. Crivello, J. V.; Song, K. Y.; Ghoshal, R., *Chem. Mat.* **2001,** *13* (5), 1932-1942.

7. Choi, H.; Lim, C.; Lee, D.; Kim, B., *Journal of Polymer Engineering* **2009,** *29* (1-3), 1-14.

8. Abe, Y.; Honda, Y.; Gunji, T., *Applied Organometallic Chemistry* **1998,** *12* (10-11), 749 - 753.

9. Chang, T.; Yeh, T.; Yang, C.; Hong, Y.; Wu, T., *Polymer* **2001,** *42* (21), 8565-8570.

10. Costa, R. O. R.; Vasconcelos, W. L., *Journal of Non-Crystalline Solids* **2002,** *304* (1-3), 84-91.

11. Innocenzi, P.; Esposto, M.; Maddalena, A., *Journal of Sol-Gel Science and Technology* **2001,** *20* (3), 293-301.

12. Tadanaga, K.; Yoshida, H.; Matsuda, A.; Minami, T.; Tatsumisago, M., *Chem. Mat.* **2003,** *15* (9), 1910-1912.

13. Raps, D.; Hack, T.; Wehr, J.; Zheludkevich, M. L.; Bastos, A. C.; Ferreira, M. G. S.; Nuyken, O., *Corrosion Science* **2009,** *51* (5), 1012-1021.

14. Rinker, E. B.; Ashour, S. S.; Sandall, O. C., *Industrial & Engineering Chemistry Research* **2000,** *39* (11), 4346-4356.

15. Zelenak, V.; Halamova, D.; Gaberova, L.; Bloch, E.; Llewellyn, P., *Microporous and Mesoporous Materials* **2008,** *116* (1-3), 358-364.

16. Hiyoshi, N.; Yogo, K.; Yashima, T., *Chemistry Letters* **2004,** *33* (5), 510-511.

17. Sakamoto, Y.; Nagata, K.; Yogo, K.; Yamada, K., *Microporous and Mesoporous Materials* **2007,** *101* (1-2), 303-311.

CHAPTER 9. RAFT-MEDIATED ALKOXYSILANE-FUNCTIONAL COPOLYMER-CLAY NANOCOMPOSITES FOR ORGANIC-INORGANIC HYBRID APPLICATIONS

9.1. Introduction

Controlled living radical polymerizations have received significant attention in recent years as a viable technique to increase control during the polymerization process, obtain very narrow polymer molecular weight breadth (PDI < 1.5), and define the polymer architecture.[1-3] Additionally, polymers possessing complex architectures, such as blocks and stars, may easily be produced through the implementation of these controlled polymerization techniques.[4-6] Of the current controlled living radical polymerization techniques, reversible addition-fragmentation chain transfer (RAFT) may be the most versatile method as this technique only requires the addition of an appropriate “RAFT agent” to the reaction mixture; the additional reaction ingredients (monomers, solvent, etc.) remain the same as in conventional free radical polymerization.[7-8]

The RAFT mechanism proceeds through five steps: initiation, reversible chain transfer, re-initiation, chain equilibration, and termination (Scheme 9.1). After initiation, the propagating polymer radicals add to the RAFT agent, typically a thiocarbonylthio compound. The resulting intermediate compound fragments to produce two species: a polymeric thiocarbonylthio compound and a new radical compound. The new radical compound serves as a site for additional monomer addition and polymer chain propagation. With RAFT polymerizations, equilibrium exists between active propagating species and the dormant polymeric compounds,

leading to the growth of polymeric chains at approximately the same rate and the formation of low polydispersity polymers. Detailed studies regarding RAFT polymerizations have been reported in comprehensive reviews.[3, 8-10]

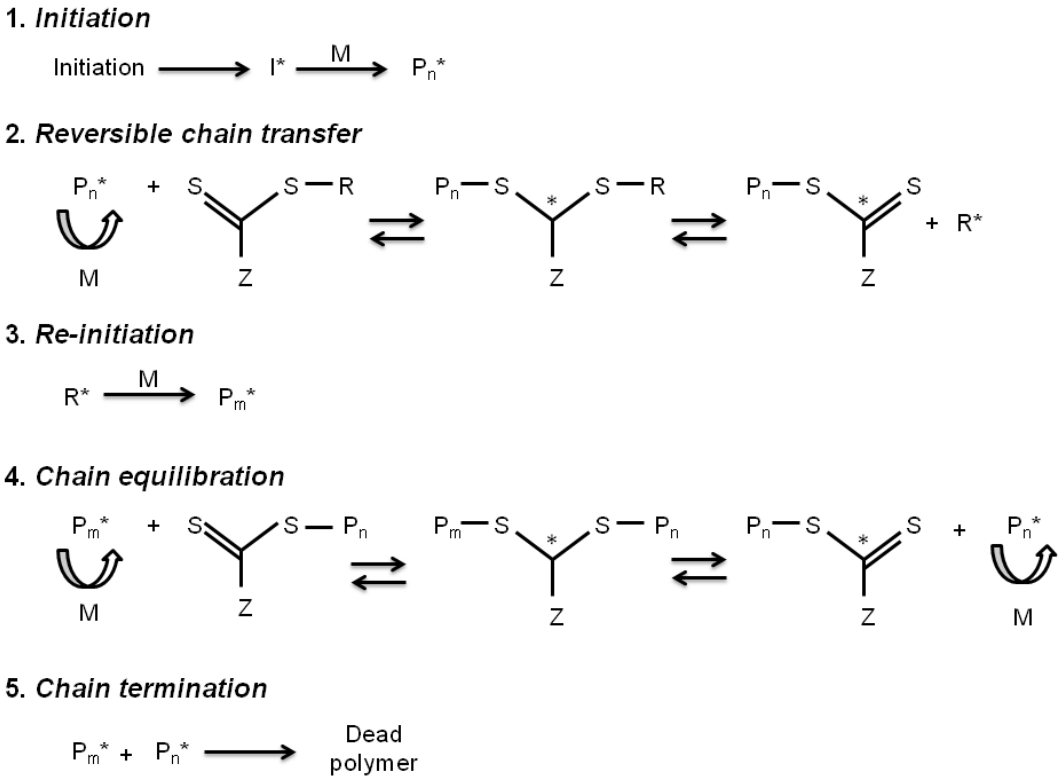

Scheme 9.1: RAFT-mediated polymerization mechanism consisting of five steps: initiation, reversible chain transfer, re-initiation, chain equilibration, and chain termination.

Recently, RAFT-mediated polymerizations have been utilized in the preparation of polymer-clay nanocomposites. Salem and Shipp reported the RAFT polymerization of polystyrene, poly(methyl methacrylate), and poly(*n*-butyl acrylate) in the preparation of polymer-clay nanocomposites.[11] Each polymer was synthesized in the presence of organically modified montmorillonite clays and with either of two RAFT agents: 4-cyano-4-methyl-4-thiobenzoylsulfanylbutyric acid and

2-(2-cyanopropyl) dithiobenzoate. Exfoliated nanocomposites were successfully prepared by the RAFT-mediated polymerization of polystyrene and poly(*n*-butyl acrylate), whereas a mixed exfoliated-intercalated morphology was achieved for the poly(methyl methacrylate) nanocomposites. Zhang et al. first reported the intercalation of a cationic RAFT agent to produce RAFT-mediated polymer-clay nanocomposites.[12] Through an ion exchange reaction, RAFT agent 10-carboxylic acid-10-dithiobenzoate-decyltrimethylammonium bromide was successfully intercalated to the surface of montmorillonite clay, then employed to control the polymerization of styrene. The polystyrene chains demonstrated low polydispersity (PDI 1.03 – 1.33), indicative of a controlled polymerization reaction, and the morphology of the nanocomposites was classified as exfoliated.

Samakande and coworkers reported the development of polystyrene-clay nanocomposites by RAFT-mediated polymerization in the presence of both initiator- and RAFT agent-functionalized montmorillonite clay.[13-14] Two cationic RAFT agents were successfully bound to the surface of montmorillonite clay, followed by the thermally-initiated RAFT polymerization of styrene to produce polystyrene-clay nanocomposites. The preparation of the RAFT agent-modified clay was shown to control the polymerization reaction of polystyrene and produce exfoliated nanocomposites. In an alternative approach to produce RAFT-mediated polystyrene-clay nanocomposites, montmorillonite clay was functionalized with 2,2'-azobis(2-(1-(2-hydroxyethyl)-2-imidazolin-2-yl)propane)dihydrochloride monohydrate ("VA060") to create initiator-bound clay platelets. The VA060-clay was combined with styrene and RAFT agent, and then styrene was polymerized by

RAFT to produce polystyrene-clay nanocomposites possessing intercalated morphologies. RAFT-mediated copolymerizations have also been employed in the preparation of polymer-clay nanocomposites. Amphiphilic polystyrene-*block*-poly(4-vinylpyridine)-clay nanocomposites were successfully developed by Zhang et al. by sequentially polymerizing styrene and 4-vinylpyridine by RAFT-mediated techniques.[15] The first step in the nanocomposite preparation was the RAFT polymerization of styrene to synthesize dithiobenzoate-terminated polystyrene. The polystyrene product, serving as a macro RAFT agent, was then employed in the RAFT-mediated polymerization of 4-vinylpyridine. Next, the polystyrene-block-poly(4-vinylpyridine) copolymer was quaternized and underwent an ion exchange reaction with montmorillonite clay to produce an amphiphilic block copolymer-clay nanocomposite. Based on X-ray diffraction (XRD) and transmission electron microscopy (TEM) analysis, exfoliated and intercalated morphologies were successfully achieved. Qu et al. also reported the preparation of block copolymer-clay nanocomposites through RAFT-mediated sequential polymerizations.[16] Polystyrene was first polymerized by RAFT technique in the presence of organically modified montmorillonite clay to create a macro RAFT agent, followed by the RAFT-mediated polymerization of acrylamide to produce poly(styrene-*b*-acrylamide)-clay nanocomposites.

In Chapter 6, the development of organic-inorganic hybrids from a precursor alkoxysilane-functional copolymer-clay nanocomposite was reported. First, copolymers were synthesized with 3-methacryloxypropyltrimethoxysilane (3-MPS) in the presence of methacrylate-functional montmorillonite clay to produce

alkoxysilane-functional clay nanocomposites. The nanocomposites was then used as a sol precursor, and underwent simultaneous hydrolysis and condensation via sol-gel chemistry to create organic-inorganic crosslinked hybrid coatings with organically-modified clay dispersed throughout the hybrid network. Improvements in barrier, thermal, and mechanical properties were observed when comparing the clay-containing organic-inorganic hybrids to the neat hybrids. In Chapters 7 and 8, amine-functional organic-inorganic hybrids were also created through a similar technique.. The first approach was the synthesis of 3-MPS with 2-(dimethylamino)ethyl methacrylate (DMAEMA), followed by hybrid formation. The second approach was to crosslink copolymer-clay nanocomposites composed of monomers 3-MPS and methyl methacrylate (MMA) with amine-functional silane coupling agent 3-aminopropyltrimethoxysilane (APTMS).

With this current study, the RAFT-mediated preparation of organic-inorganic hybrid coatings from a precursor nanocomposite sol was investigated. Two different RAFT-mediated polymerization techniques were adopted in the preparation of the hybrid coatings. First, a quaternary ammonium RAFT agent was bound to montmorillonite clay, followed by the RAFT-mediated copolymerization of 3-MPS and MMA. The resulting nanocomposite was then crosslinked with silane coupling agent tetraethyl orthosilicate (TEOS) to produce the hybrid films. The alternative approach was the RAFT-mediated copolymerization of 3-MPS and MMA in the presence of methacrylate-functional montmorillonite clay to serve as a grafting agent followed by crosslinking with TEOS to create the hybrid films. The RAFT agent functionalized clay produced copolymers with the lower polydispersity

and enhanced barrier, mechanical, and thermal properties. This study serves as an initial set of experimental RAFT-mediated copolymerizations and hybrid film formations to explore the feasibility of coupling the controlled living radical polymerization technique RAFT with the preparation of organic-inorganic hybrid films previous reported in Chapters 6 – 8.

9.2. Experimental

9.2.1. Materials

2-(dimethylamino)ethyl methacrylate (DMAEMA), 1-bromooctane, 1-dodecanethiol, sodium hydroxide, carbon disulfide, α,α-dibromo-p-xylene, dimethylethyl amine, methyl methacrylate (MMA), and anhydrous toluene were obtained from Sigma Aldrich (Milwaukee, WI). 3-methacryloxypropyltrimethoxy-silane (3-MPS) was obtained from Gelest (Morrisville, PA). Initiator 2,2-azobis(2-methylbutyronitrile), "Vazo 67", was gratefully supplied by DuPont (Belle, WV). Montmorillonite clay Cloisite® Na^+ was obtained from Southern Clay Products (Gonzales, TX). MMA was purified by passing through an activated basic column and stored at 0 °C until polymerization. 3-MPS was purified by distillation under vacuum and also storage at 0 °C. Vazo 67 was re-crystallized in ethanol prior to use. Additional materials were used as received.

9.2.2. Quaternary alkylammonium organic modifier synthesis

The quaternary alkylammonium RAFT agent, N-(4-((((dodecylthio)carbon-thioyl)thio)methyl)benzyl)-N,-dimethylethanammonium bromide (DCTBAB), was synthesized and structurally verified according to a procedure reported by Samakande et al.[17] In summary, a sodium salt compound was formed by a

reaction of 1-dodecanethiol with carbon disulfide in a solution containing sodium hydroxide, followed by the addition of 1.5 equivalents of α,α-dibromo-p-xylene to favor a monofunctional product. The intermediate was then reacted with dimethylethyl amine to produce a quaternary ammonium RAFT agent. The methacrylate-functional alkylammonium organic modifier, 2-methacryloyloxyethyloctyl-dimethylammonium bromide (MEOAB) was synthesized, according to the procedure detailed by Zeng and Lee,[18] by employing 1-bromooctane to quaternize 2-(dimethylamino)ethyl methacrylate (DMAEMA). The structures for the functional quaternary alkylammonium organic modifiers are shown in Figure 9.1.

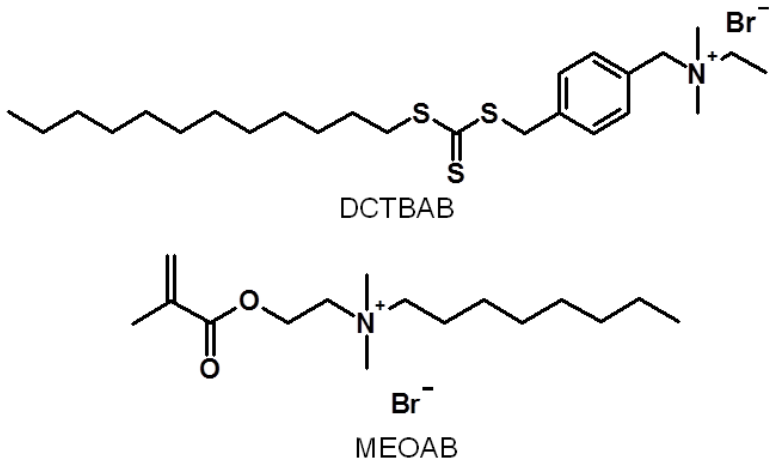

Figure 9.1: Structures of functional quaternary alkylammonium organic modifiers N-(4-((((dodecylthio)carbon-thioyl)thio)methyl)benzyl)-N,-dimethylethanammonium bromide (DCTBAB) and 2-methacryloyloxyethyloctyl-dimethylammonium bromide (MEOAB).

9.2.3. Montmorillonite clay organic modification

Unmodified montmorillonite clay Cloisite® Na^+ was functionalized with quaternary alkylammonium organic modifiers DCTBAB and MEOAB by ion exchange reactions. 4.347 g of Cloisite Na^+ were mixed with 300 mL of deionized

water for one hour, followed by the addition of 2.174 g of DCTBAB (4.125×10^{-3} mol). The DCTBAB solution was mixed overnight, filtered, rinsed with water until no bromide counterion was detected with 0.1 N $AgNO_3$, and dried at 50 °C. For the functionalization with MEOAB, 5.00 g of Cloisite Na^+ were mixed with 300 mL of deionized water for one hour. Next, 2.65 g of MEOAB (8.153×10^{-3} mol) was added, and the resulting MEOAB solution was mixed overnight, filtered, rinsed with water until no bromide counterion was detected, and dried in an oven at 50 °C. The organomodified clays, herein referred to as DCTBA-clay and MEOA-clay, were ground with a mortar and pestle until each was a fine powder.

9.2.4. RAFT-mediated copolymerization with DCTBA-clay

MMA (4.00 g, 4.00×10^{-2} mol) and 3-MPS (9.94 g, 4.00×10^{-2} mol) were mixed overnight with DCTBA-clay (0.479 g) to allow for monomer swelling in the modified clay interlayers, then added to a 100 mL Schlenk flask with initiator Vazo 67 (0.349 g, 1.81×10^{-3} mol) and anhydrous toluene (20 mL). The reaction mixture was degassed by three freeze-vacuum-thaw cycles, then transferred to a thermostated oil bath at 70 °C. The RAFT-mediated copolymerization was carried out for 24 hours and the excess solvent was then removed by a rotary evaporator.

9.2.5. RAFT-mediated copolymerization with MEOA-clay

The procedure for the RAFT-mediated copolymerization with MEOA-clay was similar to that of the procedure in 9.2.4., except MEOA-clay (.4789 g) was mixed overnight with monomers MMA and 3-MPS, and RAFT agent DCTBAB (0.158 g) was added with the initiator Vazo 67 and anhydrous toluene to the reaction flask prior to copolymerization. A control RAFT-mediated copolymerization

reaction was also conducted by the same procedure, but no organomodified clay was added to the reaction mixture.

9.2.6. Organic-inorganic hybrid coating formation via sol-gel chemistry

The RAFT-mediated alkoxysilane-functional clay nanocomposites were crosslinked via sol-gel chemistry to create organic-inorganic hybrid coatings. A stock solution of tetraethyl orthosilicate (1.00 mol), deionized water (25 mol), ethanol (5 mol), and hydrochloric acid (0.025 mol) was mixed at room temperature according to Chan and coworkers.[19] The copolymer-clay nanocomposites were mixed with the TEOS solution in a 90:10 weight ratio at room temperature for one hour, then spin-coated onto glass, aluminum, and porous membrane substrates for 20 seconds at 500 RPM. The coated hybrid films were then dried at 70 °C in a vacuum oven for three hours (thickness ≈ 20 μm). A portion of the hybrid formulations were carefully poured into a cylindrical plastic container, aged for three days at room temperature, then heated at 40 °C for several hours to create cylindrical samples for barrier testing (thickness ≈ 150 μm).

9.2.7. Characterization

Before hybrid coating formation, the copolymer backbone and physical properties of the RAFT-mediated copolymer-clay nanocomposites were characterized. Fourier-Transform infrared (FTIR) spectroscopy was employed to study the copolymer backbone composition with a Nicolet Magna-IR 850 spectrometer with detector type DTGS KBr, and spectra were obtained in absorbance mode between 400 and 4000 cm^{-1}. Gel permeation chromatography (GPC) was used to determine the copolymer molecular weight and polydispersity.

GPC measurements were performed with a Water 2410 Gel Permeation Chromatograph equipped with a refractive index detector. The copolymer samples were refluxed in a solution of tetrahydrofuran (THF) and LiCl and then centrifuged to remove the clay platelets. The resulting copolymer-THF solution was approximately 1% concentration. Calibration of the GPC instrument was performed with polystyrene standards and the flow rate was 1 mL/minute. The viscosity of the copolymer-clay nanocomposites was performed with an ICI cone and plate viscometer at 75 °C.

The conversion and theoretical number average molecular weight (M_n) were determined according to the procedure detailed by Severac et al.[20] Briefly, the final conversion was determined gravimetrically with equation (9.1) where $m_{dry}$is the weight of a completely dried sample, $m_{sample}$is the weight of the initial sample, and SC is the dry solid content at 100% conversion.

$$\chi = \frac{(m_{dry} \times 100)}{(m_{sample} \times SC)} \tag{9.1}$$

The theoretical M_n was calculated from equation (9.2) where $[RAFT]$ is the concentration of the RAFT agent DCTBAB and $(Mass\ RAFT)$ is the molecular weight of the RAFT agent DCTBAB.

$$M_n = (Mass\ of\ monomers) \times \frac{\chi}{[RAFT]} + (Mass\ RAFT) \tag{9.2}$$

X-ray diffraction (XRD) was employed to characterize the extent of organic modifier intercalation and dispersion of clay within the hybrid network. XRD was performed using a Bruker AXS' D8 Discover diffractometer in Bragg-Brentano geometry with Cu Kα radiation at a wavelength of 1.5406 Å. Each hybrid coating

was scanned from 1.5° – 50° 2θ, and the run time was 1 second/step. The barrier properties of the hybrid networks were determined by employing ASTM E96, “Standard Test Methods for Water Vapor Transmission, Water Method.” The thicker samples of hybrids previously prepared were attached a permeability cup containing distilled water, and then placed in a controlled humidity chamber with conditions of 75 ± 2% relative humidity and 20 ± 2 °C. The mass of the permeability cups was measured over time under a steady state of water vapor loss occurred. Duplicate samples were tested to verify permeability results.

The viscoelastic properties of the organic-inorganic hybrids were measured by dynamic mechanical analysis (DMA) with a TA Instruments Q800 Dynamic Mechanical Analyzer in tensile mode. Hybrid free films were cut to the dimensions of approximately 15 mm x 5 mm x 0.020 mm. DMA measurements were performed with a 1 Hz frequency, constant strain of 0.03%, and a heating rate of 5 °C/minute from -75 °C to 200 °C. A BYK-Gardner pendulum hardness tester was employed to measure the hybrid film hardness on aluminum substrates. Thermogravimetric analysis (TGA) was employed to study the thermal stability of the hybrid network with a TA Instruments Q500 Thermogravimetric Analyzer. The hybrid samples were heated from room temperature to 600 °C/minute at a rate of 20 °C/minute in a nitrogen atmosphere. The optical clarity of the hybrid films was determined by measuring percent transmittance with a Varian Cary 5000 UV-Vis Spectrometer.

9.3. Results and discussion

The goal of this study was to couple a previously developed organic-inorganic hybrid film preparation technique with the controlled living radical

polymerization technique RAFT to explore the resulting hybrid film properties. Previously, conventional free radical polymerization was employed to copolymerize monomers 3-methacryloxypropyltrimethoxysilane (3-MPS) with methyl methacrylate (MMA) or 2-(dimethylamino)ethyl methacrylate (DMAEMA) in the presence of organomodified clay to produce alkoxysilane-functional copolymer-clay nanocomposites. The nanocomposites were then crosslinked via sol-gel chemistry to create hybrid films with organomodified clay dispersed throughout the network.

With this study, the RAFT-mediated copolymerization of MMA and 3-MPS was conducted by two different approaches to create alkoxysilane-functional copolymer-clay nanocomposites. The first approach was to functionalize a quaternary ammonium RAFT agent to montmorillonite clay, then perform a RAFT-mediated copolymerization. By functionalizing the clay platelet surface with a quaternary ammonium RAFT agent, the RAFT-mediated copolymerization will be conducted within the clay interlayers leading to copolymer propagation and growth from the clay surface. Once the growing copolymer volume is in excess of the clay interlayer volume, the RAFT-mediated copolymerization may lead to clay delamination and high dispersion within the copolymer network. In addition to the possible clay exfoliation, the RAFT-mediated copolymerization will also provide control over the copolymer chain architecture and reduce chain polydispersity.

The second approach was to functionalize clay with a methacrylate-based alkylammonium organic modifier with an unattached RAFT agent as part of the reaction medium. This alternative approach was selected to compare the

properties obtained from the RAFT-functionalized clays to an unattached RAFT agent. After crosslinking with silane coupling agent tetraethyl orthosilicate (TEOS), the RAFT-mediated organic-inorganic hybrid films were characterized based on their morphological, barrier, mechanical, thermal, and optical properties. In addition to the clay-containing hybrids, a control RAFT-mediated copolymerization was conducted to compare the properties obtained. The synthesis of these three RAFT-mediated copolymer-clay nanocomposites will serve as an initial study to examine the feasibility of coupling the RAFT-mediated copolymerization technique with the organic-inorganic hybrid preparation method detailed in Chapters 6 – 8.

9.3.1. RAFT-mediated alkoxysilane-functional clay nanocomposite characterization

The successful copolymerization of monomers MMA and 3-MPS was confirmed by Fourier-transform infrared (FTIR) spectroscopy. Figure 9.2 displays the FTIR spectra for the 3-MPS monomer and the RAFT-mediated copolymers. The 1635 cm^{-1} absorption band, attributed to the $CH=CH_2$ bond of the methacrylate functional group, was not observed in the three copolymer products, suggesting the successful conversion of monomer to copolymer. The FTIR spectra also revealed that premature hydrolysis or condensation of the alkoxysilane functional groups on the copolymers did not occur. No absorption bands were observed in the 3700 – 3700 cm^{-1} region, indicating no –OH bonds formed during the RAFT-mediated copolymerization reaction. The 1080 cm^{-1} absorption band, characteristic of the $Si-OCH_3$ functional group, did not broaden in the copolymer FTIR spectra, indicating the condensation reaction to create Si-O-Si bonds did not

occur during the copolymerization. Additional absorption bands observed with each copolymer include 2920 cm^{-1} (-CH), 2850 cm^{-1} ($O-CH_3$), and 1730 cm^{-1} (C=O).

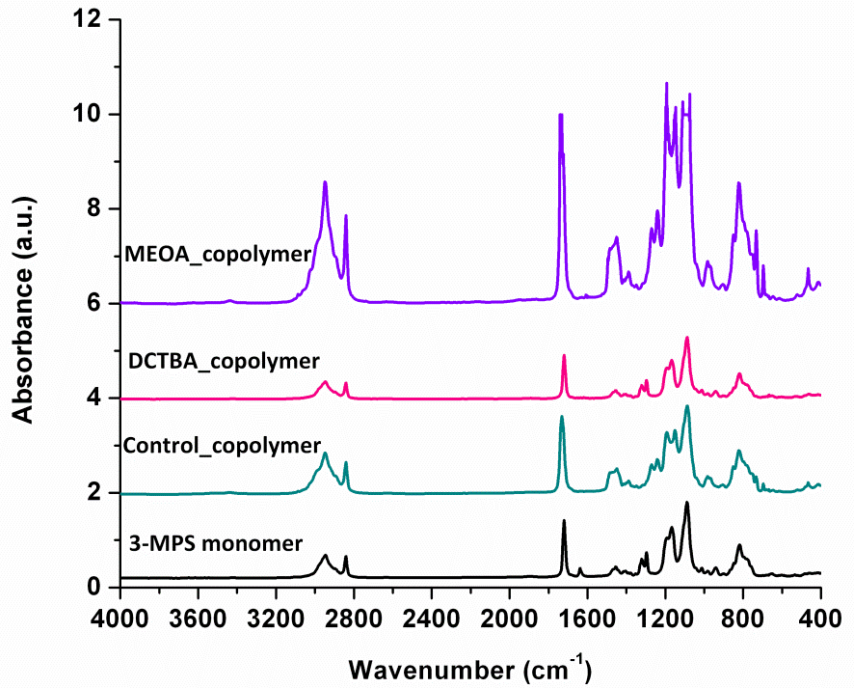

Figure 9.2: FTIR scans for 3-MPS monomer and RAFT-mediated copolymers.

Gel permeation chromatography (GPC) was used to determine the molecular weight and polydispersity (PDI) of the alkoxysilane-functional copolymers (Table 9.1). The DCTBAB organic modifier was shown to successfully control the copolymerization of the MMA and 3-MPS monomers, as observed in the control copolymerization reaction. The PDI of the Control_copolymer was determined to be 1.34. The functionalization of the unmodified montmorillonite clay with the DCTBAB organic modifier also demonstrated the ability to control the copolymerization reaction with a PDI of 1.25 for the DCTBA_copolymer. The

MEOA_copolymer PDI was 1.39, slightly higher than the Control_copolymer and DCTBA_copolymer, but was still successfully controlled.

The conversions of the RAFT-mediated copolymers ranged from 24% - 33% after a 24 hour reaction time. The conversion of the copolymers may have been lower due to an increase in viscosity with the growing copolymer chains. The theoretical number average molecular weights, M_n, were found to be in good agreement with the experimental M_n determined by GPC. The viscosities of the copolymer-clay nanocomposites were found to be in direct correlation to the alkoxysilane-functional copolymers with the highest molecular weight copolymer also being the most viscous. The increase in viscosity with higher molecular weight was attributed to more chain entanglements with the longer copolymer chains.

TABLE 9.1
RAFT-mediated alkoxysilane-functional copolymer-clay nanocomposite properties

Nanocomposite Name	M_n (g/mol)	PDI (M_w/M_n)	Conver-sion	Theo. M_n (g/mol)	Viscosity (Poise)
Control_copolymer	13,100	1.34	26%	12,700	2.0
DCTBA_copolymer	12,600	1.25	24%	11,800	1.6
MEOA_copolymer	10,100	1.39	33%	16,000	1.4

9.3.2. Hybrid morphology – X-ray diffraction

X-ray diffraction (XRD) was utilized to study the intercalation of the functional quaternary ammonium organic modifiers into the montmorillonite clay platelets and to indicate the degree of organomodified clay dispersion throughout the RAFT-mediated organic-inorganic hybrid films. As seen in Figure 9.3, the organomodified clay diffraction peaks shifted to lower 2θ values when compared to the unmodified Cloisite® Na^+ clay, indicating the successful intercalation of the

organic modifiers into the clay interlayers. The DCTBA-clay and MEOA-clay diffraction peaks occurred at approximately the same 2θ value; therefore, the increase in interlayer spacing was approximately the same for the organomodified clays. By employing Bragg's law, the *d*-spacing values for the DCTBA- and MEOA-clays was determined to be 1.48 nm, an increase from the unmodified Cloisite® Na^+ *d*-spacing value (1.08 nm).

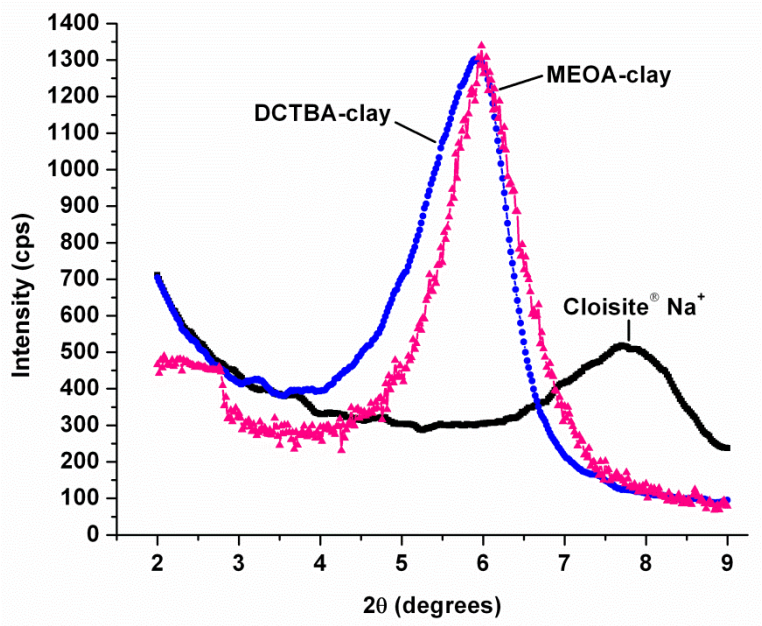

Figure 9.3: XRD scans of pristine Cloisite® Na^+, DCTBA-clay, and MEOA-clay.

Figure 9.4 displays the XRD scans for the three RAFT-mediated organic-inorganic hybrid films. No diffraction peaks were observed for any film in the low 2θ range (2 – 9 2θ), indicating a disruption of the well-ordered clay stacking. The absence of diffraction peaks indicates a high degree of clay dispersion occurred during the preparation of the organic-inorganic hybrid films. The RAFT-mediated copolymerization in the presence of the organomodified clays, an in situ intercalative copolymerization method, may have contributed to dispersing the

clays throughout the hybrid film. If the growing copolymer chain volume was larger than the organomodified clay interlayer space, the clay platelets order may have been disrupted to compensate for the propagating alkoxysilane-functional copolymer chains.

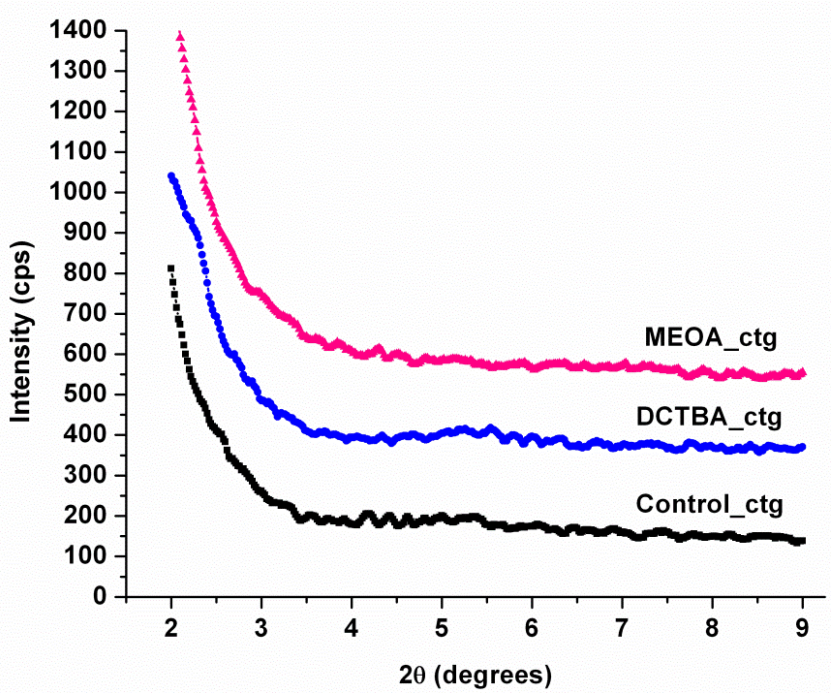

Figure 9.4: XRD scans of RAFT-mediated organic-inorganic hybrid films.

9.3.3. Barrier properties – Water vapor transmission and permeability

Water vapor transmission (WVT) and water vapor permeability (WVP) were measured, in accordance with ASTM E96, for the RAFT-mediated organic-inorganic hybrid films containing organomodified clay. From Figure 9.5, it is apparent that the transmission of water vapor through the hybrid films containing organomodified clay was reduced compared to the control hybrid film. The DCTBA_ctg measured the lowest WVT once the transmission reached a steady state.

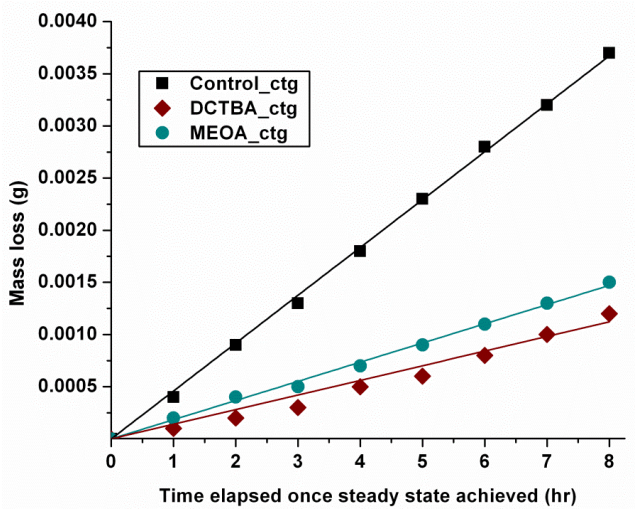

Figure 9.5: Water vapor transmission (WVT) of the RAFT-mediated organic-inorganic hybrid films in accordance with ASTM E96.

By incorporating the WVT rate with the film thickness and saturation pressure, the WVP of each film was calculated (Table 9.2). Once again, the DCTBA_ctg had the lowest measured WVP at 9.91E-12 g·m/m^2·s·Pa compared to the control hybrid film (4.58E-11 g·m/m^2·s·Pa) and the MEOA_ctg (1.93E-11 g·m/m^2·s·Pa). The incorporation of clay platelets into the organic-inorganic hybrid networks improved the barrier protection, most likely a consequence of a tortuous diffusion path. By forcing the water vapor molecules to traverse around the impermeable clay platelets, the diffusion path length may be greatly extended and decrease the WVT rate and WVP values. The barrier properties of the hybrid films containing the organomodified clay will also strongly depend on the degree of clay dispersion. Because the clay loading was equivalent for both DCTBA_ctg and MEOA_ctg, the differences in WVT rate and WVP for each film may be attributed to the clay dispersion throughout the hybrid network. Functionalizing the clay platelets with the RAFT agent, as opposed to dispersing the RAFT agent within the

reaction mixture, was found to produce hybrid films with the most improved barrier properties. This technique may then lead to better organomodified clay dispersion in the precursor copolymer-clay nanocomposite sol, leading to greater dispersion throughout the organic-inorganic hybrids.

TABLE 9.2
RAFT-mediated organic-inorganic hybrid film barrier, thermal, and optical properties characterization

Hybrid Name	WVP ($g \cdot m/m^2 \cdot s \cdot Pa$)	T_{10}% (°C)	Char yield (%)	Transmittance (%)*
Control_ctg	4.58E-11	220	8	96
DCTBA_ctg	9.91E-12	300	28	85
MEOA_ctg	1.93E-11	260	24	83

*% transmittance at 400 nm

9.3.4. Thermal stability and optical clarity – Thermogravimetric analysis and UV-visible spectroscopy

Thermogravimetric analysis (TGA) confirmed the organomodification of the unmodified montmorillonite clays and demonstrated the increased thermal stability from the incorporation of organomodified clays into the organic-inorganic hybrid network. From Figure 9.6, the organically-modified clays DCTBA-clay and MEOA-clay measured char yields of 67% and 83%, respectively, which were lower than the unmodified Cloisite® Na^+ char yield (92%). The lower char yields of the organomodified clays suggest the successful intercalation of the DCTBAB and MEOAB organic modifiers into the unmodified clay interlayers. Because the DCTBA-clay had a lower char yield than the MEOA-clay, a higher degree of DCTBAB may have functionalized to the clay platelet, leading to the higher organic content observed in the TGA degradation curve. The lower DCTBA-clay char yield

could also be a reflection of possessing a higher molecular weight organic modifier than the MEOA-clay.

Significant improvements in the RAFT-mediated thermal stability were observed with the incorporation of organomodified clays into the hybrid network. Table 9.2 reports the temperature at 10 wt.% loss (T_{10}%) and char yields for the hybrid films. The DCTBA_ctg measured the highest T_{10}% at 300 °C, a substantial improvement compared to the Control_ctg T_{10}% at 220 °C. The MEOA_ctg also measured a higher T_{10}% (260 °C) than the control hybrid film, but was significantly lower than the DCTBA_ctg (Figure 9.6).

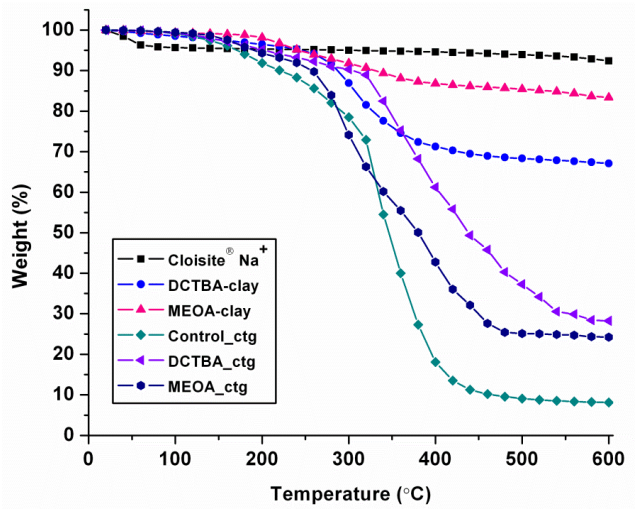

Figure 9.6: Thermogravimetric analysis (TGA) degradation curves of pristine unmodified and organomodified clays and the RAFT-mediated organic-inorganic hybrid films.

The increased thermal stability with clay incorporation was attributed to the impermeable clay platelets increasing the diffusion time of the degradation products. The higher thermal stability of the DCTBA_ctg compared to the

MEOA_ctg may be a consequence of clay dispersion. If the DCTBA_ctg had a greater degree of clay dispersion than the MEOA_ctg, the thermal stability would be greater. The optical clarity of the RAFT-mediated organic-inorganic hybrids also suggests a greater degree of clay dispersion throughout the DCTBA_ctg. As seen in Figure 9.7 and Table 9.2, the transmittance through DCTBA_ctg was higher than the MEOA_ctg through the visible spectrum. The higher optical clarity is likely a result of improved clay dispersion, where the well-dispersed clay platelets do not affect the optical clarity as significantly compared to poorer clay dispersions.

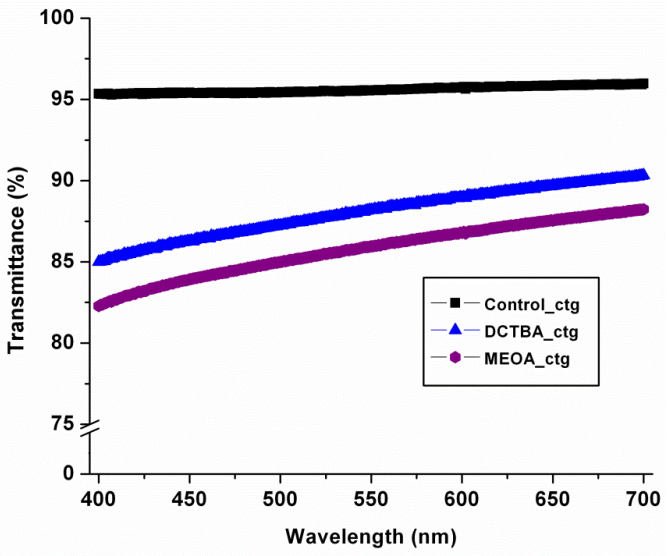

Figure 9.7: Transmittance of RAFT-mediated organic-inorganic hybrids as determined by UV-visible spectroscopy.

9.3.5. Mechanical properties – Dynamic mechanical analysis and König hardness

Increased storage moduli and crosslink densities were observed by dynamic mechanical analysis with the incorporation of the organomodified clays into the organic-inorganic hybrid network. From Figure 9.8 and Table 9.3, it is

apparent that the inclusion of organomodified clay improved the mechanical properties of the hybrid films. The Control_ctg had a storage modulus (E') of 160 MPa at room temperature, whereas the DCTBA_ctg and MEOA_ctg measured E' values of 510 and 350 MPa, respectively. The DCTBA_ctg, demonstrating the highest E' values over the -80 – 200 °C temperature range, was superior to the MEOA_ctg, most likely a result of clay dispersion within the hybrid film.

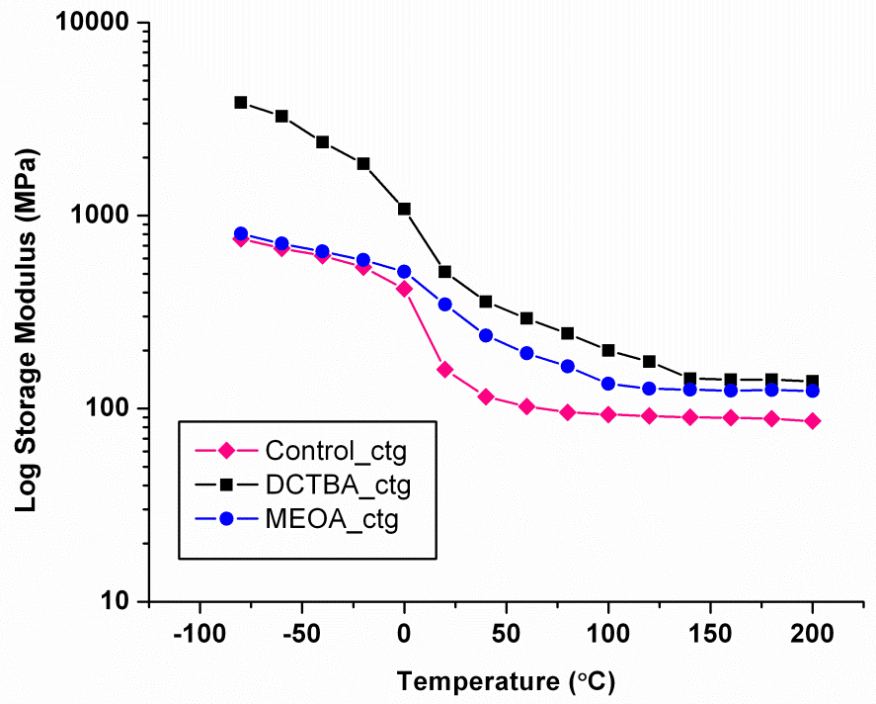

Figure 9.8: Dynamic mechanical analysis (DMA) storage modulus curves for the RAFT-mediated organic-inorganic hybrid films.

TABLE 9.3
RAFT-mediated organic-inorganic hybrid mechanical properties characterization

Hybrid Name	*E'* (MPa,25°C)	T_g (°C)	XLD (mol/cm^3)	Hardness (sec)
Control_ctg	160	65	7.20E-03	106
DCTBA_ctg	510	82	1.25E-02	136
MEOA_ctg	350	76	1.06E-02	128

Similar trends were observed with the crosslink density (XLD) of each hybrid film. The XLD of the DCTBA_ctg was highest of the three hybrid films at 1.25E-02 mol/cm^3, whereas the MEOA_ctg had a XLD of 1.06E-02 mol/cm^3. In addition to the improvement in the hybrid viscoelastic properties with organomodified clay incorporation, the hardness of the hybrid films increased with clay inclusion (Figure 9.9). The König pendulum hardness of the Control_ctg was 106 seconds, and the introduction of DCTBA-clay and MEOA-clay produced hybrids with hardness values of 136 and 128 seconds, respectively.

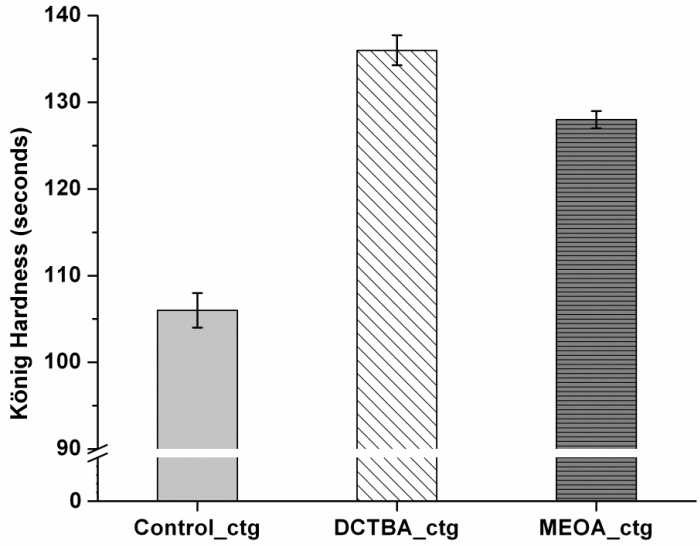

Figure 9.9: König pendulum hardness results for the RAFT-mediated organic-inorganic hybrid films.

From the mechanical property analysis of the three hybrid films, two major trends emerged which directly correlated to the barrier, thermal, and optical property comparison. The first trend observed was the improvement in the material properties with the incorporation of the organomodified clay into the hybrid network. With the inclusion of DCTBA-clay and MEOA-clay into the RAFT-mediated organic-inorganic hybrid films, improvements in the water vapor

transmission, water vapor permeability, thermal stability, mechanical strength, and hardness were observed. The enhanced material properties are attributed to the distribution of the organomodified clay throughout the hybrid network. The second trend observed throughout the material property characterization of the clay-containing hybrids was that DCTBA_ctg was superior to the MEOA_ctg. Because the level of clay loading was equivalent in each hybrid film, the more significant enhancements in the DCTBA_ctg material properties was likely a result of better clay dispersion. By grafting the RAFT agent DCTBAB to the unmodified clay platelet, the growing copolymer chain may have had a greater extent of chain intercalation between the clay interlayer, thus leading to better clay dispersion. Although the MEOA_ctg demonstrated increased material properties compared to the Control_ctg, the hybrid film properties were typically less enhanced than the DCTBA_ctg.

9.4. Conclusions

RAFT-mediated alkoxysilane-functional copolymer-clay nanocomposites were prepared to serve as precursor sol materials for the formation of organic-inorganic hybrid films. Two approaches were taken for RAFT agent incorporation. The first approach, where the RAFT agent was grafted to the montmorillonite clay platelet, was found to be most successful in enhancing the resulting hybrid film properties. Reductions in water vapor transmission and water vapor permeability were attributed to proper clay distribution throughout the hybrid network, thus providing a tortuous diffusion path. The hybrid film thermal stability, mechanical strength, and hardness also improved compared to a control hybrid film containing

no organomodified clay. The second approach, where the RAFT agent was added to the reaction medium with methacrylate-functional organomodified clay, was found to be less successful in improving the hybrid film properties. Although the improvements in the barrier, mechanical, and thermal properties were observed compared to the control hybrid, the first approach with the RAFT agent-functional clay was superior. These initial studies displayed the success of employing quaternary ammonium RAFT agents to control the copolymerization reaction in the preparation of alkoxysilane-functional copolymer-clay nanocomposites. Further copolymer reactions with high concentrations of the RAFT-functionalized clay will be studied to determine the maximum clay loading to maintain control of the copolymerization reaction while further improving the hybrid film properties.

9.5. References

1. Patten, T. E.; Xia, J.; Abernathy, T.; Matyjaszewski, K., *Science* **1996,** *272* (5263), 866.

2. Sciannamea, V.; Jérôme, R.; Detrembleur, C., *Chemical Reviews* **2008,** *108* (3), 1104-1126.

3. Chiefari, J.; YK Chong; Ercole, F.; Krstina, J.; Jeffery, J.; Le, T. P. T.; Mayadunne, R. T. A.; Meijs, G. F.; Moad, C. L.; Moad, G., *Macromolecules* **1998,** *31* (16), 5559-5562.

4. Gao, H.; Matyjaszewski, K., *Macromolecules* **2007,** *40* (3), 399-401.

5. YK Chong; Le, T. P. T.; Moad, G.; Rizzardo, E.; Thang, S. H., *Macromolecules* **1999,** *32* (6), 2071-2074.

6. Barner, L.; Davis, T. P.; Stenzel, M. H.; Barner-Kowollik, C., *Macromolecular Rapid Communications* **2007,** *28* (5), 539-559.

7. McCormick, C. L.; Lowe, A. B., *Accounts of Chemical Research* **2004,** *37* (5), 312-325.

8. Moad, G.; Rizzardo, E.; Thang, S. H., *Australian Journal of Chemistry* **2005,** *58* (6), 379-410.

9. Matyjaszewski, K., *Controlled/living radical polymerization progress in ATPR, NMP, and RAFT (ACS symposium series, vol. 768)*. American Chemical Society, Washington, DC: 2000.

10. Moad, G.; Rizzardo, E.; Thang, S. H., *Australian Journal of Chemistry* **2006,** *59* (10), 669-692.

11. Salem, N.; Shipp, D. A., *Polymer* **2005,** *46* (19), 8573-8581.

12. Zhang, B.-Q.; Pan, C.-Y.; Hong, C.-Y.; Luan, B.; Shi, P.-J., *Macromolecular Rapid Communications* **2006,** *27* (2), 97-102.

13. Samakande, A.; Juodaityte, J. J.; Sanderson, R. D.; Hartmann, P. C., *Macromolecular Materials and Engineering* **2008,** *293* (5), 428-437.

14. Samakande, A.; Sanderson, R. D.; Hartmann, P. C., *European Polymer Journal* **2009,** *45* (3), 649-657.

15. Zhang, B.-Q.; Chen, G.-D.; Pan, C.-Y.; Luan, B.; Hong, C.-Y., *Journal of Applied Polymer Science* **2006,** *102* (2), 1950-1958.

16. Qu, Y. Z.; Su, Y. N.; Sun, J. S.; Wang, K. C., *Journal of Applied Polymer Science* **2008,** *110* (1), 387-391.

17. Samakande, A.; Sanderson, R. D.; Hartmann, P. C., *Synthetic Communications* **2007,** *37* (21), 3861-3872.

18. Zeng, C.; Lee, L. J., *Macromolecules* **2001,** *34* (12), 4098-4103.

19. Chan, C. K.; Peng, S. L.; Chu, I., *Polymer* **2001,** *42* (9), 4189-4196.

20. Severac, R.; Lacroix-Desmazes, P.; Boutevin, B., *Polymer International* **2002,** *51* (10), 1117-1122.

CHAPTER 10. GENERAL CONCLUSIONS

10.1. General conclusions

The goal of this dissertation research was to explore the novel preparation of barrier coatings by incorporating layered silicates into polymeric materials to create high performance hybrids. The first approach taken was the development of UV-curable nanocomposite barrier coatings by using a novel in situ preparation technique. Hydroxy-functional organomodified clay was first dispersed at high shear with a hydroxy-functional monomer, and the resulting mixture was used in the polyesterification of an unsaturated polyester resin. This in situ intercalative polymerization technique produced highly dispersed organomodified clays throughout the polyester resin. By employing donor-acceptor chemistry, UV-curable nanocomposite films were prepared. The in situ preparation technique provided a higher degree of clay dispersion compared to an alternative clay dispersion technique of mixing and sonication. With lower levels of hydroxy-functional clay loading (1 – 2 wt.%), exfoliated morphologies were produced for the UV-curable nanocomposites prepared by the in situ technique. Several material properties were shown to improve with the in situ preparation technique compared to the sonication dispersion route, including decreased water vapor permeability, increased storage moduli, and increased thermal stability.

Interestingly, the incorporation of higher levels of clay loading (5 – 10 wt.%) did not further improve the nanocomposite material properties. Instead, decreases in the mechanical performance and thermal stability were observed with the incorporation of higher clay loading, potentially a consequence of the clay organic

modifier inducing plasticizing effects on the nanocomposite films. To explore the impact of the clay organic modifier structure and concentration on nanocomposite material properties, a series of unsaturated polyesters were synthesized in the presence of just the organic modifiers. Two common quaternary alkylammonium organic modifiers were incorporated into the polyester resins by the same in situ preparation technique previously used in the preparation of clay-containing unsaturated polyester resins, then crosslinked via donor-acceptor chemistry to produce UV-curable films. Dramatic decreases in the mechanical properties of the UV-curable films were observed with higher concentrations of the methyl, tallow, bis-2-hydroxyethyl ammonium (MTEtOH) organic modifier. Increases in the MTEtOH concentration reduced the storage moduli and crosslink densities of the UV-curable films to values even lower than the control UV-curable film.

To further induce clay dispersion in a precursor unsaturated polyester resin, a novel “reverse” in situ preparation technique was developed to produce an in situ ion exchange reaction during polyesterification. The hydroxy-functional organic modifiers were pre-dispersed with a hydroxy-functional organic modifier, then polyesterification was started. During the polyesterification, unmodified montmorillonite clay was added to the reaction mixture, and an in situ ion exchange reaction was induced. The polyesters produced through the reverse in situ technique were crosslinked by donor-acceptor chemistry via UV-irradiation to produce UV-curable films. Enhanced cure, barrier, mechanical, and thermal properties were observed for the nanocomposites prepared through the reverse in situ process compared to nanocomposites prepared through an alternative clay

dispersion technique of mixing and sonication. The improvement in nanocomposite properties was attributed to higher clay dispersion throughout the film, as confirmed by transmission electron microscopy and X-ray diffraction. The optimal clay loading was determined to be between 2 – 5 wt.% organomodified clay, as nanocomposites possessing this level of clay loading demonstrated the most significant enhancements in material properties.

In addition to the preparation and study of UV-curable polymer-clay nanocomposite systems, another branch of nanocomposite materials was studied: organic-inorganic hybrid films prepared by sol-gel chemistry. The novel preparation of organic-inorganic hybrids containing organically modified clay was studied as a relatively facile approach to incorporate the advantageous characteristics of hybrid formation by sol-gel chemistry with layered silicate incorporation. The preparation of these novel organic-inorganic hybrid films was completed in a two-step process. First, alkoxysilane-functional organic precursor 3-methacryloxypropyltrimethoxy-silane (3-MPS) was copolymerized with methyl methacrylate (MMA) in the presence of organomodified clay to create an alkoxysilane-functional copolymer-clay nanocomposite. The nanocomposite was then used as a sol precursor for the formation of organic-inorganic hybrids by utilizing sol-gel chemistry to crosslink the alkoxysilane-functional copolymers. The level of organomodified clay loading and monomer molar ratios were found to have a profound impact on the properties of the organic-inorganic hybrid films. The incorporation of organomodified clay, particularly 2 – 5 wt.%, into the hybrid network improved the film barrier, mechanical, and thermal properties. Over one magnitude reduction in the water

vapor permeability was observed with clay inclusion as well as significant improvements in the hybrids storage moduli and crosslink densities.

Due to the success in preparing high performance organic-inorganic hybrids with organomodified clay incorporated into the hybrid network, variations to the copolymer backbone and crosslinking agents were explored. In particular, amine-functionality was incorporated into the hybrid films for potential applications in CO_2 capture and separation membrane technology. Two approaches were studied to incorporate the amine-functional groups into the hybrid structure. The first approach was to copolymerize 3-MPS with 2-(dimethylamino)ethyl methacrylate (DMAEMA) to produce amine- and alkoxysilane-functional copolymer-clay nanocomposites that may undergo sol-gel crosslinking reactions to yield amine-based organic-inorganic hybrids. Once again, the organic-inorganic hybrid films demonstrated enhanced material properties, particularly barrier protection and mechanical performance, in comparison to a neat hybrid film containing no organomodified clay. Although improved material properties were seen, the resulting films were brittle and difficult to handle.

To overcome the brittleness of the amine-based organic-inorganic hybrids, a second approach to incorporate amine-functionality into the hybrid structure was explored. Similar to the first preparation technique, 3-MPS and MMA were copolymerized in the presence of organomodified clay. The nanocomposite sol precursor was then crosslinked with 3-aminopropyltrimethoxysilane (APTMS) to incorporate amine-functionality into the organic-inorganic hybrids. The weight ratio of nanocomposite precursor to APTMS crosslinker and the organomodified clay

loading were both found to impact the hybrid film properties. Striking reductions in the water vapor permeability were observed by increasing the APTMS content. The water vapor permeability decreased over three magnitudes by increasing the APTMS concentration and organomodified clay loading compared to a neat hybrid film. Higher concentrations of the APTMS crosslinker also led to increased storage moduli, crosslink density, and thermal stability.

The final variation of the preparation of novel organic-inorganic hybrid films containing organomodified clay was to incorporate the controlled living radical polymerization technique of reversible addition-fragmentation chain transfer (RAFT) into the preparation of the copolymer-clay nanocomposite precursor. A quaternary ammonium RAFT agent was synthesized and used to functionalize montmorillonite clay platelets. The RAFT-mediated copolymerization was then conducted to produce alkoxysilane-functional copolymer-clay nanocomposites. An alternative RAFT-mediated copolymerization approach was created to serve as a comparison to the RAFT-functional clay platelets. With the alternative technique, the RAFT agent was introduced into the reaction medium without being attached to the clay surface. Instead, the clay was functionalized with a methacrylate-functional quaternary ammonium surfactant. Overall, the hybrid films formed from the RAFT-functional clay exhibited lower water vapor permeability and increased mechanical strength, crosslink density, thermal stability, and optical clarity compared to the alternative RAFT-mediated copolymerization approach. By functionalizing the clay surface with the RAFT agent, the dispersion of clays was seemingly enhanced, leading to a more significant improvement in material

properties. This initial experimentation into coupling the RAFT technique with the organic-inorganic hybrid preparation method was found to be successful.

CHAPTER 11. FUTURE WORK

11.1. Future Work

The UV-curable polymer-clay nanocomposite barrier coatings prepared through two novel in situ techniques (Chapters 2 and 4) demonstrated significantly enhanced materials properties compared to nanocomposites prepared through an alternative clay dispersion technique of mixing and sonication. In particular, the implementation of the in situ preparation methods led to reductions in both water vapor transmission and water vapor permeability. Although improvements in the barrier properties of the UV-curable nanocomposite systems were observed, the transmission of water vapor through the film will largely be affected by any defects within the coating. To overcome this obstacle, multi-layer coatings may be tested to observe the impact on coating barrier performance. Variables such as number of multi-layers, thickness, and cure time between applications may all be changed to explore the optimal coating application process to achieve the best barrier protection. In addition, dramatic reductions in water vapor transmission and permeability were obtained with the novel in situ preparation techniques but no significant changes in the oxygen gas transmission rate were observed (Chapter 2). Further experimentation to study this phenomenon could include surface analysis and microscopy to examine whether the clay platelets are creating small defects if protruding from the nanocomposite film, thus increasing the permeation of oxygen gas through the films.

The development of novel organic-inorganic hybrid films with organomodified clay dispersed throughout the hybrid network exhibited significant

improvements compared to neat organic-inorganic hybrid film systems (Chapter 6). Three series of copolymer-clay nanocomposites were synthesized with the monomer molar ratio varied at 3:1, 2:1, and 1:1 and clay loading of 1 – 10 wt.% for a total of fifteen nanocomposites and thus fifteen hybrid films. With the sol-gel preparation process, several parameters will affect the final hybrid film structure including the pH of the reaction medium, solvent selection, crosslinker selection, molar ratios of water and solvent, and the time for aging, drying, and densification. Therefore, further experimentation would be warranted to explore the impact of changing a portion of these reaction parameters.

In Chapters 7 and 8, amine-based organic-inorganic hybrid films were produced by incorporating amine functionality into both the alkoxysilane-functional copolymer backbone and the silane crosslinking agent. While the initial characterization of the hybrid films demonstrated improvements in the barrier, mechanical, and thermal properties, the target application for these systems is their implementation in CO_2 capture and separation membrane technologies. Therefore, subjecting the hybrid films to CO_2 and performing sorption/desorption, transmission, and permeability experiments would be warranted to examine the feasibility of using the amine-based hybrids in CO_2 capture and separation applications. Based on the success of the initial study regarding the RAFT-mediated copolymerization in the preparation of alkoxysilane-functional copolymer-clay nanocomposite (Chapter 9), further experimentation to study the impact of clay loading on film properties and the maximum clay concentration to still control

the copolymerization would help provide a more detailed understanding of this RAFT-mediated process.